INVESTIGATING THE REGULATION OF EFFECTOR GENE EXPRESSION IN THE RICE BLAST FUNGUS *MAGNAPORTHE ORYZAE* AND THE CELLULAR DYNAMICS OF THE BLAST INFECTION ON FINGER MILLET

by

JIE ZHU

(Under the Direction of Chang Hyun Khang)

ABSTRACT

The filamentous fungal pathogen *Magnaporthe oryzae* causes devastating blast diseases on economically important staple crops including rice, wheat, and finger millet. During a plant-pathogen interaction, the pathogen secretes effector proteins to modulate the plant cell structure, function and immune responses to facilitate infection. Expression of effector genes is typically repressed during axenic growth and highly induced during plant infection, yet the mechanism of the concerted expression remains largely unknown. In this study, I systematically investigated epigenetic and transcriptional regulation of effector gene expression in *M. oryzae* using genetic, molecular, and cell biology approaches. During mycelial growth in axenic culture, I found that the silencing histone modification trimethylated histone H3 lysine 27 (H3K27me3) mainly represses expression of H3K27me3-enriched effector genes. Interestingly, expression levels of many H3K27me3-enriched effector genes are also controlled by the transcription factor MoGti1. MoGti1 overexpression in the absence of H3K27me3 synergistically upregulates expression of some effector genes during mycelial growth. In particular, most (81%) of these synergistically upregulated effector genes are also highly induced during plant infection at 36 hpi by a wild-type

M. oryae strain. Thus, these results suggest a double control of effector gene expression: the epigenetic mechanism mediated by H3K27me3 represses expression during mycelial growth, while the transcriptional mechanism mediated by MoGti1 activates expression during plant infection. To better understand effector gene expression and regulation at single cell resolution, I developed a dual-color gene expression reporter of the *PWL2* effector gene. Expression of *PWL2* is successively upregulated during appressorium-mediated penetration and invasive hyphae cell-to-cell movement. This expression is controlled by the tandem repeats in the *PWL2* promoter, specifically, the 12-bp *cis*-regulatory sequence that is required for promoter activity during biotrophic invasion of rice cells. Although the interaction between *M. oryzae* and rice is well characterized, little is known about the infection on other plants. Thus, by developing a finger millet live-cell imaging assay, I investigated cytological dynamics of the finger millet-*M. oryzae* interaction and found the formation of a novel biotrophic interfacial complex (BIC) pattern, multisite BICs, during compatible interaction. Additionally, the rare infection of a *M. oryzae* isolate from finger millet (MoE) on rice through both microscopic and macroscopic observations demonstrates the host species specificity of MoE toward rice.

INDEX WORDS: *Magnaporthe oryzae*, Effector genes, Gene expression and regulation, Epigenetics, Transcription factor (TF), *cis*-regulatory element, Biotrophic interfacial complex (BIC), Finger millet, Host species specificity.

INVESTIGATING THE REGULATION OF EFFECTOR GENE EXPRESSION IN THE RICE BLAST FUNGUS *MAGNAPORTHE ORYZAE* AND THE CELLULAR DYNAMICS OF THE BLAST INFECTION ON FINGER MILLET

by

JIE ZHU

BS, Shandong Agricultural University, China, 2010

MS, Shandong Agricultural University, China, 2013

A Dissertation Submitted to the Graduate Faculty of The University of Georgia in Partial Fulfillment of the Requirements for the Degree

DOCTOR OF PHILOSOPHY

ATHENS, GEORGIA

2020

INVESTIGATING THE REGULATION OF EFFECTOR GENE EXPRESSION IN THE RICE BLAST FUNGUS *MAGNAPORTHE ORYZAE* AND THE CELLULAR DYNAMICS OF THE BLAST INFECTION ON FINGER MILLET

by

JIE ZHU

Major Professor:	Chang Hyun Khang
Committee:	Michelle Momany
	Zachary A Lewis
	Wolfgang Lukowitz
	Anish Malladi

Electronic Version Approved:

Ron Walcott
Interim Dean of the Graduate School
The University of Georgia
August 2020

DEDICATION

To all who have supported the studies in this dissertation, professors, fellow graduate students, families and friends.

ACKNOWLEDGEMENTS

I would be truly ungrateful if I did not take a moment to acknowledge the contributions of others to the process that has led to this work and helped make it what it is.

I would like to thank my committee members for their insights, encouragement, and patience. Their efforts have helped to make this work possible and the quality product it is. I would first like to thank Dr. Chang Hyun Khang, who has been a tremendous mentor for me, encouraging my research and providing opportunities for me to gain not only scientific knowledge but also clear pictures for the future career. In particular, I am grateful to Dr. Khang for continuously praying and mentoring for my faith in Jesus Christ over the years.

I would like to thank Dr. Michelle Momany, for helping me to better understand my project and always encouraging me in fungal group, and Dr. Zachary A Lewis, for the valuable rotation time in your lab, particularly, the experience of working with you on nuclei isolation, and the knowledge and insights learned from your classes. Also, I thank Dr. Wolfgang Lukowitz and Dr. Anish Malladi for your expertise and precious time.

I would like to thank Dong Won Kim, Kiersun Jones, Cory Jenkinson, Mariel Pfeifer, Kathryn Yeary, Margaret Henderson and rotation student Benjamin Chadwick in Dr. Khang's lab for all your help in lab work and writings.

I would like to thank Abigail Courtney, Dr. Peng Qi, Hallie Wright and Ruizhe Lin for the pleasant and productive collaborations. I would like to thank Dr. Masayuki Kamei, Dr. Youbao Zhao, Dr. Yumen Fan, Dr. Shan Jing and fungal group members for your assistance with lab techniques and advice on my project.

And I want to give special thanks to my wife, Xiaoming for your love and support in my research and life, and thanks to my sons, David and Daniel for your precious and sweet company during my study and research. Thanks to my parents and my brother for being supportive and encouraging. Also, thanks to my church family for all your love and support.

Finally, I thank my God, for Your amazing creation, for the wonderful nature, for the marvelous organisms in which every cell works together in the amazing and excellent way. I could not get through the rough days of this project and all the difficulties without You. Thank you, my Father.

TABLE OF CONTENTS

Page

LIST OF TABLES

Page

LIST OF FIGURES

Page

CHAPTER 1

INTRODUCTION AND LITERATURE REVIEW

TRANSCRIPTIONAL AND EPIGENETIC REGULATIONS OF EFFECTOR GENE EXPRESSION IN FILAMENTOUS FUNGI

The emergence of filamentous pathogens is a major threat to food production. During plant infection, filamentous pathogens deploy various ways to exploit host plants and facilitate invasion, one of which is to secrete effectors. Effectors, in a broad definition, are defined as molecules secreted by an organism to manipulate an interaction with a host (e.g. avirulence (Avr) proteins, secondary metabolites (SMs) and sRNA etc.). Effectors typically function as essential determinants of pathogen pathogenesis during plant-pathogen interaction. For instance, Avr proteins can interfere with host immune responses to promote interaction (effector-triggered susceptibility, ETS) in the absence of the cognate host resistant (R) proteins. In the presence of the R proteins, however, host defense response (effector-triggered immunity, ETI) is triggered to suppress interaction. Host-selective toxins (SMs) produced by filamentous pathogens are required to invade plant tissue and induce disease by suppressing immunity of sensitive plants (Tsuge et al., 2013). The function of fungal effectors has been extensively studied in the past (Lo Presti et al., 2015b; Sanchez-Vallet et al., 2018a), but mechanisms regulating effector gene expression has not been clear yet. This review mainly covers studies of transcriptional and epigenetic regulatory mechanisms that control expression of genes encoding protein effectors in filamentous fungi.

Effector gene expression

In planta induction

Upon infection, filamentous fungi reprogram transcription to control the required machinery so as to adapt to a colonization lifestyle. Regulated expression of effector genes is one of the most critical reprogramming actions. The expression of effector genes is typically suppressed during vegetative growth but is highly induced during plant infection, which is consistent with the function of effectors to facilitate fungal invasion. For instance, transcripts of *Magnaporthe oryzae PWL2* effector gene were undetectable in axenically grown cultures, but cDNA was amplified from RNA of the infected plants (Sweigard et al., 1995a). Similarly, *Ustilago maydis* effector genes *Mig1* (for maize-induced gene) and gene cluster *Mig2s* were not expressed or barely expressed during yeast-like and filamentous growth in axenic culture but were distinctly upregulated during biotrophic infection stage (Basse et al., 2000b, 2002b). However, these studies only showed one or a few effector genes being upregulated during plant infection. Is the *in planta* induction of effector gene expression a general machinery in filamentous pathogens? This question has been investigated and confirmed by high-throughput transcriptome analysis in recent years. Wang and colleagues (2011) demonstrated for the first time that the RXLR effector repertoire was widely and transcriptionally reprogrammed during soybean infection by an oomycete pathogen *Phytophthora sojae*. Subsequently, this globally induced effector gene expression pattern was found in fungal pathogens *Colletotrichum higginsianum, Blumeria graminis* f. sp. Hordei, *M. oryzae*, *Leptosphaeria maculans*, and *U. maydis*, suggesting that the induced effector gene expression during plant infection is a conserved pattern in various plant pathogens (Dong et al., 2015; Gervais et al., 2017; Hacquard et al., 2013; Kleemann et al., 2012; Lanver et al., 2018; O'Connell et al., 2012a).

Wave expression/stage-specific pattern

During colonization of plant tissues, pathogens tightly control transcriptional reprogramming to coordinate their lifestyle transitions. This is not only associated with *in vitro* to *in vivo* (*planta*) transitions but also involves biotrophic/necrotrophic stages and biotrophy to necrotrophy transitions. Since effectors mainly function as key determinants of pathogen pathogenicity during plant-pathogen interaction, the permanently induced effector expression upon infection may increase fitness cost of pathogens. For instance, the highly constitutive expression of RXLR effector *Avh238* that should express at low level upon *P. sojae* infection greatly reduced the infection of transformants compared to a wild-type strain and a control transformant (Wang et al., 2011). Therefore, effector gene expression shows a highly stage-specific pattern as different sets of effector genes are expressed at different infection stages. The coordinated expression of effector genes along with disease development constitute successive waves of effector gene transcription, which have been connected to pathogenic transitions (Dong et al., 2015; Gervais et al., 2017; Hacquard et al., 2013; Kleemann et al., 2012; Lanver et al., 2018; O'Connell et al., 2012a; Wang et al., 2011). Consequently, the misexpression of effector genes at an inappropriate stage may impair virulence of filamentous pathogens, such as *Avh238* (Wang et al., 2011). The tight control of effector gene expression supports the function of effectors because many Avr proteins can be recognized by the host plant and trigger severe immune responses. The early expression of these Avr proteins may be recognized by plant and effective enough to confer plant immunity and to block pathogenesis development.

Signals/Host viability

The fungal infection process resembles multiple stress conditions, such as limited nutrients and oxidative stress. The expression of genes induced in stress conditions share

common patterns. For example, i) expression of stress genes is able to be rapidly and specifically activated in response to external stimuli; ii) the expression time and level are tightly controlled; iii) multiple genes are cooperatively/synchronically activated in response to the same stimulus (Weake and Workman, 2010). Upon plant infection, although many effector genes show *in planta* induction, a subset of them are only upregulated after penetration into plant cells (Basse et al., 2000a; van der Does et al., 2008). Therefore, expression of effector genes is also specifically induced, after which expression is controlled in a well-coordinated manner. In addition, induced expression of each set of effector genes at each infection stage suggests that they are cooperatively activated. All these features have been uncovered in effector genes and resemble stress gene expression, suggesting that effector gene expression may be also induced by external stimuli. Interestingly, however, few external signals have been found yet to widely activate effector gene expression in filamentous pathogens.

The similarity between effector genes and stress genes supports a hypothesis that abiotic stresses are able to induce effector gene expression even during mycelia growth in axenic culture. Recently, Meyer and colleagues (2017) determined effector gene expression in *L. maculans* using many different abiotic factors: nitrogen (N) / carbon (C) source, temperature, pH, and antibiotic stresses (cycloheximide, phleomycin). N/C source, temperature and pH only showed a limited effect on effector gene expression. Interestingly, however, cellular stresses imposed by antibiotics strongly induced effector gene expression in mycelia (Meyer et al., 2017). Unsurprisingly, these results are consistent with the function of effector proteins which antagonize stresses from the infected plant, such as oxidative stress and enzyme digestion. The un-demanded induction of effector genes due to common abiotic factors (e.g. pH and temperature) might increase fungal fitness cost. Cycloheximide inhibits protein synthesis and

phleomycin triggers DNA double strand break (DSB). Both antibiotic stresses (cycloheximide and phleomycin) highly induced effector gene expression. This suggests that filamentous fungi produce effectors under harsh environment. During a plant-pathogen interaction, a plant produces H_2O_2, SMs, and digestion enzymes to resist fungal infection, which also possibly interferes with plant protein synthesis and triggers DSB.

In planta induction of effector gene expression indicates that there may be external signals being detected by filamentous fungi to trigger their expression. Indeed, surface hydrophobicity and the cutin monomer 16-hydroxy hexadecanoic acid upregulated the expression of 47 novel effector genes in *U. maydis* (Lanver et al., 2014). *C. higginsianum candidate secreted effector-encoding gene 6* (*ChEP6*) was highly induced in appressoria formed *in planta* compared to appressoria *in vitro*, although appressoria are morphologically indistinguishable, suggesting signals from *in planta* infection induce *ChEP6* expression (O'Connell et al., 2012a). The signals can be either stress conditions like limited nutrients or plant-derived chemicals like cell wall components. For example, the expression of *Cladosporium fulvum* effector *Avr9* was highly induced during plant infection and limited nitrogen conditions but not under the *in vitro* condition with unrestricted nitrogen, suggesting nitrogen limitation induces *Avr9* expression, although the correlation between nitrogen limitation and plant infection has not been clear yet (Van den Ackerveken et al., 1994). Recently, chemical signals derived from plants have been uncovered to induce effector gene expression. Plett et al. (2012) first demonstrated that expression of *Laccaria bicolor* effector *MiSSP7* was induced by rutin and quercitin belonging to flavonoids which are typically found in exudates of plant roots. The external signals must be sensed by fungal pathogens to reprogram transcriptions. Indeed, *U. maydis* plasma membrane proteins Sho1 and Msb2 are required for expression of 26 surface cue-

induced effectors, suggesting they are putative sensors of plant surface cues (Lanver et al., 2014). Currently, although only little evidence has been found to support the hypothesis that external signals during plant infection trigger effector gene expression, identification of external signals regulating effector gene expression in the future will surely give us a new perspective to block fungal disease.

The induced expression of *MiSSP7* by flavonoids rutin and quercitin suggests that the activation of *MiSSP7* is not host plant specific as long as plants can produce flavonoids. Indeed, *MiSSP7* expression was able to be induced by both host (poplar) and non-host (*Arabidopsis thaliana*) roots (Plett et al., 2011). This non-host specific expression pattern of effector genes was also found in barley powdery mildew *Blumeria graminis* f. sp. Hordei. Transcriptomic studies of *B. graminis* on immunocompromised *Arabidopsis* mutants revealed that large sets of effector genes were comparably expressed during early stage of both compatible and incompatible interactions (Hacquard et al., 2013). These results indicate that non-host specific induction of effector genes seems to be a conserved pattern upon plant infection. However, this is not always the case. The expression of *F. oxysporum Six1* was not induced on non-host plants *Arabidopsis thaliana*, *Zea mays* and *Nicotiana benthamiana* compared on host tomato, although it was induced by cell culture of the non-host *N. benthamiana* (van der Does et al., 2008). This was further demonstrated by a transcriptomic study of the wheat pathogen *Zymoseptoria tritici* on a compatible wheat host *Triticum aestivum* and a noncompatible grass host *Brachypodium distachyon*. Expression of genes encoding proteins with putative secretion signals was specifically upregulated during early stage of wheat infection compared to noncompatible grass, suggesting a host-specific regulatory program (Kellner et al., 2014). The reason why effector genes show host/non-host expression pattern remains unknown. Interestingly, however,

transcripts of *B. graminis* effector genes were reduced when an active *MLA1* R gene is in the non-host *Arabidopsis,* indicating the presence of *MLA1* R gene results in a recognition between non-host *Arabidopsis* and the pathogen (Hacquard et al., 2013). This is similar to the observation in noncompatible interaction between *Z. tritici* and *B. distchyon*. *Z. tritici* infects *B. distchyon* leaf surface through stomata but proliferation ceases in the substomatal cavity, suggesting an early recognition between plant and pathogen (Kellner et al., 2014). This indicates an early recognition between host and pathogen. Pathogen can reprogram transcription of effector genes to manipulate host defenses in compatible interaction and/or to be suppressed by plant defenses in noncompatible interaction. The hypothesis that certain interaction/recognition between effector and cognate R proteins plays a vital role in deciding how to reprogram effector gene expression needs to be explored in the future.

Interaction/recognition between effector and R proteins at the early infection stage indicates that plants have to be metabolically active to response pathogen invasion. Consequently, living plant cells may be required for expression of some effector genes. Several lines of evidence support this hypothesis. For instance, *F. oxysporum* effector *Six1* was unable to express on dead plant tissue and ground plant materials, suggesting the cue(s) inducing *Six1* expression is only present in living plant (van der Does et al., 2008). Similarly, transcriptomic analysis of *F. graminearum* on living and dead wheat revealed that expression of a limited number of effector genes required the living plant (Boedi et al., 2016). Both *F. oxysporum* and *F. graminearum* have biotrophic growth phase during early infection, which is similar to *Z. tritici* and *B. graminis* infections. Thus, exclusively induced expression of effector genes on living plant suggests that these effector genes might be specifically essential during the biotrophic phase, such as subduing the plant immune system or maintaining plant cell viability.

Transcriptional regulation

Cis-regulatory element

Once receiving a signal, a transcriptional activator is recruited to promoter region of effector genes to bind specific DNA sequence (*cis*-regulatory element) and then activates the transcription of effector genes. Compared to transcriptional activators that regulate effector gene expression, *cis*-regulatory elements seem to be more identifiable because promoter sequences of known and putative effector genes have been available for researchers. Sequence alignment followed by promoter mutation analysis provide us a straightforward approach to elucidate how *cis*-regulatory elements control effector gene expression.

Currently, promoter deletion assay reveals that a short upstream region of effector genes is typically sufficient to confer full promoter activity. For instance, a 350-bp upstream fragment of *U. maydis* effector gene *Mig2-5* contained all elements for the strong induction *in planta* (Farfsing et al., 2005). Similarly, this was observed for *Parastagonospora nodorum* effector gene *Tox3* (Lin et al., 2018). The full promoter activity includes both positive and negative regulation. For example, none of deletions and substitutions of *Mig2-5* promoter showed increased promoter activity during filamentous growth in axenic culture, indicating that the strong transcriptional activity of *Mig2-5 in planta* is mediated by positive *cis*-elements (Farfsing et al., 2005). However, promoter activities of *Mig1* and *Mig2-1* effector genes were controlled by both positive and negative *cis*-regulatory elements through successive promoter deletion coupled with GFP reporter assay (Basse et al., 2002a; Basse et al., 2000a).

The identification of *cis*-regulatory elements through promoter mutation analysis is a time and effort-consuming process, although it is straightforward. Nevertheless, effectors belonging to a gene family or cluster will make this approach easy since we can take advantage

of the alignment of promoter sequences to analyze modules or features that are conserved in a family or cluster. For example, the promoter alignment of five effector genes in *Mig2* cluster identified three conserved regions (box I, II, III). Substitution of box III with random sequence showed more severe impact for *Mig2-5* promoter activity than that of box I and box II (Farfsing et al., 2005). Further substitution and sequence analysis identified that a consensus motif 5'-MNMNWNCCAMM-3' in box III was essential for promoter activity (Farfsing et al., 2005). Lately, it was demonstrated that this *cis*-regulatory element was deployed by the transcriptional activator Mzr1 (see discussion in next session) to control *Mig2-5* promoter activity (Zheng et al., 2008). Interestingly, there are nine copies of 5'-CCA-3' motif in core promoter region of *Mig2-5*. Although the substitution of three copies only partially affected prompter activity, the substitution of six copies completely abolished promoter activity. Furthermore, reconstruction of heterologous promoters with six copies of CCA-containing regions showed stronger promoter activity than that of four copies (Farfsing et al., 2005). These results suggest that the number of *cis*-regulatory element plays an important role in controlling the strength of promoter activity.

The identification of *cis*-regulatory elements, even a short fragment that is essential for effector promoter activity, will advance understandings on regulatory machinery of effector gene expression. For example, Lin et al., (2018) identified that a 25-bp region in the *Tox3* promoter was required for its transcriptional induction through promoter deletion and DNase I foot-printing. Then, two-repeats of 25-bp region were used as bait to successfully prey the interacting transcriptional activator PnCon7 (Lin et al., 2018). Additionally, successive wave pattern of effector gene expression indicates that the same wave of effector genes expressing at same time was co-transcribed by same one/type transcriptional activator (Lanver et al., 2018). Thus,

effectors in the same expression wave may share a *cis*-regulatory element. Consequently, the identified *cis*-regulatory element can be used to predict novel candidate effector genes.

With the development of high-throughput sequencing technologies, it not only makes more genome sequences available, but also allows us to identify *cis*-regulatory elements more efficiently and effectively. First, we have large amounts of sequence resources of effector promoters to identify putative *cis*-regulatory elements using bioinformatic analysis. For instance, miniature inverted-repeat transposable elements (MITEs) are associated with *SIX* effector genes and a mimp exists in the promoter region of all *SIX* genes in *F. oxysporum* through bioinformatic analysis. Thus, the presence of mimps in prompters was successfully used to predict novel candidate effector genes, although the deletion of mimp on two *SIX* gene promoters had no influence for gene expression (Schmidt et al., 2013). In addition, chromatin immunoprecipitation followed by sequencing (ChIP-seq) assay of a transcriptional activator is able to simultaneously determine a *cis*-regulatory element and any effector genes that are directly regulated by this transcriptional activator.

Trans-acting regulators

A trans-regulatory element encodes a transcription factor that recognizes and binds a specific *cis*-regulatory element of target genes to directly regulate gene expression. Regulation of effector gene expression by various types of transcription factors has been well reviewed recently (Tan and Oliver, 2017b). Thus far, 13 TFs from four transcription factor families (Zinc finger, APSES (ASM-1, Phd1, StuA, EFG1, and Sok2), WOPR, and fork head) have been reported to affect effector or candidate effector gene expression, either positively or negatively. This review emphasizes how a transcription factor regulating expression of effector genes can be identified.

Homology search

Critical roles that effectors play in pathogenicity have been extensively highlighted in different pathosystems, as mentioned previously. This leads to a hypothesis that reduced pathogenicity of a transcription factor mutant results from decreased expression of effector genes. Indeed, the less virulent mutant of SnStuA, a APSES (ASM-1, Phd1, StuA, EFG1, and Sok2) TF, showed about 6-fold less expression of an effector gene *SnTox3* than in the wild-type strain, suggesting a potential function of SnStuA in regulating effector gene expression (IpCho et al., 2010). This study first indicated that StuA TF is involved in regulation of effector gene expression. Later, Soyer et al. (2015) identified a StuA homology in *L. manculans* and demonstrated that gene silencing of *LmStuA* down-regulated expression of *AvrLm4-7, AvrLm1*, and *AvrLm6* effector genes during infection, further suggesting that StuA TF affects effector gene expression. Currently, whether StuA TFs function as a regulator of effector gene expression in other filamentous fungi still remains unknown. However, as the APSES proteins family share a conserved DNA-binding domain in diverse fungi, the function of StuA on effector gene expression might be conserved (Zhao et al., 2015). Therefore, homology search provides a strategy to efficiently identify a TF that possibly involves effector gene expression in various fungi. Simultaneously, this approach allows us to predict whether the function of a TF on effector gene regulation is conserved in different pathosystems.

Another well studied example of identifying a TF that affects effector gene expression through homology search is white-opaque regulator 1 (Wor1) protein. Wor1 was initially characterized as a master regulator of morphological switching and virulence in human fungal pathogen *Candida albican* (Huang et al., 2006). Subsequently, an insertional mutagenesis screen in *F. oxysporum* identified *SIX gene expression 1* (*Sge1*), a Wor1 ortholog, that was essential for

fungal virulence on tomatoes and functioned as a positive regulator for expression of four effector genes *SIX1*, *SIX2*, *SIX3* and *SIX5* (Michielse et al., 2009a). Thereafter, the Wor1 ortholog in *Verticillium dahliae* VdSge1, *Fusarium verticillioides* Sge1, *Cladosporium fulvum* CfWor1, *Z. tritici* ZtWor1, *M. oryzae* MoGti1, and *U. maydis* Ros1 were identified by homology search and demonstrated to affect effector gene expression (Table 1.1) (Brown et al., 2014b; Li et al., 2016b; Mirzadi Gohari et al., 2014a; Okmen et al., 2014a; Santhanam and Thomma, 2013; Tollot et al., 2016). Interestingly, all Wor1 knockout mutants in various fungal pathogens cause significantly reduced or no pathogenicity during pant infection, further suggesting that deletions of Wor1 orthologs downregulated effector gene expression. Surprisingly, however, most Wor1 orthologs were able to not only positively affect effector gene expression but they can affect them negatively as well (Brown et al., 2014b; Li et al., 2016b; Mirzadi Gohari et al., 2014a; Okmen et al., 2014a; Santhanam and Thomma, 2013; Tollot et al., 2016). Considering that Wor1 functioned as a master regulator of morphological switching and regulated expression of phase specific genes in *C. albican* (Huang et al., 2006; Zordan et al., 2007), the WOPR protein may mainly control a subset of effector gene expression to facilitate fungal invasion. For example, Ros1 downregulated expression of 128 effector genes involved in the establishment of biotrophic development but upregulated 70 effector genes that are essential for the late infection stage (Tollot et al., 2016). This is consistent with the successive wave expression pattern of effector genes, indicating that WOPR protein functions during phase switching.

The expression profiles of WOPR proteins in different fungi vary. For instance, expression levels of *ZtWor1* and *CfWor1* were much higher *in vitro* than during infection, which contrasted with the upregulation of *FoSge1*, *VdSge1* and *MoGti1* during infection (Brown et al., 2014b; Li et al., 2016b; Mirzadi Gohari et al., 2014a; Okmen et al., 2014a; Santhanam and

Thomma, 2013). This raises a question why expression of WOPR proteins is associated with different development stages of different fungi, although all deletion mutants showed significantly reduced pathogenicity. The answer to this question will shed light on targets of WOPR proteins and whether they are specific regulators of effector gene expression in plant pathogenic fungi. Expression levels of *ZtWor1* and *CfWor1* showed more correlation with development transitions, suggesting that they are involved in more fungal developmental processes (Mirzadi Gohari et al., 2014a; Okmen et al., 2014a). This is consistent with the overexpression phenotype of *CfWor1*, which resulted in the reduced conidiation and virulence on the susceptible plant than wild-type (Okmen et al., 2014a). Similarly, all the deletion mutants of WOPR proteins lead to reduced conidiation and/or abnormal hyphal growth (Brown et al., 2014b; Li et al., 2016b; Mirzadi Gohari et al., 2014a; Okmen et al., 2014a; Santhanam and Thomma, 2013; Tollot et al., 2016). However, this cannot rule out the possibility that WOPR proteins directly target effector genes. As demonstrated recently, Ros1 directly regulated effector gene expression through RNA-seq and ChIP-seq analyses (Tollot et al., 2016). Currently, the machinery of WOPR proteins regulating effector gene expression still remains unexplored. The effector genes whose expression is affected by WOPR proteins in different fungi have not been compared yet, but it might provide a hint on how WOPR proteins involve effector gene expression. For example, the occurrence of shared motif in promoters of upregulated effector genes by WOPR proteins may suggest that they are directly regulated by WOPR proteins. Otherwise, WOPR proteins indirectly affect effector gene expression through regulating direct targets. This has been demonstrated by the heterodimeric transcription factor bE/bW that controls the *U. maydis* lifestyle transition from saprophytic to a pathogenic stage (yeast-like to filamentous hyphae), in which downstream responsive genes, including effectors, were not

directly regulated by bE/bW proteins but by a second transcription factor Rbf1 that was activated by bE/bW (Heimel et al., 2010).

Cis-regulatory element-based assay

Promoter deletion and motif search generates many short DNA fragments containing putative *cis*-regulatory elements. This makes it possible to identify the interacting transcription factor through a yeast one-hybrid or electrophoretic mobility shift assay (EMSA) coupled with a mass spectrometry (MS) technique. Recently, for instance, a 25-bp region in the promoter of *P. nodorum Tox3* effector was identified through promoter deletion and DNase I foot-printing (Lin et al., 2018). Then yeast one-hybrid with 2 copies of 25-bp fragment identified the putative transcription factor PnCon7. Subsequent gene silencing of *PnCon7* caused reduced expression of *Tox3* in a dose-dependent manner, suggesting PnCon7 directly regulated *Tox3* expression. Another three predicted effectors of which promoters contain the conserved region of 25-bp fragment were also demonstrated to be directly regulated by PnCon7. Interestingly, PnCon7 also regulated two necrotrophic effectors *ToxA* and *Tox1*, although they had no conserved binding motif in promoters, suggesting an indirect regulation. Compared to a homology search, a *cis*-regulatory element-based assay has the ability to determine direct/indirect regulation more efficiently based on the presence or absence of *cis*-regulatory elements. However, the regulation function of the transcription factor identified by a *cis*-regulatory element-based assay might not be conserved in different fungi, even if they share the same binding motif. For example, *C. albicans* Wor1 and *S. cerevsive* Mit1 target different sets of genes involved in different types of morphological alternations in two species, although they are homologous and bind to the same DNA motif (Cain et al., 2012; Lohse et al., 2010).

Transcriptional co-regulation

Transcriptional co-regulation of the same kind of genes typically indicates that these genes are correlated with respect to their biological functions. For example, a same set of effector genes is co-regulated at the biotrophic stage to promote the establishment and maintenance of biotrophic invasion. Transcriptional co-regulation of different kinds of genes indicates that genes are associated with biological processes. For example, the co-regulation of transcription factors and effector genes during infection may suggest that the transcription factors positively regulate expression of these effector genes. This hypothesis gives us another strategy to identify transcription factors that regulate effector gene expression. Zheng et al. (2008) first successfully used this strategy to identify a TF Mzr1 regulating effector gene expression in *U. maydis*. Mzr1 showed the highest expression during biotrophic growth, which was consistent to the *Mig2* effector genes. Subsequent *Mzr1* knockout mutant showed undetectable GFP signals of *Mig2-5* transcriptional fusion, but the ectopic expression of *Mzr1* restored *Mig2-5* prompter activity. Overexpression of *Mzr1* strongly activated *Mig2-5* prompter activity during filamentous growth in axenic culture. Additionally, Mzr1 was unable to activate the activity of the *Mig2-5* promoter that contained substitutions of previously identified *cis*-regulatory element, suggesting Mzr1 directly regulates *mig2-5* promoter activity using the same *cis*-regulatory element during plant infection. Interestingly, however, Mzr1 only regulated expression of *mig2-4, mig2-5* and *mig2-6* but not *mig2-1*, *mig2-2*, *mig2-3*, even though they were in the same gene cluster. This is possibly because promoters of individual genes in this cluster have lost the ability of to be activated by Mzr1 during long time coevolution of effector-R interaction. Surprisingly, *Mzr1* deletion was not critical for fungal virulence, possibly due to the loss of function of effectors to avoid being recognized by plant R protein through a selective sweep.

Although Mzr1 is unable to control disease development, transcriptional co-regulation of TFs and effector genes typically indicates that TFs may play a regulatory function during pathogenic development. For instance, *P. nodorum* PnPf2 has been demonstrated recently to control pathogenic development by regulating effector gene expression (Rybak et al., 2017). The expression profile of *PnPf2* and necrotrophic effector (NEs) *SnTox3* showed a co-regulated pattern during both axenic culture and wheat infection but only during wheat infection for *SnToxA* effector. The deletion of *PnPf2* strongly reduced pathogen virulence and expression of *SnToxA* and *SnTox3*, but only biochemical complementation of effector proteins *SnToxA* and *SnTox3* restored virulent activity of *PnPf2* deletion mutant. These results suggest that PnPf2 is a transcriptional regulator of *SnToxA* and *SnTox3*, which leads to control disease development. Similarly, the forkhead transcription factor Fox1 in *U. maydis* was exclusively and highly expressed during biotrophic invasion (Zahiri et al., 2010). *Fox1* deletion significantly reduced expression of several effector genes, which subsequently resulted in impaired pathogenic development.

The wave expression pattern of effector genes suggests that different sets of effector genes are co-regulated by transcription factor(s) at each stage. Taking advantage of RNA-seq technology, the consecutive waves of effector gene expression during infection process can be uncovered, which allows us to determine all co-regulated effector genes and transcription factors in each wave. Consequently, we will get a global overview of regulatory networks for effector gene expression. Recently, the biotrophic development of *U. maydis* has been investigated by RNA-seq analysis. The putative transcriptional regulators of each effector wave were identified through the strongest connectivity in a weighted co-expression network of all differentially expressed effector genes and transcriptional factor genes (Lanver et al., 2018). Therefore, the

large-scale transcriptome analysis provides a comprehensive temporal view of gene expression during fungal invasion process. This analysis not only allows us to visualize the utilization of certain effectors but also associated transcription factors that involve effector gene regulation at each colonization stage.

Epigenetic regulation

Filamentous fungi are multicellular organisms. All cells are genetically homogeneous but show structurally and functionally heterogeneity at different development stages because of the differential expression of genes. Expression of effector genes are typically repressed under *in vitro* conditions, such as in mycelia and conidia, but highly induced during plant infection, such as in appressoria and invasive hyphae. Therefore, the stably altered and heritably maintained effector gene expression in the same organism before and after plant infection indicates that expression of effector genes is under control of epigenetic regulation. Soyer et al. (2014) first demonstrated that epigenetic control tightly repressed *L. maculans* effector gene expression during mycelia growth in axenic culture. The silencing of *heterochromatin protein 1* (*HP1*) and histone methyltransferase *DIM-5* (H3K9me3) resulted in the upregulation of many effector genes during mycelia growth which is a non-inducible condition in wild-type strain. Additionally, induced expression of effector genes (*AvrLm1* and *AvrLm4-7*) during mycelia growth was correlated with the reduced H3K9me3 in *HP1* and *DIM5* silenced strains. This suggests that an epigenetic reprogramming before and after plant infection regulates expression of fungal effector genes. However, interestingly, silenced transformants had no affect for effector gene expression during plant infection. These results lead to a two-layer regulatory hypothesis that expression of the effector gene undergoes chromatin-mediated repression *in vitro* and the lifestyle switch from vegetative to pathogenic growth lifts the repression in order to activate effector gene expression

(Soyer et al., 2015). Currently, the epigenetic reprogramming at effector gene loci after plant infection has not been demonstrated, and the percentage of effector genes undergoing epigenetic regulation has yet to be elucidated.

Similarly, fungal SM gene clusters were also found to be regulated by histone modifications. For instance, the deletion of histone methyltransferase *KMT6* (H3K27me3) depressed expression of genes predominantly involved in secondary metabolite pathways in *F. graminearum* (Connolly et al., 2013a). The endophyte *Epichloe festucae* only synthesizes secondary metabolites lolitrems (ltm) and ergot alkaloids (eas) *in planta*. It has been found that H3K9me3 and H3K27me3 levels were reduced in alkaloid gene loci *in planta* compared to axenic culture through ChIP-qPCR (Chujo and Scott, 2014b). This leads to the hypothesis that induced SM genes *ltm* and *eas* in *planta* result from the reduced the H3K9me3 and H3K27me3 levels. Indeed, deletion of H3K9 and H3K27-methyltransferases derepressed expression of *ltm* and *eas* genes in axenic culture, which was correlated with the corresponding reduction of H3K9m3 and H3K27me3 levels at these loci in the deletion mutant (Chujo and Scott, 2014b). Since both SM and effector genes are mainly suppressed *in vitro* but induced *in planta* and are associated with transposable elements (TE)-rich regions of the genome, it is possible that the global epigenetic reprogramming at effector gene loci after plant infection remodels the chromatin structure (histone modifications) to allow for the accessibility of transcription factor(s); this leads to a massively concerted expression of effector genes (Soyer et al., 2015).

Thus far, only HP1 and H3K9me3 have been determined to control effector gene expression (Soyer et al., 2014b). Absence of H3K27me3 in *F. graminearum* allowed expression of putative secreted pathogenicity factors, indicating that H3K27me3 also controls effector gene expression (Connolly et al., 2013a). H3K27 methylation shows high enrichment in subtelomeric

regions in all chromosomes of *N. crassa*, *F. graminearum* and *C. neoformans* (Lewis, 2017a). The subtelomeric regions typically contain many TE-rich regions that are co-localized with many putative and known effector genes in *M. oryzae* and *P. infestans* (Farman, 2007; Haas et al., 2009). This further suggests that effector gene expression is under control of the H3K27me3. Notably, the extensive colocalization of H3K27me3 and H3K36me3 was observed in *F. graminearum* and the removal of H3K36 methylation in *N. crassa* did not redistribute H3K27 methylation, suggesting there is certain crosstalk between different histone modifications (Lewis, 2017a). Nevertheless, whether the H3K36me3 and its crosstalk with H3K27me3 are involved in effector gene regulation has yet to be confirmed.

Coordinate control of transcriptional and epigenetic regulations

Studies have revealed that the transcriptional and epigenetics control play a significant role in effector gene expression. How do epigenetic and transcriptional regulations coordinately control effector gene expression during fungal development? As mentioned previously, a two-layer regulatory hypothesis has been proposed that expression of effector genes is repressed via chromatin-mediated control *in vitro.* Furthermore, open chromatin allows for the accessibility of transcription factor(s) to activate expression of effector genes during plant infection (Fig. 1.1A) (Soyer et al., 2015). However, this model cannot explain some observations in effector gene expression. For instance, in *P. nodorum*, the expression of *PnPf2* and *SnToxA* only co-regulated during wheat infection, although *PnPf2* expression was also highly induced during axenic culture (Rybak et al., 2017). Similarly, the expression of *MoGti1* was highly induced before penetration but *BAS4* expression was not until after penetration in *M. oryzae* (Chapter 2). This suggests that other possible mechanisms might exist to collectively govern effector gene expression in a right

spatial and temporal manner. Based on the current observations, there are two other hypothetical models to elucidate the coordinated regulation of effector gene expression.

Chromatin modifying proteins histone acetytranferases (HATs) and histone deacetylases (HDACs) can not only modify histone proteins, but also non-histone proteins such as transcription factors. Therefore, HATs or HDACs post-translationally modifying TFs might change their binding or specificity to allow or inhibit TFs activating effector gene expression (Fig. 1.1D) (Trivedi et al., 2010). If this is true, it might explain why highly induced *PnPf2 in vitro* was unable to upregulate effector gene expression. One possibility is that additional modification of a TF is required to initiate transcription of effector genes. Another possibility is that extra modification of a TF prevents its activation.

Overexpression of *CfWor1* induces expression of some effector genes in the axenic culture of *C. fulvum* (Okmen et al., 2014a). This was also observed for *MoGti1* in *M. oyrzae*, for which overexpression significantly upregulated expression of some effector genes in mycelia (Chapter 2). If epigenetics represses expression of effector genes *in vitro*, how is a TF able to access the open chromatin to activate their expression? Interestingly, chromatin modifiers can be recruited to specific loci by a TF to steer the transcription of downstream genes (Yang et al., 2014b). This suggests that overexpression of a TF might recruit chromatin modifiers to increase the chromatin accessibility, leading to the continuation of effector gene transcriptions (Fig. 1.1E).

Two other hypothetical models are also possible, although there is no evidence to support them currently. The transcription activators that regulate effector gene expression are kept in a repressed state by epigenetic chromatin marks prior to infection; and the signal triggers the derepression of TFs to allow them to upregulate expression of the corresponding effector genes

(Fig. 1.1B). However, it might also be possible that TFs are expressed but the epigenetic regulation prevents them from binding the *cis*-regulatory elements of effector genes. The release of epigenetic repression provides an accessible chromatin state to upregulate expression of effector genes (Fig. 1.1C). While most studies have uncovered the roles of transcription regulation, the understanding of epigenetics and integration of the two mechanisms is only just beginning. Considering the significant roles effectors play in plant-pathogen interaction, it will be necessary to study the coordinated regulation of transcription and epigenetics in controlling effector gene expression, although it is challenging and complex.

Conclusions and Future directions

The study of effector biology has made the use of effectors a possible tool to improve plant resistance against various plant pathogens through breeding (Vleeshouwers and Oliver, 2014). A better understanding of effector regulation in fungal pathogens will provide us with another potentially great strategy to inhibit fungal diseases. For instance, signals triggering the switch of effector gene expression from repression to activation remain largely unknown, although some physical and chemical signals have the ability to affect effector gene expression (Meyer et al., 2017). Therefore, identification of signals regulating effector gene expression will give us novel insights to block fungal disease. Considering the fitness benefits of effector gene expression, they must antagonize stresses from the infected plant, such as oxidative stress and enzyme digestion. Thus, it might be possible that signals regulating effector gene expression are the same signals that cause a stress response in fungi.

As the sequencing technology becomes more economical and convenient, ChIP-seq will be a good way to study a transcriptional activator genome-wide because we can investigate both its DNA-binding motif and potential targets. With the help of promoter deletion or mutation

analyses, we will easily determine the exact *cis*-element and downstream target. Since expression of effector genes show a stage specific pattern and different sets of effector genes express at different infection stages, there must be multiple transcriptional activators functioning at various stages (Lanver et al., 2018). RNA-seq coupled with ChIP-seq will allow us to construct a global regulatory network of the effector gene expression. The implementation of these combined approaches will not only help us to understand the regulatory mechanism of effector gene expression, but will also reveal mechanisms through which filamentous fungi undergo stress responses during plant infection.

UNDERSTANDING OF FINGER MILLET INFECTION BY THE BLAST FUNGUS

M. oryzae is a causal agent of the economically important blast disease on many crop plants including rice, wheat, finger millet and barley etc. (Ceresini et al., 2019; Dean et al., 2005; Gladieux et al., 2018; Kamoun et al., 2019; Takan et al., 2012). For instance, rice blast disease causes 10-30% losses of overall global rice yield every year, and the loss is estimated to feed 60 million people (Dean et al., 2005; Wilson and Talbot, 2009). In addition to the heavy loss on rice, blast disease has threatened other important staple crops such as wheat and finger millet. Wheat blast was first found in Brazil in 1985 and now is well established in South America (Ceresini et al., 2019). In 2016, wheat blast appeared in Bangladesh and caused a sudden outbreak with yield loss up to 100% (Inoue et al., 2017; Kamoun et al., 2019). Finger millet (*Eleusine coracana*) is a staple food for people in the semi-arid tropics of East Africa, but its production is mainly constrained by blast disease (Takan, 2004). Thus, blast disease continues to pose a global threat of food supplies despite effort to control this disease in these decades. Much effort has been focused on controlling rice blast disease, whereas knowledge of blast infection on other important crop plants (e.g. finger millet) remains limited.

M. oryzae infects and causes disease on a wide range of host plants (Talbot, 2003), but individual isolates typically have narrow host range (Choi et al., 2013; Kang et al., 1995) and are categorized into several pathotypes that are pathogenic to specific hosts including *Oryza* spp. (rice), *Triticum* spp. (wheat), *Eleusine* spp. (finger millet) etc. (Couch et al., 2005; Murakami et al., 2000; Yoshida et al., 2016). Host specificity has two types: host cultivar specificity and host species specificity (Murakami et al., 2003; Sweigard et al., 1995b). Host cultivar specificity depends on plant cultivars that a pathogen can infect (Murakami et al., 2003). Host cultivar specificity of *M. oryzae Oryza* (MoO) pathotype has been well studied, and the cultivar resistance involved is controlled by gene-for-gene interactions (Murakami et al., 2003; Murakami et al., 2000; Sweigard et al., 1995b). Host species specificity depends on whether or not a plant species is a host for a pathogen (Murakami et al., 2003). Knowledge of host species specificity still remains poorly understood, although some progress has been made recently. For example, AVR genes *PWL2* and *PWT3* in *M. oryzae* have been revealed to be determinants of host species specificity toward weeping lovegrass and wheat, respectively (Inoue et al., 2017; Kang et al., 1995; Sweigard et al., 1995b). Apparently, understandings of the host specificity of blast fungus on different hosts will provide us new perspective to control blast disease. However, less information is available on the finger millet crops that are resistant to blast compared to other crops such as rice.

M. oryzae infection on rice is well studied but not on other host specific plants. On the rice leaf surface, a conidium of blast fungus develops a melanized cell called an appressorium, which has high turgor pressure, to directly penetrate a rice epidermal cell (de Jong et al., 1997). Then the fungus produces invasive hyphae (IH) to proliferate in the first-invaded rice cell and moves into adjacent cells (Kankanala et al., 2007). Cytological studies have revealed that rice

blast fungus is a hemibiotrophic pathogen (Kankanala et al., 2007). Each newly invaded rice cell during initial invasion remains alive but loses viability when the IH spread into neighbor cells (Jones et al., 2017; Kankanala et al., 2007). During initial biotrophic invasion, fungal IH are sealed in the extra-invasive hyphal membrane (EIHM) (Kankanala et al., 2007). As IH continue to grow in the first-invaded rice cell, EIHM is disrupted and subsequently rice vacuole rupture and death of the invaded rice cell (Jones et al., 2017). To manipulate plant cell structure/function and suppress plant immune response, *M. oryzae* secretes and delivers effector proteins using a specialized structure - biotrophic interfacial complex (BIC) - to cross EIHM into plant cytoplasm (Khang et al., 2010a). Live-cell imaging studies reveal that BIC is a spatially and temporally dynamic structure. BIC is firstly observed at the tip of the initially filamentous hyphae and then left behind beside the first-differentiated bulbous IH cell as the fungal hyphae continue to grow (Khang et al., 2010a). Disease lesions typically become visible between 72 - 96 hours after inoculation with conidial suspension on rice seedings, and sporulation occurs under humid conditions (Wilson and Talbot, 2009).

Blast disease on finger millet is destructive and results in more than 50 % reduction of the yield when the panicle is infected, thereby becoming a key factor constraining finger millet production in the East African region (Shittu, 2018). Nevertheless, the current understanding of *M. oryzae* infection on finger millet is limited. Host specificity of *M. oryzae* isolates from finger millet toward different host plants have been reported (Chiapello et al., 2015; Gladieux et al., 2018; Kang et al., 1995; Takan et al., 2012), but the mechanism of such host specificity is unknown. Moreover, we barely know if the infection of host-adapted blast fungi on other plants (e.g. finger millet) cytologically resembles rice. Currently, the finger millet disease is mainly managed by cultural practices (e.g. crop rotation) and chemical control, but less information on

the finger millet resistance to blast is available compared to other crops such as rice (Shittu, 2018). Lack of knowledge of the blast pathogen infection on finger millet has hindered efforts to develop strategies to manage blast disease. Therefore, understanding of the blast fungus infection and host species specificity on finger millet will provide us insights to better control blast disease on finger millet and other host plants.

References

Basse, C.W., Kolb, S., and Kahmann, R. (2002). A maize-specifically expressed gene cluster in *Ustilago maydis*. Molecular Microbiology *43*, 75-93.

Basse, C.W., Stumpferl, S., and Kahmann, R. (2000). Characterization of a *Ustilago maydis* gene specifically induced during the biotrophic phase: evidence for negative as well as positive regulation. Molecular and Cellular Biology *20*, 329-339.

Brown, D.W., Busman, M., and Proctor, R.H. (2014). *Fusarium verticillioides* SGE1 is required for full virulence and regulates expression of protein effector and secondary metabolite biosynthetic genes. Mol Plant Microbe Interact *27*, 809-823.

Cain, C.W., Lohse, M.B., Homann, O.R., Sil, A., and Johnson, A.D. (2012). A conserved transcriptional regulator governs fungal morphology in widely diverged species. Genetics *190*, 511-521.

Ceresini, P.C., Castroagudín, V.L., Rodrigues, F.Á., Rios, J.A., Aucique-Pérez, C.E., Moreira, S.I., Croll, D., Alves, E., de Carvalho, G., and Maciel, J.L.N. (2019). Wheat blast: from its origins in South America to its emergence as a global threat. Molecular plant pathology *20*, 155-172.

Chiapello, H., Mallet, L., Guerin, C., Aguileta, G., Amselem, J., Kroj, T., Ortega-Abboud, E., Lebrun, M.-H., Henrissat, B., and Gendrault, A. (2015). Deciphering genome content and evolutionary relationships of isolates from the fungus *Magnaporthe oryzae* attacking different host plants. Genome biology and evolution *7*, 2896-2912.

Choi, J., Park, S.-Y., Kim, B.-R., Roh, J.-H., Oh, I.-S., Han, S.-S., and Lee, Y.-H. (2013). Comparative analysis of pathogenicity and phylogenetic relationship in *Magnaporthe grisea* species complex. PloS one *8*.

Chujo, T., and Scott, B. (2014). Histone H3K9 and H3K27 methylation regulates fungal alkaloid biosynthesis in a fungal endophyte-plant symbiosis. Mol Microbiol *92*, 413-434.

Connolly, L.R., Smith, K.M., and Freitag, M. (2013). The *Fusarium graminearum* histone H3 K27 methyltransferase KMT6 regulates development and expression of secondary metabolite gene clusters. PLoS Genet *9*, e1003916.

Couch, B.C., Fudal, I., Lebrun, M.-H., Tharreau, D., Valent, B., Van Kim, P., Nottéghem, J.-L., and Kohn, L.M. (2005). Origins of host-specific populations of the blast pathogen *Magnaporthe oryzae* in crop domestication with subsequent expansion of pandemic clones on rice and weeds of rice. Genetics *170*, 613-630.

de Jong, J.C., McCormack, B.J., Smirnoff, N., and Talbot, N.J. (1997). Glycerol generates turgor in rice blast. Nature *389*, 244.

Dean, R.A., Talbot, N.J., Ebbole, D.J., Farman, M.L., Mitchell, T.K., Orbach, M.J., Thon, M., Kulkarni, R., Xu, J.-R., and Pan, H. (2005). The genome sequence of the rice blast fungus *Magnaporthe grisea*. Nature *434*, 980.

Dong, Y., Li, Y., Zhao, M., Jing, M., Liu, X., Liu, M., Guo, X., Zhang, X., Chen, Y., Liu, Y., *et al.* (2015). Global genome and transcriptome analyses of *Magnaporthe oryzae* epidemic isolate 98-06 uncover novel effectors and pathogenicity-related genes, revealing gene gain and lose dynamics in genome evolution. PLoS Pathogen *11*, e1004801.

Farfsing, J.W., Auffarth, K., and Basse, C.W. (2005). Identification of cis-active elements in *Ustilago maydis mig2* promoters conferring high-level activity during pathogenic growth in maize. Molecular Plant-Microbe Interactions *18*, 75-87.

Farman, M.L. (2007). Telomeres in the rice blast fungus *Magnaporthe oryzae*: the world of the end as we know it. FEMS Microbiology Letters *273*, 125-132.

Gervais, J., Plissonneau, C., Linglin, J., Meyer, M., Labadie, K., Cruaud, C., Fudal, I., Rouxel, T., and Balesdent, M.H. (2017). Different waves of effector genes with contrasted genomic location are expressed by *Leptosphaeria maculans* during cotyledon and stem colonization of oilseed rape. Molecular Plant Pathology *18*, 1113-1126.

Gladieux, P., Condon, B., Ravel, S., Soanes, D., Maciel, J.L.N., Nhani, A., Chen, L., Terauchi, R., Lebrun, M.-H., and Tharreau, D. (2018). Gene flow between divergent cereal-and grass-specific lineages of the rice blast fungus *Magnaporthe oryzae*. MBio *9*, e01219-01217.

Haas, B.J., Kamoun, S., Zody, M.C., Jiang, R.H., Handsaker, R.E., Cano, L.M., Grabherr, M., Kodira, C.D., Raffaele, S., Torto-Alalibo, T., *et al.* (2009). Genome sequence and analysis of the Irish potato famine pathogen *Phytophthora infestans*. Nature *461*, 393-398.

Hacquard, S., Kracher, B., Maekawa, T., Vernaldi, S., Schulze-Lefert, P., and Ver Loren van Themaat, E. (2013). Mosaic genome structure of the barley powdery mildew pathogen and conservation of transcriptional programs in divergent hosts. Proceedings of the National Academy of Sciences *110*, E2219-2228.

Heimel, K., Scherer, M., Vranes, M., Wahl, R., Pothiratana, C., Schuler, D., Vincon, V., Finkernagel, F., Flor-Parra, I., and Kamper, J. (2010). The transcription factor Rbf1 is the

master regulator for b-mating type controlled pathogenic development in *Ustilago maydis*. PLoS Pathog *6*, e1001035.

Huang, G., Wang, H., Chou, S., Nie, X., Chen, J., and Liu, H. (2006). Bistable expression of WOR1, a master regulator of white–opaque switching in *Candida albicans*. Proceedings of the National Academy of Sciences *103*, 12813-12818.

Inoue, Y., Vy, T.T., Yoshida, K., Asano, H., Mitsuoka, C., Asuke, S., Anh, V.L., Cumagun, C.J., Chuma, I., and Terauchi, R. (2017). Evolution of the wheat blast fungus through functional losses in a host specificity determinant. Science *357*, 80-83.

IpCho, S.V., Tan, K.C., Koh, G., Gummer, J., Oliver, R.P., Trengove, R.D., and Solomon, P.S. (2010). The transcription factor StuA regulates central carbon metabolism, mycotoxin production, and effector gene expression in the wheat pathogen *Stagonospora nodorum*. Eukaryot Cell *9*, 1100-1108.

Jones, K., Zhu, J., Jenkinson, C.B., Kim, D.W., and Khang, C.H. (2017). Disruption of the interfacial membrane leads to *Magnaporthe oryzae* effector re-location and lifestyle switch during rice blast disease. bioRxiv, 177147.

Kamoun, S., Talbot, N.J., and Islam, M.T. (2019). Plant health emergencies demand open science: Tackling a cereal killer on the run. PLoS Biology *17*, e3000302.

Kang, S., Sweigard, J.A., and Valent, B. (1995). The PWL host specificity gene family in the blast fungus *Magnaporthe grisea*. MPMI-Molecular Plant Microbe Interactions *8*, 939-948.

Kankanala, P., Czymmek, K., and Valent, B. (2007). Roles for rice membrane dynamics and plasmodesmata during biotrophic invasion by the blast fungus. Plant Cell *19*, 706-724.

Kellner, R., Bhattacharyya, A., Poppe, S., Hsu, T.Y., Brem, R.B., and Stukenbrock, E.H. (2014). Expression profiling of the wheat pathogen *Zymoseptoria tritici* reveals genomic patterns of transcription and host-specific regulatory programs. Genome biology and evolution *6*, 1353-1365.

Khang, C.H., Berruyer, R., Giraldo, M.C., Kankanala, P., Park, S.-Y., Czymmek, K., Kang, S., and Valent, B. (2010). Translocation of *Magnaporthe oryzae* effectors into rice cells and their subsequent cell-to-cell movement. The Plant Cell *22*, 1388-1403.

Kleemann, J., Rincon-Rivera, L.J., Takahara, H., Neumann, U., Ver Loren van Themaat, E., van der Does, H.C., Hacquard, S., Stuber, K., Will, I., Schmalenbach, W., *et al.* (2012). Sequential delivery of host-induced virulence effectors by appressoria and intracellular hyphae of the phytopathogen *Colletotrichum higginsianum*. PLoS Pathogen *8*, e1002643.

Lanver, D., Berndt, P., Tollot, M., Naik, V., Vranes, M., Warmann, T., Munch, K., Rossel, N., and Kahmann, R. (2014). Plant surface cues prime *Ustilago maydis* for biotrophic development. PLoS Pathog *10*, e1004272.

Lanver, D., Muller, A.N., Happel, P., Schweizer, G., Haas, F.B., Franitza, M., Pellegrin, C., Reissmann, S., Altmuller, J., Rensing, S.A., *et al.* (2018). The Biotrophic Development of *Ustilago maydis* Studied by RNA-Seq Analysis. Plant Cell *30*, 300-323.

Lemmens, M., Schuhmacher, R., Guldener, U., *et al.* (2016). Comparison of *Fusarium graminearum* transcriptomes on living or dead wheat differentiates substrate-responsive and defense-responsive genes. Frontiers in Microbiology *7*, 1113.

Lewis, Z.A. (2017). Polycomb Group Systems in Fungi: New Models for Understanding Polycomb Repressive Complex 2. Trends Genet *33*, 220-231.

Li, Y., Wang, G., Xu, J.R., and Jiang, C. (2016). Penetration peg formation and invasive hyphae development require stage-specific activation of MoGti1 in *Magnaporthe oryzae*. Mol Plant Microbe Interact *29*, 36-45.

Lin, S.Y., Chooi, Y.H., and Solomon, P.S. (2018). The global regulator of pathogenesis PnCon7 positively regulates *Tox3* effector gene expression through direct interaction in the wheat pathogen *Parastagonospora nodorum*. Molecular microbiology *109*, 78-90.

Lo Presti, L., Lanver, D., Schweizer, G., Tanaka, S., Liang, L., Tollot, M., Zuccaro, A., Reissmann, S., and Kahmann, R. (2015). Fungal effectors and plant susceptibility. Annu Rev Plant Biol *66*, 513-545.

Lohse, M.B., Zordan, R.E., Cain, C.W., and Johnson, A.D. (2010). Distinct class of DNA-binding domains is exemplified by a master regulator of phenotypic switching in Candida albicans. Proceedings of the National Academy of Sciences *107*, 14105-14110.

Meyer, M., Bourras, S., Gervais, J., Labadie, K., Cruaud, C., Balesdent, M.H., and Rouxel, T. (2017). Impact of biotic and abiotic factors on the expression of fungal effector-encoding genes in axenic growth conditions. Fungal Genet Biol *99*, 1-12.

Michielse, C.B., van Wijk, R., Reijnen, L., Manders, E.M., Boas, S., Olivain, C., Alabouvette, C., and Rep, M. (2009). The nuclear protein Sge1 of *Fusarium oxysporum* is required for parasitic growth. PLoS Pathog *5*, e1000637.

Mirzadi Gohari, A., Mehrabi, R., Robert, O., Ince, I.A., Boeren, S., Schuster, M., Steinberg, G., de Wit, P.J., and Kema, G.H. (2014). Molecular characterization and functional analyses of ZtWor1, a transcriptional regulator of the fungal wheat pathogen *Zymoseptoria tritici*. Mol Plant Pathol *15*, 394-405.

Murakami, J., Tomita, R., Kataoka, T., Nakayashiki, H., Tosa, Y., and Mayama, S. (2003). Analysis of host species specificity of *Magnaporthe grisea* toward foxtail millet using a genetic cross between isolates from wheat and foxtail millet. Phytopathology *93*, 42-45.

Murakami, J., Tosa, Y., Kataoka, T., Tomita, R., Kawasaki, J., Chuma, I., Sesumi, Y., Kusaba, M., Nakayashiki, H., and Mayama, S. (2000). Analysis of host species specificity of *Magnaporthe grisea* toward wheat using a genetic cross between isolates from wheat and foxtail millet. Phytopathology *90*, 1060-1067.

O'Connell, R.J., Thon, M.R., Hacquard, S., Amyotte, S.G., Kleemann, J., Torres, M.F., Damm, U., Buiate, E.A., Epstein, L., Alkan, N., *et al.* (2012). Lifestyle transitions in plant pathogenic *Colletotrichum* fungi deciphered by genome and transcriptome analyses. Nat Genet *44*, 1060-1065.

Okmen, B., Collemare, J., Griffiths, S., van der Burgt, A., Cox, R., and de Wit, P.J. (2014). Functional analysis of the conserved transcriptional regulator CfWor1 in *Cladosporium fulvum* reveals diverse roles in the virulence of plant pathogenic fungi. Mol Microbiol *92*, 10-27.

Plett, J.M., Kemppainen, M., Kale, S.D., Kohler, A., Legué, V., Brun, A., Tyler, B.M., Pardo, A.G., and Martin, F. (2011). A secreted effector protein of *Laccaria bicolor* is required for symbiosis development. Current Biology *21*, 1197-1203.

Rybak, K., See, P.T., Phan, H.T., Syme, R.A., Moffat, C.S., Oliver, R.P., and Tan, K.C. (2017). A functionally conserved Zn2 Cys6 binuclear cluster transcription factor class regulates necrotrophic effector gene expression and host-specific virulence of two major Pleosporales fungal pathogens of wheat. Mol Plant Pathol *18*, 420-434.

Sanchez-Vallet, A., Fouche, S., Fudal, I., Hartmann, F.E., Soyer, J.L., Tellier, A., and Croll, D. (2018). The Genome Biology of Effector Gene Evolution in Filamentous Plant Pathogens. Annu Rev Phytopathol.

Santhanam, P., and Thomma, B.P. (2013). *Verticillium dahliae* Sge1 differentially regulates expression of candidate effector genes. Molecular plant-microbe interactions *26*, 249-256.

Schmidt, S.M., Houterman, P.M., Schreiver, I., Ma, L., Amyotte, S., Chellappan, B., Boeren, S., Takken, F.L., and Rep, M. (2013). MITEs in the promoters of effector genes allow prediction of novel virulence genes in *Fusarium oxysporum*. BMC genomics *14*, 119.

Shittu, T.A. (2018). Population analysis of the finger millet blast pathogen *Magnaporthe oryzae* in Eastern Africa.

Soyer, J.L., El Ghalid, M., Glaser, N., Ollivier, B., Linglin, J., Grandaubert, J., Balesdent, M.H., Connolly, L.R., Freitag, M., Rouxel, T., *et al.* (2014). Epigenetic control of effector gene expression in the plant pathogenic fungus *Leptosphaeria maculans*. PLoS Genet *10*, e1004227.

Soyer, J.L., Rouxel, T., and Fudal, I. (2015). Chromatin-based control of effector gene expression in plant-associated fungi. Curr Opin Plant Biol *26*, 51-56.

Sweigard, J.A., Carroll, A.M., Kang, S., Farrall, L., Chumley, F.G., and Valent, B. (1995). Identification, cloning, and characterization of *PWL2*, a gene for host species specificity in the rice blast fungus. The plant cell *7*, 1221-1233.

Takan, J. (2004). Finger millet blast pathogen diversity and management in East Africa: A summary of project activities and outputs. International sorghum and millets newsletter *45*, 66-69.

Takan, J., Chipili, J., Muthumeenakshi, S., Talbot, N., Manyasa, E., Bandyopadhyay, R., Sere, Y., Nutsugah, S., Talhinhas, P., and Hossain, M. (2012). *Magnaporthe oryzae* populations adapted to finger millet and rice exhibit distinctive patterns of genetic diversity, sexuality and host interaction. Molecular biotechnology *50*, 145-158.

Talbot, N.J. (2003). On the trail of a cereal killer: exploring the biology of *Magnaporthe grisea*. Annual Reviews in Microbiology *57*, 177-202.

Tan, K.C., and Oliver, R.P. (2017). Regulation of proteinaceous effector expression in phytopathogenic fungi. PLoS Pathog *13*, e1006241.

Tollot, M., Assmann, D., Becker, C., Altmuller, J., Dutheil, J.Y., Wegner, C.E., and Kahmann, R. (2016). The WOPR protein Ros1 Is a master regulator of sporogenesis and late effector gene expression in the maize pathogen *Ustilago maydis*. PLoS Pathogen *12*, e1005697.

Trivedi, C.M., Zhu, W., Wang, Q., Jia, C., Kee, H.J., Li, L., Hannenhalli, S., and Epstein, J.A. (2010). Hopx and Hdac2 interact to modulate Gata4 acetylation and embryonic cardiac myocyte proliferation. Dev Cell *19*, 450-459.

Tsuge, T., Harimoto, Y., Akimitsu, K., Ohtani, K., Kodama, M., Akagi, Y., Egusa, M., Yamamoto, M., and Otani, H. (2013). Host-selective toxins produced by the plant pathogenic fungus *Alternaria alternata*. FEMS Microbiol Rev *37*, 44-66.

Van den Ackerveken, G., Dunn, R., Cozijnsen, A., Vossen, J., Van den Broek, H., and De Wit, P. (1994). Nitrogen limitation induces expression of the avirulence gene *avr9* in the tomato pathogen *Cladosporium fulvum*. Molecular and General Genetics MGG *243*, 277-285.

van der Does, H.C., Duyvesteijn, R.G., Goltstein, P.M., van Schie, C.C., Manders, E.M., Cornelissen, B.J., and Rep, M. (2008). Expression of effector gene *SIX1* of *Fusarium oxysporum* requires living plant cells. Fungal Genetics and Biology *45*, 1257-1264.

Vleeshouwers, V.G., and Oliver, R.P. (2014). Effectors as tools in disease resistance breeding against biotrophic, hemibiotrophic, and necrotrophic plant pathogens. Molecular plant-microbe interactions *27*, 196-206.

Wang, Q., Han, C., Ferreira, A.O., Yu, X., Ye, W., Tripathy, S., Kale, S.D., Gu, B., Sheng, Y., Sui, Y., *et al.* (2011). Transcriptional programming and functional interactions within the *Phytophthora sojae* RXLR effector repertoire. Plant Cell *23*, 2064-2086.

Weake, V.M., and Workman, J.L. (2010). Inducible gene expression: diverse regulatory mechanisms. Nat Rev Genet *11*, 426-437.

Wilson, R.A., and Talbot, N.J. (2009). Under pressure: investigating the biology of plant infection by *Magnaporthe oryzae*. Nature Reviews Microbiology *7*, 185-195.

Yang, Y., Cheng, X., Tian, W., Zhou, B., Wu, X., Xu, H., Fang, F., Fang, M., and Xu, Y. (2014). MRTF-A steers an epigenetic complex to activate endothelin-induced pro-inflammatory transcription in vascular smooth muscle cells. Nucleic Acids Res *42*, 10460-10472.

Yoshida, K., Saunders, D.G., Mitsuoka, C., Natsume, S., Kosugi, S., Saitoh, H., Inoue, Y., Chuma, I., Tosa, Y., and Cano, L.M. (2016). Host specialization of the blast fungus *Magnaporthe oryzae* is associated with dynamic gain and loss of genes linked to transposable elements. BMC genomics *17*, 370.

Zahiri, A., Heimel, K., Wahl, R., Rath, M., and Kämper, J. (2010). The *Ustilago maydis* forkhead transcription factor Fox1 is involved in the regulation of genes required for the

attenuation of plant defenses during pathogenic development. Molecular plant-microbe interactions *23*, 1118-1129.

Zhao, Y., Su, H., Zhou, J., Feng, H., Zhang, K.Q., and Yang, J. (2015). The APSES family proteins in fungi: characterizations, evolution and functions. Fungal Genet Biol *81*, 271-280.

Zheng, Y., Kief, J., Auffarth, K., Farfsing, J.W., Mahlert, M., Nieto, F., and Basse, C.W. (2008). The *Ustilago maydis* Cys2His2-type zinc finger transcription factor Mzr1 regulates fungal gene expression during the biotrophic growth stage. Mol Microbiol *68*, 1450-1470.

Zordan, R.E., Miller, M.G., Galgoczy, D.J., Tuch, B.B., and Johnson, A.D. (2007). Interlocking transcriptional feedback loops control white-opaque switching in *Candida albicans*. PLoS Biol *5*, e256.

Table

Table 1.1 Summary for characterization of Wor1 proteins in various fungal pathogens

Fungus*	***F. oxysporum* KO**	***V. dahliae* KO**	***F. verticillioides* KO**	***C. fulvum* KO**	***C. fulvum* O/E**	***Z. tritici* KO**	***M. oryzae* KO**	***U. maydis* KO**
Gene name	*Sge1*	*Sge1*	*Sge1*	*CfWor1*	*CfWor1*	*ZtWor1*	*MoGti1*	*Ros1*
Virulence	Reduced	Reduced	Reduced	No	Reduced	Reduced	Reduced	Reduced
Reduced conidiation	Yes	Yes	No	Yes	Yes	Yes	Yes	Reduced teliospore
Abnormal hyphal growth	No	Yes	No	Yes	No	Yes	No	No
Altered conidia germination rate	No	No	–	–	–	No	Delayed	–
Expression profile	Highly induced during infection with maximal expression eight days after inoculation.	–	*Sge1* is expressed under multiple growth conditions.	*CfWor1* expression is five times higher in vitro than during infection of tomato.	*CfWor1* expression is five times higher in vitro than during infection of tomato.	It highly expresses in mycelia, lower expression in spores and induced at early and late infection stages.	Highly induced during plant infection, even before penetration.	*Ros1* is highly induced at late infection stage and shows a very low expression *in vitro*.
Effector expression	positively regulate *Six1/2/3/5*	required for the expression of six putative effector genes and two of them are negatively regulated.	Tend to positively regulate effector gene expression	Expression of *Avr2*, *Avr4E*, *Avr4*, *Avr9* and *Ecp6* was significantly lower in the *Δcfwor1* mutants during infection. But they are either up- or down-regulated in mycelia.	Expression of *Avr2*, *Avr9* and *Ecp6* is downregulated in overexpression strain during both infection and *in vitro*. But some effectors are upregulated *in vitro.*	ZtWor1 either positively or negatively regulates SSPs.	Either positively or negatively regulate effector gene expression during plant infection.	128 putative effector genes that involve in biotrophic development are downregulated and 70 late effectors are upregulated.
Note	*Sge1* mutant is capable of penetrating the surface.	Required for radial growth; pigmentation of the mycelium also was affected; deletion mutant is not able to infect and colonize tomato plants.		*cfwor1* mutants secrete an extracellular matrix (ECM) of unknown composition that completely covers the hyphae and sclerotium-like structures.	Conidia phenotype change; the expression level of overexpression strain was higher than wildtype at early stage but was comparable to that observed for wild-type at late stages of infection.	ZtWor1 is much more involved in developmental processes than as a specific regulator of effector genes.		Binding site is similar to Wor1 and Mit1.
Reference	Michielse et al., 2009	Santhanam et al., 2013	Brown et al., 2014	Okmen et al., 2014	Okmen et al., 2014	Mirzadi Gohari et al., 2014	Li et al., 2016	Tollot et al., 2016

*KO and O/E indicate gene knock out and overexpression strain, respectively.

Figure

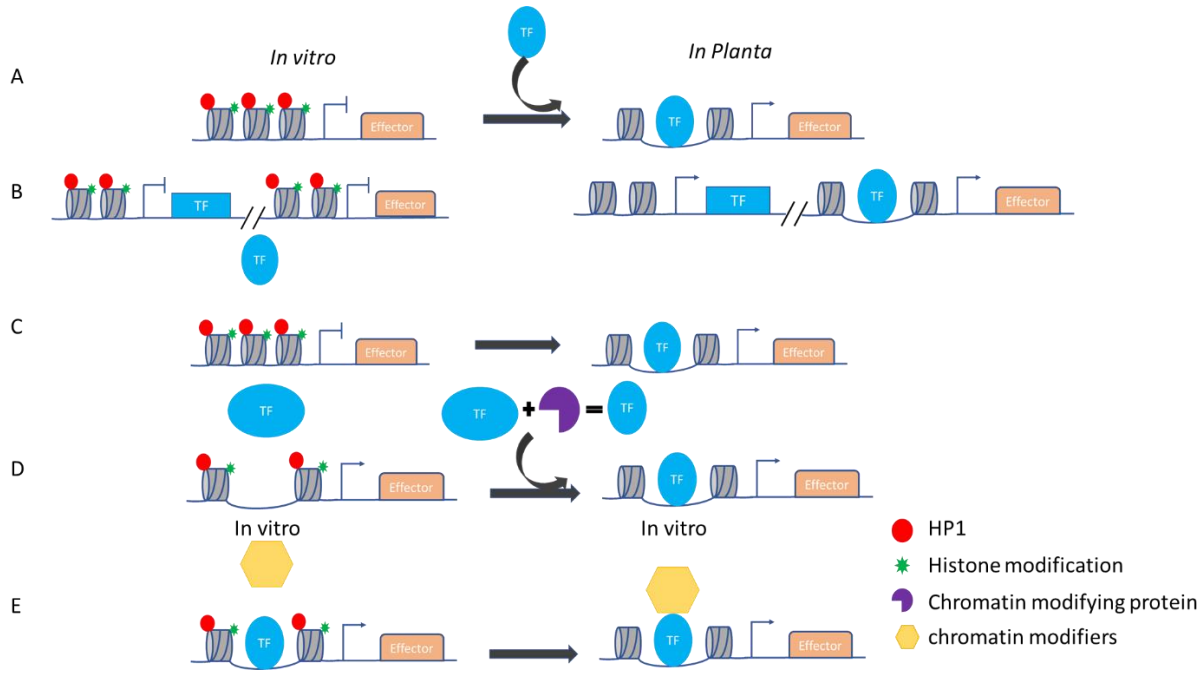

Figure 1.1 Models of coordinate control of transcriptional and epigenetic regulations on effector gene expression

CHAPTER 2

EPIGENETIC AND TRANSCRIPTIONAL CONTROL OF EFFECTOR GENE EXPRESSION IN RICE BLAST FUNGUS *MAGNAPORTHE ORYZAE*[1]

[1] Jie Zhu, Abigail J. Courtney, Peng Qi, Katrien Devos, Zarchary A. Lewis and Chang Hyun Khang. To be submitted to PLoS Genetics.

Abstract

The rice blast fungus *Magnaporthe oryzae* secretes effector proteins that suppress plant immunity and facilitate colonization. Expression of effector genes is often repressed during mycelial growth in axenic culture and strongly induced during plant infection, yet the mechanism of this concerted expression remains largely unknown. Using chromatin immunoprecipitation followed by high throughput sequencing (ChIP-seq) we found that 40% of a total of 178 known and predicted effector genes are enriched by silencing histone modification trimethylated histone H3 lysine 27 (H3K27me3) during mycelial growth. H3K27me3 loss by *MoKMT6* deletion significantly depressed overall expression of H3K27me3-enriched effector genes, but did not affect non H3K27me3-enriched effector genes in qRT-PCR and transcriptome analyses. Interestingly, expression levels of many H3K27me3-enriched effector genes were also significantly induced by ectopic overexpression of the transcription factor *MoGti1* during mycelial growth, although we did not observe reprogrammed H3K27me3 pattern at both individual effector gene loci and genome wide. The *MoGti1* overexpression in the absence of H3K27me3, synergistically upregulated the expression of 21 effector genes during mycelial growth. In particular, 81% (17/21) of these synergistically upregulated effector genes were also highly induced during the biotrophic stage of infection in a wild-type *M. oryzae* strain. Taken together, these results suggest that epigenetic control, mediated by H3K27me3, represses the expression of H3K27me3-enriched effector genes during mycelial growth, but the transcriptional control, mediated by MoGti1, activates expression of a subset of effector genes during plant infection.

Introduction

The emergence of filamentous fungal pathogens is a major threat to the global food production. During plant infection, fungal pathogens secrete effector molecules to exploit host plants and to facilitate invasion. Effectors typically function as essential pathogenicity determinants of plant-pathogen interactions. For instance, avirulence (Avr) effector proteins can interfere with plant immune response to promote interaction (effector-triggered susceptibility, ETS) in the absence of the cognate host resistant (R) proteins. In the presence of the R proteins, however, plant defense response (effector-triggered immunity, ETI) is triggered to suppress interaction. While the function of fungal effectors has been extensively studied (Lo Presti et al., 2015a; Sanchez-Vallet et al., 2018b), the mechanisms of regulating effector gene expression remain largely unknown.

During plant infection, filamentous fungi reprogram transcription to control required machineries for the colonization lifestyle. Regulated expression of effector genes is one of the most critical reprogramming actions. Expression of effector genes is typically suppressed during mycelial growth in axenic culture but is highly induced during plant infection, which is consistent with an *in planta*-specific function of effectors, to facilitate fungal invasion. Transcriptomic studies during plant infection have revealed that concerted wave expression of effector genes during different infection stages is a general machinery in filamentous pathogens, including both oomycetes and fungi, suggesting that the globally induced effector gene expression during plant infection is a conserved pattern in pathogens (Dong et al., 2015; Gervais et al., 2017; Hacquard et al., 2013; Kleemann et al., 2012; Lanver et al., 2018; O'Connell et al., 2012b). Thus, this expression pattern raises the question on how expression of effector genes is globally repressed during mycelial growth but is concertedly activated during plant infection.

Filamentous fungi are multicellular organisms. All cells are genetically homogeneous but can be structurally and functionally heterogeneous at different development stages, because of the differential expression of genes. As mentioned above, expression of effector genes is typically repressed under *in vitro* conditions, such as in mycelia and conidia, but highly induced during plant infection, such as in appressoria and invasive hyphae. Therefore, the stably altered and heritably maintained effector gene expression in the same organism, before and after plant infection, indicates that expression of effector genes is under epigenetic control. Indeed, in *Leptosphaeria maculans*, the silence of *Heterochromatin Protein 1* (*HP1*) and *DIM5* catalyzing trimethylation of H3 lysine 9 (H3K9me3) results in induced expression of small secreted protein (SSP)-encoding genes during growth in axenic culture which is a typical non-inducible condition for effector gene expression (Soyer et al., 2014a). It still remains to be investigated whether other epigenetic machineries (e.g. trimethylation of H3 lysine 27, H3K27me3) are involved in regulation of effector gene expression. Nonetheless, absence of H3K27me3 derepresses expression of secondary metabolite (SM) genes as well as putative secreted pathogenicity factors in *Fusarium graminearum* (Connolly et al., 2013b), possibly indicating that H3K27me3 also plays roles in effector gene expression. Additionally, a recent study reports that deletion of *KMT1* and *KMT6* catalyzing trimethylation of H3K9 and H3K27, respectively, deregulates expression of pathogenicity-related genes, including some putative effector genes, in *Zymoseptoria tritici* (Soyer et al., 2019).

H3K27 methylation shows high enrichment in subtelomeric regions in all chromosomes of filamentous fungi *Neurospora crassa*, *F. graminearum*, and *Cryptococcus neoformans* (Lewis, 2017b). Interestingly, the subtelomeric regions typically contain TE-rich regions that co-localize with many putative and known effector genes in *Magnaporthe oryzae* and *Phytophthora*

infestans (Farman, 2007; Haas et al., 2009; Peng et al., 2019). This further implies that expression of effector genes is under control of H3K27me3. Because H3K27me3 is a transcriptionally repressive mark, this suggests that it might repress expression of effector genes under non-inducible conditions.

The concerted transcription of effector genes during plant infection indicates an existence of a global transcriptional regulator. One good example is the WOPR transcription factor, which is initially characterized as a master regulator of morphological switching and virulence in human fungal pathogen *Candida albicans* (white-opaque regulator 1, Wor1; (Huang et al., 2006)). Wor1 homologs were subsequently identified in various plant pathogenic fungi; and all deletion mutants show altered expression of many effector genes either positively or negatively (Brown et al., 2014a; Li et al., 2016a; Michielse et al., 2009b; Mirzadi Gohari et al., 2014b; Okmen et al., 2014b; Santhanam and Thomma, 2013; Tollot et al., 2016). However, it is still unknown whether the WOPR transcription factor is under control of epigenetic regulation or can regulate effector gene expression in a coordinate manner with epigenetic machinery.

In this study, we profiled genome-wide distributions of histone modifications (H3K4me2, H3K9me3, H3K27me3 and H3K36me3) during mycelial growth of rice blast fungus *Magnaporthe oryzae* using chromatin immunoprecipitation followed by high-throughput sequencing (ChIP-seq). We found that a large proportion of known and predicted effector genes in *M. oryzae* are enriched with H3K27me3. Then we demonstrated that H3K27me3 is involved in epigenetic repression of effector gene expression during mycelial growth using RNA-seq and quantitative PCR (qRT-PCR). Interestingly, many derepressed effector genes due to H3K27me3 loss by *MoKMT6* knockout during mycelial growth were also induced during plant infection of a wild-type strain at 36 hours post inoculation (hpi), suggesting a correlation between H3K27me3

loss at effector gene loci and effector gene expression during plant infection. To investigate transcriptional activation of effector genes, we overexpressed MoGti1, Wor1 homolog in *M. oryzae*, and found that expression of some effector genes was significantly upregulated even during mycelia growth. Then, we explored the outcome of possible interplay between epigenetic (H3K27me3) and transcriptional (MoGti1) regulation on effector gene expression and uncovered a synergistic effect when *MoGti1* was overexpressed in the mutant strain without H3K27me3. Our data showed H3K27me3-mediated repression of effector genes during mycelial growth and MoGti1-mediated activation of effector genes during plant infection and strongly suggests a coordinate control of effector gene expression by epigenetic and transcriptional regulations in a temporal manner.

Materials and Methods

Strains and growth conditions

M. oryzae field isolate O-137 was used as the wild-type strain and the recipient of fungal transformations. *M. oryzae* strains used in this study are listed in Table S2.9. The fungi were maintained in frozen storage (-20°C) and cultured on oatmeal agar (OMA) plates at 25°C under continuous light (Valent et al., 1991).

Vector construction and fungal transformation

To obtain a *MoKMT6* knock-out mutant of *M. oryzae*, a homologous gene replacement strategy was applied as previously described (Khang et al., 2005). Briefly, the 5'- (1.4 kb) and 3'- (1.3kb) flanking regions of *MoKMT6* were amplified by PCR from genomic DNA of *M. oryzae* isolate O-137 using the primers shown in Table S2.12. The *Neomycin phosphotransferase–II* (*NTPII*) gene was cloned from pBV141 (Kim et al., 2011). Each primer was designed with a restriction enzyme site at 5' end. PCR was performed using Phusion High-

Fidelity PCR Master Mix with HF Buffer (Thermo Scientific™). The PCR cycling program consisted of an initial denaturation for 2 min at 98°C, two cycles of 30 s denaturation at 98°C, 30 s annealing at 56°C, 1 min extension at 72°C and 25 cycles of 30 s denaturation at 98°C, 30 s annealing at 62°C, 1 min extension at 72°C, followed by a final extension for 10 min at 72°C. PCR products were isolated from gels using E.Z.N.A.® Gel Extraction Kit (Omega Bio-tek). The three fragments were first cloned in pJET1.2 using CloneJET PCR Cloning Kit (Thermo Fisher Scientific) for sequence analysis and later into binary vector pBV108 (pGKO2)(Khang et al., 2005). *NTPII* gene was constructed between the two flanking regions using a restriction ligation strategy. Fungal transformation was performed using *Agrobacterium tumefaciens* mediated transformation (ATMT) according to previous description (Khang et al., 2005). After two rounds of selections on TB3 (0.3% yeast extract, 0.3% casamino acid, 20% sucrose) and V8 (8% V8 vegetable juice (Campbell's), pH6.97) media containing 800 µg/ml of G418 (Fisher BioReagents) and 200 µM of Cerfotaxime (Gold Biotechnology), 72 independent fungal transformants were screened by negative selection on V8 media containing 800 µg/ml of G418, 200 µM of Cerfotaxime and 5 µM of (+)-5-Fluoro-2"-deoxyuridine (F2dU, Aros organics). Eleven fungal transformants after negative selection were analyzed for gene replacement events by two different PCR amplification strategies that were used previously (Fig. S2.4) (Fernandez et al., 2012; van der Does et al., 2008; Wilson et al., 2010). Then the selected knock-out transformant was further confirmed by qRT-PCR assay.

Genetic complementation of *MoKMT6* deletion mutant was performed by introducing a wild-type allele of *MoKMT6* ectopically into *Δmokmt6* genome, which resulted in a complemented strain carrying the wild-type allele of *MoKMT6* at a random locus. Genomic sequences containing *MoKMT6* coding sequence with its 5'- and 3' flanking regions were

amplified from genomic DNA of *M. oryzae* isolate O-137 with primers shown in Table S2.12 and first cloned into pJET1.2 and later into binary vector pCK1806. pCK1806 was generated by replacing *Xho*I-*EcoR*I fragment of pBV141 with *Nourseothricin acetyltransferase* gene (*Nat1*) amplified from pDONR207 (generously shared by Ane Sesma at Universidad Politécnica de Madrid, Madrid, Spain). Twenty independent transformants were selected on V8 media containing 400 µg/ml nourseothricin (Gold Biotechnology) and analyzed by PCR amplification. Then, two transformants were further confirmed by qRT-PCR analysis of *BAS4* expression and ChIP-seq analysis of H3K27me3.

To construct MoGti1 overexpression cassette, *MoGti1* coding sequence with 300-bp of 3'-flanking region after stop codon was amplified from genomic DNA of *M. oryzae* O-137 with primers in Table S2.12. 1-kb of the strong constitutive *M. oryzae* ribosomal protein (P27) promoter was isolated from *EcoR*I-*BamH*I fragment of pBV126 (Khang et al., 2010b). Two fragments were first cloned into pJET1.2 and later into binary vector pCK1806. Twelve independent transformants were selected and behaved similarly to wild-type strain under microscopy examination. Then four transformants with wild-type and recipient strains were inoculated into liquid complete medium (CM, 10 mg/ml of sucrose, 6 mg/ml of casamino acids, and 6 mg/ml of yeast extract) for 5 days to isolate RNA for determining *MoGti1* expression level (Fig. S2.7).

To obtain dual transformants of *Δmokmt6*-MoGti1oe, we introduced *MoGti1* overexpression construct into a *MoKMT6* deletion mutant. Twelve independent transformants were selected on V8 media containing 400 µg/ml nourseothricin. Then four transformants with wild-type and recipient strains were inoculated into liquid CM for 5 days to isolate RNA for determining *MoGti1* expression level (Fig. S2.9).

To monitor *BAS4* expression at signal cell resolution, 1-kb 5'- and 0.5-kb 3'-flanking region of *BAS4* coding sequence were amplified, respectively, from genomic DNA of *M. oryzae* isolate O-137 with primers in Table S2.12. EGFP was isolated from *BamH*I-*BsrG*I fragment of pGXT (Chen et al., 2009), and the protein degradation signal peptide PEST was isolated from *BsrG*I-*Not*I fragment of pBV118 (pd2EGFP-1)(Li et al., 1998). EGFP:PEST was constructed between the two flanking regions using a restriction ligation strategy. All four fragments were fused into binary vector pBV1(pBHt2) (Mullins et al., 2001). After fungal transformation, ten independent transformants were selected on V8 media containing 200 µg/ml hygromycin (Fisher) and purified by single spore isolation.

Genomic DNA isolation

Fungal conidia were harvested from ~10-day-old culture on OMA plates. $1x10^5$ spores/ml in distilled water were inoculated into liquid complete medium and shaken at 25°C, 100 rpm for 5 days under dark environment. Then fungal mycelia were collected and washed by filtration to remove extra water, and frozen immediately in liquid nitrogen and stored at −80°C for subsequent DNA extraction. The CTAB (cetyltrimethyl ammonium bromide) DNA extraction method was used to isolate genomic DNA from the mycelia samples (Clarke, 2009).

Preparation of infected rice sheath and mycelia samples for gene expression analysis

To examine expression of effector genes and the transcription factor *MoGti1* during plant infection, a time course qRT-PCR assay was performed. Briefly, rice sheath inoculations were performed by inoculating fungal spores at concentration of 1×10^5 spores/ml in distilled water as described (Kankanala et al., 2007). 8cm-long sheath pieces from ~20-day-old plants were used. Fifteen of infected rice sheath samples at each time point of 18 hours post inoculation (hpi),

24hpi, 33hpi and 40hpi were collected as described (Mosquera et al., 2009), and frozen immediately in liquid nitrogen and stored at −80°C for subsequent RNA extraction.

Preparation of mycelia samples for RNA extraction was performed as exactly as mycelia samples for genomic DNA extraction and ChIP-seq assay.

ChIP-seq, ChIP-seq library construction and data analysis

For preparation of mycelia for ChIP-seq samples, fungal mycelia after 5 days growth in CM were washed once by 1% phosphate-buffered saline (PBS) and transferred into 50 ml flasks containing 10 ml of PBS with 1% formaldehyde to perform chemical cross-linking at room temperature on a rotating platform for 30 min. The reaction was quenched with 125 mM glycine. ChIP methods were performed as described previously (Ferraro and Lewis, 2018). Antibodies used for ChIP are listed in Table S2.11. For Illumina sequencing, ChIP-seq libraries were prepared using 10 ng of immunoprecipitated DNA and were constructed by end repair and A-tailing using the NEB End Repair Module (cat. # E7546S). Illumina adaptors were ligated to repaired DNA molecules using the NEB Ligation Module (cat #E7595S). Ligation products were amplified to generate dual-indexed libraries using NEBNext Ultra II Q5 Hot Start HiFi PCR Master Mix (cat. # M0543S). Libraries were pooled and sequenced on a NextSeq500 instrument at the Georgia Genomics and Bioinformatics Core to generate 75-bp reads.

For ChIP-seq data analysis, short reads (<20-bp) and adaptor sequences were removed using TrimGalore (version 0.4.4) (Krueger, 2015), cutadapt version 1.1 (Martin, 2011), and Python 2.7.8, with fastqc command (version 0.11.3). Trimmed Illumina reads were aligned to the current *Magnaporthe oryzae* 70-15 MG8 genome assembly (accession# GCA_000002495.2) using BWA (version 0.7.15) (Li, 2013), using the mem algorithm, which randomly assign multi-mapped reads to a single location. Files were sorted and indexed using SAMtools (version 1.9)

(Li, 2013). To plot the relative distribution of mapped reads, read counts were determined for each 25-bp window across the genome using igvtools and data were displayed using the Integrated Genome Viewer (Robinson et al., 2011). The Hypergeometric Optimization of Motif EnRichment (HOMER) software package (version 4.8) (Heinz et al., 2010) was used to identify H3K27me3 peaks in wildtype against input using "findPeaks.pl" with the following parameters: -style histone. Bedtools (version 2.27.1) "intersect" (version 2.26.0) (Quinlan and Hall, 2010) was used to determine the fraction/number of peaks that intersect with annotated genes. HOMER was also used to construct heatmaps using "annotatePeaks.pl" with the following options: -hist 10 -size 2000/6000 -ghist for heatmaps centered on TSS and centered on K27me3 peaks, respectively. Heatmaps were constructed with R using the pheatmap package using a k-means of two and separately hierarchical clustering of rows for heatmaps with effector genes (Kolde, 2012). The 95th percentile value was set as the maximum value and pheatmap was used to generate heatmaps using HOMER -ghist matrix files as input. Karyotype plots of all assembled chromosomes with H3K27me3 enrichment and effector gene positions were generated using karyoploteR package (Gel and Serra, 2017) in R using the wildtype H3K27me3 bam file. A custom cytoband file was created with the genomic coordinates of known effector genes from literature. Hierarchical clustering of all H3K27me3 ChIP experiments and replicates was generated using DiffBind (Stark and Brown, 2011) to show sample similarity. Separate ChIP bam files from replicate experiments were merged to create the combined sequence data heatmaps.

RNA isolation, quantitative RT-PCR, RNA-seq library construction and RNA-seq analysis

Total RNAs from mycelia and infected rice sheaths were extracted using a Trizol method (Invitrogen). Genomic DNA was removed by treatment with Turbo™ DNase (Ambion, Cat# AM1907) according to manufacturer's instructions. 2 µg of total RNA extracted from infected rice tissue or mycelia grown for 5 days in CM was used to synthesize cDNA with ImProm II Reverse Transcriptase system (Promega). qRT-PCR was performed with the MX3005P (Stratagene) and CFX96™ (Bio-Rad) systems using the PowerUp™ SYBR™ Green Master Mix (Thermo Fisher/applied biosystem). Thermocycler conditions were as follows: 2 min at 50°C, 10 min at 95°C, followed by 40 cycles of 95°C for 30 sec, 60°C for 30 sec, and 72°C for 30 sec. A final dissociation cycle was incorporated to ensure the specificity of each primer pair. Each qRT-PCR mixture (final volume 14 µl) contained 7 µl of PowerUp™ SYBR™ Green Master Mix, 1.5 µl of forward and reverse primers (3.3 nM concentrations for each), 2 µl of cDNA template and 2 µl of distilled water. Primers used for qRT-PCR assays are listed in Table S2.12. The relative expression level of each gene was calculated by the $2^{-\Delta\Delta CT}$ method (Livak and Schmittgen, 2001), with the *M. oryzae actin* gene (MGG_03982) as a control housekeeping gene. Briefly, the average threshold cycle (Ct) was normalized to that of *actin* gene for each of the treated samples as $2^{-\Delta Ct}$, where $\Delta Ct = (Ct, _{\text{effector gene}} - Ct, _{\text{actin}})$. The fold changes between the wild-type and mutants during mycelia growth in liquid CM were calculated as $2^{-\Delta\Delta Ct}$, where $\Delta\Delta Ct = (Ct, _{\text{effector gene}}-Ct, _{\text{actin}})_{\text{mutant}} - (Ct, _{\text{effector gene}} - Ct, _{\text{actin}})_{\text{wild-type}}$. Two technical replications for each of two or three biological replications were performed. Mean and standard deviation were calculated from qRT-PCR results of three biological replicates.

RNA-seq libraries were prepared from 1μg of total RNA and constructed with the Illumina Truseq Stranded mRNA Library Prep kit (cat #20020594) according to directions. Libraries were pooled and sequenced on a NextSeq500 instrument at the Georgia Genomics and Bioinformatics Core to generate 75-bp reads.

For RNA-seq data analysis, Illumina paired-end reads were mapped to the current *Magnaporthe oryzae* 70-15 MG8 genome assembly (accession# GCA_000002495.2) using the Hierarchical Indexing for Spliced Alignment of Transcripts 2 (HISAT2: version 2.1.0) (Kim et al., 2015) with parameters –RNA-strandness RF then sorted and indexed using SAMtools (version 1.9) (Li et al., 2009). FeatureCounts from Subread (version 1.6.2) (Liao et al., 2014) was used to generate gene level counts for all RNA bam files. Raw counts were imported into R and differential gene expression analysis was conducted using Bioconductor: DeSeq2 (Love et al., 2014). Distance matrix, volcano, and box plots generated in R using DeSeq2 and ggplot2 (Wickham, 2016), respectively. Heatmaps were constructed using the pheatmap package with scale "row" for all sample heatmap, pairwise comparisons were generated the same with the addition of hierarchical clustering of rows for H3K27me3 enriched and unenriched groups separately.

Microarray analysis and comparison

Microarray data of *M. oryzae* O-137 infected rice sheath at 36 hpi were downloaded from NCBI Gene Expression Omnibus (GEO), accession number GSE8517 (www.ncbi.nlm.nih.gov/geo) (Mosquera et al., 2009). Probe IDs and corresponding sequences from previously published microarray dataset (GSE8517) were compiled into a FASTA file and their corresponding genes were identified using BLAST against a local database of the current *Magnaporthe oryzae* 70-15 MG8 genome assembly (accession# GCA_000002495.2). Only

genes that had two-fold upregulated in comparison to wildtype were used for further analysis and comparisons. Genes with the same fold change criteria were used for comparison. Venn diagrams were constructed to show the overlap of the gene sets using R package VennDiagram (Chen and Boutros, 2011). UpSet plots were generated with the same gene sets using R package UpSetR (Conway et al., 2017).

Effector prediction and data set

The *M. oryzae* secretome data was previously generated by Zhang et al. (2018), which included 1426 secretory proteins. This secretome was used to predict *M. oryzae* effector genes by EffectorP 2.0 (http://effectorp.csiro.au/)(Sperschneider et al., 2018), a machine learning method trained with characterized fungal effectors to predict effector proteins from secretomes. A total of 449 effector genes were identified from EffectorP2.0. Then BLAST (e-value cut-off = 1e-5) search of 449 effector genes identified that 434 effectors had homologous sequences in the genome of *M. oryzae* isolate O-137. Among them, 36 known *M. oryzae* effector genes that were reported in literatures were included, but another 14 known effector genes were not. Thus, we combined 434 predicted effector genes and 14 known effector genes as our dataset (a total of 448 known and predicted effector genes) for the further analysis.

Pathogenicity assay

Rice (*Oryza sativa)* cultivar YT16 was planted as described (Jones et al., 2016b). Long day conditions (14/10 h, day/night) in a growth chamber with daytime temperature of 28°C and nighttime temperature of 24 °C were applied for plant growth. About 20-day-old rice was used for whole-plant infection with 3×10^4 spores/ml in distilled gelatin solution (0.25%) to assess mutant phenotypes. Seven days after inoculation, symptoms on the inoculated plants were recorded (Valent et al., 1991) and evaluated (Matsunaga et al., 2017) as described. Briefly, the

youngest leaf that was expanded when being inoculated was examined and documented by using EPSON perfection 4870 Photo with 24-bit color, 600 dpi resolutions and same document size (8.5 inch of width and 11.7 inch of height). Then, ImageJ (Schneider et al., 2012) was used to process and measure diseased leaf area. Pixels in images were converted to centimeters with the Set Scale command, and a single leaf was analyzed each time. To measure the whole and diseased leaf area, we used Color Threshold with HSB color space. Appropriate thresholds to whole leaf area and specifically diseased leaf area were selected and measured, respectively.

Confocal Microscopy

Confocal microscopy was performed on a Zeiss LSM 880 Confocal Microscope with an upright microscope stand. Excitation/emission wavelengths were 488 nm/496 to 544 nm for EGFP and 543 nm/565 to 617 nm for tdTomato. Images were processed using Zen Black software (version 10.0, Zeiss).

Results

Histone modifications of known and predicted effector genes in *M. oryzae*

To investigate a role of histone modifications in regulating effector gene expression, we determined the genome-wide distributions of histone H3 (H3) lysine methylations H3K4me2, H3K9me3, H3K27me3 and H3K36me3 in *M. oryzae* using ChIP-seq. Chromatin was extracted from *M. oryzae* mycelia cultured in complete medium (axenic culture in this study), in which most of *M. oryzae* effector genes are transcriptionally repressed (Mosquera et al., 2009). Our ChIP-seq results revealed that two repressing histone marks, namely H3K9me3 and H3K27me3, were predominantly enriched in presumed heterochromatin regions, such as chromosomal ends, which contrasts to the distribution of the activating H3K4me2 marks (Fig. 2.1 and Fig. S2.1). Interestingly, distributions of H3K9me3 and H3K27me3 were not precisely colocalized but

neighboring. Each mark was deposited at distinct genomic regions with little or no overlap (Fig. 2.1 and Fig. S2.1).

In literature, we identified 24 *M. oryzae* effector genes, whose expression has been experimentally demonstrated to be repressed during mycelial growth in axenic culture but activated during various infection stages (Table S2.1). These effector genes include avirulence genes and pathogenicity genes. Interestingly, we found all these effector genes were located in or nearby the H3K27me3-enriched regions (Fig. 2.1). Further analysis revealed that most of these effector genes were highly enriched with H3K27me3 during mycelial growth (Fig. S2.2 and Table S2.1). This striking association of the repressed effector genes with silencing H3K27me3 marks prompted us to expand our analysis to a total of 448 known and predicted effector genes that we identified in *M. oryzae* isolate O-137. We found that ~30% of these effector genes (132 of a total of 448 genes) are enriched with H3K27me3 (>70% coverage), but only ~6.2% (819/13,144) of annotated *M. oryzae* genes are enriched with comparable level of H3K27me3. Then, we performed a hierarchical clustering with 448 known and predicted effector genes using k-means clustering of two, which gave us a comprehensive overview of H3K27me3 distribution across all the 2-kb transcription start site (TSS) regions during mycelial growth (Fig. 2.2). This analysis revealed that these genes are grouped into two clusters, thus are named cluster 1 and cluster 2. The effector genes in cluster 1 were highly enriched by H3K27me3 (40%, 178/448). H3K27me3 enrichment at effector gene loci of the cluster 1 tended to colocalize with high levels of H3K36me3 (Fig. 2.2). However, the effector genes in cluster 2 had low enrichment of H3K27me3 (Fig. 2.2), including a constitutively expressed effector gene *MC69* (Saitoh et al., 2012). In addition, H3K36me3 enrichment at effector gene loci of the cluster 2 seemed to be lower than that of the cluster 1 (Fig. 2.2). We also found that the enrichment of another silencing

mark H3K9me3 at effector gene loci in mycelia was comparable to the genome-wide level (the percentage is also comparable ~1%), but the activating mark H3K4me2 at effector gene loci was lower than that on all genes (Fig. 2.2B).

Deletion of the histone methyltransferase *MoKMT6* eliminates H3K27 trimethylation in *M. oryzae*

To further characterize the role of the histone methylation in regulating effector gene expression, we decided to focus on *MoKMT6* (MGG_00152) in *M. oryzae*. *MoKMT6* was previously cloned from a wheat-pathogenic strain of *M. oryzae* and shown to encode a histone methyltransferase responsible for catalyzing methylation of H3K27 (Pham et al., 2015). We first identified the same gene in the rice-pathogenic *M. oryzae* strain O-137 by BLAST analysis and used a homologous recombination strategy to generate *MoKMT6* deletion mutants (Fig. S2.4). All deletion mutants (n=8), compared to WT and ectopic strains, produced noticeably fewer dark mycelia when grown on conidia-inducing OMA media, indicating they were defective in conidiation. Indeed, the Δ*mokmt6* deletion mutant strain CKF3472 (chosen for further studies) showed reduced conidiation and also virulence on rice (Fig. 2.3A and Table S2.2). Complementation of the deletion strain with the WT allele restored virulence defects but not conidiation (Fig. 2.3A and Table S2.2). These phenotypes were consistently observed when *MoKMT6* was disrupted in a wheat-pathogenic strain of *M. oryzae* (Pham et al., 2015). ChIP-seq analysis clearly showed that the enrichment of H3K27me3 was lost in the Δ*mokmt6* mutant but was restored in the complementation strain (Fig. 2.3B), confirming that *MoKMT6* is responsible for deposition of H3K27me3 in *M. oryzae*.

Loss of H3K27me3 results in de-repression of effector gene expression

We used qRT-PCR to compare the expression of nine effector genes during mycelial growth in axenic culture of WT and Δ*mokmt6*. These effector genes include five AVR genes (*AVR-Pik*, *AVRPiz-t*, *AVR-Pi9*, *ACE1*, and *PWL2*), two biotrophy-associated genes (*BAS3* and *BAS4*), and two virulence genes (*Slp1* and *MC69*). Seven out of nine genes were enriched with H3K27me3 in WT during mycelial growth, but the enrichment was removed in the Δ*mokmt6* mutant (Fig. 2.4, Fig. S2.6 and Table S2.3). We found that the transcript levels of all seven effector genes in the Δ*mokmt6* mutant were significantly increased, ranging from 3.5-fold (i.e, *PWL2*) to even above 150-fold (i.e, *AVRPiz-t* and *BAS4*), compared with those in WT (Fig. 2.4A, 2.4B, Fig. S2.5 and Table S2.3). These results indicate that H3K27me3 is involved in repressing expression of these effector genes during mycelial growth in axenic culture and that, consequently, loss of H3K27me3 results in de-repression of their expression. Furthermore, we found that the expression of *MC69*, which has no enrichment of H3K27me3 during mycelial growth of WT strain, was not changed in the Δ*mokmt6* mutant (Fig. 2.4C). Interestingly, *AVR-Pi9* was clustered into the group of low H3K27me3 enrichment in our hierarchical clustering, but genome-wide loss of H3K27me3 led to its derepressed expression during mycelial growth (Fig. 2.4A), indicating the indirect involvement of H3K27me3 on effector gene expression.

Regulation of effector gene expression by the transcription factor MoGti1

Gene expression is increasingly shown to be regulated by both histone modifications and transcription factors (TFs) (Fischer et al., 2018; Mayran et al., 2018). To investigate the coordinated regulation of H3K27me3 and TFs in effector gene expression, we focused on the *M. oryzae* TF MoGti1 and effector gene *BAS4*. MoGti1 is a homolog of the Wor1 TF, and deletion of *MoGti1* in *M. oryzae* results in altered expression of several effector genes, including *BAS4*

(Li et al., 2016a). *BAS4* expression was strongly induced immediately after appressorium-mediated host penetration at 25 hpi (Fig. 2.5A and 2.5B). We found that the *BAS4* promoter contains the core motif (TTAAAGTTT), recognized by Wor1 (Lohse et al., 2010), suggesting that the expression of *BAS4* is directly regulated by MoGti1. This is further supported by qRT-PCR results revealing coordinately induced expression of *MoGti1* and *BAS4*, with an earlier induction of *MoGti1*, during the course of plant infection while repressed in axenic growth (Fig. 2.5B).

To further confirm that MoGti1 positively regulates *BAS4* expression, we transformed *M. oryzae* ectopically with the *MoGti1* coding sequence under control of the constitutive promoter of the ribosomal protein *RP27* gene. Four randomly selected transformants showed more than 10-fold increase of *MoGti1* expression, compared to WT, in axenic culture (Fig. S2.7). One transformant (MoGti1oe; CKF3790AB) that exhibited the highest fold increase, ~55-fold, was chosen for further experiments. We found that the transcript level of *BAS4* was significantly increased, ~250-fold, in MoGti1oe relative to WT in axenic culture (Fig. 2.5C).

We then examined another eight effector genes (*AVR-Pik*, *AVR-Pi9*, *AVRPiz-t*, *PWL2*, *ACE1*, *MC69*, *Slp1*, and *BAS3*, Table S2.3) in both WT and MoGti1oe during mycelial growth in axenic culture (Fig. 2.5C and Fig. S2.8). Similar to *BAS4*, the expression of *AVR-Pik*, *PWL2*, and *BAS3* was significantly upregulated in MoGti1oe compared to WT. Interestingly, we also found that the expression of some effector genes was downregulated (i.e., *AVR-Pi9*), or not altered (i.e., *AVRPiz-t*, *ACE1*, *Slp1*, and *MC69*) in MoGti1oe compared to WT. Taken together, we suggest that MoGti1 plays both a positive and a negative role in regulating expression of a subset of effector genes in *M. oryzae*.

Double control of effector gene expression by H3K27me3 and MoGti1

Since deletion of *MoKMT6* (*Δmokmt6*) or overexpression of *MoGti1* (MoGti1oe) leads to increased expression of *BAS4* and other effector genes (Fig. 2.4, 2.5, and Fig. S2.5, S2.8), we asked whether the combination of *Δmokmt6* and MoGti1oe has an additive or synergistic effect on effector gene expression. To answer this, we generated *M. oryzae* strains, ectopically overexpressing *MoGti1* in the *Δmokmt6* mutant and subsequently identified one strain, CKF4034 (*Δmokmt6*-MoGti1oe), in which the level of *MoGti1* overexpression was comparable to that in the MoGti1oe strain (Fig. S2.9B). The qRT-PCR assays with RNA isolated from axenic cultures showed that *Δmokmt6* or MoGti1oe alone increased the *BAS4* transcripts by ~150-fold or ~250-fold, respectively, but the *Δmokmt6* and MoGti1oe combination increased the *BAS4* expression by ~20,000-fold (Fig. 2.6A). Similar result was also observed in another independent *Δmokmt6*-MoGti1oe transformant. This synergistic effect was consistently observed for other effector genes, such as *AVR-Pik, BAS3* and *PWL2*, whose expression, just like *BAS4*, was increased by *Δmokmt6* or MoGti1oe alone (Fig. S2.11A and Table S2.3).

To gain insight into the synergistic effect of *Δmokmt6* and MoGti1oe on effector gene expression, we first tested if H3K27me3 plays a role in regulating *MoGti1* expression by examining *MoGti1* transcript in *Δmokmt6* using qRT-PCR. We found that *MoGti1* expression was significantly induced (~3-fold) in *Δmokmt6* compared to WT, indicating that H3K27me3 is involved in repressing *MoGti1* expression (Fig. 2.6B). In *F. graminearum* and *N. crassa*, H3K27me3 loss can upregulate both H3K27me3-marked and non-H3K27me3-marked genes (Connolly et al., 2013b; Jamieson et al., 2013). To determine if *MoGti1* is a H3K27me3-marked gene, we examined H3K27me3 distribution at the *MoGti1* locus in axenic culture. Our ChIP-seq analysis showed that H3K27me3 was not enriched at *MoGti1* locus, indicating *MoGti1* is a non-

H3K27me3-marked gene (Fig. 2.6B). Taken together, these results suggest that H3K27me3 is implicated with repressing *MoGti1* expression indirectly.

Four effector genes (*AVR-Pik*, *BAS3*, *BAS4*, and *PWL2*) in our qRT-PCR analysis showed the increased expression in MoGti1oe, and these genes are enriched with H3K27me3 in WT (Fig. S2.11 and Table S2.3). We then tested if *MoGti1* overexpression can alter H3K27me3 pattern at these gene loci. To this end, we first measured the transcripts of *MoKMT6* in both WT and MoGti1oe and no significant difference of *MoKMT6* expression was found between them (Fig. 2.6C). ChIP-seq result showed no noticeable difference of the H3K27me3 enrichment from WT at individual gene locus (Fig. 2.6C and Fig. 2.S10). Similarly, we found almost indistinguishable difference of H3K4me2, H3K9me3, H3K27me3 and H3K36me3 in MoGti1oe from WT when viewed at whole chromosome scale (Fig. 2.6D). These suggest that altered expression of effector genes due to MoGti1oe does not involve changes in histone modifications, including silencing mark H3K27me3 and active mark H3K4me2.

Previously, we showed that MoGti1 overexpression upregulated expression of a subset of effector genes (Fig. 2.5C and Fig. S2.8). The deletion of *MoKMT6* was able to induce expression of both *MoGti1* and effector genes in axenic culture (Fig. 2.4, 2.6B and Fig. S2.5). This raises a question whether induced effector gene expression by *MoKMT6* deletion is solely due to upregulated *MoGti1* expression. Because of the comparable expression of *MoGti1* in both MoGti1oe and *Δmokmt6*-MoGti1oe strains (Fig. S2.9B), any differences of effector gene expression between these two strains is likely due to the presence or absence of H3K27me3. We observed that H3K27me3 loss lead to the remarkable upregulation of effector gene expression (*AVR-Pik*, *BAS3*, *BAS4*, and *PWL2*) in *Δmokmt6*-MoGti1oe compared to in MoGti1oe. This suggests that the induced effector gene expression (*AVR-Pik*, *BAS3*, *BAS4*, and *PWL2*) by

MoKMT6 deletion is not solely due to upregulated *MoGti1* expression but also because of the loss of H3K27me3. This was further confirmed by induced expression of effector genes *ACE1*, *AVRPiz-t* and *AVR-Pi9* in *Δmokmt6*. Because their expression was not or negatively regulated by MoGti1 (Fig. 2.5), the upregulated expression of these effector genes in *Δmokmt6* must be due to the loss of H3K27me3.

Trimethylation of H3K27 and the transcription factor MoGti1 globally control expression of effector genes

To investigate effects of H3K27me3 and MoGti1 on expression of effector genes on a genome-wide scale, we performed RNA-seq on wild-type, *Δmokmt6* and MoGti1oe strains during mycelial growth in axenic culture. We found that expression of seven out of nine qRT-PCR- tested effector genes showed consistent expression pattern to RNA-seq data in *Δmokmt6* and MoGti1oe respectively (Table S2.4). The remaining two effector genes *AVR-Pik* and *PWL2* lacked reads in wild-type strain but were detected in *Δmokmt6* and MoGti1oe based on RNA-seq, suggesting upregulated expression, which is also consistent with qRT-PCR results. Thus, the consistency between qRT-PCR and RNA-seq results confirms our RNA-seq profile. Overall, the expression levels of 32.1% (144/448) of effector genes were differentially regulated by the removal of H3K27me3 during mycelial growth, including 125 upregulated and 19 downregulated effector genes (Table S2.5). Similarly, the overexpression of MoGti1 in mycelia led to an altered expression of ~20% (89/448) of effector genes, where we found 63 upregulated effector genes including *BAS3*, *BAS4* and *SPD5*, and 26 downregulated effector genes, including *AVR-Pi9* (Table S2.5). Considering that effector genes only represent 3.4% (448/13144) of the genes in the entire *M. oryzae* genome, we suggest that both H3K27me3 and MoGti1 globally control expression of effector genes in *M. oryzae*.

H3K27me3 is involved in repressing expression of genome-wide effector genes

We then addressed the question whether expression of genome-wide effector genes correlates with H3K27me3 in the expected manner. We compared expression levels of H3K27me3-enriched and -unenriched effector genes in wild-type and *Δmokmt6*. As expected, expression levels of H3K27me3-enriched effector genes in wild-type strain were less than that of H3K27me3-unenriched effector genes (Fig. 2.7 and Fig. S2.12). However, the loss of H3K27me3 in *Δmokmt6* mutant resulted in a significantly induced expression of H3K27me3-enriched effector genes, but not for H3K27me3-unenriched effector genes (Fig. 2.7 and Fig. S2.12). These suggest that H3K27me3 enrichment on effector genes plays an important role in repressing expression of effector genes in genome-wide. This is also supported by the higher percentage of upregulated effector genes (87%, 125/144) in *Δmokmt6* than that of downregulated ones (13%, 19/144). In particular, many of the known effector genes (15 out of a total of 24 genes), of which expression is repressed during mycelial growth (Table S2.1), were detected to be upregulated, while none was downregulated (Table S2.5). For the remaining 424 effector genes, the number of upregulated effector genes were about six times higher than that of downregulated ones (110 vs. 19). In addition, contrary to H3K27me3-unenriched effector genes, H3K27me3-enriched effector genes tended to have a relatively lower enrichment of H3K4me2 at their loci, consistent with their lower expression levels during mycelial growth (Fig. 2.2).

Effector genes upregulated during biotrophic invasion are enriched with H3K27me3-enriched effector genes during mycelial growth

As expression of 15/24 (62.5%) known effector genes was derepressed due to the loss of H3K27me3 in *Δmokmt6* (Table S2.4), and they are also known to be induced during plant infection (Table S2.1) in WT, we explored if expression of the effector genes which are enriched

by H3K27me3 during mycelial growth is induced during plant infection. To this end, we analyzed the transcriptomic data generated from infected rice sheath by *M. oryzae* O-137 at 36 hpi from the previous study (Mosquera et al., 2009). As expected, many effector genes (33.7%, 151/448) were upregulated more than two-fold change at 36 hpi, including 18/24 known effector genes, when compared to only 10.3% of genome-wide genes being upregulated (Table S2.5). In particular, expression of 48.3% (86/178) of the effector genes which are enriched by H3K27me3 during mycelial growth was induced more than two-fold change at 36 hpi, but only 24.3% (65/268) of the effector genes which are not enriched by H3K27me3 during mycelial growth was induced (Table S2.5). This suggests that, indeed, expression of the effector genes which are enriched by H3K27me3 during mycelial growth tends to be induced during plant infection. Considering that expression of different effector genes is concertedly expressed at various infection stages (Dong et al., 2015; Kleemann et al., 2012), 86 induced effector genes which are enriched by H3K27me3 during mycelial growth only represent a specific fungal infection stage at 36 hpi. It is possible that more effector genes that are enriched by H3K27me3 during mycelial growth will be induced if we investigate other infection stages.

We next investigated if induced effector gene expression during plant infection correlates with removal of H3K27me3 at effector gene loci which are enriched by H3K27me3 during mycelial growth. Thus, we examined and compared expression patterns of effector genes which are enriched by H3K27me3 during mycelial growth in mycelia of the *Δmokmt6* mutant and in infected plant by a wild-type strain at 36 hpi. In contrast of H3K27me3-unenriched effector genes, expression of H3K27me3-enriched effector genes was overall more upregulated in mycelia of the *Δmokmt6* mutant (42.1% of H3K27me3-enriched effector genes compared to 11.6% of unenriched effector genes, Table S2.5). Among these, ~43.4% (46/106) of upregulated

effector genes during mycelial growth of *Δmokmt6* were also significantly upregulated more than two-fold change during plant infection at 36 hpi (Table S2.6 and S2.8). Interestingly, the majority of these upregulated effector genes were H3K27me3-enriched ones (80%, 37/46), including 7 known effector genes of which expression is repressed during mycelial growth such as *AVRPiz-t* and *BAS4* (Table S2.6 and S2.8). This suggests a strong correlation between concertedly induced effector gene expression and removal of H3K27me3 at effector gene loci during plant infection.

Synergistic effect of H3K27me3 and MoGti1 on effector gene expression

Finally, we addressed the question if H3K27me3 and MoGti1 have a synergistic effect on induction of effector genes through RNA-seq of the *Δmokmt6*-MoGti1oe strain in comparison with *Δmokmt6* and MoGti1oe. We found that *Δmokmt6*-MoGti1oe strain had a comparable number of upregulated effector genes to the total number of that in both *Δmokmt6* and MoGti1oe strains (41% vs. 42% = combined %, Table S2.4). Notably, the expression of a total of 36 effector genes was significantly upregulated in both *Δmokmt6* mutant and MoGti1oe (Table S2.7). Among them, expression levels of 21/36 effector genes were also significantly upregulated in *Δmokmt6*-MoGti1oe strain, which was higher than the sum of their individual expression levels in *Δmokmt6* mutant and MoGti1oe, respectively, including qRT-PCR tested *BAS3* and *BAS4* (Table S2.7). Taken together, these suggest that H3K27me3 and MoGti1 synergistically control expression of subset of effector genes in *M. oryzae.* Interestingly, 17/21 (81%) of these synergistically upregulated effector genes in *Δmokmt6*-MoGti1oe were also highly induced during biotrophic invasion of the rice sheath at 36 hpi by a wild-type *M. oryzae* strain (Table S2.7), indicating a temporal correlation between H3K27me3-MoGti1 regulatory mechanism on effector gene expression and biotrophic invasion stage.

Discussion

In this study, we have found that expression of effector genes in *M. oryzae* is controlled by two layers of regulatory mechanisms: epigenetic (H3K27me3) and transcriptional (MoGti1) regulations (Fig. 2.8). Specifically, histone H3K27 trimethylation, deposited by MoKMT6, plays a role in repressing expression of effector genes that are enriched with H3K27me3 during mycelial growth (Fig. 2.1, 2.2, 2.3, 2.4 and Fig. S2.2, S2.3, S2.5, S2.6). During plant infection, our data suggests a redistribution of H3K27me3 at effector gene loci (Table S2.6 and S2.8). This redistribution allows MoGti1 to directly or indirectly regulate a subset of effector genes (Fig. 2.5, S2.8 and Fig. S2.11A). Additionally, the regulation of both H3K27me3 and MoGti1 on effector gene expression has been investigated in two ways in our study. First, we find that, even in the presence of highly enriched H3K27me3 on effector genes, MoGti1 is still able to transcriptionally regulate their expression. The evidence is that we do not observe reprogrammed H3K27me3 pattern as well as another three histone modifications H3K4me2, H3K9me3 and H3K36me3, when MoGti1 is overexpressed during mycelial growth, although expression of effector genes was differentially regulated (Fig. 2.5C, 2.6 and Fig. S2.8, S2.10, S2.11). This also indicates that MoGti1 does not result in redistribution of histone modifications at effector gene loci during plant infection. Second, the synergistically upregulated expression of effector genes (*AVR-Pik, BAS3, BAS4* and *PWL2* etc.) when MoGti1 is overexpressed in *Δmokmt6* (Fig. 2.6A, Fig. S2.11A and Table S2.7) indicates that the removal of H3K27me3 at these effector gene loci greatly increases transcription, possibly by improving binding efficiency of transcription factors at accessible promoters of effector genes. In particular, the majority of synergistically upregulated effector genes are also upregulated during plant infection of a wild-type strain at 36 hpi (Table S2.7 and S2.8), further supporting the coordinate control of effector gene expression

during plant infection by redistribution of H3K27me3 and activation of MoGti1 (Fig. 2.5B and Table S2.6, S2.7).

Control of effector gene expression by other regulations besides H3K27me3 and MoGti1

Our study indicates that expression of effector genes is also under control of other regulations besides H3K27me3 and MoGti1 in *M. oryzae*. One evidence is that we observed unaltered expression of *MC69* either by removal of H3K27me3 or by overexpression of MoGti1 (Fig 4C and S8 Fig). One possibility is the regulation by other histone modifications in addition to H3K27me3. Our ChIP-seq result reveals that 40% (178/446) of effector genes have relative high enrichment of H3K27me3 during mycelial growth of *M. oryzae* (Fig. 2.2 and Table S2.8). Among them, H3K27me3 loss derepresses expression of 42.1% (75/178) of effector genes during mycelial growth, which includes many known effector genes, such as *AVRPiz-t*, *AVR-Pik*, *ACE1*, *BAS3*, *BAS4*, *PWL2* and *Slp1* (Fig. 2.4, Fig. S2.5 and Table S2.3, S2.8). That only a subset of H3K27me3-enriched effector genes was derepressed indicates that activating signals may be required to upregulate expression of other H3K27me3-enriched effector genes in addition to H3K27me3 loss. However, there are still 60% (268/446) of effector genes with low or no H3K27me3 enrichment at the same growth stage and condition, such as *MC69*, of which expression is not controlled by H3K27me3 (Fig. 2.2 and Table S2.3, S2.8). These results indicate that H3K27me3 plays a role, but not only, in repressing effector gene expression during mycelial growth of *M. oryzae*. As discussed in *L. maculans* and *Z. tritici*, expression of effector or putative effector genes is up-regulated due to the absence of H3K9me3 in axenic culture (Soyer et al., 2014a; Soyer et al., 2019). Interestingly, we also found an enrichment of H3K9me3 in a

small subset of effector genes (Fig. S2.3), although future investigation is needed to confirm the role of H3K9me3 on effector gene expression in *M. oryzae*.

Another possibility is the regulation by various transcription factors. Indeed, MoGti1 has been previously shown to control expression of a subset of, but not all, effector genes in *M. oryzae* (Li et al., 2016a). Our MoGti1 overexpression study confirms this observation and includes more new observations that provide a more complete understanding of the regulation of MoGti1 on effector gene expression (Fig. 2.5, Fig. S2.8 and Table S2.3, S2.8). Similarly, in *Ustilago maydis*, MoGti1 ortholog Ros1 has been reported as a transcriptional regulator for downregulation of effector genes that are essential during early infection but upregulation of effector genes during late infection (Lanver et al., 2018; Tollot et al., 2016). In addition to Ros1, multiple transcriptional regulators have been identified in *U. maydis*, like Rbf1 and Fox1, to control expression of effector genes at different infection stages (Lanver et al., 2018). Interestingly, we have also noticed that *MoGti1* expression during plant infection coincides with *BAS4* and *AVR-Pik* upregulation and *AVR-Pi9* downregulation around similar appressorium-mediated penetration stage (Fig. 2.5B, chapter 3 and (Wu et al., 2015)). This temporal association between expression of *MoGti1* and various effector genes suggests that MoGti1 is only one of the transcriptional regulators to control expression of effector genes at a specific stage. Although no other TFs have been demonstrated to regulate effector gene expression in *M. oryzae*, so far 13 TFs from different families in various fungi have been found to control expression of effector or candidate effector genes (Tan and Oliver, 2017a). Thus, it is possible that, in addition to MoGti1, multiple other TFs are also involved in effector gene regulation during plant infection of *M. oryzae*.

Re-distribution of H3K27me3 derepresses effector gene expression during plant infection

It is not clear yet if highly and widely upregulated effector gene expression during plant infection is due to altered histone modifications. Previously, the reduced H3K9me3 level derepresses expression of effector genes in axenic culture but does not change expression pattern of effector genes during primary infection of *L. maculans* (Soyer et al., 2014a), indicating that the repressive histone modification (H3K9me3) might be reduced at effector gene loci during plant infection. In our study, absence of H3K27me3 derepresses expression of H3K27me3-enriched effector genes under non-inducible conditions (Fig. 2.4, Fig. S2.5 and Table S2.8). Interestingly, expression of many known and predicted effector genes that are enriched by H3K27me3 during mycelial growth is also highly upregulated during plant infection (Fig. S2.2 and Table S2.1, S2.6, S2.8). Particularly, the transcript level of *BAS4* during plant infection of wild-type strain at 25 hpi is massively induced and is significantly higher than that even during mycelial growth of Δ*mokmt6*-MoGti1oe strain (Fig. S2.13). These results indicate that the highly induced expression of H3K27me3-enriched effector genes during plant infection may be correlated with H3K27me3 removal at corresponding effector gene loci. Indeed, ChIP-qPCR *in vitro* and *in planta* analyses of a putative effector gene in *Z. tritici* reveals that reduced H3K27me3 level at this putative effector gene locus is correlated with its upregulated expression *in planta* (Soyer et al., 2019). Additionally, *in planta* exclusively induced SM genes *lolitrems* (*ltm*) and *ergot alkaloids* (*eas*) are also correlated with the reduced H3K27m3 levels at each locus when compared to axenic culture in *Epichloe festucae* (Chujo and Scott, 2014a). These results suggest that fungal H3K27me3 redistributes at individual H3K27me3-enriched gene locus during plant infection to allow efficient transcription. The similar observation has been reported

in mouse AtT-20 cells, for instance, high H3K9me2 levels are strongly depleted but H3K4me1 and H3K27ac levels are increased after the pioneer factor Pax7 action at pioneered sites, which facilitates the binding of other TFs and coactivators to promote transcription (e.g. p300) (Mayran et al., 2018). Thus, it is possible that the genome-wide redistribution of H3K27me3 during plant infection results in open chromatin and gain of active histone modifications (e.g. H3K4me2 and H3K27ac) at effector gene loci to accelerate transcription. Alternatively, the huge discrepancy of *BAS4* expression levels during plant infection of wild-type strain compared to during mycelial growth of Δ*mokmt6*-MoGti1oe indicates the involvement of a different layer of regulatory, like sRNA, lncRNA or repressor. It will be interesting to investigate whether and how the genome-wide redistribution of H3K27me3 and other histone modifications occur to play roles in expression of *M. oryzae* effector genes during plant infection.

MoGti1 overexpression is not able to reprogram H3K27me3 pattern but might override repressive effect of H3K27me3 on effector gene expression

We did not find any evidence that ectopic overexpression of the transcription factor MoGti1 changed the H3K27me3 pattern during mycelial growth in *M. oryzae* (Fig. 2.6C, D and Fig. S2.10), although ectopic expression of transcription factors mediating epigenetic reprogramming has been reported in animal studies. For example, in human cell lines having the physiologic phosphatidylinositol 3-kinase (PI3K) pathway, overexpression of the master transcription factor Nrf2 that plays roles in cellular detoxification system decreases levels of H3K27me3 but increases H3K4me3 in promoters of the Nrf2's targets *mTOR* and *NQO1* (Bendavit et al., 2016). Additionally, the ectopic expression of four transcription factors — OCT4, SOX2, KLF4 and MYC (OSKM) in mouse embryonic fibroblasts leads to the genome-wide change of H3K4me2 but H3K27me3 remains largely unchanged (Koche et al., 2011).

Interestingly, we also did not observe distinguishable alterations of H3K4me2, H3K9me3 and H3K36me3 when MoGti1 was ectopically overexpressed in mycelia of *M. oryzae* compared to wild type strain. Thus, it is possible that MoGti1 alone is not sufficient to reprogram epigenomes in *M. oryzae*. Alternatively, ectopic overexpression of MoGti1 could result in epigenetic reprogramming (e.g. H3K27ac) that we did not investigate in this study.

Despite the unaltered H3K27me3 pattern both globally and locally when MoGti1 is ectopically overexpressed during mycelial growth of *M. oryzae*, expression of many H3K27me3-enriched effector genes is still significantly induced (Fig. 2.5C, Fig. S2.8 and Table S2.8). It appears that repression of effector genes by H3K27me3 can be overridden by overexpression of MoGti1 under our experimental condition. How is a transcription factor able to access the condensed chromatin to activate gene expression? We propose two possible explanations. First, overexpression of the transcription factor MoGti1 might recruit chromatin modifiers to increase the chromatin accessibility leading to the transcription of effector genes. For instance, chromatin modifiers BRG1/BRM can be recruited to promoters of pro-inflammatory genes by a transcription co-factor MRTF-A to steer the transcription of downstream genes in animal cells (Yang et al., 2014a). Second, Petruck et al. (2017) found the delayed H3K27me3 accumulation on nascent DNA after DNA replication following induction of embryonic stem cell differentiation, thus providing a "window of opportunity" for recruitment of induced transcription factors to their binding sites (Petruk et al., 2017). Therefore, it is possible that MoGti1 that is constitutively overexpressed during mycelial growth gains access to its binding sites on nascent DNA right after DNA replication to lead to expression of downstream effector genes.

References

Bendavit, G., Aboulkassim, T., Hilmi, K., Shah, S., and Batist, G. (2016). Nrf2 transcription factor can directly regulate mTOR: linking cytoprotective gene expression to a major metabolic regulation that generates redox activity. Journal of Biological Chemistry *291*, 25476-25488.

Brown, D.W., Busman, M., and Proctor, R.H. (2014). *Fusarium verticillioides* SGE1 is required for full virulence and regulates expression of protein effector and secondary metabolite biosynthetic genes. Molecular Plant-Microbe Interactions *27*, 809-823.

Chen, H., and Boutros, P.C. (2011). VennDiagram: a package for the generation of highly-customizable Venn and Euler diagrams in R. BMC bioinformatics *12*, 35.

Chen, S., Songkumarn, P., Liu, J., and Wang, G.L. (2009). A versatile zero background T-vector system for gene cloning and functional genomics. Plant Physiology *150*, 1111-1121.

Chujo, T., and Scott, B. (2014). Histone H3K9 and H3K27 methylation regulates fungal alkaloid biosynthesis in a fungal endophyte-plant symbiosis. Molecular Microbiology *92*, 413-434.

Clarke, J.D. (2009). Cetyltrimethyl ammonium bromide (CTAB) DNA miniprep for plant DNA isolation. Cold Spring Harbor Protocol *2009*, pdb prot5177.

Connolly, L.R., Smith, K.M., and Freitag, M. (2013). The *Fusarium graminearum* histone H3K27 methyltransferase KMT6 regulates development and expression of secondary metabolite gene clusters. PLoS genetics *9*, e1003916.

Conway, J.R., Lex, A., and Gehlenborg, N. (2017). UpSetR: an R package for the visualization of intersecting sets and their properties. Bioinformatics *33*, 2938-2940.

Dong, Y., Li, Y., Zhao, M., Jing, M., Liu, X., Liu, M., Guo, X., Zhang, X., Chen, Y., Liu, Y., *et al.* (2015). Global genome and transcriptome analyses of *Magnaporthe oryzae* epidemic isolate 98-06 uncover novel effectors and pathogenicity-related genes, revealing gene gain and lose dynamics in genome evolution. PLoS Pathogen *11*, e1004801.

Farman, M.L. (2007). Telomeres in the rice blast fungus *Magnaporthe oryzae*: the world of the end as we know it. FEMS Microbiology Letters *273*, 125-132.

Fernandez, J., Wright, J.D., Hartline, D., Quispe, C.F., Madayiputhiya, N., and Wilson, R.A. (2012). Principles of carbon catabolite repression in the rice blast fungus: Tps1, Nmr1-3, and a MATE-family pump regulate glucose metabolism during infection. PLoS genetics *8*, e1002673.

Ferraro, A.R., and Lewis, Z.A. (2018). ChIP-Seq Analysis in *Neurospora crassa*. In Fungal Genomics (Springer), pp. 241-250.

Fischer, J., Muller, S.Y., Netzker, T., Jager, N., Gacek-Matthews, A., Scherlach, K., Stroe, M.C., Garcia-Altares, M., Pezzini, F., Schoeler, H., *et al.* (2018). Chromatin mapping identifies BasR, a key regulator of bacteria-triggered production of fungal secondary metabolites. Elife *7*.

Gel, B., and Serra, E. (2017). karyoploteR: an R/Bioconductor package to plot customizable genomes displaying arbitrary data. Bioinformatics *33*, 3088-3090.

Gervais, J., Plissonneau, C., Linglin, J., Meyer, M., Labadie, K., Cruaud, C., Fudal, I., Rouxel, T., and Balesdent, M.H. (2017). Different waves of effector genes with contrasted

genomic location are expressed by *Leptosphaeria maculans* during cotyledon and stem colonization of oilseed rape. Molecular Plant Pathology *18*, 1113-1126.

Haas, B.J., Kamoun, S., Zody, M.C., Jiang, R.H., Handsaker, R.E., Cano, L.M., Grabherr, M., Kodira, C.D., Raffaele, S., Torto-Alalibo, T., *et al.* (2009). Genome sequence and analysis of the Irish potato famine pathogen *Phytophthora infestans*. Nature *461*, 393-398.

Hacquard, S., Kracher, B., Maekawa, T., Vernaldi, S., Schulze-Lefert, P., and Ver Loren van Themaat, E. (2013). Mosaic genome structure of the barley powdery mildew pathogen and conservation of transcriptional programs in divergent hosts. Proceedings of the National Academy of Sciences *110*, E2219-2228.

Heinz, S., Benner, C., Spann, N., Bertolino, E., Lin, Y.C., Laslo, P., Cheng, J.X., Murre, C., Singh, H., and Glass, C.K. (2010). Simple combinations of lineage-determining transcription factors prime cis-regulatory elements required for macrophage and B cell identities. Molecular cell *38*, 576-589.

Huang, G., Wang, H., Chou, S., Nie, X., Chen, J., and Liu, H. (2006). Bistable expression of WOR1, a master regulator of white–opaque switching in *Candida albicans*. Proceedings of the National Academy of Sciences *103*, 12813-12818.

Jamieson, K., Rountree, M.R., Lewis, Z.A., Stajich, J.E., and Selker, E.U. (2013). Regional control of histone H3 lysine 27 methylation in *Neurospora*. Proceedings of the National Academy of Sciences *110*, 6027-6032.

Jones, K., Kim, D.W., Park, J.S., and Khang, C.H. (2016). Live-cell fluorescence imaging to investigate the dynamics of plant cell death during infection by the rice blast fungus *Magnaporthe oryzae*. BMC Plant Biology *16*, 69.

Kankanala, P., Czymmek, K., and Valent, B. (2007). Roles for rice membrane dynamics and plasmodesmata during biotrophic invasion by the blast fungus. Plant Cell *19*, 706-724.

Khang, C.H., Berruyer, R., Giraldo, M.C., Kankanala, P., Park, S.Y., Czymmek, K., Kang, S., and Valent, B. (2010). Translocation of *Magnaporthe oryzae* effectors into rice cells and their subsequent cell-to-cell movement. Plant Cell *22*, 1388-1403.

Khang, C.H., Park, S.Y., Lee, Y.H., and Kang, S. (2005). A dual selection based, targeted gene replacement tool for *Magnaporthe grisea* and *Fusarium oxysporum*. Fungal Genetics and Biology *42*, 483-492.

Kim, D., Langmead, B., and Salzberg, S.L. (2015). HISAT: a fast spliced aligner with low memory requirements. Nature methods *12*, 357-360.

Kim, H.-S., Park, S.-Y., Lee, S., Adams, E.L., Czymmek, K., and Kang, S. (2011). Loss of cAMP-dependent protein kinase A affects multiple traits important for root pathogenesis by *Fusarium oxysporum*. Molecular Plant-Microbe Interactions *24*, 719-732.

Kleemann, J., Rincon-Rivera, L.J., Takahara, H., Neumann, U., Ver Loren van Themaat, E., van der Does, H.C., Hacquard, S., Stuber, K., Will, I., Schmalenbach, W., *et al.* (2012). Sequential delivery of host-induced virulence effectors by appressoria and intracellular hyphae of the phytopathogen *Colletotrichum higginsianum*. PLoS Pathogen *8*, e1002643.

Koche, R.P., Smith, Z.D., Adli, M., Gu, H., Ku, M., Gnirke, A., Bernstein, B.E., and Meissner, A. (2011). Reprogramming factor expression initiates widespread targeted chromatin remodeling. Cell Stem Cell *8*, 96-105.

Kolde, R. (2012). Pheatmap: pretty heatmaps. R package version *61*, 617.

Krueger, F. (2015). Trim galore. A wrapper tool around Cutadapt and FastQC to consistently apply quality and adapter trimming to FastQ files *516*, 517.

Lanver, D., Muller, A.N., Happel, P., Schweizer, G., Haas, F.B., Franitza, M., Pellegrin, C., Reissmann, S., Altmuller, J., Rensing, S.A., *et al.* (2018). The Biotrophic Development of *Ustilago maydis* Studied by RNA-Seq Analysis. Plant Cell *30*, 300-323.

Lewis, Z.A. (2017). Polycomb group systems in fungi: new models for understanding polycomb repressive complex 2. Trends in Genetics *33*, 220-231.

Li, H. (2013). Aligning sequence reads, clone sequences and assembly contigs with BWA-MEM. arXiv preprint arXiv:13033997.

Li, H., Handsaker, B., Wysoker, A., Fennell, T., Ruan, J., Homer, N., Marth, G., Abecasis, G., and Durbin, R. (2009). The sequence alignment/map format and SAMtools. Bioinformatics *25*, 2078-2079.

Li, X., Zhao, X., Fang, Y., Jiang, X., Duong, T., Fan, C., Huang, C.-C., and Kain, S.R. (1998). Generation of destabilized green fluorescent protein as a transcription reporter. Journal of Biological Chemistry *273*, 34970-34975.

Li, Y., Wang, G., Xu, J.R., and Jiang, C. (2016). Penetration peg formation and invasive hyphae development require stage-specific activation of *MoGTI1* in *Magnaporthe oryzae*. Molecular Plant-Microbe Interactions *29*, 36-45.

Liao, Y., Smyth, G.K., and Shi, W. (2014). featureCounts: an efficient general purpose program for assigning sequence reads to genomic features. Bioinformatics *30*, 923-930.

Livak, K.J., and Schmittgen, T.D. (2001). Analysis of relative gene expression data using real-time quantitative PCR and the $2^{-\Delta\Delta CT}$ method. Methods *25*, 402-408.

Lo Presti, L., Lanver, D., Schweizer, G., Tanaka, S., Liang, L., Tollot, M., Zuccaro, A., Reissmann, S., and Kahmann, R. (2015). Fungal effectors and plant susceptibility. Annual Review of Plant Biology *66*, 513-545.

Lohse, M.B., Zordan, R.E., Cain, C.W., and Johnson, A.D. (2010). Distinct class of DNA-binding domains is exemplified by a master regulator of phenotypic switching in Candida albicans. Proceedings of the National Academy of Sciences *107*, 14105-14110.

Love, M.I., Huber, W., and Anders, S. (2014). Moderated estimation of fold change and dispersion for RNA-seq data with DESeq2. Genome biology *15*, 550.

Martin, M. (2011). Cutadapt removes adapter sequences from high-throughput sequencing reads. EMBnet journal *17*, 10-12.

Matsunaga, T.M., Ogawa, D., Taguchi-Shiobara, F., Ishimoto, M., Matsunaga, S., and Habu, Y. (2017). Direct quantitative evaluation of disease symptoms on living plant leaves growing under natural light. Breed Science *67*, 316-319.

Mayran, A., Khetchoumian, K., Hariri, F., Pastinen, T., Gauthier, Y., Balsalobre, A., and Drouin, J. (2018). Pioneer factor Pax7 deploys a stable enhancer repertoire for specification of cell fate. Nature Genetics *50*, 259-269.

Michielse, C.B., van Wijk, R., Reijnen, L., Manders, E.M., Boas, S., Olivain, C., Alabouvette, C., and Rep, M. (2009). The nuclear protein Sge1 of *Fusarium oxysporum* is required for parasitic growth. PLoS Pathogen *5*, e1000637.

Mirzadi Gohari, A., Mehrabi, R., Robert, O., Ince, I.A., Boeren, S., Schuster, M., Steinberg, G., de Wit, P.J., and Kema, G.H. (2014). Molecular characterization and functional analyses of ZtWor1, a transcriptional regulator of the fungal wheat pathogen *Zymoseptoria tritici*. Molecular Plant Pathology *15*, 394-405.

Mosquera, G., Giraldo, M.C., Khang, C.H., Coughlan, S., and Valent, B. (2009). Interaction transcriptome analysis identifies *Magnaporthe oryzae* BAS1-4 as Biotrophy-associated secreted proteins in rice blast disease. Plant Cell *21*, 1273-1290.

Mullins, E.D., Chen, X., Romaine, P., Raina, R., Geiser, D.M., and Kang, S. (2001). *Agrobacterium*-mediated transformation of *Fusarium oxysporum*: an efficient tool for insertional mutagenesis and gene transfer. Phytopathology *91*, 173-180.

O'Connell, R.J., Thon, M.R., Hacquard, S., Amyotte, S.G., Kleemann, J., Torres, M.F., Damm, U., Buiate, E.A., Epstein, L., Alkan, N., *et al.* (2012). Lifestyle transitions in plant pathogenic *Colletotrichum* fungi deciphered by genome and transcriptome analyses. Nature Genetics *44*, 1060-1065.

Okmen, B., Collemare, J., Griffiths, S., van der Burgt, A., Cox, R., and de Wit, P.J. (2014). Functional analysis of the conserved transcriptional regulator CfWor1 in *Cladosporium fulvum* reveals diverse roles in the virulence of plant pathogenic fungi. Molecular Microbiology *92*, 10-27.

Peng, Z., Oliveira-Garcia, E., Lin, G., Hu, Y., Dalby, M., Migeon, P., Tang, H., Farman, M., Cook, D., and White, F.F. (2019). Effector gene reshuffling involves dispensable mini-chromosomes in the wheat blast fungus. PLoS Genetics *15*, e1008272.

Petruk, S., Cai, J., Sussman, R., Sun, G., Kovermann, S.K., Mariani, S.A., Calabretta, B., McMahon, S.B., Brock, H.W., and Iacovitti, L. (2017). Delayed accumulation of H3K27me3 on nascent DNA is essential for recruitment of transcription factors at early stages of stem cell differentiation. Molecular Cell *66*, 247-257. e245.

Pham, K.T., Inoue, Y., Vu, B.V., Nguyen, H.H., Nakayashiki, T., Ikeda, K., and Nakayashiki, H. (2015). MoSET1 (histone H3K4 methyltransferase in *Magnaporthe oryzae*) regulates global gene expression during infection-related morphogenesis. PLoS Genetics *11*, e1005385.

Quinlan, A.R., and Hall, I.M. (2010). BEDTools: a flexible suite of utilities for comparing genomic features. Bioinformatics *26*, 841-842.

Robinson, J.T., Thorvaldsdóttir, H., Winckler, W., Guttman, M., Lander, E.S., Getz, G., and Mesirov, J.P. (2011). Integrative genomics viewer. Nature biotechnology *29*, 24-26.

Saitoh, H., Fujisawa, S., Mitsuoka, C., Ito, A., Hirabuchi, A., Ikeda, K., Irieda, H., Yoshino, K., Yoshida, K., Matsumura, H., *et al.* (2012). Large-scale gene disruption in *Magnaporthe oryzae* identifies MC69, a secreted protein required for infection by monocot and dicot fungal pathogens. PLoS Pathogen *8*, e1002711.

Sanchez-Vallet, A., Fouche, S., Fudal, I., Hartmann, F.E., Soyer, J.L., Tellier, A., and Croll, D. (2018). The Genome Biology of Effector Gene Evolution in Filamentous Plant Pathogens. Annual Review of Phytopathology.

Santhanam, P., and Thomma, B.P. (2013). *Verticillium dahliae* Sge1 differentially regulates expression of candidate effector genes. Molecular Plant-Microbe Interactions *26*, 249-256.

Schneider, C.A., Rasband, W.S., and Eliceiri, K.W. (2012). NIH Image to ImageJ: 25 years of image analysis. Nature Methods *9*, 671.

Soyer, J.L., El Ghalid, M., Glaser, N., Ollivier, B., Linglin, J., Grandaubert, J., Balesdent, M.H., Connolly, L.R., Freitag, M., Rouxel, T., *et al.* (2014). Epigenetic control of effector gene expression in the plant pathogenic fungus *Leptosphaeria maculans*. PLoS Genetics *10*, e1004227.

Soyer, J.L., Grandaubert, J., Haueisen, J., Schotanus, K., and Holtgrewe Stukenbrock, E. (2019). In planta chromatin immunoprecipitation in Zymoseptoria tritici reveals chromatin-based regulation of putative effector gene expression. bioRxiv.

Sperschneider, J., Dodds, P.N., Gardiner, D.M., Singh, K.B., and Taylor, J.M. (2018). Improved prediction of fungal effector proteins from secretomes with EffectorP 2.0. Molecular Plant Pathology *19*, 2094-2110.

Stark, R., and Brown, G. (2011). DiffBind: differential binding analysis of ChIP-Seq peak data. R package version *100*, 4-3.

Tan, K.C., and Oliver, R.P. (2017). Regulation of proteinaceous effector expression in phytopathogenic fungi. PLoS Pathogen *13*, e1006241.

Tollot, M., Assmann, D., Becker, C., Altmuller, J., Dutheil, J.Y., Wegner, C.E., and Kahmann, R. (2016). The WOPR protein Ros1 Is a master regulator of sporogenesis and late effector gene expression in the maize pathogen *Ustilago maydis*. PLoS Pathogen *12*, e1005697.

Valent, B., Farrall, L., and Chumley, F.G. (1991). *Magnaporthe grisea* genes for pathogenicity and virulence identified through a series of backcrosses. Genetics *127*, 87-101.

van der Does, H.C., Duyvesteijn, R.G., Goltstein, P.M., van Schie, C.C., Manders, E.M., Cornelissen, B.J., and Rep, M. (2008). Expression of effector gene *SIX1* of *Fusarium oxysporum* requires living plant cells. Fungal Genetics and Biology *45*, 1257-1264.

Wickham, H. (2016). ggplot2: elegant graphics for data analysis (Springer).

Wilson, R.A., Gibson, R.P., Quispe, C.F., Littlechild, J.A., and Talbot, N.J. (2010). An NADPH-dependent genetic switch regulates plant infection by the rice blast fungus. Proceedings of the National Academy of Sciences *107*, 21902-21907.

Wu, J., Kou, Y., Bao, J., Li, Y., Tang, M., Zhu, X., Ponaya, A., Xiao, G., Li, J., Li, C., *et al.* (2015). Comparative genomics identifies the *Magnaporthe oryzae* avirulence effector

AvrPi9 that triggers Pi9-mediated blast resistance in rice. New Phytologist *206*, 1463-1475.

Yang, Y., Cheng, X., Tian, W., Zhou, B., Wu, X., Xu, H., Fang, F., Fang, M., and Xu, Y. (2014). MRTF-A steers an epigenetic complex to activate endothelin-induced pro-inflammatory transcription in vascular smooth muscle cells. Nucleic Acids Research *42*, 10460-10472.

Tables

Table S2.1. A total of 24 *M. oryzae* effector genes that are repressed during mycelial growth in culture but induced in planta

Gene Name	MGG_#	Chromosome	H3K27me3 enrichment[a]	Repressed in mycelia[b]	Induced in planta[c]	Reference
ACE1	MGG_12447	2	High	+	+, 16hpi	Bohnert et al., 2004; Fudal et al., 2007
AVR-Pi9	MGG_12655	7	Low	+	+, 12hpi	Wu et al., 2015
AVR-Pik	MGG_15972	2	High	+	+, 24hpi	de Guillen et al, 2015; Dong et al., 2015
AVR-Pita1	MGG_15370	6	Low	+	+	Mosquera et al., 2009;
AVRPiz-t	MGG_18041	7	High	+	+, 24 hpi	Li et al., 2009; Park et al., 2012; Dong et al., 2015
BAS1	MGG_04795	1	High	+	+	Mosquera et al., 2009
BAS2	MGG_09693	4	Low	+	+	Mosquera et al., 2009
BAS3	MGG_11610	5	High	+	+, 16hpi, 24hpi,	Mosquera et al., 2009; de Guillen et al, 2015; Mogga et al., 2016
BAS4	MGG_10914	5	High	+	+, 24hpi	Mosquera et al., 2009; Mogga et al., 2016
BAS107	MGG_10020	4	High	+	+	Mosquera et al., 2009; Dong et al., 2015
MAX	MGG_02546	7	High	+	+, 24, 48hpi	Dong et al., 2015; de Guillen et al, 2015
MAX	MGG_08414	2	High	+	+, 24hpi	de Guillen et al, 2015
MAX	MGG_08482	4	High	+	+, 24hpi	de Guillen et al, 2015
MAX	MGG_09675	7	High	+	+, 24hpi	de Guillen et al, 2015; Dong et al., 2015
MoCDIP3	MGG_07986	2	High	+	+, App, 96hpi	Chen et al., 2013
MoCDIP4	MGG_08409	2	Low	+	+, App, and 72hpi	Chen et al., 2013
MoCDIP5	MGG_10234	Unplaced	Low	+	+, App, 96hpi	Chen et al., 2013
MoHEG6	MGG_08506	4	High	+	+, 24hpi	Dong et al., 2015; Mogga et al., 2016
MoHEG9	MGG_00043	5	High	+	+, 24hpi	Mosquera et al., 2009; Dong et al., 2015; Mogga et al., 2016
MoHEG12	MGG_06224	4	High	+	+	Mosquera et al., 2009; Dong et al., 2015; Mogga et al., 2016
PWL2	MGG_04301	6	High	+	+	Sweigard et al., 1995; Mosquera et al., 2009
SLP1	MGG_10097	4	High	+	+	Mentlak et al., 2012; Dong et al., 2015
SPD5	MGG_02154	1	High	+	+	Dong et al., 2015; Sharpee et al., 2017
SPD8	MGG_09379	6	High	+	+	Mosquera et al., 2009; Dong et al., 2015; Sharpee et al., 2017

[a]H3K27me3 enrichment is profiled by ChIP-seq of *M. oryzae* mycelia grown in axenic culture.

[b]Undetectable expression of effector genes either by RT-PCR, qRT-PCR, fluorescent reporter or RNA-seq during fungal growth in axenic culture. "+" means yes.

[c]Induced expression during plant infection process including appressorium stage and invasive growth stage. "+" means yes.

Table S2.2. Phenotypic characterization of *MoKMT6* knock-out and *MoGti1* overexpression strains

Strain	Mycelial growth (mm)[a]	Conidiation (x10^5/mL)[b]	Conidia germination (%)[c]	Appressorium formation(%)[d]
Wild-type	69.0 ± 2.2	12.8 ± 4.1	99.0 ± 2.73	99.2 ± 1.27
Δmokmt6	66.9 ± 0.50	0.15 ± 0.05**	98.4 ± 2.97	93.7 ± 11.2*
Δmokmt6-MoKMT6	67.5 ± 1.5	3.3 ± 1.1*	98.5 ± 3.5	97.5 ± 3.54
MoGti1oe	59 ± 1.2**	14.3 ± 4.8	98.1 ± 2.87	96.4 ± 3.43*

[a]Vegetative growth of fungal mycelia was measured at 14 days post-inoculation on complete medium plates.

[b]Conidia were counted after 12 days of growth on 5cm of OMA media incubated at 24°C under continues light. Conidia were harvested by suspending them with 5 ml of distilled water per plate.

[c]Germination rate was measured 21-25 hours after inoculating on hydrophobic glass coverslips with conidia from 12-day-old OMA cultures. Germination rate was measured as the percentage ratio of germinated conidia to all counted conidia.

[d]Appressorium formation rates were calculated 21-25 hours after inoculating on glass coverslips from 12-day-old OMA cultures under a confocal microscope. Appressorium formation rate was measured as the percentage ratio of mature appressoria to germinated conidia.

All data are presented as means ± SD from four biological replicates. Data were analyzed with two-tailed student t-test. *, $p<0.05$; **, $p<0.01$.

Table S2.3. Summary of qRT-PCR tested effector genes in different fungal strains

Effector	MGG#	H3K27me enrichment	Induced in *Δmokmt6* (+:Yes, -:No)	Regulated by MoGti1	Relative expression (qRT-PCR, Log_2Fold change)			Relative expression (RNA-seq, Log_2FC)		
					Δmokmt6	MoGti1oe	*Δmokmt6*-MoGti1oe	*Δmokmt6*	MoGti1oe	*Δmokmt6*-MoGti1oe
AVR-Pik	MGG_15972	High	+	Positive	4.2	0.8	7.8	NA	NA	4.9
BAS4	MGG_10914	High	+	Positive	7.3	8.0	14.3	3.9	5.2	10.6
BAS3	MGG_11610	High	+	Positive	2.1	2.1	6.2	2.0	2.2	6.1
PWL2	MGG_04301	High	+	Positive	1.8	2.8	7.9	NA	NA	NA
AVRPiz-t	MGG_18041	High	+	No influence	7.6	NC	7.9	6.8	NC	6.8
ACE1	MGG_12447	High	+	No influence	3.4	NC	2.6	5.3	NC	4.8
Slp1	MGG_10097	High	+	No influence	4.4	NC	5.3	4.9	NC	7.0
MC69	MGG_02848	Low	-	No influence	NC	NC	NC	NC	NC	NC
AVR-Pi9	MGG_12655	Low	+	Negative	2.4	-2.3	NC	2.4	-5.1	NC

NA means Log_2Fold change is not available. Quantification of expression data in RNA-seq is impacted by lack of reads in wild-type.

NC means there is no change for expressions compared to wild-type ($p>0.05$).

Table S2.4. Percentage of up-/down-regulated genes and effector genes during mycelial growth of different strains

		Up-regulated[d]			Down-regulated[d]		
		Δ*mokmt6* vs. wt	**MoGti1oe vs. wt**	**Δ*mokmt6*-MoGti1oe vs. wt**	**Δ*mokmt6* vs. wt**	**MoGti1oe vs. wt**	**Δ*mokmt6*-MoGti1oe vs. wt**
Whole-genome (13144)[a]		1858 (14.1%)	1524 (11.6%)	2979 (22.7%)	935 (7.1%)	1228 (9.3%)	2098 (16.0%)
Effector genes (448)	Predicted effectors[b]	110 (24.6%)	60 (13.4%)	167 (37.3%)	19 (4.2%)	25 (5.6%)	31 (6.9%)
	Known effectors[c]	15 (3.3%)	3 (0.7%)	16 (3.6%)	0	1 (0.2%)	0

[a]Total number of genes with MGG_#: 13144

[b]Total number of effector genes that are predicted by EffectorP: 424

[c]Total number of known effector genes of which expression are repressed in mycelia: 24

[d]Up regulated genes: Log_2foldchange>0; Down regulated genes: Log_2foldchange<0.

padjusted <0.05

Table S2.5. High percentage of H3K27me3-enriched effector genes are upregulated in Δ*mokmt6* mycelia and at 36hpi of WT

	Up-regulated in mycelia ($Log_2FC>2$)			**Up-regulated in planta (36hpi)[d] ($Log_2FC>2$)**
	Δ*mokmt6* vs. wt	**MoGti1oe vs. wt**	**Δ*mokmt6*-MoGti1oe vs. wt**	**WT**
Whole-genome (13144)[a]	1053 (8.0%)	462 (3.5%)	1470 (11.2%)	1351 (10.3%)
H3K27me3-enriched effector genes (178)[b]	75 (42.1%)	23 (12.9%)	97 (54.5%)	86 (48.3%)
H3K27me3-unenriched effector genes (268)[c]	31 (11.6%)	21 (7.8%)	58 (21.6%)	65 (24.3%)

[a]Total number of genes with MGG_#: 13144

[b]Total number of effector genes which show high enrichment of H3K27me3 during mycelial growth: 178

[c]Total number of effector genes which show low enrichment of H3K27me3 during mycelial growth: 268

[d]Data is from Mosquera et al., 2009.

padjusted <0.05

Table S2.6. Majority of effector genes upregulated both in *Δmokmt6* mycelia and at 36hpi of WT show high enrichment of H3K27me3 during mycelial growth

#	MGG_#	H3K27me3	Note
1	MGG_01956	High	
2	MGG_02154	High	*SPD5*
3	MGG_05424	High	
4	MGG_06224	High	*MoHEG12*
5	MGG_07357	High	
6	MGG_07880	High	
7	MGG_07919	High	
8	MGG_08355	High	
9	MGG_08399	High	
10	MGG_08414	High	*MAX*
11	MGG_08480	High	
12	MGG_08482	High	*MAX*
13	MGG_08506	High	*MoHEG6*
14	MGG_08610	High	
15	MGG_08817	High	
16	MGG_09378	High	
17	MGG_10318	High	
18	MGG_10455	High	
19	MGG_10477	High	
20	MGG_10914	High	*BAS4*
21	MGG_11072	High	
22	MGG_15046	High	
23	MGG_15443	High	
24	MGG_15620	High	
25	MGG_15924	High	
26	MGG_16041	High	
27	MGG_16058	High	
28	MGG_16585	High	
29	MGG_16619	High	
30	MGG_16693	High	
31	MGG_16698	High	
32	MGG_17244	High	
33	MGG_17556	High	
34	MGG_17567	High	
35	MGG_17582	High	
36	MGG_18035	High	
37	MGG_18041	High	*AVRPiz-t*
38	MGG_02239	Low	
39	MGG_05403	Low	
40	MGG_07556	Low	
41	MGG_08407	Low	
42	MGG_08428	Low	
43	MGG_08435	Low	
44	MGG_09377	Low	
45	MGG_09693	Low	*BAS2*
46	MGG_12655	Low	*AVR-Pi9*

[a]H3K27me3 enrichment is profiled by ChIP-seq of *M. oryzae* mycelia grown in axenic culture.

Table S2.7. Majority of synergistically upregulated effector genes by H3K27me3 loss and MoGti1 overexpression are also upregulated at 36hpi of WT

#	MGG_#	Fold change			Synergistically up-regulated[a] (+:Yes; -:No)	Induced at 36 hpi[b] (+:Yes; -:No)	H3K27me3 enrichment[c]
		Δ*mokmt6*	MoGti1oe	Δ*mokmt6*-MoGti1oe			
1	MGG_01956	5.8	4.4	48.4	+	+	High
2	MGG_08355	44.9	21.5	309.3	+	+	High
3	MGG_08399	388.2	71.4	1651.4	+	+	High
4	MGG_08480	167.9	231.7	725.5	+	+	High
5	MGG_08610	913.7	187.0	2591.7	+	+	High
6	MGG_10455	38.3	100.3	1783.1	+	+	High
7	MGG_10914(*BAS4*)	14.8	37.6	1531.8	+	+	High
8	MGG_11072	386.8	712.5	1114.4	+	+	High
9	MGG_11610(*BAS3*)	4.0	4.7	69.2	+	+	High
10	MGG_15046	70.8	19.2	400.4	+	+	High
11	MGG_15620	19.4	11.0	2494.7	+	+	High
12	MGG_16057	3.7	3.6	10.4	+	+	High
13	MGG_16058	108.6	8.7	194.0	+	+	High
14	MGG_16585	17.2	37.0	1374.2	+	+	High
15	MGG_17556	5.1	6.0	19.0	+	+	High
16	MGG_18035	21.0	20.4	54.7	+	+	High
17	MGG_08428	33.0	61.6	763.6	+	+	Low
18	MGG_08376	23.0	7.6	89.6	+	-	Low
19	MGG_08941	4.4	7.0	12.4	+	-	Low
20	MGG_10456	7.2	2.1	11.2	+	-	Low
21	MGG_17580	32.1	5.6	340.0	+	-	High
22	MGG_02154(*SPD5*)	9.1	60.4	58.3	-	+	High
23	MGG_00614	2.1	5.0	3.9	-	+	Low
24	MGG_01974	1.8	2.1	3.6	-	+	Low
25	MGG_05531	2.2	2.5	1.3[d]	-	+	Low
26	MGG_07556	37.3	3.4	33.2	-	+	Low
27	MGG_07558	9.9	4.7	1.3[d]	-	-	High
28	MGG_16188	2.2	4.2	5.4	-	-	High
29	MGG_16553	192.3	19.4	52.2	-	-	High
30	MGG_05406	1.8	1.6	1.7	-	-	Low
31	MGG_05982	25.5	3.3	10.2	-	-	Low
32	MGG_08543	8.6	2.9	4.5	-	-	Low
33	MGG_09842	7.7	102.6	1.8[d]	-	-	Low
34	MGG_10531	41.9	56.2	50.4	-	-	Low
35	MGG_14195	44.5	15.9	36.3	-	-	Low
36	MGG_16869	2.2	7.5	7.5	-	-	Low

[a]Synergistically upregulated effector genes are defined that expression levels of effector genes in *Δmokmt6*-MoGti1oe are higher than the sum of individual expression levels in *Δmokmt6* mutant and MoGti1oe, respectively.

[b]Data is from Mosquera et al., 2009

[c]H3K27me3 enrichment is profiled by ChIP-seq of *M. oryzae* mycelia grown in axenic culture.

[d]Not statistically significant (padjusted>0.05).

Table S2.8. Summary of expression data for 448 known and predicted effector genes of *M. oryzae* O-137

			Differential Expression RNA-seq samples				Overlap between RNA-seq samples and 36hpi in planta microarray data		
Input ID	**Transcript Product Description**	**H3K27me3 enrichment status**	**Differential Expression in Δ*mokmt6* strain**	**Differential Expression in MoGti1oe strain**	**Differential Expression in Δ*mokmt6*-MoGti1oe strain**	**Expression Change in 36hpi microarray data**	**Overlap between Δ*mokmt6* and 36hpi**	**Overlap between MoGti1oe and 36hpi**	**Overlap between Δ*mokmt6*-MoGti1oe and 36hpi**
MGG_00043	MoHEG9	Enriched	No Change	No Change	No Change	Up≥2fold	-	-	-
MGG_00225	hypothetical protein	Enriched	No Change	No Change	No Change	Down<2fold	-	-	-
MGG_00230	hypothetical protein	Enriched	No Change	Up	Up	Up≥2fold	-	+	+
MGG_00269	hypothetical protein	Enriched	Up	No Change	Up	Down<2fold	-	-	-
MGG_00281	hypothetical protein	Enriched	Up	No Change	Up	Down<2fold	-	-	-
MGG_00305	hypothetical protein	Enriched	No Change	No Change	No Change	Down<2fold	-	-	-
MGG_01956	hypothetical protein	Enriched	Up	Up	Up	Up≥2fold	+	+	+
MGG_01964	hypothetical protein	Enriched	No Change	No Change	Up	Up≥2fold	-	-	-
MGG_02139	hypothetical protein	Enriched	Up	No Change	Up	Down<2fold	-	-	-
MGG_02154	SPD5	Enriched	Up	Up	Up	Up< 2fold	+	+	+
MGG_02166	hypothetical protein	Enriched	No Change	No Change	Up	Down<2fold	-	-	+
MGG_02207	hypothetical protein	Enriched	Up	No Change	Up	Down<2fold	-	-	-
MGG_02222	hypothetical protein	Enriched	No Change	No Change	Up	Down<2fold	-	-	-
MGG_02223	BAS4c	Enriched	Up	No Change	Up	Down≥2fold	-	-	+
MGG_02339	hypothetical protein	Enriched	No Change	No Change	No Change	Down<2fold	-	-	-
MGG_02546	MAX	Enriched	No Change	No Change	No Change	Up≥2fold	-	-	-
MGG_02590	hypothetical protein	Enriched	Up	No Change	Up	N/A	-	-	-
MGG_04258	hypothetical protein	Enriched	No Change	Down	Down	Down<2fold	-	-	-
MGG_04259	hypothetical protein	Enriched	No Change	No Change	No Change	N/A	-	-	-
MGG_04301	PWL2	Enriched	No Change	No Change	No Change	N/A	-	-	-
MGG_04546	hypothetical protein	Enriched	No Change	No Change	No Change	Down≥2fold	-	-	-
MGG_04735	hypothetical protein	Enriched	No Change	No Change	No Change	Down≥2fold	-	-	-
MGG_04795	BAS1	Enriched	No Change	No Change	No Change	Up≥2fold	-	-	-
MGG_05389	hypothetical protein	Enriched	No Change	No Change	No Change	Down≥2fold	-	-	-
MGG_05410	hypothetical protein	Enriched	No Change	No Change	Up	Up≥2fold	-	-	+
MGG_05424	hypothetical protein	Enriched	Up	No Change	No Change	Up≥2fold	+	-	-
MGG_05608	hypothetical protein	Enriched	No Change	No Change	No Change	Down<2fold	-	-	-
MGG_06231	hypothetical protein	Enriched	Up	No Change	No Change	Down<2fold	-	-	-
MGG_06234	hypothetical protein	Enriched	Up	No Change	Up	Down<2fold	-	-	-
MGG_06359	hypothetical protein	Enriched	No Change	No Change	No Change	Down<2fold	-	-	-
MGG_07357	hypothetical protein	Enriched	Up	No Change	Up	Up≥2fold	+	-	+
MGG_07363	hypothetical protein	Enriched	Up	No Change	Up	Down<2fold	-	-	-
MGG_07372	hypothetical protein	Enriched	No Change	No Change	No Change	Down<2fold	-	-	-
MGG_07411	MoHEG17	Enriched	Up	No Change	No Change	N/A	-	-	-
MGG_07424	hypothetical protein	Enriched	No Change	No Change	Up	Down<2fold	-	-	-
MGG_07566	hypothetical protein	Enriched	No Change	No Change	No Change	Down<2fold	-	-	-
MGG_07625	hypothetical protein	Enriched	No Change	Up	Up	Down<2fold	-	-	-
MGG_07715	hypothetical protein	Enriched	No Change	No Change	Down	Down≥2fold	-	-	-
MGG_07834	hypothetical protein	Enriched	No Change	No Change	No Change	Up≥2fold	-	-	-
MGG_07871	hypothetical protein	Enriched	Up	No Change	Up	Down<2fold	-	-	-
MGG_07880	hypothetical protein	Enriched	Up	No Change	Up	Up≥2fold	+	-	+
MGG_07900	hypothetical protein	Enriched	No Change	No Change	Up	Down≥2fold	-	-	+
MGG_07955	endo-1,4-beta-xylanase I	Enriched	No Change	No Change	Up	Down<2fold	-	-	-
MGG_07993	hypothetical protein	Enriched	Up	No Change	Up	Down<2fold	-	-	-
MGG_07994	hypothetical protein	Enriched	No Change	No Change	Up	N/A	-	-	-
MGG_08020	endoglucanase-4	Enriched	No Change	No Change	Down	Down<2fold	-	-	-
MGG_08230	hypothetical protein	Enriched	No Change	No Change	No Change	Up≥2fold	-	-	-
MGG_08373	hypothetical protein	Enriched	No Change	Down	Down	Down<2fold	-	-	-

MGG_08407	hypothetical protein	Enriched	Up	No Change	Up	Up≥2fold	+	-	+
MGG_08424	endo-1,4-beta-xylanase I	Enriched	No Change	No Change	Up	Down<2fold	-	-	-
MGG_08435	hypothetical protein	Enriched	Up	No Change	Up	Down≥2fold	+	-	+
MGG_08480	alpha/beta hydrolase	Enriched	Up	Up	Up	Down≥2fold	+	+	+
MGG_08481	hypothetical protein	Enriched	Up	No Change	Up	Down<2fold	-	-	-
MGG_08482	MAX	Enriched	Up	No Change	Up	Up≥2fold	+	-	+
MGG_08506	MoHEG6	Enriched	Up	No Change	Up	Up≥2fold	+	-	+
MGG_08529	hypothetical protein	Enriched	No Change	No Change	No Change	Down<2fold	-	-	-
MGG_08543	hypothetical protein	Enriched	Up	Up	Up	Down<2fold	-	-	-
MGG_08609	hypothetical protein	Enriched	Up	No Change	Up	Down<2fold	-	-	-
MGG_08610	hypothetical protein	Enriched	Up	Up	Up	Down≥2fold	+	+	+
MGG_08789	hypothetical protein	Enriched	Up	No Change	Up	Down<2fold	-	-	-
MGG_08817	hypothetical protein	Enriched	Up	Down	No Change	Up≥2fold	+	-	-
MGG_08818	hypothetical protein	Enriched	No Change	No Change	No Change	Down<2fold	-	-	-
MGG_08941	hypothetical protein	Enriched	Up	Up	Up	Down<2fold	-	-	-
MGG_09109	hypothetical protein	Enriched	No Change	No Change	No Change	Down<2fold	-	-	-
MGG_09321	hypothetical protein	Enriched	Down	Up	Up	Up≥2fold	-	+	+
MGG_09379	SPD8	Enriched	No Change	No Change	Up	N/A	-	-	-
MGG_09387	MoHEG8	Enriched	No Change	No Change	Up	N/A	-	-	-
MGG_09425	MAX	Enriched	No Change	No Change	No Change	Down≥2fold	-	-	-
MGG_09439	hypothetical protein	Enriched	No Change	No Change	No Change	Down<2fold	-	-	-
MGG_09452	hypothetical protein	Enriched	No Change	No Change	No Change	Down<2fold	-	-	-
MGG_09675	MAX	Enriched	No Change	No Change	Up	Up≥2fold	-	-	+
MGG_09693	BAS2	Enriched	Up	No Change	Up	Up≥2fold	+	-	+
MGG_09842	hypothetical protein	Enriched	Up	Up	No Change	Down<2fold	-	-	-
MGG_09848	hypothetical protein	Enriched	No Change	No Change	Up	Down<2fold	-	-	-
MGG_09998	hypothetical protein	Enriched	No Change	No Change	No Change	Down<2fold	-	-	-
MGG_10020	BAS107	Enriched	No Change	No Change	No Change	Up≥2fold	-	-	-
MGG_10026	cystein rich protein	Enriched	No Change	No Change	Up	Down<2fold	-	-	-
MGG_10097	SLP1/intracellular hyphae protein 1	Enriched	Up	No Change	Up	Down<2fold	-	-	-
MGG_10120	hypothetical protein	Enriched	No Change	No Change	No Change	Up≥2fold	-	-	-
MGG_10217	hypothetical protein	Enriched	Up	No Change	Up	Down<2fold	-	-	-
MGG_10231	hypothetical protein	Enriched	Up	No Change	Up	Down<2fold	-	-	-
MGG_10234	MoCDIP5	Enriched	Up	No Change	Up	Down<2fold	-	-	-
MGG_10315	hydrophobin-like protein MPG1	Enriched	No Change	Down	Down	Down<2fold	-	-	-
MGG_10335	SPD7	Enriched	No Change	No Change	No Change	Down<2fold	-	-	-
MGG_10394	hypothetical protein	Enriched	Down	Down	Down	Down<2fold	-	-	-
MGG_10456	hypothetical protein	Enriched	Up	Up	Up	Down<2fold	-	-	-
MGG_10531	hypothetical protein	Enriched	Up	Up	Up	Down<2fold	-	-	-
MGG_10774	hypothetical protein	Enriched	No Change	No Change	No Change	N/A	-	-	-
MGG_10914	BAS4	Enriched	Up	Up	Up	Up≥2fold	+	+	+
MGG_11072	hypothetical protein	Enriched	Up	Up	Up	Up≥2fold	+	+	+
MGG_11091	hypothetical protein	Enriched	Up	No Change	No Change	Down<2fold	-	-	-
MGG_11610	BAS3	Enriched	Up	Up	Up	Up≥2fold	-	+	+
MGG_11627	hypothetical protein	Enriched	No Change	No Change	Up	N/A	-	-	-
MGG_12016	hypothetical protein	Enriched	Up	Down	Down	Down<2fold	-	-	-
MGG_12445	hypothetical protein	Enriched	No Change	No Change	No Change	N/A	-	-	-
MGG_12447	ACE1/polyketide synthase/peptide synthetase	Enriched	Up	No Change	Up	Down<2fold	-	-	-
MGG_12509	hypothetical protein	Enriched	No Change	No Change	Up	Down<2fold	-	-	-
MGG_12930	hypothetical protein	Enriched	No Change	No Change	No Change	N/A	-	-	-
MGG_13868	hypothetical protein	Enriched	No Change	No Change	No Change	N/A	-	-	-
MGG_14006	hypothetical protein	Enriched	No Change	No Change	No Change	Down<2fold	-	-	-
MGG_14156	hypothetical protein	Enriched	No Change	No Change	No Change	N/A	-	-	-
MGG_14195	hypothetical protein	Enriched	Up	Up	Up	N/A	-	-	-
MGG_14344	hypothetical protein	Enriched	No Change	No Change	No Change	Up≥2fold	-	-	-
MGG_14374	hypothetical protein	Enriched	No Change	No Change	Up	N/A	-	-	-
MGG_14422	SPD4	Enriched	Up	Down	Up	N/A	-	-	-

MGG_14600	hypothetical protein	Enriched	No Change	No Change	No Change	Down<2fold	-	-	-
MGG_14830	hypothetical protein	Enriched	Up	No Change	Up	N/A	-	-	-
MGG_14965	MoHEG4	Enriched	No Change	No Change	No Change	N/A	-	-	-
MGG_15031	hypothetical protein	Enriched	No Change	No Change	Up	Down<2fold	-	-	-
MGG_15044	SPD9	Enriched	No Change	No Change	No Change	N/A	-	-	-
MGG_15046	hypothetical protein	Enriched	Up	Up	Up	Down≥2fold	+	+	+
MGG_15212	null	Enriched	No Change	No Change	No Change	Down<2fold	-	-	-
MGG_15371	hypothetical protein	Enriched	No Change	No Change	Up	N/A	-	-	-
MGG_15376	hypothetical protein	Enriched	No Change	No Change	No Change	Down≥2fold	-	-	-
MGG_15391	hypothetical protein	Enriched	No Change	No Change	No Change	Down<2fold	-	-	-
MGG_15443	hypothetical protein	Enriched	Up	No Change	Up	Up≥2fold	+	-	+
MGG_15458	hypothetical protein	Enriched	No Change	No Change	No Change	N/A	-	-	-
MGG_15459	hypothetical protein	Enriched	No Change	No Change	Up	N/A	-	-	-
MGG_15620	hypothetical protein	Enriched	Up	Up	Up	Down≥2fold	+	+	+
MGG_15625	hypothetical protein	Enriched	Up	No Change	Up	Down<2fold	-	-	-
MGG_15793	hypothetical protein	Enriched	Up	No Change	No Change	N/A	-	-	-
MGG_15908	hypothetical protein	Enriched	No Change	No Change	No Change	Down<2fold	-	-	-
MGG_15911	hypothetical protein	Enriched	No Change	No Change	No Change	Down<2fold	-	-	-
MGG_15924	hypothetical protein	Enriched	Up	No Change	Up	Up≥2fold	+	-	+
MGG_15972	AVR-Pik	Enriched	No Change	No Change	Up	Up≥2fold	-	-	+
MGG_15973	hypothetical protein	Enriched	No Change	No Change	No Change	N/A	-	-	-
MGG_16041	hypothetical protein	Enriched	Up	No Change	Up	Down≥2fold	+	-	+
MGG_16057	hypothetical protein	Enriched	Up	Up	Up	Down≥2fold	-	-	+
MGG_16058	hypothetical protein	Enriched	Up	Up	Up	Up≥2fold	+	+	+
MGG_16059	hypothetical protein	Enriched	No Change	No Change	No Change	Down<2fold	-	-	-
MGG_16080	hypothetical protein	Enriched	Up	No Change	No Change	Down<2fold	-	-	-
MGG_16171	hypothetical protein	Enriched	No Change	No Change	No Change	Up≥2fold	-	-	-
MGG_16175	hypothetical protein	Enriched	Down	Up	No Change	Up≥2fold	-	+	-
MGG_16188	hypothetical protein	Enriched	Up	Up	Up	Down<2fold	-	-	-
MGG_16382	hypothetical protein	Enriched	No Change	Up	No Change	Down<2fold	-	-	-
MGG_16404	hypothetical protein	Enriched	Up	No Change	Up	Down<2fold	-	-	-
MGG_16422	hypothetical protein	Enriched	No Change	No Change	No Change	N/A	-	-	-
MGG_16475	hypothetical protein	Enriched	No Change	No Change	No Change	Down<2fold	-	-	-
MGG_16489	hypothetical protein	Enriched	No Change	No Change	No Change	Up≥2fold	-	-	-
MGG_16545	hypothetical protein	Enriched	No Change	No Change	No Change	N/A	-	-	-
MGG_16553	hypothetical protein	Enriched	Up	Up	Up	N/A	-	-	-
MGG_16562	hypothetical protein	Enriched	No Change	No Change	No Change	N/A	-	-	-
MGG_16585	hypothetical protein	Enriched	Up	Up	Up	Up< 2fold	+	+	+
MGG_16593	hypothetical protein	Enriched	No Change	No Change	No Change	N/A	-	-	-
MGG_16603	hypothetical protein	Enriched	No Change	No Change	Up	Down<2fold	-	-	-
MGG_16647	hypothetical protein	Enriched	No Change	No Change	Up	Up< 2fold	-	-	+
MGG_16660	hypothetical protein	Enriched	Up	No Change	Up	Down<2fold	-	-	-
MGG_16693	hypothetical protein	Enriched	Up	No Change	Up	Up≥2fold	+	-	+
MGG_16698	hypothetical protein	Enriched	Up	No Change	Up	Up≥2fold	+	-	+
MGG_16759	hypothetical protein	Enriched	No Change	No Change	No Change	Down≥2fold	-	-	-
MGG_16789	hypothetical protein	Enriched	No Change	No Change	No Change	Down≥2fold	-	-	-
MGG_16953	hypothetical protein	Enriched	No Change	No Change	No Change	Down≥2fold	-	-	-
MGG_17028	hypothetical protein	Enriched	No Change	No Change	No Change	Down<2fold	-	-	-
MGG_17237	hypothetical protein	Enriched	No Change	No Change	No Change	N/A	-	-	-
MGG_17240	hypothetical protein	Enriched	No Change	No Change	No Change	Down≥2fold	-	-	-
MGG_17244	hypothetical protein	Enriched	Up	No Change	Up	Down≥2fold	+	-	+
MGG_17249	hypothetical protein	Enriched	No Change	No Change	Up	Up≥2fold	-	-	+
MGG_17250	hypothetical protein	Enriched	No Change	No Change	No Change	Up≥2fold	-	-	-
MGG_17255	hypothetical protein	Enriched	No Change	No Change	No Change	Down<2fold	-	-	-
MGG_17266	hypothetical protein	Enriched	No Change	Up	Up	Down≥2fold	-	-	+
MGG_17303	hypothetical protein	Enriched	Up	No Change	No Change	Down<2fold	-	-	-
MGG_17556	hypothetical protein	Enriched	Up	Up	Up	Up≥2fold	+	+	+
MGG_17563	hypothetical protein	Enriched	No Change	No Change	Up	Down≥2fold	-	-	+
MGG_17567	hypothetical protein	Enriched	Up	No Change	Up	Down<2fold	+	-	+

MGG_17579	hypothetical protein	Enriched	No Change	No Change	Up	Down<2fold	-	-	-
MGG_17580	hypothetical protein	Enriched	Up	Up	Up	Down<2fold	-	-	-
MGG_17582	hypothetical protein	Enriched	Up	No Change	Up	Up≥2fold	+	-	+
MGG_17597	hypothetical protein	Enriched	No Change	No Change	No Change	Down<2fold	-	-	-
MGG_17628	hypothetical protein	Enriched	No Change	No Change	No Change	Up≥2fold	-	-	-
MGG_17767	hypothetical protein	Enriched	No Change	No Change	Up	N/A	-	-	-
MGG_17799	hypothetical protein	Enriched	No Change	No Change	No Change	Down<2fold	-	-	-
MGG_17800	hypothetical protein	Enriched	No Change	No Change	No Change	Down<2fold	-	-	-
MGG_18020	hypothetical protein	Enriched	No Change	No Change	Up	Down≥2fold	-	-	+
MGG_18035	hypothetical protein	Enriched	Up	Up	Up	Up< 2fold	+	+	+
MGG_18041	AVRPiz-t	Enriched	Up	No Change	Up	Up< 2fold	+	-	+
MGG_18062	hypothetical protein	Enriched	No Change	No Change	No Change	Down≥2fold	-	-	-
MGG_18078	hypothetical protein	Enriched	No Change	No Change	No Change	N/A	-	-	-
MGG_18122	hypothetical protein	Enriched	No Change	No Change	Up	Down<2fold	-	-	-
MGG_18140	hypothetical protein	Enriched	Up	No Change	Up	Down<2fold	-	-	-
MGG_00052	hypothetical protein	Unenriched	No Change	No Change	Down	Down<2fold	-	-	-
MGG_00081	hypothetical protein	Unenriched	No Change	No Change	Up	Up≥2fold	-	-	-
MGG_00148	hypothetical protein	Unenriched	Down	No Change	Down	N/A	-	-	-
MGG_00245	hypothetical protein	Unenriched	No Change	Down	Up	Up≥2fold	-	-	+
MGG_00283	hypothetical protein	Unenriched	No Change	Down	Up	Down<2fold	-	-	-
MGG_00321	hypothetical protein	Unenriched	No Change	No Change	No Change	Down<2fold	-	-	-
MGG_00380	hypothetical protein	Unenriched	No Change	No Change	No Change	N/A	-	-	-
MGG_00511	hypothetical protein	Unenriched	No Change	No Change	No Change	Down<2fold	-	-	-
MGG_00614	hypothetical protein	Unenriched	Up	Up	Up	Up≥2fold	-	+	-
MGG_00618	pectinesterase	Unenriched	No Change	No Change	No Change	Down<2fold	-	-	-
MGG_00677	endoglucanase-1	Unenriched	Down	No Change	Down	Down<2fold	-	-	-
MGG_00703	MAS3 protein	Unenriched	No Change	Down	No Change	Down≥2fold	-	-	-
MGG_00732	hypothetical protein	Unenriched	No Change	No Change	No Change	Down<2fold	-	-	-
MGG_00737	MoHEG5	Unenriched	No Change	Down	No Change	Down<2fold	-	-	-
MGG_00992	hypothetical protein	Unenriched	No Change	No Change	Up	Down≥2fold	-	-	-
MGG_01149	MoHEG16	Unenriched	No Change	No Change	Up	Down<2fold	-	-	-
MGG_01173	hydrophobin	Unenriched	No Change	No Change	No Change	Down<2fold	-	-	-
MGG_01188	hypothetical protein	Unenriched	No Change	No Change	No Change	Down<2fold	-	-	-
MGG_01195	acetylesterase	Unenriched	Up	Down	Down	N/A	-	-	-
MGG_01328	endoglucanase	Unenriched	No Change	Up	Up	Down<2fold	-	-	-
MGG_01367	hypothetical protein	Unenriched	Up	No Change	No Change	Down<2fold	-	-	-
MGG_01403	fungal cellulose binding domain-containing protein	Unenriched	No Change	Up	Up	Down<2fold	-	-	-
MGG_01455	hypothetical protein	Unenriched	No Change	No Change	No Change	Up< 2fold	-	-	-
MGG_01530	hypothetical protein	Unenriched	No Change	No Change	No Change	Down<2fold	-	-	-
MGG_01542	glycosyl hydrolase family 10	Unenriched	Down	Down	Down	Down<2fold	-	-	-
MGG_01575	hypothetical protein	Unenriched	No Change	Down	No Change	Down<2fold	-	-	-
MGG_01851	hypothetical protein	Unenriched	Up	No Change	Down	Down<2fold	-	-	-
MGG_01974	hypothetical protein	Unenriched	Down	Up	Up	Up< 2fold	-	-	-
MGG_01986	hypothetical protein	Unenriched	Down	No Change	Up	Up≥2fold	-	-	-
MGG_01993	hypothetical protein	Unenriched	No Change	No Change	No Change	N/A	-	-	-
MGG_01994	hypothetical protein	Unenriched	No Change	No Change	No Change	Down<2fold	-	-	-
MGG_02073	hypothetical protein	Unenriched	No Change	No Change	No Change	Up≥2fold	-	-	-
MGG_02090	hypothetical protein	Unenriched	No Change	Up	Up	Up≥2fold	-	+	+
MGG_02234	hypothetical protein	Unenriched	No Change	No Change	Down	Down<2fold	-	-	-
MGG_02239	MoHEG14	Unenriched	Up	No Change	No Change	Up≥2fold	+	-	-
MGG_02338	hypothetical protein	Unenriched	No Change	No Change	No Change	Down<2fold	-	-	-
MGG_02635	hypothetical protein	Unenriched	No Change	No Change	No Change	Down≥2fold	-	-	-
MGG_02638	hypothetical protein	Unenriched	No Change	Down	Down	Down<2fold	-	-	-
MGG_02715	hypothetical protein	Unenriched	No Change	No Change	No Change	Down≥2fold	-	-	-
MGG_02848	MC69	Unenriched	No Change	No Change	No Change	Down≥2fold	-	-	-
MGG_02918	hypothetical protein	Unenriched	No Change	Up	Up	Down<2fold	-	-	-
MGG_02989	hypothetical protein	Unenriched	No Change	No Change	No Change	Down<2fold	-	-	-
MGG_02990	hypothetical protein	Unenriched	No Change	No Change	No Change	Up≥2fold	-	-	-

MGG_03072	DNA-directed RNA polymerase III subunit RPC10	Unenriched	No Change	No Change	No Change	Down<2fold	-	-	-
MGG_03079	hypothetical protein	Unenriched	No Change	No Change	No Change	Down<2fold	-	-	-
MGG_03085	hypothetical protein	Unenriched	No Change	No Change	No Change	Down<2fold	-	-	-
MGG_03308	hypothetical protein	Unenriched	No Change	No Change	Up	Down<2fold	-	-	-
MGG_03315	hypothetical protein	Unenriched	No Change	No Change	No Change	Down<2fold	-	-	-
MGG_03326	hypothetical protein	Unenriched	Down	Down	No Change	Down<2fold	-	-	-
MGG_03338	cellulose-binding protein	Unenriched	No Change	No Change	No Change	Down<2fold	-	-	-
MGG_03350	cu/Zn superoxide dismutase	Unenriched	No Change	No Change	No Change	Down<2fold	-	-	-
MGG_03356	MoCDIP1/ricin B lectin:Parallel beta-helix	Unenriched	No Change	No Change	Down	Down<2fold	-	-	-
MGG_03369	hypothetical protein	Unenriched	No Change	No Change	No Change	Down≥2fold	-	-	-
MGG_03439	acid phosphatase	Unenriched	No Change	Up	Up	Up≥2fold	-	-	+
MGG_03461	chitin deacetylase	Unenriched	No Change	No Change	No Change	Down<2fold	-	-	-
MGG_03466	hypothetical protein	Unenriched	No Change	No Change	No Change	Down<2fold	-	-	-
MGG_03495	hypothetical protein	Unenriched	Down	No Change	Down	Down<2fold	-	-	-
MGG_03507	hypothetical protein	Unenriched	No Change	No Change	No Change	Down<2fold	-	-	-
MGG_03671	hypothetical protein	Unenriched	No Change	No Change	Up	Down≥2fold	-	-	-
MGG_03685	AVR-Pi54	Unenriched	Down	Down	Down	Down<2fold	-	-	-
MGG_03806	hypothetical protein	Unenriched	Up	No Change	Up	Down<2fold	-	-	-
MGG_04057	hypothetical protein	Unenriched	No Change	No Change	No Change	Down<2fold	-	-	-
MGG_04208	hypothetical protein	Unenriched	No Change	No Change	No Change	Down<2fold	-	-	-
MGG_04348	pectate lyase	Unenriched	Up	No Change	Up	N/A	-	-	-
MGG_04354	hypothetical protein	Unenriched	No Change	No Change	No Change	Down<2fold	-	-	-
MGG_04355	hypothetical protein	Unenriched	No Change	No Change	No Change	Down<2fold	-	-	-
MGG_04384	hypothetical protein	Unenriched	No Change	No Change	No Change	Down<2fold	-	-	-
MGG_04439	endosomal protein P24B	Unenriched	No Change	No Change	Down	Down<2fold	-	-	-
MGG_04451	hypothetical protein	Unenriched	No Change	No Change	No Change	Down<2fold	-	-	-
MGG_04507	synbindin	Unenriched	No Change	No Change	No Change	Down<2fold	-	-	-
MGG_04547	endoglucanase II	Unenriched	No Change	No Change	Up	Down<2fold	-	-	-
MGG_04573	hypothetical protein	Unenriched	No Change	No Change	No Change	Down<2fold	-	-	-
MGG_04579	hypothetical protein	Unenriched	No Change	No Change	No Change	Down<2fold	-	-	-
MGG_04580	hypothetical protein	Unenriched	No Change	No Change	No Change	Up≥2fold	-	+	-
MGG_04859	hypothetical protein	Unenriched	No Change	Up	Up	Down<2fold	-	-	-
MGG_04889	hypothetical protein	Unenriched	No Change	No Change	No Change	N/A	-	-	-
MGG_04928	hypothetical protein	Unenriched	No Change	No Change	No Change	Down<2fold	-	-	-
MGG_04973	carbonate dehydratase	Unenriched	Down	Down	Down	Down<2fold	-	-	-
MGG_05023	chitin deacetylase 1	Unenriched	No Change	No Change	No Change	Down<2fold	-	-	-
MGG_05100	hypothetical protein	Unenriched	No Change	No Change	No Change	Down<2fold	-	-	-
MGG_05127	hypothetical protein	Unenriched	No Change	No Change	Up	Down<2fold	-	-	-
MGG_05232	hypothetical protein	Unenriched	No Change	No Change	No Change	Down<2fold	-	-	-
MGG_05344	MSP1/SnodProt1	Unenriched	No Change	No Change	No Change	Down≥2fold	-	-	-
MGG_05403	hypothetical protein	Unenriched	Up	No Change	Up	Down≥2fold	+	-	+
MGG_05406	hypothetical protein	Unenriched	Down	Down	Down	Down<2fold	-	-	-
MGG_05429	hypothetical protein, variant	Unenriched	No Change	Up	Up	Down<2fold	-	-	-
MGG_05504	hypothetical protein	Unenriched	No Change	No Change	No Change	Down<2fold	-	-	-
MGG_05518	hypothetical protein	Unenriched	No Change	No Change	No Change	Up≥2fold	-	-	-
MGG_05531	MoCDIP2	Unenriched	Up	Up	No Change	Down≥2fold	-	-	-
MGG_05538	hypothetical protein	Unenriched	No Change	No Change	No Change	Up≥2fold	-	-	-
MGG_05640	hypothetical protein	Unenriched	No Change	No Change	No Change	Down<2fold	-	-	-
MGG_05744	hypothetical protein	Unenriched	Up	No Change	No Change	Down<2fold	-	-	-
MGG_05749	hypothetical protein	Unenriched	No Change	No Change	No Change	Down<2fold	-	-	-
MGG_05751	hypothetical protein	Unenriched	Down	No Change	Down	Down≥2fold	-	-	-
MGG_05785	BAS113/levanase	Unenriched	No Change	Up	Up	Up≥2fold	-	-	-
MGG_05818	hypothetical protein	Unenriched	No Change	No Change	Up	Down<2fold	-	-	-
MGG_05831	hypothetical protein	Unenriched	Up	No Change	Up	Down<2fold	-	-	-
MGG_05875	pectate lyase	Unenriched	No Change	No Change	No Change	Down≥2fold	-	-	-

MGG_05896	hypothetical protein	Unenriched	No Change	Up	Up	Up≥2fold	-	+	+
MGG_05943	hypothetical protein	Unenriched	No Change	No Change	No Change	Down<2fold	-	-	-
MGG_05982	hypothetical protein	Unenriched	Up	Up	Up	Down<2fold	-	-	-
MGG_06224	MoHEG12	Unenriched	Up	No Change	Up	Up≥2fold	+	-	+
MGG_06523	hypothetical protein	Unenriched	No Change	No Change	No Change	Down<2fold	-	-	-
MGG_06621	hypothetical protein	Unenriched	No Change	No Change	No Change	Down<2fold	-	-	-
MGG_06771	hypothetical protein	Unenriched	Down	No Change	No Change	Down<2fold	-	-	-
MGG_07153	hypothetical protein	Unenriched	Down	No Change	Down	Down<2fold	-	-	-
MGG_07246	hypothetical protein	Unenriched	No Change	Up	No Change	Down<2fold	-	-	-
MGG_07294	feruloyl esterase B	Unenriched	No Change	No Change	No Change	Down<2fold	-	-	-
MGG_07300	cellulose-growth-specific protein	Unenriched	No Change	No Change	Down	Down<2fold	-	-	-
MGG_07311	hypothetical protein	Unenriched	No Change	Up	Up	Down<2fold	-	-	-
MGG_07352	hypothetical protein	Unenriched	No Change	No Change	No Change	Down<2fold	-	-	-
MGG_07556	hypothetical protein	Unenriched	Up	Up	Up	Up≥2fold	+	-	+
MGG_07558	hypothetical protein	Unenriched	Up	Up	No Change	Down<2fold	-	-	-
MGG_07607	hypothetical protein	Unenriched	No Change	No Change	No Change	Down<2fold	-	-	-
MGG_07624	hypothetical protein	Unenriched	No Change	Up	Up	Up≥2fold	-	+	+
MGG_07630	hypothetical protein	Unenriched	No Change	No Change	No Change	Up≥2fold	-	-	-
MGG_07677	rhamnogalacturonan acetylesterase	Unenriched	Up	No Change	Up	Down<2fold	-	-	-
MGG_07699	hypothetical protein	Unenriched	No Change	No Change	Up	Down≥2fold	+	-	+
MGG_07749	BAS2c	Unenriched	No Change	No Change	No Change	Down<2fold	-	-	-
MGG_07766	hypothetical protein	Unenriched	No Change	Up	Up	Down<2fold	-	-	-
MGG_07810	hypothetical protein	Unenriched	No Change	No Change	No Change	Up≥2fold	-	-	-
MGG_07919	hypothetical protein	Unenriched	Up	No Change	Up	Up< 2fold	+	-	+
MGG_07969	BAS2b	Unenriched	No Change	Down	Down	Down<2fold	-	-	-
MGG_07986	MoCDIP3	Unenriched	Up	No Change	Up	Down<2fold	-	-	-
MGG_08214	hypothetical protein	Unenriched	Up	No Change	Up	Down<2fold	-	-	-
MGG_08254	hypothetical protein	Unenriched	No Change	Up	No Change	Down<2fold	-	-	-
MGG_08275	hypothetical protein	Unenriched	Down	No Change	Down	Down<2fold	-	-	-
MGG_08291	hypothetical protein	Unenriched	No Change	No Change	No Change	Down<2fold	-	-	-
MGG_08331	endo-1,4-beta-xylanase B	Unenriched	Up	No Change	No Change	Down<2fold	-	-	-
MGG_08350	hypothetical protein	Unenriched	Up	No Change	Up	Down<2fold	-	-	-
MGG_08355	hypothetical protein	Unenriched	Up	Up	Up	Up≥2fold	+	+	+
MGG_08376	hypothetical protein	Unenriched	Up	Up	Up	Down<2fold	-	-	-
MGG_08399	MoHEG3	Unenriched	Up	Up	Up	Up≥2fold	+	+	+
MGG_08409	MoCDIP4/cellulose-growth-specific protein	Unenriched	Up	No Change	Up	Down<2fold	-	-	-
MGG_08414	MAX	Unenriched	Up	No Change	No Change	Up≥2fold	+	-	-
MGG_08428	hypothetical protein	Unenriched	Up	Up	Up	Up≥2fold	+	+	+
MGG_08432	hypothetical protein	Unenriched	No Change	No Change	No Change	Down<2fold	-	-	-
MGG_08451	hypothetical protein	Unenriched	No Change	No Change	No Change	Down<2fold	-	-	-
MGG_08454	elicitor	Unenriched	No Change	Down	No Change	Down<2fold	-	-	-
MGG_08469	hypothetical protein	Unenriched	Up	No Change	Up	Down<2fold	-	-	-
MGG_08546	hypothetical protein	Unenriched	Up	No Change	Up	Down≥2fold	-	-	+
MGG_08607	hypothetical protein	Unenriched	No Change	No Change	No Change	Down<2fold	-	-	-
MGG_08796	hypothetical protein	Unenriched	No Change	No Change	No Change	Down<2fold	-	-	-
MGG_09055	MoHEG7	Unenriched	Up	Down	No Change	Down<2fold	-	-	-
MGG_09106	hypothetical protein	Unenriched	Up	No Change	Up	Down<2fold	-	-	-
MGG_09377	hypothetical protein	Unenriched	Up	No Change	Up	Up≥2fold	+	-	+
MGG_09378	MoHEG13	Unenriched	Up	No Change	Up	Down<2fold	+	-	+
MGG_09465	hypothetical protein	Unenriched	No Change	No Change	No Change	Down≥2fold	-	-	-
MGG_09474	hypothetical protein	Unenriched	No Change	No Change	No Change	Down<2fold	-	-	-
MGG_09569	hypothetical protein	Unenriched	No Change	No Change	Down	Down<2fold	-	-	-
MGG_09666	hypothetical protein	Unenriched	No Change	No Change	Up	Down<2fold	-	-	-
MGG_09709	endoglucanase II	Unenriched	No Change	No Change	Down	Down<2fold	-	-	-
MGG_09722	hypothetical protein	Unenriched	No Change	No Change	No Change	Down<2fold	-	-	-
MGG_09740	hypothetical protein	Unenriched	No Change	No Change	Up	Up≥2fold	-	-	+
MGG_09810	hypothetical protein	Unenriched	No Change	No Change	No Change	Up≥2fold	-	-	-

MGG_09844	hypothetical protein	Unenriched	Up	No Change	Up	Down<2fold	-	-	-
MGG_10259	hypothetical protein	Unenriched	No Change	No Change	No Change	Down<2fold	-	-	-
MGG_10280	hypothetical protein	Unenriched	No Change	No Change	No Change	Up≥2fold	-	-	-
MGG_10282	MoHEG18	Unenriched	No Change	No Change	No Change	Down<2fold	-	-	-
MGG_10318	hypothetical protein	Unenriched	Up	No Change	Up	Down≥2fold	+	-	+
MGG_10424	hypothetical protein	Unenriched	Up	No Change	Up	Down<2fold	-	-	-
MGG_10455	hypothetical protein	Unenriched	Up	Up	Up	Down≥2fold	+	+	+
MGG_10477	hypothetical protein	Unenriched	Up	No Change	Up	Down≥2fold	+	-	+
MGG_10532	necrosis and ethylene inducing peptide	Unenriched	Up	No Change	Up	Down<2fold	-	-	-
MGG_10732	hypothetical protein	Unenriched	No Change	No Change	No Change	Down<2fold	-	-	-
MGG_10796	hypothetical protein	Unenriched	Up	No Change	Up	Down<2fold	-	-	-
MGG_11719	hypothetical protein	Unenriched	No Change	Up	Up	Down≥2fold	-	+	+
MGG_11967	hypothetical protein	Unenriched	No Change	No Change	No Change	Up≥2fold	-	-	-
MGG_11991	SPD10	Unenriched	Up	No Change	Up	Down<2fold	-	-	-
MGG_12272	trm-112	Unenriched	Down	No Change	Down	N/A	-	-	-
MGG_12337	MAS3 protein	Unenriched	No Change	No Change	No Change	Down<2fold	-	-	-
MGG_12426	hypothetical protein	Unenriched	Up	No Change	Up	N/A	-	-	-
MGG_12551	hypothetical protein	Unenriched	No Change	No Change	No Change	Down<2fold	-	-	-
MGG_12552	hypothetical protein	Unenriched	No Change	No Change	No Change	Down<2fold	-	-	-
MGG_12654	hypothetical protein	Unenriched	No Change	No Change	No Change	Down≥2fold	-	-	-
MGG_12655	AVR-Pi9	Unenriched	Up	Down	No Change	Up≥2fold	+	-	-
MGG_12690	hypothetical protein	Unenriched	No Change	No Change	Up	N/A	-	-	-
MGG_12937	hypothetical protein	Unenriched	No Change	No Change	No Change	Down<2fold	-	-	-
MGG_12942	SPD2	Unenriched	Down	Down	Down	Down<2fold	-	-	-
MGG_13009	hypothetical protein	Unenriched	No Change	Down	Down	Down<2fold	-	-	-
MGG_13019	hypothetical protein	Unenriched	No Change	No Change	No Change	Down<2fold	-	-	-
MGG_13654	hypothetical protein	Unenriched	No Change	No Change	Down	N/A	-	-	-
MGG_13670	hypothetical protein	Unenriched	No Change	No Change	Up	Up≥2fold	-	-	+
MGG_13836	hypothetical protein	Unenriched	No Change	No Change	No Change	Down<2fold	-	-	-
MGG_13863	PWL2	Unenriched	No Change	No Change	No Change	Up≥2fold	-	-	-
MGG_14093	hypothetical protein	Unenriched	No Change	No Change	No Change	Up≥2fold	-	-	-
MGG_14652	hypothetical protein	Unenriched	No Change	No Change	No Change	Down<2fold	-	-	-
MGG_14725	hypothetical protein	Unenriched	No Change	No Change	No Change	N/A	-	-	-
MGG_14734	hypothetical protein	Unenriched	No Change	No Change	No Change	Down<2fold	-	-	-
MGG_14834	hypothetical protein	Unenriched	Up	No Change	Up	Down<2fold	-	-	-
MGG_14879	hypothetical protein	Unenriched	No Change	No Change	No Change	Down<2fold	-	-	-
MGG_14966	hypothetical protein	Unenriched	No Change	Down	Down	N/A	-	-	-
MGG_15106	hypothetical protein	Unenriched	No Change	No Change	No Change	Down<2fold	-	-	-
MGG_15207	hypothetical protein	Unenriched	No Change	Up	No Change	Down<2fold	-	-	-
MGG_15370	AVR-Pita1	Unenriched	No Change	No Change	No Change	Up≥2fold	-	-	-
MGG_15375	hypothetical protein	Unenriched	No Change	No Change	No Change	N/A	-	-	-
MGG_15539	hypothetical protein	Unenriched	No Change	No Change	No Change	Down≥2fold	-	-	-
MGG_15547	hypothetical protein	Unenriched	No Change	No Change	No Change	Down<2fold	-	-	-
MGG_15633	hypothetical protein	Unenriched	No Change	No Change	No Change	Down<2fold	-	-	-
MGG_15703	hypothetical protein	Unenriched	No Change	No Change	No Change	N/A	-	-	-
MGG_15751	hypothetical protein	Unenriched	No Change	No Change	No Change	Down<2fold	-	-	-
MGG_15814	peptidyl-prolyl cis-trans isomerase B	Unenriched	No Change	No Change	Down	Down<2fold	-	-	-
MGG_15843	hypothetical protein	Unenriched	No Change	No Change	No Change	Down<2fold	-	-	-
MGG_15878	hypothetical protein	Unenriched	No Change	No Change	Up	Down<2fold	-	-	-
MGG_15883	hypothetical protein	Unenriched	No Change	No Change	No Change	Down<2fold	-	-	-
MGG_16026	hypothetical protein	Unenriched	No Change	No Change	No Change	Up≥2fold	-	-	-
MGG_16071	hypothetical protein	Unenriched	No Change	No Change	No Change	Down<2fold	-	-	-
MGG_16090	hypothetical protein	Unenriched	No Change	No Change	No Change	Down<2fold	-	-	-
MGG_16187	hypothetical protein	Unenriched	No Change	No Change	No Change	Down<2fold	-	-	-
MGG_16238	hypothetical protein	Unenriched	No Change	No Change	No Change	Down<2fold	-	-	-
MGG_16339	hypothetical protein	Unenriched	No Change	No Change	No Change	Down<2fold	-	-	-
MGG_16357	hypothetical protein	Unenriched	No Change	No Change	No Change	Down<2fold	-	-	-
MGG_16379	hypothetical protein	Unenriched	No Change	No Change	No Change	N/A	-	-	-

MGG_16415	hypothetical protein	Unenriched	No Change	No Change	Up	Up≥2fold	-	-	+
MGG_16496	hypothetical protein	Unenriched	No Change	No Change	No Change	Down<2fold	-	-	-
MGG_16619	hypothetical protein	Unenriched	Up	No Change	Up	Down<2fold	+	-	+
MGG_16654	hypothetical protein	Unenriched	Up	No Change	Up	Down<2fold	-	-	-
MGG_16703	hypothetical protein	Unenriched	Up	No Change	Up	N/A	-	-	-
MGG_16714	hypothetical protein	Unenriched	Down	No Change	Up	N/A	-	-	-
MGG_16719	hypothetical protein	Unenriched	No Change	No Change	Down	Down<2fold	-	-	-
MGG_16737	hypothetical protein	Unenriched	No Change	No Change	No Change	Down<2fold	-	-	-
MGG_16811	hypothetical protein	Unenriched	No Change	No Change	No Change	Up≥2fold	-	-	-
MGG_16829	hypothetical protein	Unenriched	No Change	No Change	No Change	Up≥2fold	-	-	-
MGG_16836	hypothetical protein	Unenriched	No Change	No Change	No Change	Down≥2fold	-	-	-
MGG_16840	hypothetical protein	Unenriched	No Change	No Change	Up	Down<2fold	-	-	-
MGG_16860	hypothetical protein	Unenriched	No Change	No Change	No Change	Down<2fold	-	-	-
MGG_16869	hypothetical protein	Unenriched	Up	Up	Up	Down<2fold	-	-	-
MGG_16892	hypothetical protein	Unenriched	No Change	No Change	No Change	Up≥2fold	-	-	-
MGG_16925	hypothetical protein, variant	Unenriched	No Change	No Change	Up	Down<2fold	-	-	-
MGG_16939	hypothetical protein	Unenriched	No Change	No Change	No Change	Down≥2fold	-	-	-
MGG_16977	hypothetical protein	Unenriched	Up	No Change	Up	N/A	-	-	-
MGG_16989	hypothetical protein	Unenriched	No Change	No Change	Up	Down<2fold	-	-	+
MGG_17015	hypothetical protein	Unenriched	No Change	No Change	No Change	Down<2fold	-	-	-
MGG_17063	hypothetical protein	Unenriched	No Change	No Change	No Change	N/A	-	-	-
MGG_17082	hypothetical protein	Unenriched	No Change	No Change	No Change	Down<2fold	-	-	-
MGG_17132	hypothetical protein	Unenriched	No Change	Down	No Change	Down<2fold	-	-	-
MGG_17148	hypothetical protein	Unenriched	No Change	No Change	Up	Down<2fold	-	-	-
MGG_17154	hypothetical protein	Unenriched	No Change	Up	Up	Down<2fold	-	-	-
MGG_17155	hypothetical protein	Unenriched	No Change	Up	Up	Down≥2fold	-	+	+
MGG_17248	hypothetical protein	Unenriched	No Change	No Change	No Change	N/A	-	-	-
MGG_17301	hypothetical protein	Unenriched	No Change	No Change	No Change	Down<2fold	-	-	-
MGG_17319	hypothetical protein	Unenriched	No Change	No Change	No Change	Down<2fold	-	-	-
MGG_17334	hypothetical protein	Unenriched	No Change	No Change	No Change	Down<2fold	-	-	-
MGG_17353	hypothetical protein	Unenriched	No Change	No Change	No Change	Down<2fold	-	-	-
MGG_17425	hypothetical protein	Unenriched	Down	Down	Down	Up≥2fold	-	-	-
MGG_17463	hypothetical protein	Unenriched	No Change	No Change	No Change	Down<2fold	-	-	-
MGG_17464	hypothetical protein	Unenriched	No Change	No Change	Up	N/A	-	-	-
MGG_17478	hypothetical protein	Unenriched	No Change	No Change	No Change	Down<2fold	-	-	-
MGG_17532	hypothetical protein	Unenriched	Down	Down	Down	Down<2fold	-	-	-
MGG_17550	hypothetical protein	Unenriched	No Change	No Change	Up	Down≥2fold	-	-	+
MGG_17587	hypothetical protein	Unenriched	No Change	No Change	No Change	N/A	-	-	-
MGG_17614	hypothetical protein	Unenriched	No Change	No Change	No Change	Down<2fold	-	-	-
MGG_17635	hypothetical protein	Unenriched	No Change	No Change	No Change	Down<2fold	-	-	-
MGG_17666	hypothetical protein	Unenriched	No Change	No Change	No Change	Down<2fold	-	-	-
MGG_17667	hypothetical protein	Unenriched	No Change	No Change	No Change	Up≥2fold	-	-	-
MGG_17711	hypothetical protein	Unenriched	No Change	No Change	No Change	Down<2fold	-	-	-
MGG_17760	hypothetical protein	Unenriched	No Change	No Change	Up	N/A	-	-	-
MGG_17840	hypothetical protein	Unenriched	No Change	No Change	No Change	Up< 2fold	-	-	-
MGG_17885	hypothetical protein	Unenriched	No Change	No Change	No Change	Down<2fold	-	-	-
MGG_17894	hypothetical protein	Unenriched	No Change	Up	Up	N/A	-	-	-
MGG_17899	hypothetical protein	Unenriched	No Change	No Change	No Change	Down<2fold	-	-	-
MGG_17902	hypothetical protein	Unenriched	No Change	No Change	No Change	Down<2fold	-	-	-
MGG_17997	hypothetical protein	Unenriched	No Change	No Change	No Change	Down<2fold	-	-	-
MGG_18005	hypothetical protein	Unenriched	No Change	No Change	No Change	Down<2fold	-	-	-
MGG_18013	hypothetical protein	Unenriched	No Change	No Change	No Change	Down<2fold	-	-	-
MGG_18015	hypothetical protein	Unenriched	No Change	No Change	No Change	Down<2fold	-	-	-
MGG_18019	hypothetical protein	Unenriched	No Change	No Change	No Change	Up≥2fold	-	-	-
MGG_18076	hypothetical protein	Unenriched	No Change	No Change	No Change	Down<2fold	-	-	-
MGG_18141	hypothetical protein	Unenriched	Up	No Change	Up	Down<2fold	-	-	-

Table S2.9. *Magnaporthe oryzae* strains used in this study

Strain	**CKF#**	**Genotype**	**Reference**
O-137	CKF558*	Wild-type, a field isolate from rice in China.	Orbach et al., 2000
PWL2 reporter strain(nuclear)	CKF2962	Transformant of CKF558, expressing both a constitutive, nuclear tdTomato reporter gene, and a fusion of the *PWL2* promoter with sfGFP:NLS reporter gene; Hyg^R	This study
Δ*mokmt6*	CKF3472*	*MoKMT6* deletion mutant of CKF2962; Hyg^R $G418^R$	This study
	CKF3473	*MoKMT6* deletion mutant of CKF2962; Hyg^R $G418^R$	This study
MoKMT6E	CKF3477	Ectopic transformant with Δ*mokmt6* deletion construct; Hyg^R $G418^R$	This study
Δ*mokmt6*-*MoKMT6*	CKF3721	Complementation strain of Δ*mokmt6* mutant (CKF3472); Hyg^R $G418^R$ NTC^R	This study
	CKF3722	Complementation strain of Δ*mokmt6* mutant (CKF3472); Hyg^R $G418^R$ NTC^R	This study
PWL2 reporter strain (cytoplasmic)	CKF3538	Transformant of CKF558, expressing both a constitutive, cytoplasmic tdTomato reporter gene, and a fusion of the *PWL2* promoter with EGFP:PEST reporter gene; Hyg^R $G418^R$	This study
MoGti1oe	CKF3790AB*	MoGti1 overexpression transformant of CKF3538; Hyg^R $G418^R$ NTC^R	This study
	CKF3791AB	MoGti1 overexpression transformant of CKF3538; Hyg^R $G418^R$ NTC^R	This study
	CKF3792AB	MoGti1 overexpression transformant of CKF3538; Hyg^R $G418^R$ NTC^R	This study
	CKF3793AB	MoGti1 overexpression transformant of CKF3538; Hyg^R $G418^R$ NTC^R	This study

	CKF4030	MoGti1 overexpression transformant of Δ*mokmt6* deletion mutant (CKF3472); Hyg^R $G418^R$ NTC^R	This study
	CKF4031	MoGti1 overexpression transformant of Δ*mokmt6* deletion mutant (CKF3472); Hyg^R $G418^R$ NTC^R	This study
	CKF4033	MoGti1 overexpression transformant of Δ*mokmt6* deletion mutant (CKF3472); Hyg^R $G418^R$ NTC^R	This study
Δ*mokmt6*-MoGti1oe	CKF4034*	MoGti1 overexpression transformant of Δ*mokmt6* deletion mutant (CKF3472); Hyg^R $G418^R$ NTC^R	This study
BAS4 reporter strain	CKF3666	Transformant of CKF558, expressing both a constitutive, cytoplasmic tdTomato reporter gene, and a fusion of the *BAS4* promoter with EGFP:PEST reporter gene; Hyg^R $G418^R$	This study

*Representative strains were used for ChIP-seq, RNA-seq and qRT-PCR throughout this study unless otherwise noted.

Table S2.10. Key plasmids used in this study

Clone	Description
pCK1292	tdTomato expression binary vector derived from pBV141(pBGt, Kim et al., 2011), consisting of 0.5-kb P27 promoter (*Eco*RI-*BamH*I fragment), and 1.7-kb tdTomato: *N.crassa* β-tubulin terminator (*BamH*I-*Hind*III fragment) cloned in *Eco*RI-*Hind*III sites of pBV141(pBGt).
pCK1533	*PWL2* nuclear reporter vector, consisting of 1-kb *PWL2* promoter (*Eco*RI-*BamH*I fragment), 1.3-kb sfGFP plus nuclear localization signal and *PWL2* 3'-UTR (*BamH*I-*Sac*I fragment), and 2.8-kb P27 promoter:tdTomato plus nuclear localization signal and terminator (*Sac*I-*Hind*III fragment), cloned in *Eco*RI-*Hind*III sites of pBV1(pBHt2, Mullins et al., 2001).
pCK1637	*MoKMT6* knockout vector, consisting of 1.2-kb 5'-upstream sequence of *MoKMT6* (*Sal*I-*Eco*RI fragment), 1.1-kb *NTPII* fragment (*Eco*RI-*Xba*I) cloned from pBV141, and 1.2-kb 3'-downstream sequence of *MoKMT6* (*Xba*I-*BamH*I fragment), cloned in *Sal*I-*BamH*I sites of pBV108 (pGKO2, Khang et al., 2005).
pCK1714	*PWL2* cytoplasmic reporter vector, consisting of 1.7-kb *PWL2* promoter:EGFP (*Eco*RI-*BsrG*I fragment), 0.12-kb protein degradation signal peptide PEST (*BsrG*I-*Not*I fragment) from pBV118(pd2EGFP-1), and 0.5-kb *PWL2* 3'-UTR (*Not*I-*Xho*I fragment), cloned in *Eco*RI-*Sal*I sites of pBV1(pBHt2).
pCK1743	*BAS4* cytoplasmic reporter vector, consisting of 1-kb *BAS4* promoter (*Eco*RI-*BamH*I fragment), 0.8-kb EGFP:PEST(*BamH*I-*Not*I fragment) from pCK1714, and 0.5-kb *BAS4* 3'-UTR (*Not*I-*Hind*III fragment), cloned in *Eco*RI-*Hind*III sites of pBV1(pBHt2).

pCK1806	0.9-kb *NAT1* plus *Aspergillus nidulans* TrpC promoter fragment from pDONR207 (Ane Sesma at Universidad Politécnica de Madrid, Madrid, Spain) in *Xho*I-*EcoR*I sites of pBV141(pBGt).
pCK1811	*MoKMT6* complementary vector, consisting of 6-kb *MoKMT6* sequence (5'-upstream:coding seqeuce: 3'-downstream, *Mfe*I-*BamH*I fragment), cloned in *EcoR*I-*BamH*I sites of pCK1806.
pCK1900	*MoGti1* overexpression vector, consisting of 1-kb P27 promoter (*EcoR*I-*BamH*I fragment) and 1.7-kb *MoGti1* coding sequence plus *MoGti1* 3'-UTR (*BamH*I-*Hind*III fragment) cloned in *EcoR*I-*Hind*III sites of pCK1806.

Table S2.11. Antibodies used in this study

Antigen	**Purpose**	Provider	**Catalog number**
H3K4me2	ChIP-seq of wild-type and MoGti1oe	Active motif	39679 (32)
H3K9me3	ChIP-seq of wild-type and MoGti1oe	Active motif	13509002(53), 39161(53), 14418003(84)
H3K27me3	ChIP-seq of wild-type, *Δmokmt6*, *Δmokmt6*-MoKMT6 and MoGti1oe	Cell signal	Lot:8 (59), 9733S(59), Lot:14(81)
H3K36me3	ChIP-seq of wild-type and MoGti1oe	Abcam	ab9050(56)

Table S2.12. PCR primers used in this study

Name	Sequence [a] (5'-3')	Applications
CKP412	*GC*GTCGACTAAGTCCGGTAGTGTGAAGAGG	*MoKMT6* upstream for knockout
CKP413	*CG*GAATTCCTTGTCACTTTTGCTCCCTCC	*MoKMT6* upstream for knockout
CKP421	GGATCCGAAGTTCAACCGGCTCGC	*MoKMT6* downstream for knockout
CKP428	TCTAGAAAGTCCTACGGGCACAAGGC	*MoKMT6* downstream for knockout
CKP416	*CG*GAATTCTCGACAGAAGATGATATTG	*NTPII* sequence
CKP420	TCTAGATTAGAAGAACTCGTCAAG	*NTPII* sequence/ *MoKMT6* knockout screening
CKP443	AGGCTCGGTCGAGAATTGAC	*MoKMT6* knockout screening
CKP459	GGCAGGAGGGAGCAAAAGTGAC	*MoKMT6* knockout/ complementation screening
CKP460	ATTCCGCCTTGTGCCCGTAG	*MoKMT6* knockout/ complementation screening
CKP719J	GGATCCATGACGGGCAAGCTCGG	*MoKMT6* sequence for complementation
CKP720J	TCTAGAGAGCAGCACAGGCCAAGG	*MoKMT6* sequence for complementation
CKP565	GAATTCGCTGGGTAACTGATATTGAAGG	*Nat1* sequence
CKP566	CTCGAGTCAGGGGCAGGGCATG	*Nat1* sequence
CKP591	GGATCCATGTCGACTACGGGACAAGG	*MoGti1* sequence for overexpression
CKP592	AAGCTTTCGCTTGAGAAATAATATGTATTCAGGC	*MoGti1* sequence for overexpression
CKP110	GAATTCGGTAGCTTCTACGGATGC	*BAS4* 1-kb upstream for expression reporter
CKP234	GGATCCCAT TGTGAA AAGATTCGTTGTGG	*BAS4* 1-kb upstream for expression reporter
CKP548	GCGGCCGCGAGGGTTCTTTCACCTCG	*BAS4* 0.5-kb downstream for expression reporter
CKP549	AAGCTTCGGGGCTTTTGACAGTACCC	*BAS4* 0.5-kb downstream for expression reporter
CKP348	ACGGTGACCATATCGAGTGC	*ACE1* qRT-PCR
CKP349	CGCGCTTATACGTCTCCTGG	*ACE1* qRT-PCR
CKP795J	AGGTGACGCCAAGATTTCCG	*AVR-Pi9* qRT-PCR
CKP796J	ACCAGTGCGTCTTTTCGACT	*AVR-Pi9* qRT-PCR
CKP679J	CACTTTGGGAACTGTCGCTG	*AVR-Pik* qRT-PCR
CKP680J	TCGGGTACAGGAATACCAGGG	*AVR-Pik* qRT-PCR
CKP793J	CGATAAGGAAGAAGGCGGGT	*AVR-Pizt* qRT-PCR
CKP794J	TGTACGGGTGACGCGTTTTT	*AVR-Pizt* qRT-PCR
CKP611	TTGAGGAATTGTGCCCCGAC	*BAS3* qRT-PCR
CKP612	CGCAGTCGATGACGCAGAT	*BAS3* qRT-PCR
CKP329	TGCGACGACTGCACTATCTG	*BAS4* qRT-PCR
CKP330	CGCCAAGGTTAGGGCATTTC	*BAS4* qRT-PCR
CKP546	GTCATCACCCCCATCACCAAG	*MC69* qRT-PCR
CKP547	TTTGGCAGGTCCGCGAAG	*MC69* qRT-PCR
CKP333	CGACGTCCGAAAGGATCTGT	*Moactin* qRT-PCR
CKP334	TGCATACGGTCCGAAAGACC	*Moactin* qRT-PCR
CKP615	GCTCAGGTTACTTGTGGGCT	*MoGti1* qRT-PCR
CKP616	AGGTGATGGCTGACACCTTG	*MoGti1* qRT-PCR
CKP789J	TGTAATGGACACACGCACGA	*MoKMT6* qRT-PCR
CKP790J	GGAGGTGTAACTGGTCAGCC	*MoKMT6* qRT-PCR
CKP327	GGCGGGTGGACTAACAAACA	*PWL2* qRT-PCR
CKP328	TACCATCCTATCGGGCCCTC	*PWL2* qRT-PCR
CKP544	GTTCGCTACCATCACCACCC	*Slp1* qRT-PCR
CKP545	GTTGCCCTGCACCGTGTAG	*Slp1* qRT-PCR

[a]Underlined sequences correspond to restriction enzyme sites used for cloning:

*BamH*I (GGATCC), *Eco*RI (GAATTC), *Hind*III (AAGCTT), *Not*I (CGGCCG), *Sal*I (GTCGAC), *Xba*I (TCTAGA) and *Xho*I (CTCGAG).

Figures

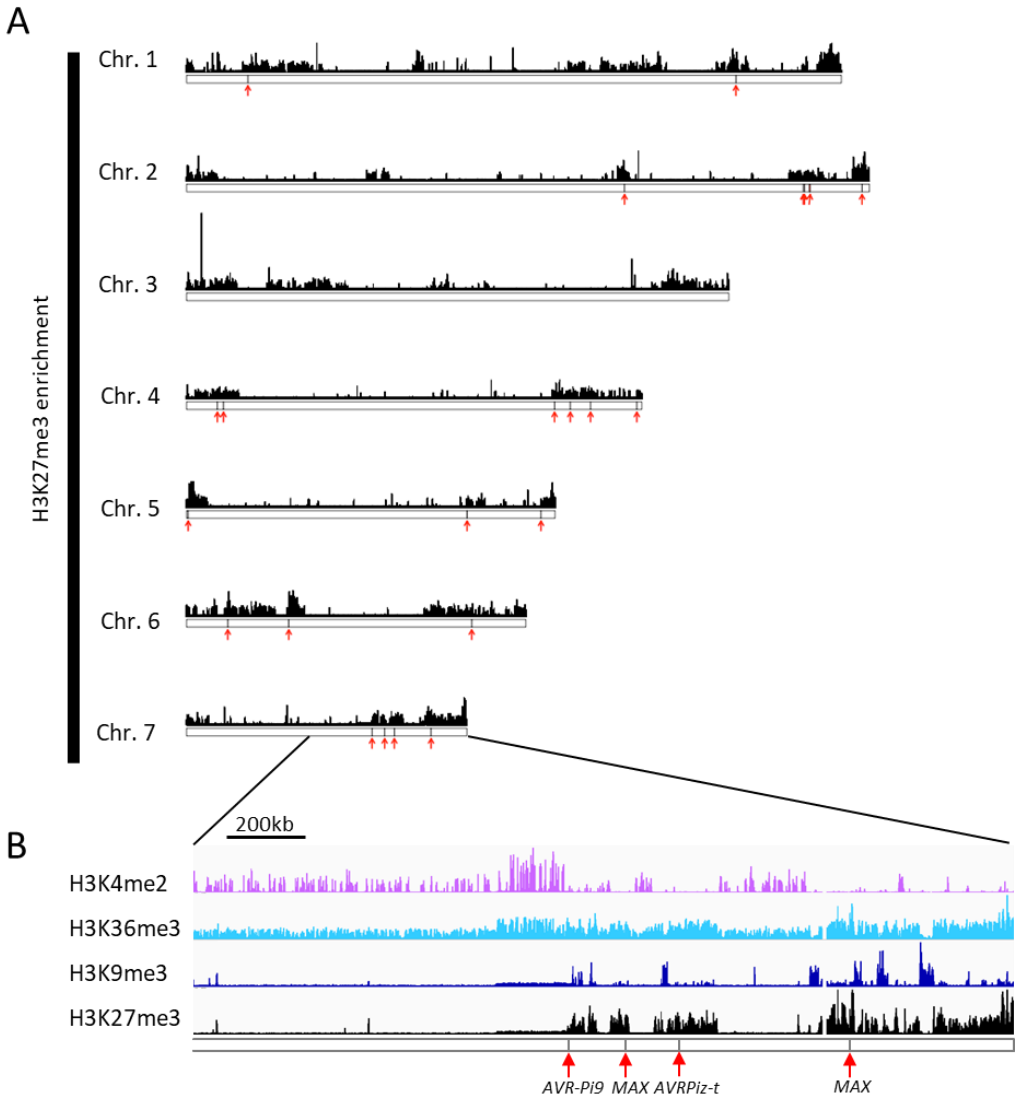

Figure 2.1. 24 known effector genes are found in regions enriched for H3K27me3. (A) Karyotype plot for all chromosomes, showing genome wide location of H3K27me3 ChIP enrichment. Red arrows indicate genomic location of 23 known effector genes. The location of one effector gene (MGG_10234) is unplaced in seven chromosomes but still found in H3K27me3-enriched regions. (B) Profile of ChIP for H3K4me2, H3K9me3, H3K36me3, and H3K27me3 enrichment for partial of Chromosome VII. Gray bars and red arrows indicate known effector genes.

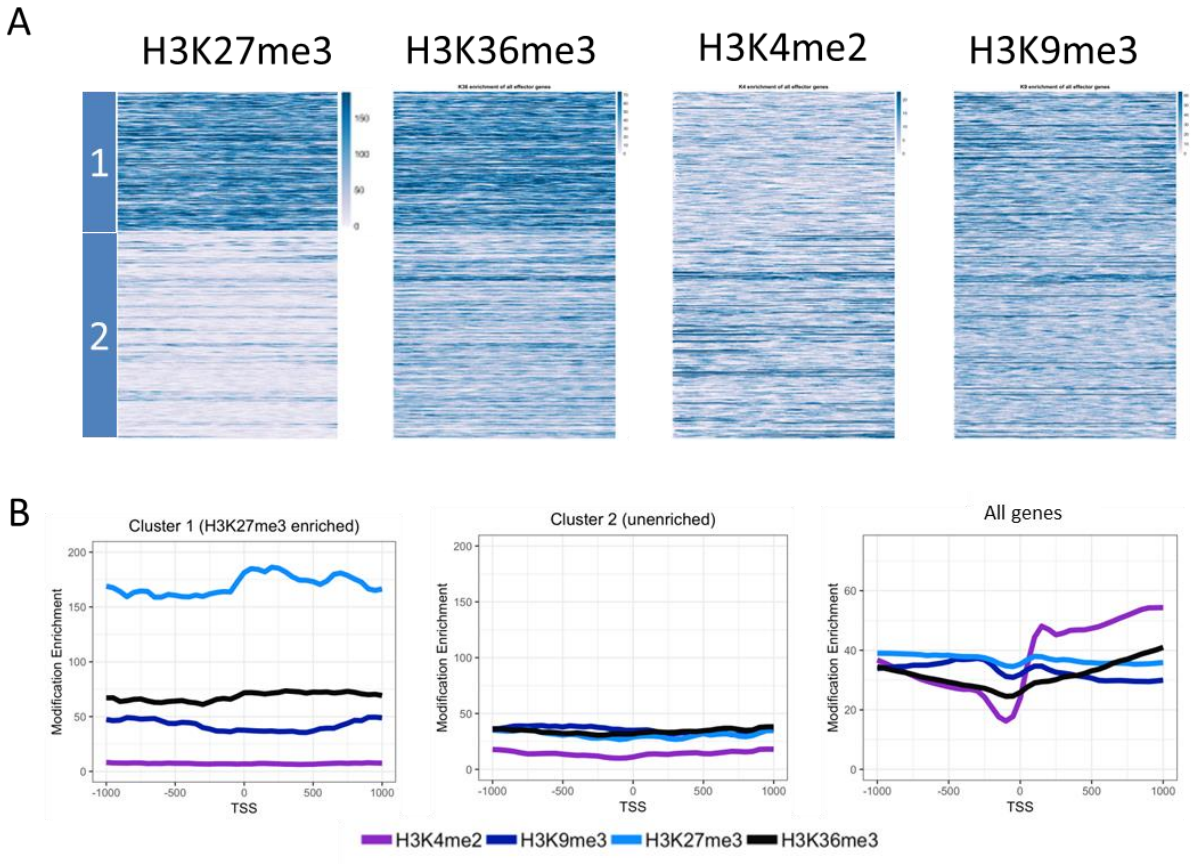

Figure 2.2. Effector genes cluster into two classes based on H3K27me3 enrichment status. (A) Heatmaps for all effector genes centered on the transcription start site (TSS) +/-1000bp for a total window size of 2000bp. H3K27me3 heatmap was clustered using k-means of two, to divide effector genes into enriched (cluster 1: top), vs unenriched (cluster 2: bottom). All other modifications are plotted in the same order as the H3K27me3 heatmap. (B) Metaplot of H3K27me3, H3K36me3, H3K4me2, H3K9me3 at all effector genes centered on TSS and +/-1000bp for a total window size of 2000bp, for cluster 1, cluster 2 (left/middle: on same scale) and all genes (right: on different scale).

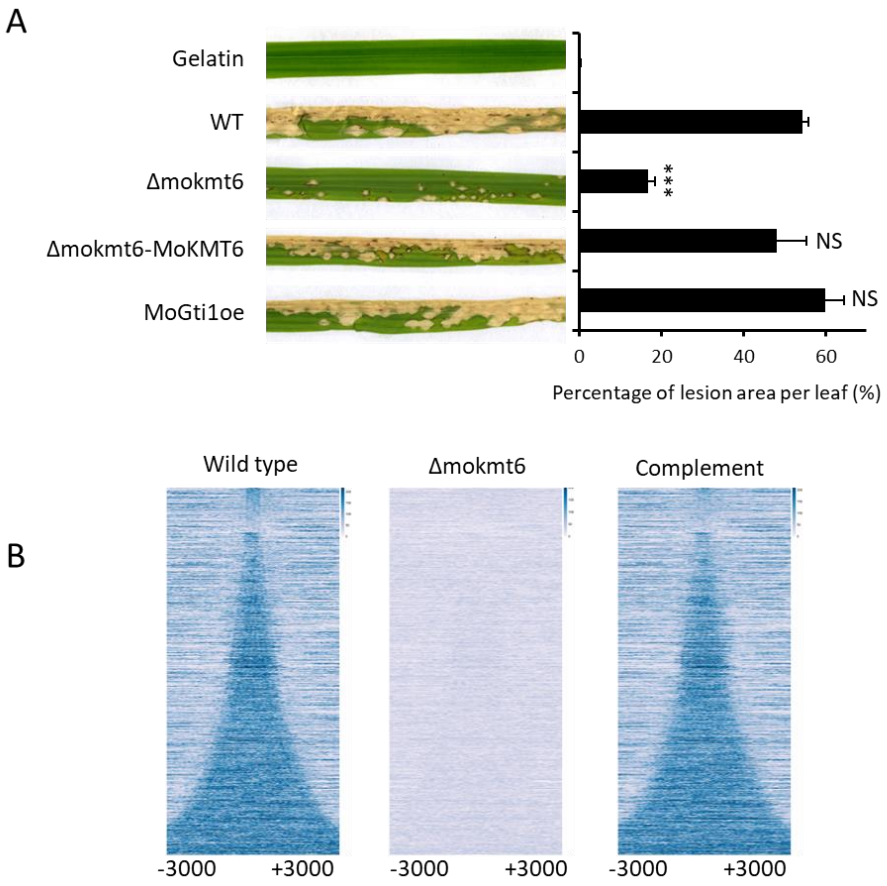

Figure 2.3. *MoKMT6* is required for the full virulence of *M. oryzae* and deposition of H3K27me3. (A) Targeted deletion of *MoKMT6* gene resulted in reduced pathogenicity on a fully susceptible rice cultivar YT16 in whole plant spray inoculation assay. Overexpression of *MoGti1* gene did not affect pathogenicity. Inoculation with 0.25% of gelatin was used as the negative control. Bar chart showed the percentage of lesion area per marked leaf after infection with fungal spores from different strains. Error bar equals standard deviation of the mean. *** $p<0.001$ (Two-tailed student t-test). NS means no significant difference. (B) Heatmaps for all ~800 H3K27me3 peaks in genome ordered from smallest to largest. Heatmaps are centered on peak center and +/-3000bp for a total window size of 6000bp. Deletion of *MoKMT6* abolishes H3K27me3 peaks (middle), and reintroduction of wild-type *MoKMT6* restores all H3K27me3 peaks (right).

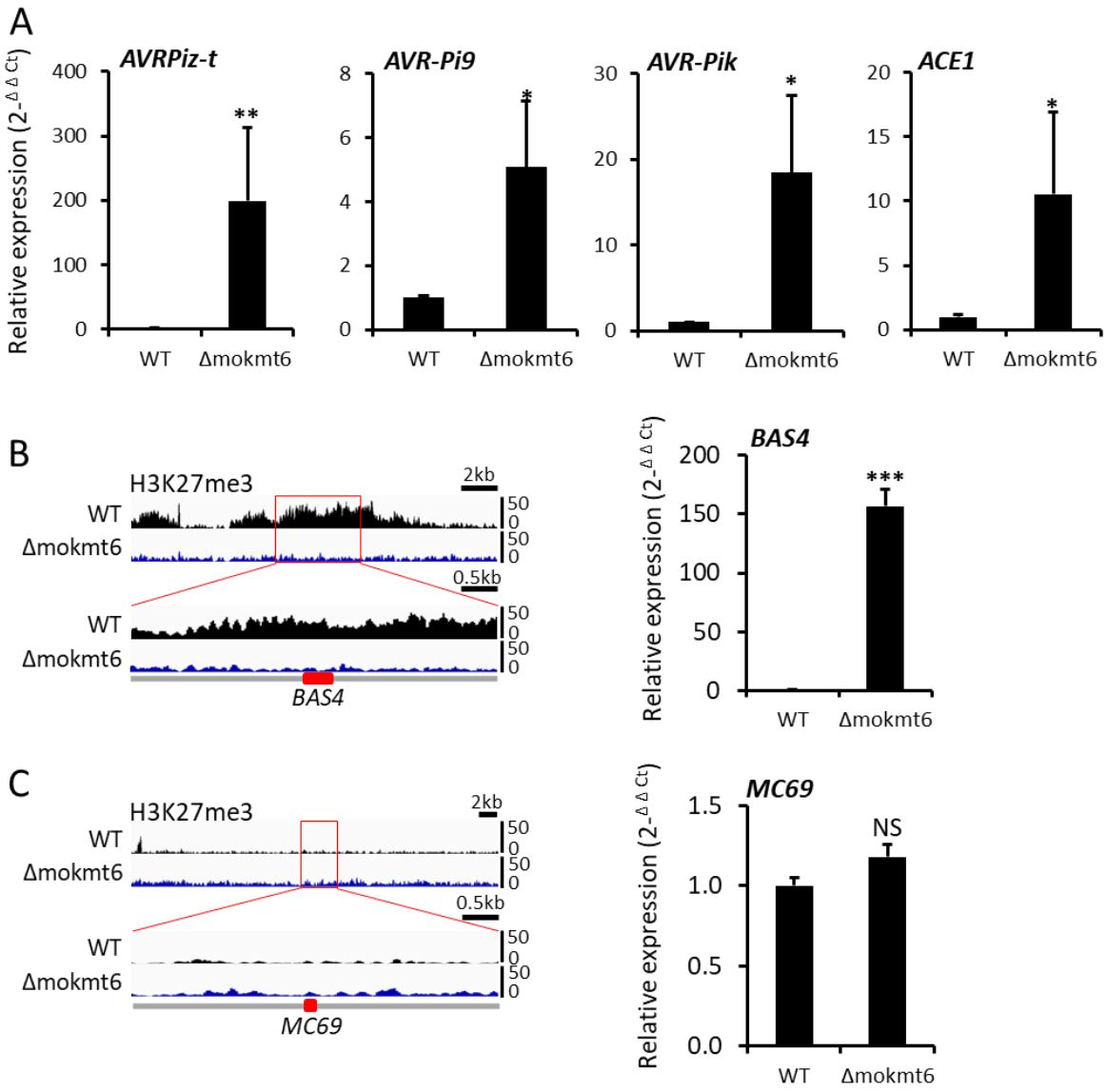

Figure 2.4. H3K27me3 is involved in repressing effector gene expression during mycelial growth of *M. oryzae*. (A) The expression of effector genes enriched with H3K27me3 were analyzed in strains of wild-type O-137 and *Δmokmt6* that were grown in CM. Quantitative RT-PCR analysis of expression were used to measure relative transcripts of avirulence genes to *M. oryzae actin* gene. (B) *BAS4* expression was derepressed in the absence of H3K27me3 during mycelial growth. Left panel shows reduced H3K27me3 enrichment at *BAS4* and nearby loci in *Δmokmt6* compared to a wild-type. Right panel shows derepressed *BAS4* expression in mycelia of *Δmokmt6*. (C) *MC69*

expression was remained in the absence of H3K27me3 during mycelial growth. No H3K27me3 enrichment was observed at *MC69* and nearby loci (left panel) and no expression change was detected in *Δmokmt6* compared to a wild-type (right panel). The abundance of effector gene transcripts in mutant is expressed relative to a value of 1 in the wild-type O-137. Mean values and standard deviation were calculated from three biological replicates. Two-tailed student t-test was performed to determine statistical difference. * indicates $p<0.05$, ** indicates $p<0.01$, *** indicates $p<0.001$ and NS means no significant difference was detected. See more examples in supplemental Figure S2.5.

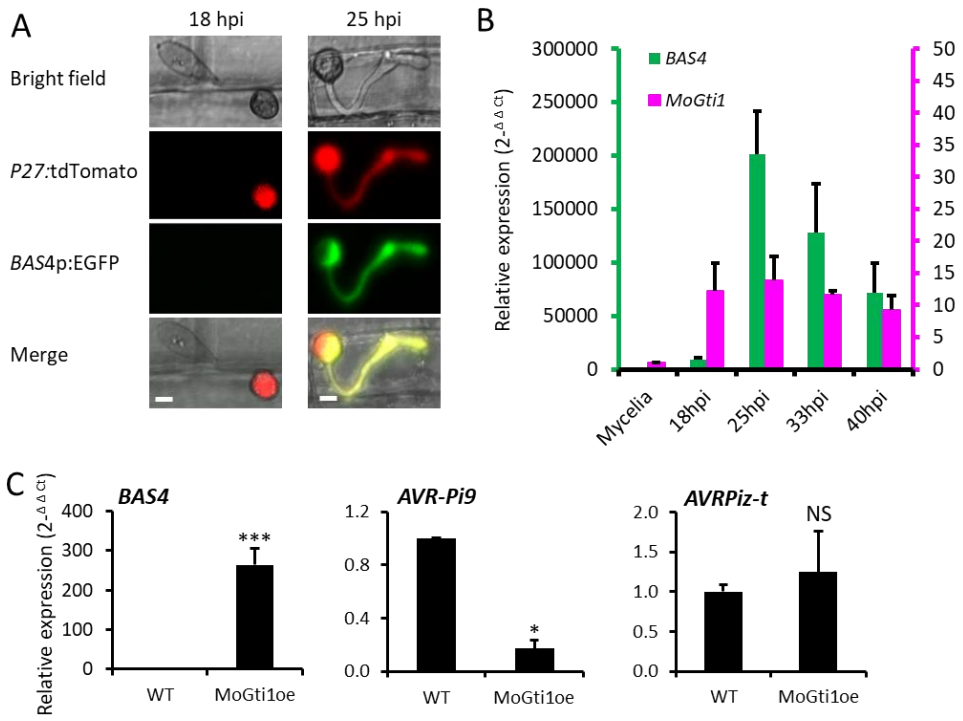

Figure 2.5. The transcription factor MoGti1 differentially regulates a subset of effector genes. Expression of *BAS4* during rice sheath infection was monitored by a fluorescent reporter strain (A) and qRT-PCR analysis (B). (A) At 18 hours post inoculation (hpi), only tdTomato control fluorescence was observed in an appressorium. But both EGFP fluorescence indicative of *BAS4* expression and tdTomato fluorescence were observed at 25 hpi in appressorium and invasive hyphae. All images are projections of multiple z-stacks. Bars: 10 μm. (B) Time-course qRT-PCR analysis at different time points (18, 25, 33, 40 hpi) confirmed the *BAS4* expression pattern and also indicated a coincide expression of *BAS4* and *MoGti1* during plant infection. (C) MoGti1 overexpression upregulated *BAS4* expression during mycelial growth (left panel), downregulated *AVR-Pi9* expression (middle panel), and did not alter *AVRPiz-t* expression (right panel) when compared to that in a wild-type. See more examples in supplemental Figure S2.8. Mean values and standard deviation were calculated from three biological replicates. * indicates $p<0.05$, *** indicates $p<0.001$ and NS means no significant difference was detected.

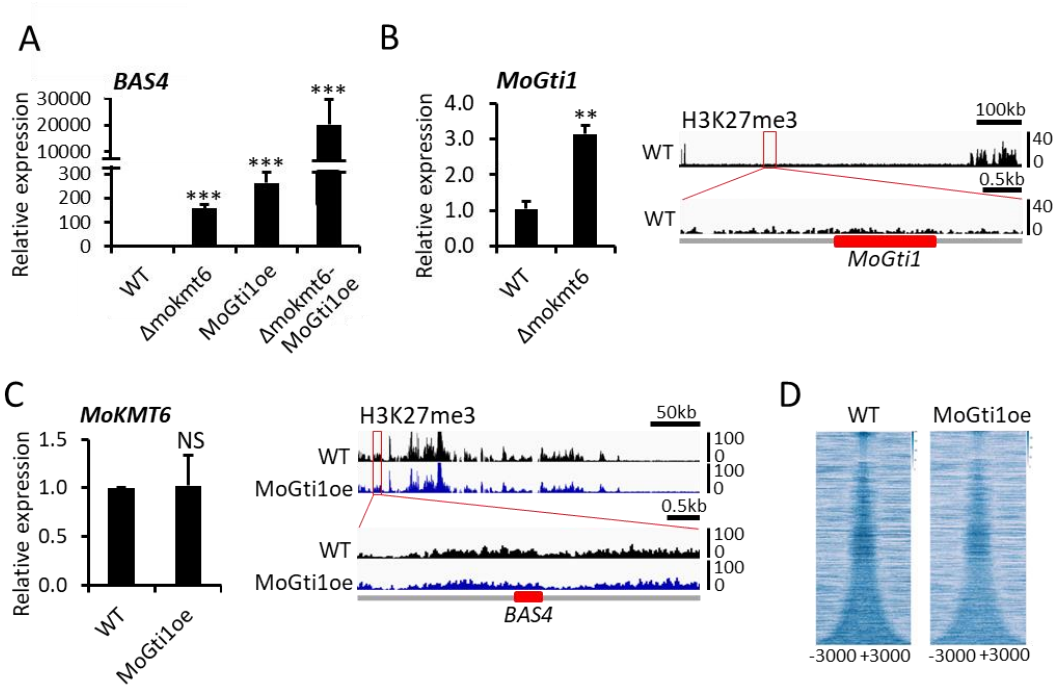

Figure 2.6. Double control of effector gene expression by H3K27me3 and MoGti1. (A) *BAS4* expression was synergistically upregulated during mycelial growth of Δ*mokmt6*-MoGti1oe strain compared to that of Δ*mokmt6* and MoGti1oe strain respectively by a qRT-PCR analysis. *BAS4* expression in Δ*mokmt6* and MoGti1oe strains was calculated from the same dataset to the Figure 2.4B and 2.5C. All four samples were prepared and run at same time. Mean values and standard deviation were calculated from three biological replicates. *** indicates $p<0.001$. (B) *MoGti1* expression was upregulated during mycelial growth of Δ*mokmt6* compared to wild-type ($p<0.01$, left panel), though no H3K27me3 enrichment was observed at *MoGti1* and nearby loci (right panel). (C) Neither *MoKMT6* expression level (left panel) nor H3K27me3 pattern at *BAS4* and nearby loci (right panel) was affected by MoGti1 overexpression during mycelial growth. (D) Overexpression of MoGti1 does not change H3K27me3 in *M. oryzae*. Heatmaps for all ~800 H3K27me3 peaks in genome ordered from smallest to largest. Heatmaps are centered on peak center and +/-3000bp for a total window size of 6000bp. Wildtype (left), and overexpression MoGti1 peaks (right).

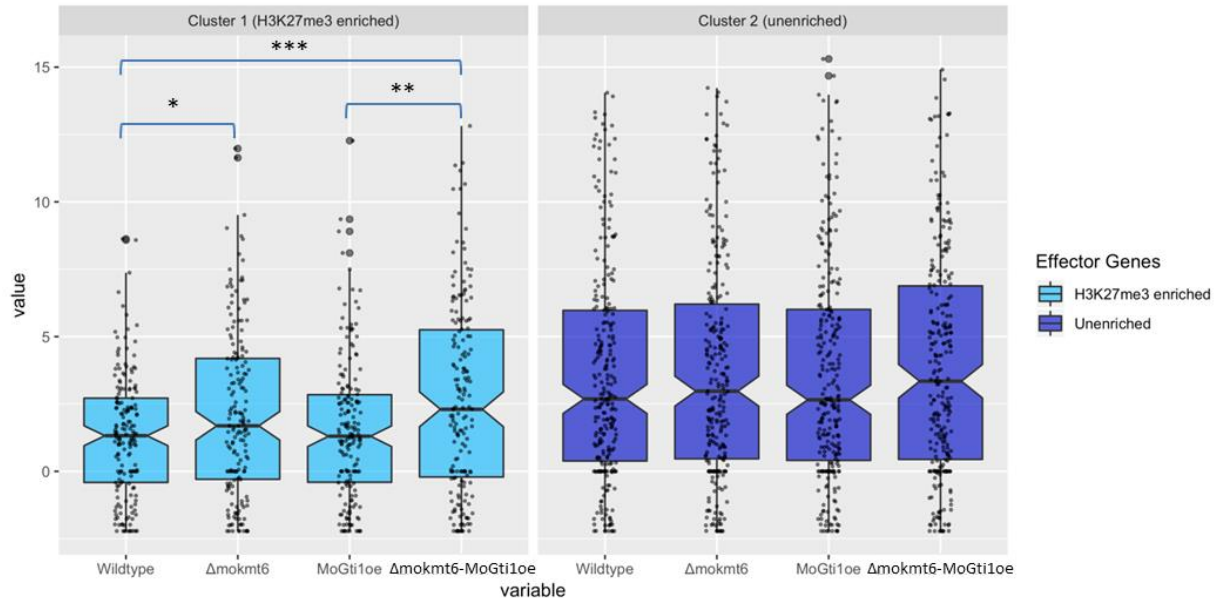

Figure 2.7. Effector genes show distinct expression changes according to H3K27me3 status. Boxplots of rlog normalized counts for effector genes enriched in H3K27me3 (left) and unenriched (right). Statistical significance indicated by *, using the Kruskal-Wallis test.

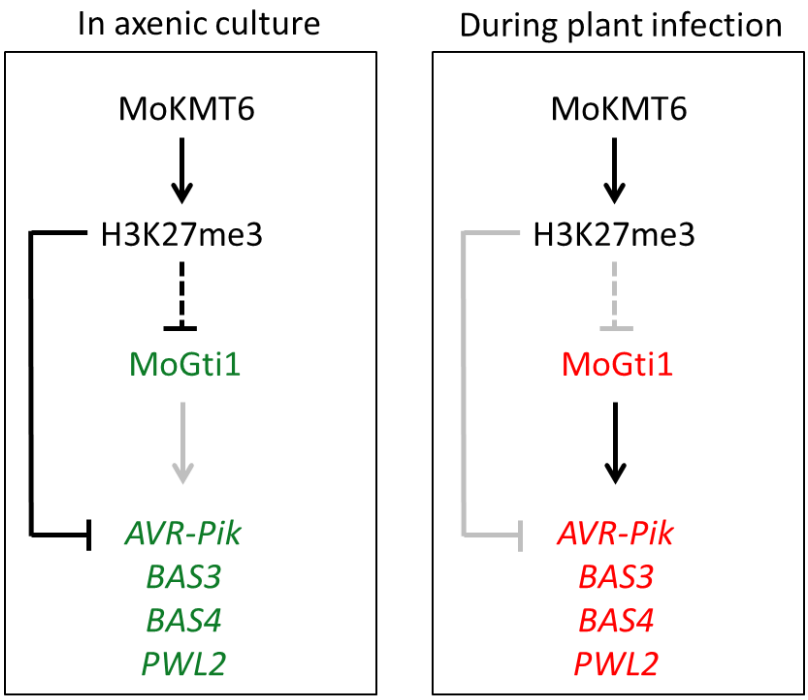

Figure 2.8. Expression of effector genes is coordinately controlled by histone modification H3K27me3 and transcription factor MoGti1. During growth in axenic culture, H3K27me3, deposited by MoKMT6, is highly enriched at effector gene loci and thereby involves repressing effector gene expression. Meanwhile, MoGti1 expression is repressed by H3K27me3, although no H3K27me3 enrichment is observed at MoGti1 locus. During plant infection, H3K27me3 enrichment is redistributed at effector gene loci and MoGti1 expression is upregulated. This allows MoGti1 or unknow transcription factors to efficiently access effector gene loci to regulate expression of effector genes. Green and red colors indicate repressed and upregulated expression respectively. Black and grey lines indicate enriched and removed H3K27me3 at effector gene loci.

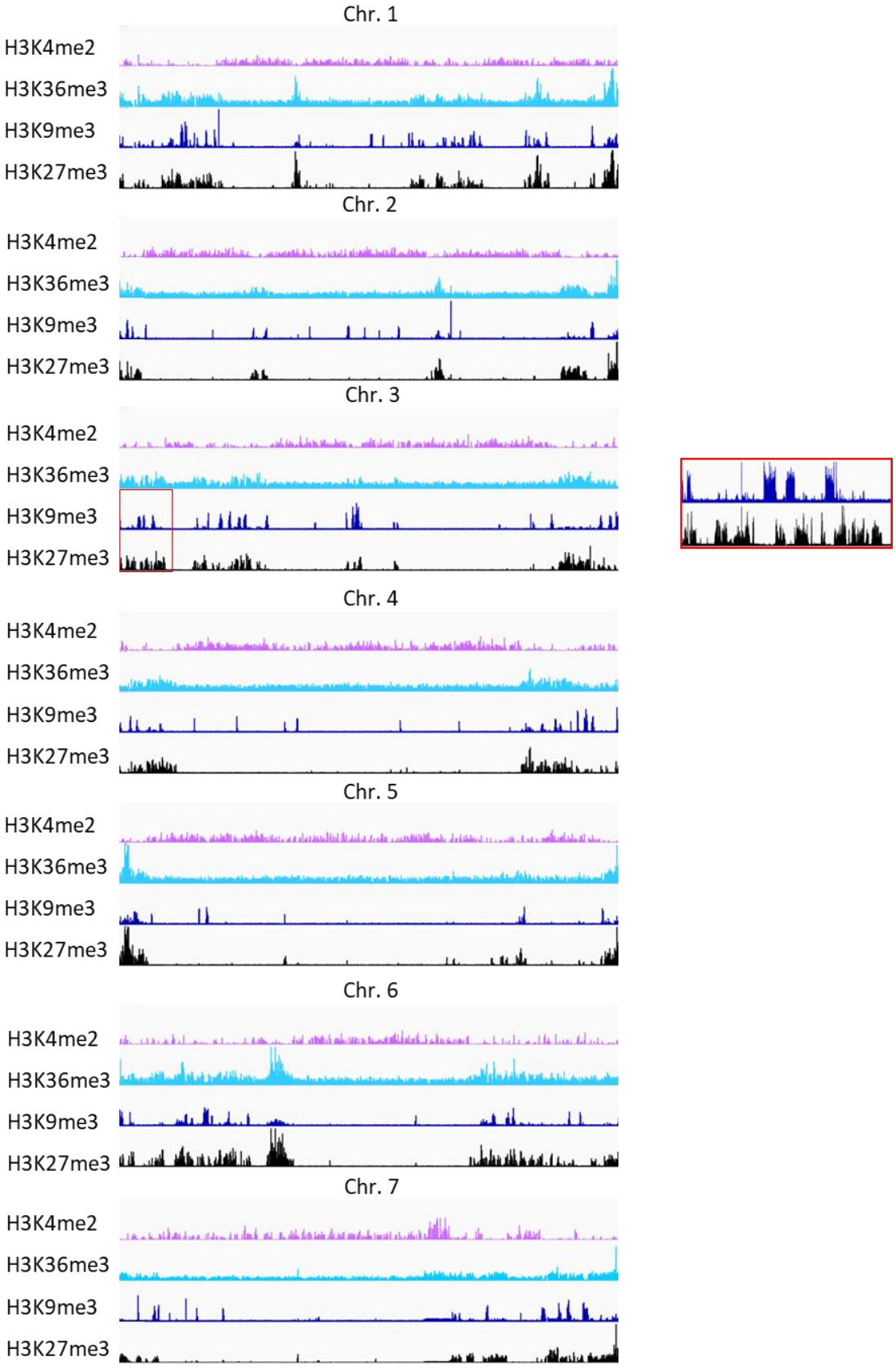
Chr. 1
H3K4me2
H3K36me3
H3K9me3
H3K27me3
Chr. 2
H3K4me2
H3K36me3
H3K9me3
H3K27me3
Chr. 3
H3K4me2
H3K36me3
H3K9me3
H3K27me3
Chr. 4
H3K4me2
H3K36me3
H3K9me3
H3K27me3
Chr. 5
H3K4me2
H3K36me3
H3K9me3
H3K27me3
Chr. 6
H3K4me2
H3K36me3
H3K9me3
H3K27me3
Chr. 7
H3K4me2
H3K36me3
H3K9me3
H3K27me3

Figure S2.1. Profile of ChIP for H3K4me2, H3K36me3, H3K9me3, and H3K27me3 enrichment for all chromosomes in *M. oryzae*. H3K27me3 (black) is predominantly enriched in, although not restricted to, the ends of chromosomes, which distribution is mutually exclusive of H3K4me2 (purple). H3K36me3 (cyan) is found throughout the genome with relative higher enrichment at chromosome ends of the wild-type strain. Selected region of Chromosome III near the telomere (inset) is expanded to detail some mutually exclusive H3K27me3 and H3K9me3 domains.

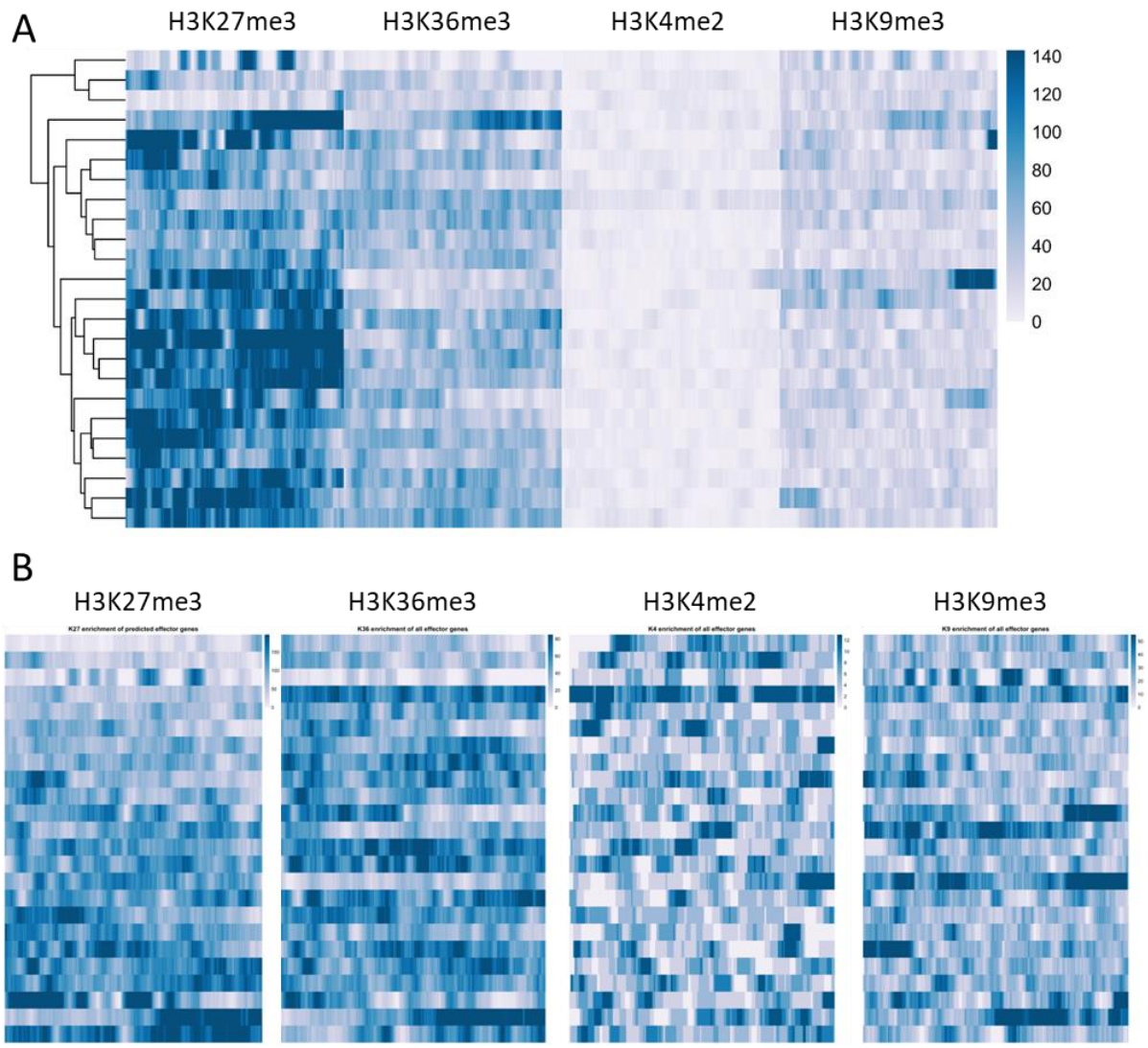

Figure S2.2. Most of 24 known effector genes are enriched for H3K27me3. (A) Hierarchical clustering by row of an underlying histogram containing all modifications for combinatorial clustering of 24 known effector genes. (B) Heatmaps of all modifications ordered by H3K27me3 enrichment level (top: lowest, bottom: highest). Each heatmap is on its own scale. Both sets of heatmaps are centered on the TSS +/-1000bp for a total window size of 2000bp.

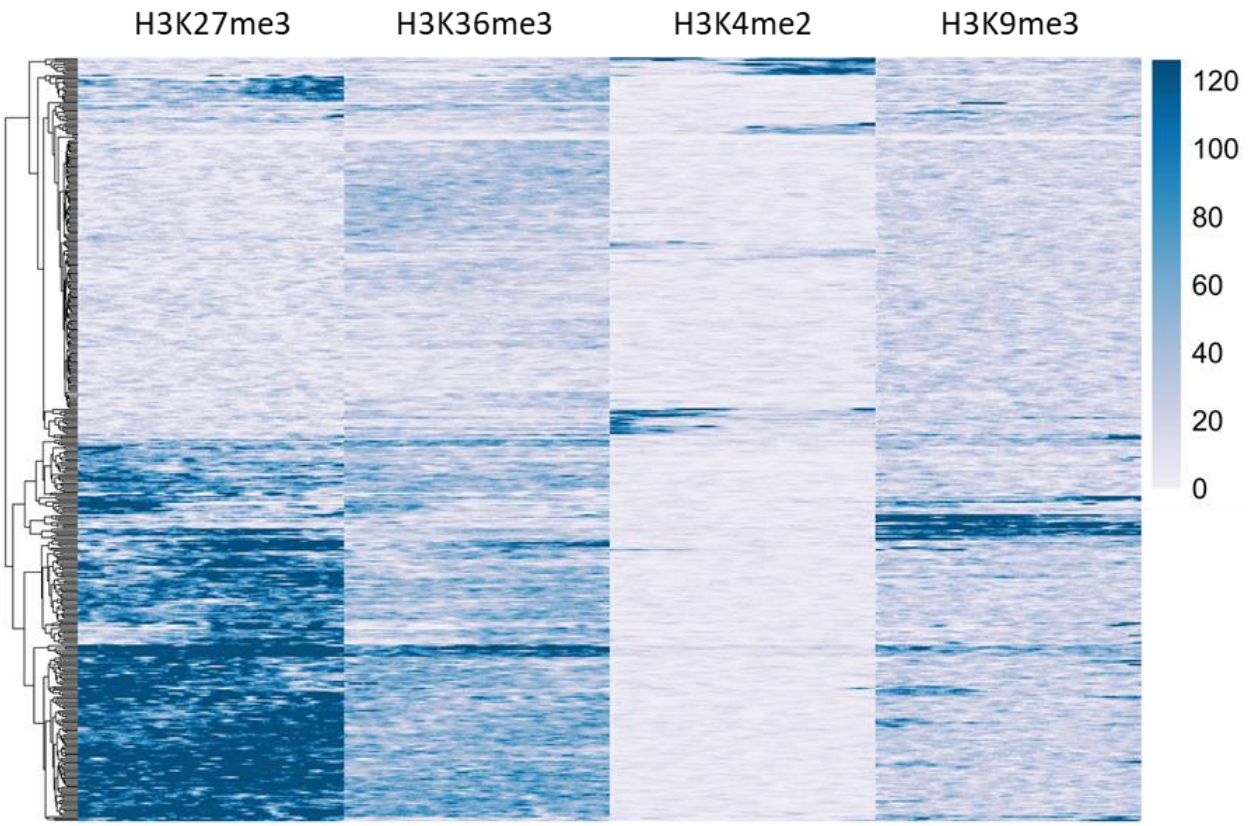

Figure S2.3. Hierarchical clustering of H3K27me3, H3K36me3, H3K4me2, H3K9me3 for all known and predicted effector genes. Hierarchical clustering by row of an underlying histogram containing all modifications for combinatorial clustering of 448 known and predicted effector genes (only 446 are shown due to lack of sequencing coverage for two).

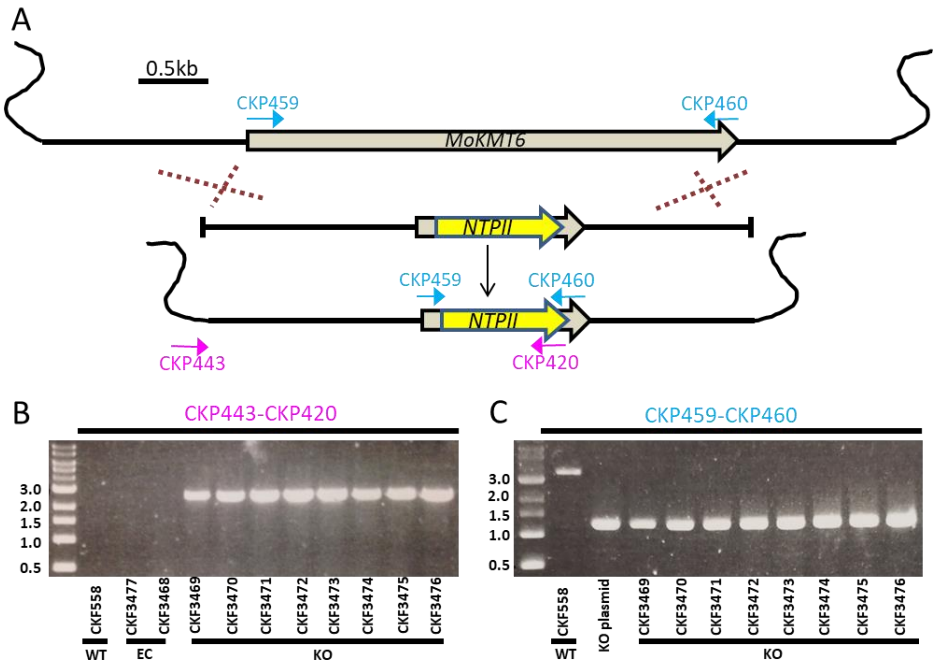

Figure S2.4. Gene replacement analysis of *MoKMT6*. (A) Schematic diagram of *MoKMT6* (grey arrow) genomic locus. The gene replacement construct contained the *NTPII* gene (yellow arrow) flanked by 1.4-kb of upstream and 1.3-kb of downstream sequences of the *MoKMT6* coding sequence. The construct was inserted through homologous recombination at *MoKMT6* locus. Primer combinations (See Table S2.12) to check for the correct insertion of the construct are indicated (pink and blue). CKP443 is right outside of 1.4-kb of upstream of *MoKMT6* and CKP420 is the reverse primer of *NTPII* gene. CKP459/CKP460 is the primer pair to amplify *MoKMT6*. (B) and (C) PCR analyses were performed from the knock-out construct, wild-type, ectopic transformants and independent knock-out mutants. No amplifications from wild-type (WT) and ectopic(EC) strains using CKP443/CKP420 suggested that there is either no *NTPII* gene (WT) or CKP443/CKP420 are not in same fragment, even same chromosome (EC). This was further confirmed by same size amplifications from knock-out construct and mutants (*NTPII*, 1.2-kb) but 3.5-kb from WT (*MoKMT6*) using the primer pair CKP459/CKP460.

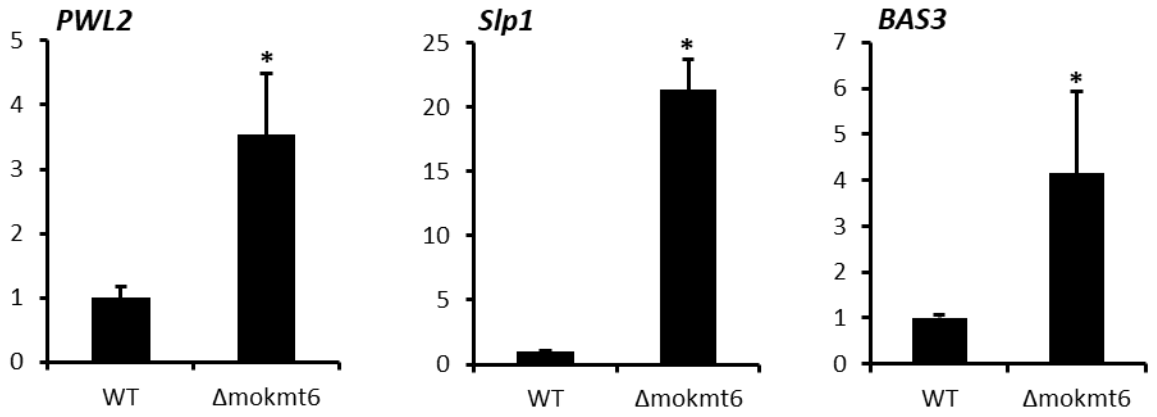

Figure S2.5. Expression of effector genes enriched with H3K27me3 is derepressed in *MoKMT6* deletion mutant during mycelial growth. The expression of effector genes enriched with H3K27me3 was analyzed in strains of wild-type O-137 and *Δmokmt6* that were grown in CM for 5 days. Mean values and standard deviation were calculated from three biological samples. Two-tailed student t-test was performed to determine if effector gene expression in *Δmokmt6* was significantly different from expression in the wild-type. * $p<0.05$.

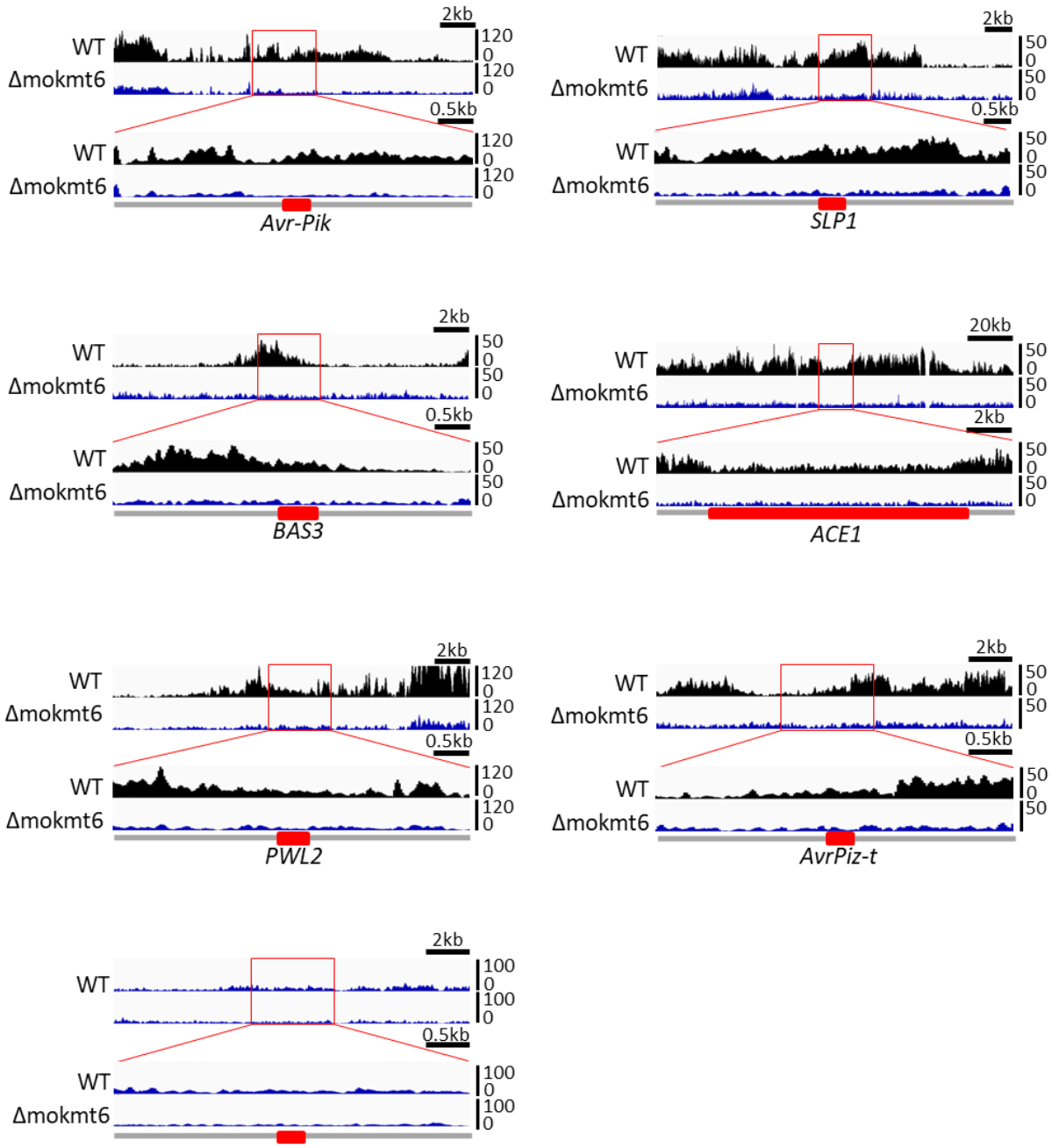

Figure S2.6. H3K27me3 enrichment is reduced at qRT-PCR tested effector gene loci and nearby loci during mycelial growth of *Δmokmt6* compared to a wild-type.

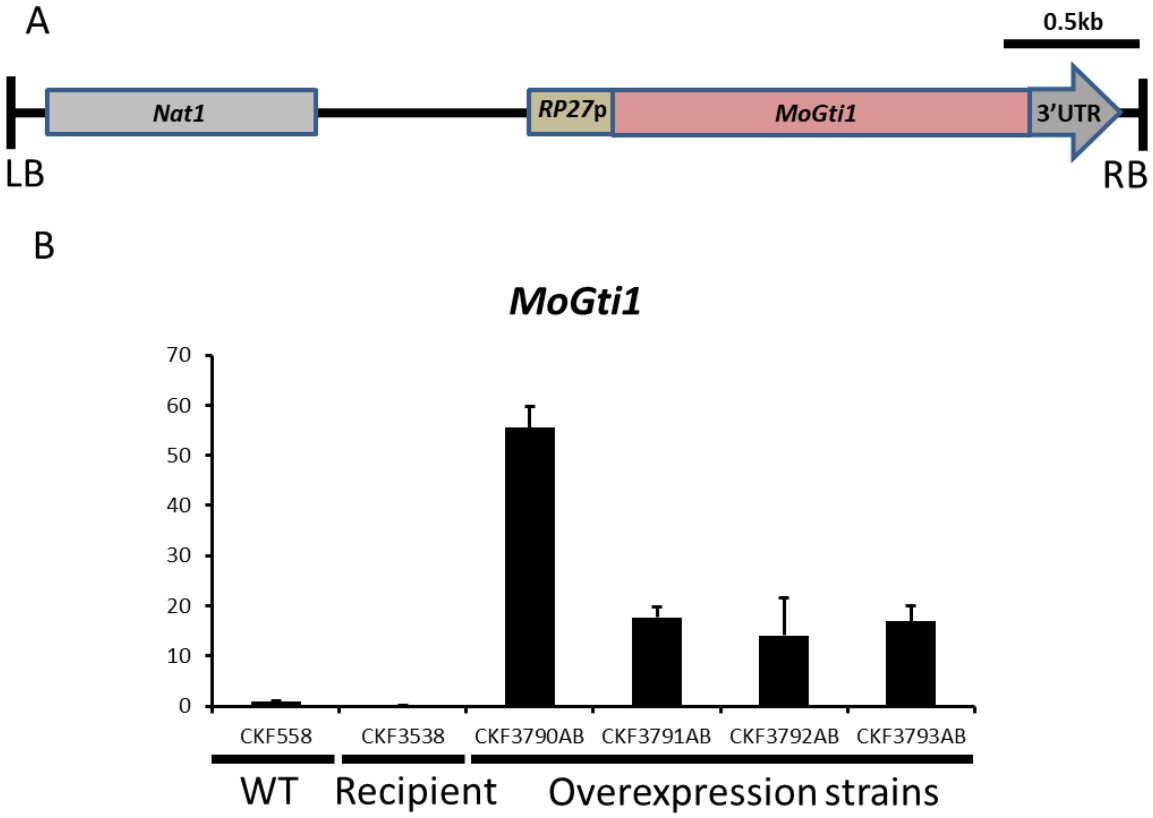

Figure S2.7. Generation of overexpression strains for *MoGti1* gene. (A) *MoGti1* was amplified from *M. oryzae* isolate O-137 using primer pairs in Table S2.12. *M. oryzae* constitutive promoter *RP27* (0.3-kb) was fused to *MoGti1* coding sequence with its 3'-flanking region (0.3-kb). The constructed vector has a *Nourseothricin acetyltransferase* gene (*Nat1*) that is resistance to nourseothricin. Fungal conidia from a *PWL2* reporter strain (CKF3538) was transformed with this construct. LB: left border, RB: right border. (B) qRT-PCR assay of *MoGti1* expression. Four transformants with wild-type and recipient strains were inoculated into liquid CM for 5 days to determine *MoGti1* expression level using qRT-PCR assay. CKF3790AB showed the highest expression of *MoGti1* and was selected for the following study.

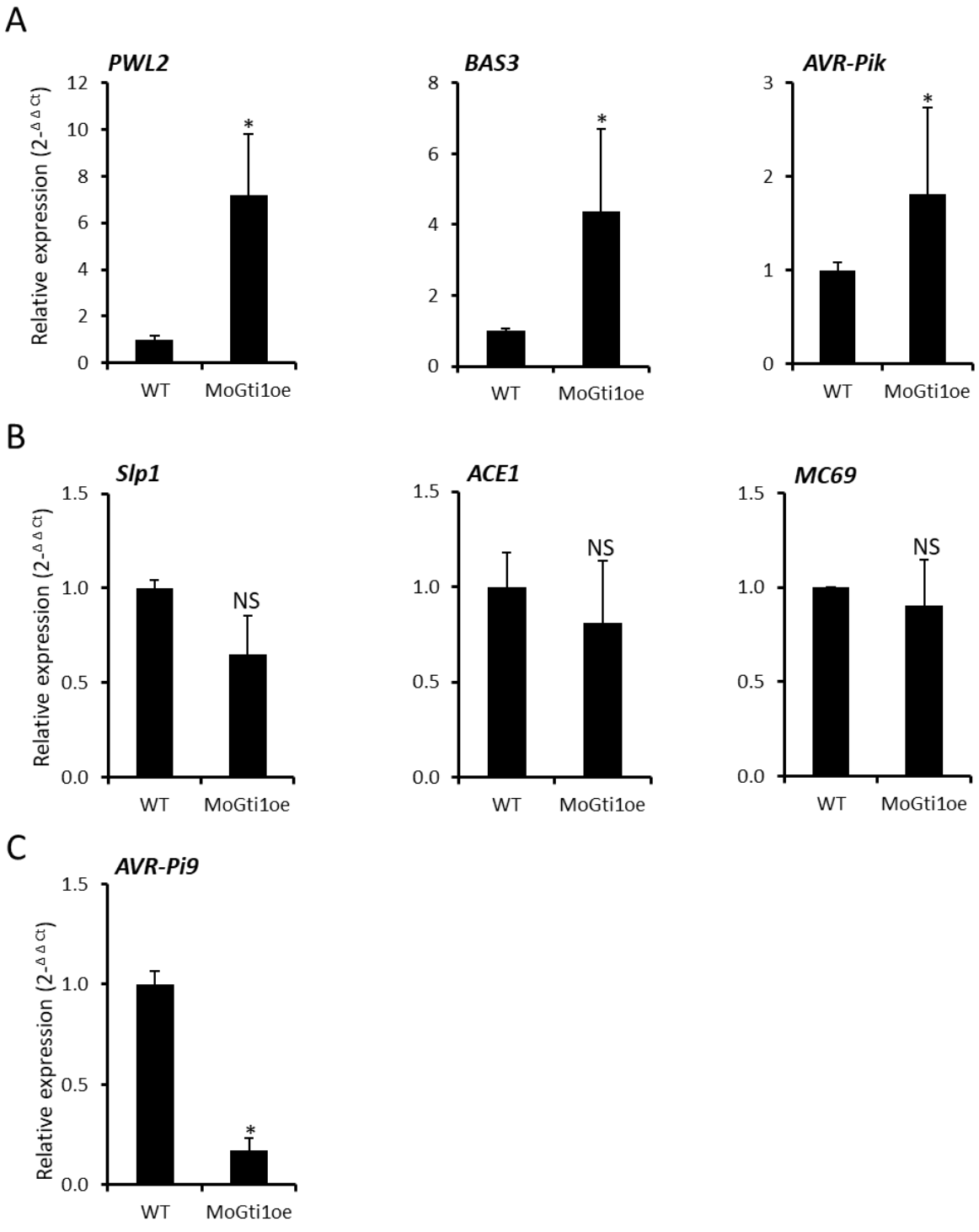

Figure S2.8. Expression of *M. oryzae* effector genes in MoGti1 overexpression strain during mycelial growth. MoGti1 overexpression upregulated (A), downregulated (C) and did not affect (B) expression of effector genes. The expression of effector genes was analyzed in strains of

wild-type O-137 and MoGti1oe that were grown in CM for 5 days. Mean values and standard deviation were calculated from three biological samples. Two-tailed student t-test was performed to determine if effector gene expression in MoGti1oe was significantly different from expression in the wild-type. * $p<0.05$. NS means no significant difference was detected.

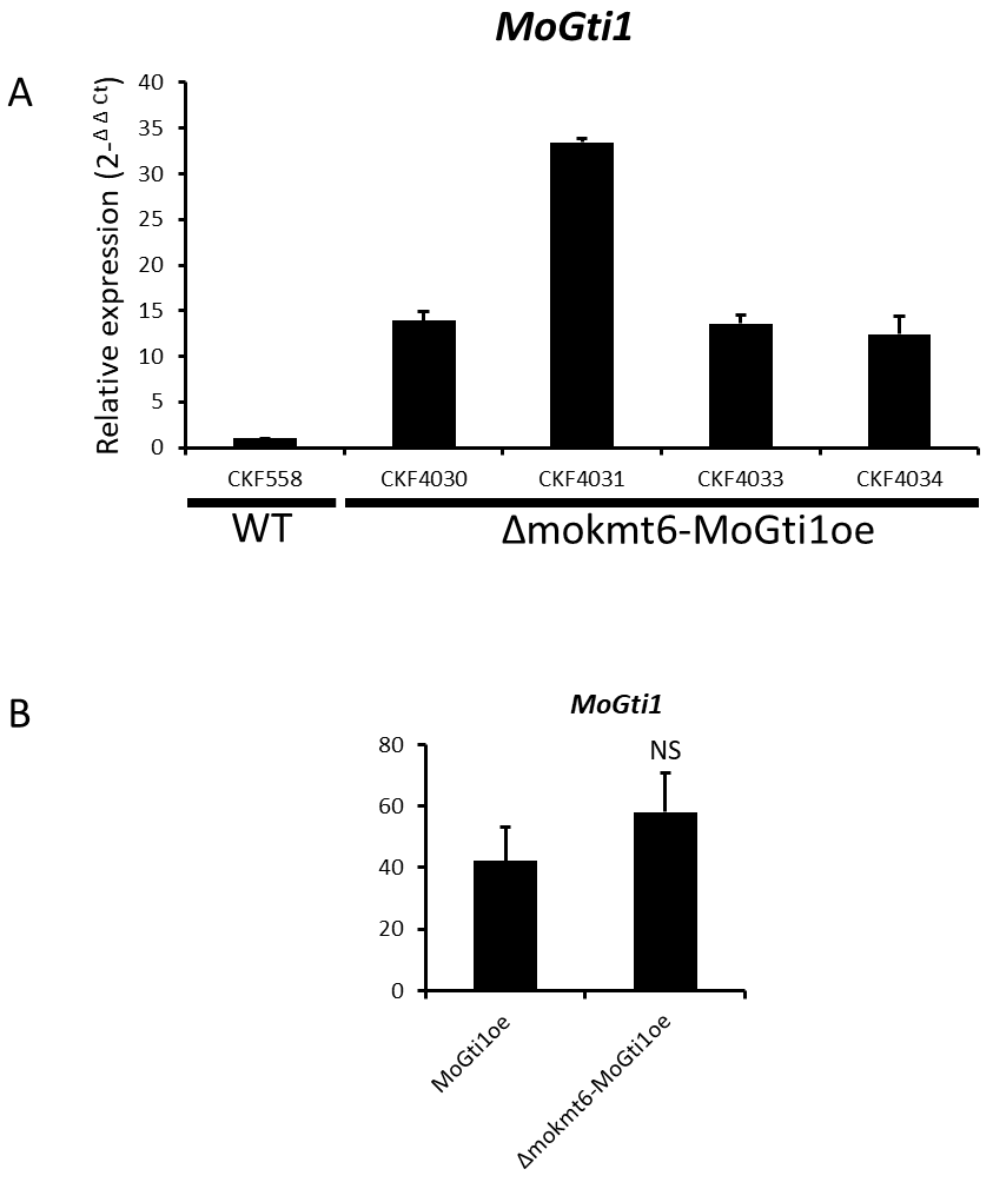

Figure S2.9. Generation of MoGti1 overexpression strains in *MoKMT6* deletion mutant. (A) *MoGti1* overexpression construct was transformed into a *MoKMT6* deletion mutant (CKF3472). Four transformants with wild-type were inoculated into liquid CM for 5 days to determine *MoGti1* expression level using qRT-PCR assay. CKF4034 was selected for the following study. (B) The comparable *MoGti1* expression level in the MoGti1oe and *Δmokmt6*-MoGti1oe strains. NS means no significant difference was detected.

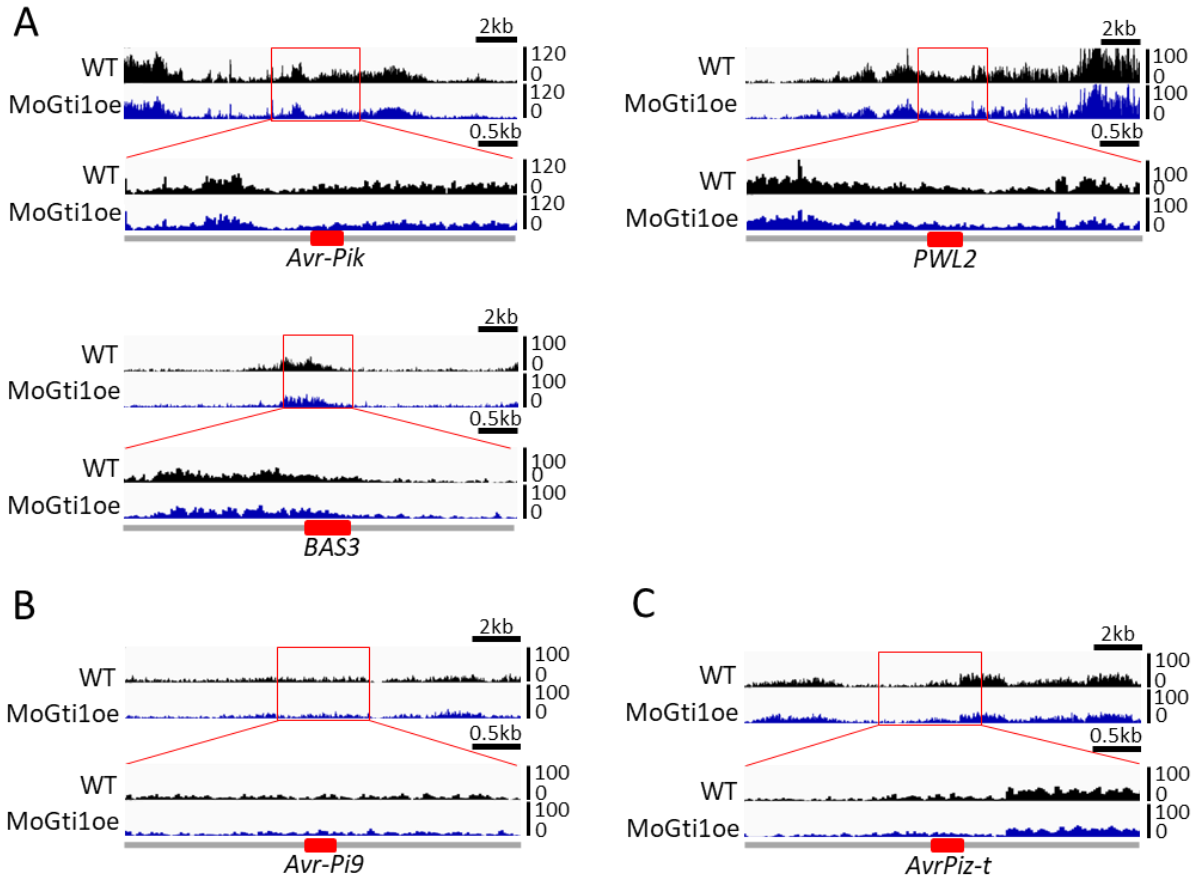

Figure S2.10. No noticeable difference of H3K27me3 was observed at individual effector gene loci in MoGti1 overexpressed strain. Although MoGti1 overexpression upregulated (A), downregulated (B) and did not affect (C) expression of effector genes, H3K27me3 distributions at loci of all these effector genes were not changed. (C) shows an example of unchanged H3K27me3 at loci of effector genes of which expression were not affected by MoGti1 overexpression.

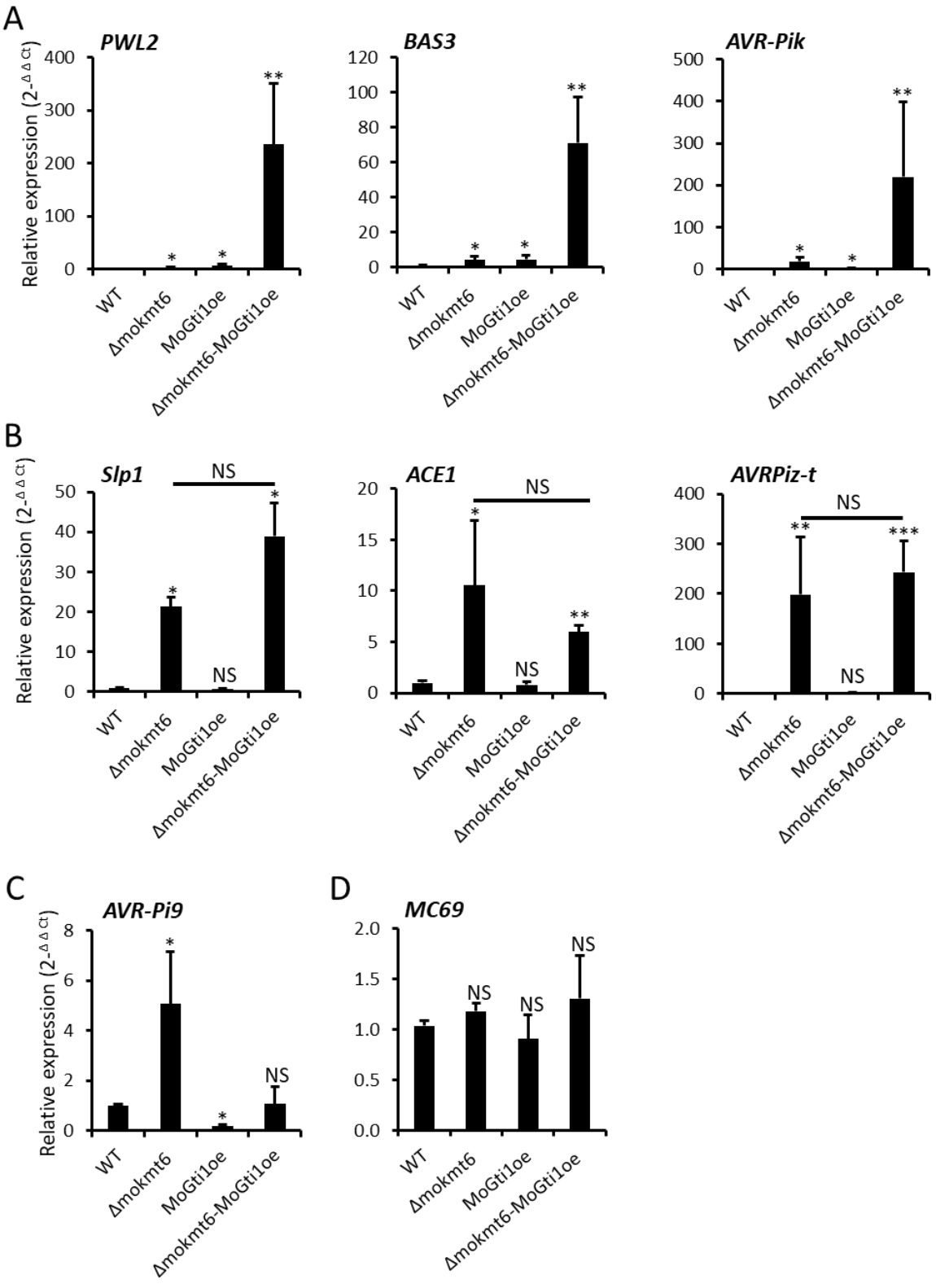
A
PWL2
BAS3
AVR-Pik
Relative expression (2-ΔΔCt)
WT
Δmokmt6
MoGti1oe
Δmokmt6-MoGti1oe
B
Slp1
ACE1
AVRPiz-t
NS
C
AVR-Pi9
D
MC69

Figure S2.11. Expression of effector genes is regulated by two different mechanisms, epigenetic and transcriptional. The effector gene expression was monitored in wild-type, *Δmokmt6*, MoGti1oe and *Δmokmt6*-MoGti1oe strains following growth in CM for 5 days. (A) Expression of effector genes that are controlled by both H3K27me3 loss and MoGti1 overexpression was synergistically upregulated in *Δmokmt6*-MoGti1oe. (B) Expression of effector genes showed no significant difference in both *Δmokmt6* and *Δmokmt6*-MoGti1oe, suggesting that they are only controlled by H3K27me3 but not by MoGti1. (C) Counteract of up/down regulation of *AVR-Pi9* by H3K27me3 loss and MoGti1 overexpression resulted in nonsignificant difference of *AVR-Pi9* expression in *Δmokmt6*-MoGti1oe compared to wild-type. (D) Neither H3K27me3 loss nor MoGti1 overexpression controlled *MC69* expression. Mean values and standard deviation were calculated from three biological samples. Two-tailed student t-test was performed to determine if effector gene expression was significantly different between different strains. * $p<0.05$, ** $p<0.01$, *** $p<0.001$. NS means no significant difference was detected.

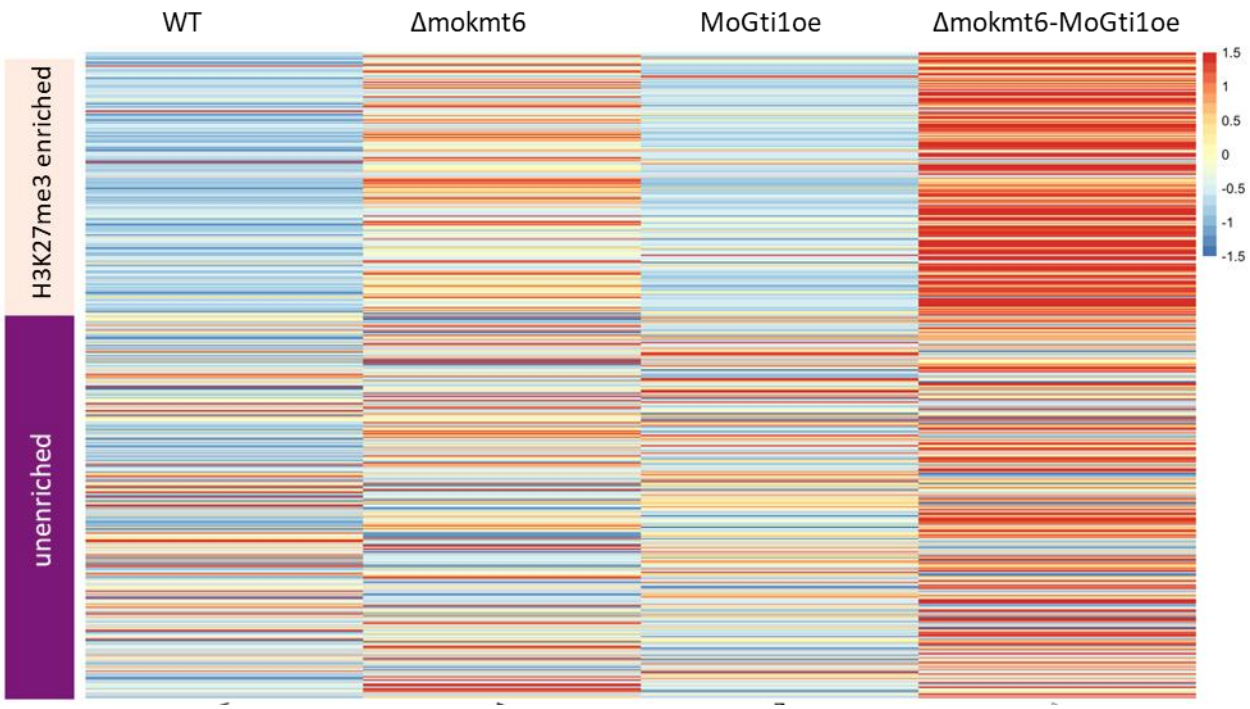

Figure S2.12: Effector genes classes have distinct expression changes. Heatmap shows all RNA-seq replicates for each sample and is ordered by classes of effector genes that have H3K27me3 enrichment (top) and effector genes that are unenriched (bottom). H3K27me3-enriched effector genes show upregulated expression when *MoKMT6* is deleted, with less dramatic expression changed in the unenriched class.

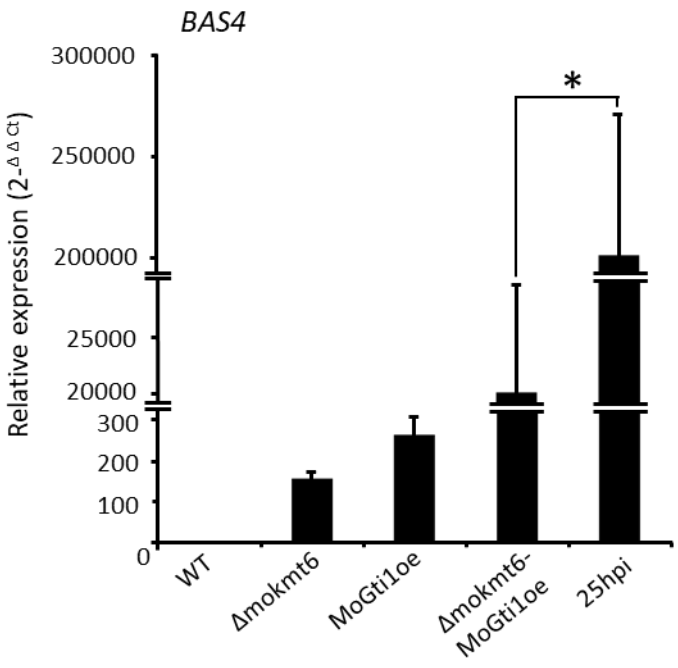

Figure S2.13. Expression of *BAS4* is regulated by epigenetic, transcriptional and unknown mechanisms. To determine if expression of *BAS4* is exclusively under control of H3K27me3 and MoGti1during plant infection, we compared transcript levels of *BAS4* in *Δmokmt6*-MoGti1oe strain following growth in CM for 5 days and in wild-type strain during plant infection (25 hpi). *BAS4* expression level is significantly higher during plant infection than that in *Δmokmt6*-MoGti1oe strain. Mean values and standard deviation were calculated from three biological samples. Two-tailed student t-test was performed to determine if *BAS4* gene expression was significantly different between different strains. * $p<0.05$.

CHAPTER 3

TANDEM DNA REPEATS CONTAIN *CIS*-REGULATORY SEQUENCES THAT ACTIVATE BIOTROPHY-SPECIFIC EXPRESSION OF *MAGNAPORTHE* EFFECTOR GENE *PWL2*[2]

[2] Jie Zhu, Jun Seop Jeong, Chang Hyun Khang. Submitted to New Phytologist.

Abstract

During plant infection fungi secrete effector proteins in coordination with distinct infection stages. The success of infection is determined by precise control of effector gene expression. We analyzed the *PWL2* effector gene of the rice blast fungus *Magnaporthe oryzae* to understand how genes are activated specifically during the early biotrophic invasion of rice cells.

We used confocal live-cell imaging of *M. oryzae* transformants with various *PWL2* promoter fragments fused to sensitive GFP reporter genes to analyze the expression pattern and the promoter activity at the cellular level, together with qRT-PCR analyses at the tissue level.

PWL2 expression was coupled with sequential biotrophic invasion, starting in the appressorium upon penetration into a rice cell (living), but greatly declining to in highly branched hyphae in the first-invaded cell (dead), then re-increasing as the hyphae penetrate into adjacent cells (living). The expression of *PWL2* required fungal penetration into living plant cells of either host rice or nonhost onion. Deletion and mutagenesis experiments revealed that the tandem repeats in the *PWL2* promoter contains 12-bp motifs required for expression.

We conclude that biotrophy-specific *PWL2* expression is activated by an unknown signal commonly present in living plant cells and requires 12-bp *cis*-regulatory sequences in the promoter.

Introduction

Fungal infections on susceptible plants are facilitated by hundreds of secreted proteins, collectively known as effectors, that modulate host cell structure, metabolism and function (Giraldo and Valent, 2013; Sanchez-Vallet et al., 2018b). The success and degree of infection is essentially influenced by the precise control of effector gene expression. There is growing evidence that distinct sets of effector genes are coordinately expressed in successive waves during the course of infection while these genes are transcriptionally repressed during vegetative growth (Dong et al., 2015; Gervais et al., 2017; Hacquard et al., 2013; Kleemann et al., 2012; Lanver et al., 2018; O'Connell et al., 2012b; Tan and Oliver, 2017a). In hemibiotrophic pathogens, including the rice blast fungus *Magnaporthe oryzae*, some effector genes (biotrophy-specific effector genes) are expressed during a biotrophic stage of infection and other effector genes during a later necrotrophic stage of infection (Mosquera et al., 2009; O'Connell et al., 2012b). What specific conditions trigger effector gene expression and how the expression is transcriptionally regulated in an infection stage-specific manner remain largely unknown but answering these questions has the potential to reveal processes unique to fungal pathogens that can be exploited as novel targets for disease control.

Magnaporthe oryzae causes devastating blast disease in rice and other economically important crops. Recent live-cell imaging studies, making use of a rice sheath infection assay and various fluorescent reporters, have revealed cellular dynamics associated with the early biotrophic stage of rice blast infection (Giraldo and Valent, 2013; Jones et al., 2017; Kankanala et al., 2007; Khang et al., 2010b; Pfeifer and Khang, 2018; Sakulkoo et al., 2018; Shipman et al., 2017) Fig. 3.1a). *Magnaporthe oryzae* biotrophic invasion begins when a single-celled appressorium produces a penetration peg that breaches the rice cell wall, allowing the fungus to enter a living rice cell. Once inside the first-invaded rice cell, the penetration peg expands to

form a filamentous primary hypha. As the primary hypha switches from filamentous to depolarized growth, the nucleus in the appressorium begins mitosis, and one nucleus undergoes a long-distance migration to the swollen tip of the primary hypha, followed by a septation, to produce the first bulbous invasive hyphal cell. The bulbous invasive hyphae (IH) continue colonizing the first-invaded host cell for 8-12 hours before moving into adjacent cells using IH pegs that co-opt plasmodesmata (Kankanala et al., 2007; Sakulkoo et al., 2018). The first-invaded rice cell is alive but dies when the fungus penetrates adjacent living cells, establishing the successive biotrophic invasion. *M. oryzae* secretes biotrophy-specific effector proteins, including PWL2, into the biotrophic interfacial complex (BIC) presumed to mediate effector translocation into host cells. The BIC first appears at the tip of the penetrating hypha (tip-BIC), but then is repositioned to the side of the first bulbous cell (side-BIC) in the first- and subsequently-invaded cells (Fig. 3.1a). *PWL2* is one of the well characterized blast effector genes, which was initially cloned as an avirulence gene, preventing the fungus from infecting weeping lovegrass, and belongs to a multigene family present in various host-adapted isolates of *M. oryzae* (Kang et al., 1995; Sweigard et al., 1995b). Previous studies have demonstrated that *PWL2* is highly expressed during infection, while its expression is rarely detectable in axenically grown cultures (Mosquera et al., 2009; Nishimura et al., 2016; Sweigard et al., 1995b).

In this study, we analyzed the *PWL2* gene to understand how effector genes are activated specifically during the early biotrophic invasion of rice cells. The *PWL2* expression pattern and the promoter activity were determined using confocal live-cell imaging of *M. oryzae* transformants with various *PWL2* promoter fragments fused to sensitive GFP reporter genes (destabilized or nuclear-targeted) at the cellular level, together with time-course qRT-PCR analyses at the tissue level. We found that *PWL2* expression was coupled with sequential

biotrophic invasion, and that the expression required fungal penetration into living plant cells of either host rice or nonhost onion. Deletion and mutagenesis experiments revealed that the tandem repeats in the *PWL2* promoter contains 12-bp sequences required for expression. Taken together, these results show that biotrophy-specific *PWL2* expression is activated by an unknown signal commonly present in living plant cells and requires 12-bp *cis*-regulatory sequences in the promoter.

Materials and Methods

Strains, fungal transformation and plasmid construction

M. oryzae wild-type strain O-137 was used as a recipient strain to generate fungal transformants using *Agrobacterium tumefaciens*-mediated transformation (Khang et al., 2005). *M. oryzae* strains were cultured on oatmeal agar plates at 24°C under continuous light and stored frozen at -20°C to maintain full pathogenicity (Valent et al., 1991). See Table S3.3 and S3.4 for the list of *M. oryzae* strains and plasmids used in this study. To monitor *PWL2* expression at signal cell resolution, *M. oryzae* transformant CKF3538 was made by sequential transformation of pCK1292 and pCK1714 into wild-type strain O-137. pCK1292 was generated by cloning 0.5-kb *Eco*RI-*BamH*I fragment of pBV167 (*RP27* promoter) (Shipman et al., 2017) and 1.7-kb *BamH*I-*Hind*III fragment of pAN582 (pBV359, tdTomato:Nos terminator) (Nelson et al., 2007) in *Eco*RI-*Hind*III sites of pBV141 (pBGt) (Kim et al., 2011). pCK1714 was generated by cloning 1.7-kb *Eco*RI-*BsrG*I fragment of pCK1298 (PWL2p:EGFP), 0.12-kb *BsrG*I-*Not*I fragment of pBV118 (pd2EGFP-1)(Li et al., 1998), and 0.5-kb *Not*I-*Xho*I fragment of pBV1102 (*PWL2* 3'-UTR) in *Eco*RI-*Sal*I sites of pBV1 (pBHt2) (Mullins et al., 2001).

To identify the *cis*-element in the *PWL2* promoter, fungal transformants with fluorescently labeled nuclei were generated. In particular, *M. oryzae* transformant CKF3276 was

generated by sequential transformation of pCK1528 and pCK1586 into wild-type strain O-137. pCK1528 was generated by cloning 1.0-kb *EcoR*I-*BamH*I fragment of pBV126 (*RP27* promoter) (Khang et al., 2010b), 1.4-kb *BamH*I-*BsrG*I fragment of pAN582 (tdTomato:NLS), and 0.4-kb *BsrG*I-*Hind*III fragment of pBV578 (Nos terminator) in *EcoR*I-*Hind*III sites of pBV141. pCK1586 was generated by cloning 872-bp *EcoR*I-*BamH*I fragment of pCK1574 (*PWL2* promoter), 1.3-kb *BamH*I-*Xho*I fragment pCK1576 (sfGFP w/o ATG:NLS:*PWL2* 3'-UTR) in *EcoR*I-*Sal*I sites of pBV1. *sfGFP* was first cloned from sfGFP-Lifeact-7 (pCK1349), a gift from Michael Davidson (Addgene plasmid # 54739). A series of constructs with deletions, replacements and mutations in the *PWL2* promoter were generated by restriction enzyme digestion and ligation, or PCR using primers in Table S3.5 (Fig. S3.8,S3.9). The intact or manipulated *PWL2* URS fragments and sfGFP-NLS-PWL2 3'UTR were first cloned into pJET1.2 (Thermo Fisher Scientific) to confirm the introduction of the desired alteration by sequencing, and later the fragments were inserted into a binary vector pBV1.

After two rounds of selections on TB3 (0.3% yeast extract, 0.3% casamino acid, 20% sucrose) and V8 (8% V8 vegetable juice (Campbell's, pH7)) media containing 200 µg/ml of hygromycin or 800 µg/ml of G418 (Fisher BioReagents) and 200 µM of cefotaxime (Gold Biotechnology). At least ten independent transformants for each construct were selected. All positive transformants showed similar fluorescence patterns and behaved indistinguishably when compared to wild-type strain under microscopy examination and further purified by single spore isolation. Due to the position effect of transgenic genes (Chen and Zhang, 2016; Soanes et al., 2002), two-to-three independent transformants for each construct were randomly chosen for further analysis.

Infection assays

Rice sheath inoculations were performed using the susceptible rice cultivar YT16 as previously described (Jones and Khang, 2018). Briefly, excised leaf sheaths (5-8 cm long) from 19 - to 21-day old plants were inoculated with a spore suspension (1×10^5 spores/ml in distilled water). The inoculated sheaths were hand-trimmed and immediately used for confocal microscopy. Inoculations on onion epidermal peels were performed as previously described (Xu et al., 1997). In heat-killed inoculations, pre-trimmed sheaths or onion epidermal peels were incubated in 70°C water for 25 min and then inoculated with a spore suspension.

RNA isolation and quantitative RT-PCR (qRT-PCR)

For the qRT-PCR assay, fifteen infected rice sheaths at each time point of 18 hours post inoculation (hpi), 25 hpi, 33 hpi and 38 hpi were collected as described (Mosquera et al., 2009), frozen immediately in liquid nitrogen, and stored at −80°C for RNA extraction. The Trizol method (Invitrogen) was used to extract total RNAs. Genomic DNA was eliminated by Turbo™ DNase (Ambion, Cat# AM1907), according to manufacturer's instructions. Complementary DNA (cDNA) was synthesized using the ImProm II Reverse Transcriptase system (Promega) from 500 ng of total RNAs extracted from infected tissue or mycelia grown for 5 days in complete medium (CM). qRT-PCR was performed with the MX3005P (Stratagene) systems using the VeriQuest SYBR Green qPCR Master Mix (2X, Thermo Fisher). Each reaction (final volume 14 µl) contained 7 µl of VeriQuest SYBR Green qPCR Master Mix, 1.5 µl of each the forward and reverse primer (3.3 nM concentrations for each, Table S3.5), 2 µl of cDNA and 2 µl of distilled water. Thermocycler conditions were as follows: 2 min at 50°C, 10 min at 95 °C, followed by 40 cycles of 95°C for 30 sec, 60°C for 30 sec, and 72°C for 30 sec. The specificity of each primer pair was checked by incorporation of a final dissociation cycle. The relative

expression level was calculated using the $2^{-\Delta Ct}$ method (Livak and Schmittgen, 2001) with the *M. oryzae actin* gene (MGG_03982) as a reference gene (Che Omar et al., 2016). Briefly, the average threshold cycle (Ct) was normalized to that of the *actin* gene for each sample as $2^{-\Delta Ct}$, where $\Delta Ct = (Ct, _{\text{target gene}} - Ct, _{\text{actin}})$. Two technical replications for each of three biological replications were performed. Mean and standard deviation were calculated from three biological replicates.

Confocal microscopy and quantification of fluorescence intensity

Confocal microscopy was performed on a Zeiss LSM 510 Meta laser scanning, and a Zeiss LSM 880 confocal microscope. Excitation/emission wavelengths were 488 nm/496 to 544 nm for EGFP/sfGFP and 543 nm/565 to 617 nm for tdTomato. Images were processed using Zen Black software (v10.0, Zeiss). To quantify and compare fluorescence intensity for each experiment, pinhole size and detector gain were optimized to maximize detection range to avoid saturated pixels. Identical image acquisition and processing settings were used to analyze all images for each experiment. Quantification of fluorescence intensity was performed using ImageJ (https://imagej.nih.gov/ij/) as previously described (Hartig, 2013; Jensen, 2013). Briefly, an image was first maximum-projected and split into different channels. The image threshold was adjusted until all fluorescence areas were selected. Intensity measurements were then performed for each nucleus. *PWL2* promoter activity was defined as normalized sfGFP intensity from 0 to 1, with 0 being background intensity as determined in nuclei without fluorescence, and 1 being the highest intensity value in nuclei of the fungal transformant with the 872-bp *PWL2* promoter as determined by subtraction of background intensity.

Sequence analysis and effector prediction

DNA sequence analyses were performed using Geneious software (v8.1.2, https://www.geneious.com/) with sequences obtained from the NCBI database. The 1000-bp upstream sequences of *M. oryzae* genes were obtained from the Broad institute (https://www.broadinstitute.org/). The sequences were then imported into Geneious and used as the database for a BLASTn analysis. The 12-bp motif was used for a motif occurrence search by FIMO (MEME v4.12.0, http://meme-suite.org/tools/fimo) with default parameters (Grant et al., 2011) against the 1000-bp upstream sequences of *M. oryzae* effector genes. The alignment of *PWL2* sequences was conducted using ClustalW (Thompson et al., 2003) implemented in Geneious. The previously generated *M. oryzae* secretome data (Zhang et al., 2018) was used to predict effector genes using EffectorP 1.0 (Sperschneider et al., 2016), a machine learning method trained with characterized fungal effectors to predict effector proteins.

Results

Development of *PWL2* promoter reporter strains of *M. oryzae*

To determine the *PWL2* expression pattern, we generated a transcriptional reporter construct by fusing the *PWL2* promoter (PWL2p, 872-bp) and 3' untranslated region (UTR, 500-bp), respectively, at the 5'- and 3'-end of a reporter gene that encodes the destabilized version of enhanced GFP (EGFP). The rapid turnover of destabilized EGFP allows tracking the transient increase and decrease of gene expression in living cells (Li et al., 1998). The resulting construct (PWL2p:EGFP) was introduced at an ectopic location into the *M. oryzae* strain, constitutively expressing tdTomato under control of *M. oryzae* ribosomal protein *RP27* promoter (RP27p:tdTomato) (Fig. 3.1b). Our initial confocal imaging of ten randomly selected transformants consistently showed bright EGFP fluorescence mainly in IH growing inside rice

cells, compared to tdTomato fluorescence in all developmental stages of *M. oryzae* (Fig. 3.1S). We identified one transformant (*M. oryzae* strain CKF3538), showing brighter fluorescence than others. We then used qRT-PCR to determine the expression patterns of the native *PWL2* gene, and the ectopically inserted *EGFP* under control of the *PWL2* promoter in this strain (Fig. 3.1b). We found that both *PWL2* and *EGFP* display a similar pattern of expression during infection on rice, with expression peaking at 25 hpi and 38 hpi, while basal levels at 18 hpi and 33 hpi or not detectable in mycelia cultured in complete medium (Fig. 3.1c). We also noticed that the overall transcription level was higher for *EGFP* than *PWL2* likely due to the position effect of transgene integration into the genome. The consistent expression pattern of the native *PWL2* gene and the *EGFP* transgene (PWL2p:EGFP), together with the used of destabilized EGFP, confirms that the *PWL2* promoter reporter strain CKF3538 (PWL2p:EGFP and RP27p:tdTomato) can be used to monitor the transient transcriptional induction in real-time during infection.

Induced expression of *PWL2* during appressorium-mediated penetration and hyphal cell-to-cell movement

To determine the expression pattern of *PWL2* at the cellular level, we used confocal microscopy of *M. oryzae* transformant CKF3538 (PWL2p:EGFP and RP27p:tdTomato) invading rice cells. EGFP fluorescence (PWL2p:EGFP) was barely detectable in mature appressoria that had not yet penetrated rice cells (18 hpi; n=66) but was strongly detected in appressoria that had penetrated rice cells and in subsequently grown young invasive hyphae (25 hpi; n=178). As the fungus continued to grow in the first-invaded rice cell and formed highly branched hyphae, EGFP fluorescence declined to a barely detectable level (33 hpi; n=46) but then strongly increased again in IH that had spread into adjacent cells (38 hpi; n=36). We confirmed that lack of strong EGFP fluorescence at 18 hpi and 33 hpi was not due to artifacts related to cell death

because there was consistent tdTomato fluorescence (RP27p:tdTomato) in all fungal cells (Fig. 3.1d and Fig. S3.1). The pattern of EGFP fluorescence (PWL2p:EGFP) peaking at 25 hpi and 38 hpi with lack of strong fluorescence at 18 hpi and 33 hpi was consistent with the qRT-PCR result (Fig. 3.1c). These results indicate that the timing of activation of the *PWL2* promoter coincides with the timing of penetrations from appressoria into the first rice cells or from IH to adjacent cells. Consistently, we observed EGFP fluorescence in the appressorium that produced very short filamentous primary IH (~11 μm) but not in the proximately located appressorium that did not produce IH (Fig. S3.2). Using time-lapse confocal imaging, we further demonstrated the transition from absence of EGFP fluorescence to strong fluorescence immediately after the fungus penetrated rice cells and produced even ~10 μm IH in the first invaded cell (Fig. 3.1e) or 4-8μm IH in adjacent rice cells (Fig. 3.1f). Taken together, our results revealed that induction of *PWL2* expression repeatedly occurs immediately after appressorium-mediated penetration and hyphal cell-to-cell movement.

Induction of *PWL2* expression requires penetration into living plant cells

Rice cells that are initially invaded by young biotrophic hyphae are viable, but the invaded cells subsequently lose viability when the hyphae are fully expanded (Jones et al., 2016a; Jones et al., 2017). Given that *PWL2* was expressed in the fungus penetrating in presumed living rice cells (25 hpi and 38 hpi), but the expression was greatly declined in the fully expanded hyphae in presumed dead rice cells (33 hpi) (Fig. 3.1d), we hypothesized that living rice cells are required for *PWL2* expression. To test this, we examined EGFP expression using confocal microscopy of CKF3538 (PWL2p:EGFP and RP27p:tdTomato) inoculated on a heat-killed rice leaf sheath. After the fungus penetrated heat-killed rice cells, EGFP fluorescence was barely detectable, which was in stark contrast to the strong EGFP fluorescence when living

cells were penetrated while tdTomato fluorescence was comparable in both penetrations (n=42; Fig. 3.2a, S3.3a).

To determine whether the induced *PWL2* expression is specific to the host rice plant, we tested *PWL2* expression using an onion peel penetration assay (Xu et al., 1997). Onion is not a natural host of *M. oryzae*, but the fungus penetrates onion epidermal cells using the appressorium. We observed the similar results as in heat-killed rice cells. That is, EGFP fluorescence (PWL2p:EGFP) was strongly detected when the fungus penetrated living onion cells, whereas the fluorescence was barely detectable when it penetrated heat-killed onion cells even observed at saturated fluorescence levels (Fig. 3.2b, S3.3b). Taken together, we conclude that highly induced *PWL2* expression requires penetration into living plant cells, and the induction is not host specific.

Tandem repeats are required for *PWL2* expression

The *PWL2* promoter contains three imperfect repeat sequences, of which role in transcriptional regulation has not been explored (Sweigard et al., 1995b). These repeats are located at a position between -331 and -182 relative to the translation start site and occur three times in tandem, and thus are named R1 (48 bp), R2 (49 bp) and R3 (48 bp) in this study (Fig. 3.3a). R1 shares 92% sequence identity with each of R2 and R3, and R2 shares 88% identity with R3 (Fig. 3.3a). From the NCBI database, we identified DNA sequences of the *PWL2* locus in the genome sequences of *M. oryzae* strains adapted to rice or wheat. Sequence comparison revealed that the promoter regions are highly conserved across the strains, but the copy number of the repeats varied, ranging from two to three copies (Fig. 3.3b, S3.4).

To determine the role of the tandem repeats in *PWL2* expression, we compared the transcriptional activity of the *PWL2* promoter (PWL2p) and the *PWL2* promoter with deletion of

all three tandem repeats (PWL2p*Δ*repeats). Each promoter was fused to a fast folding superfolder GFP with a nuclear localization signal (sfGFP:NLS reporter) to facilitate precise detection and quantitation of the intensity of sfGFP fluorescence localized in nuclei when the promoter is activated. Each reporter construct (PWL2p:sfGFP:NLS or PWL2p*Δ*repeats:sfGFP:NLS) was introduced into the *M. oryzae* strain constitutively expressing tdTomato fused to NLS as a control of visualizing nuclei of viable fungal cells (RP27p:tdTomato:NLS) (Fig. 3.3c and Fig. S3.5). Using confocal microscopy we first demonstrated that sfGFP fluorescence of the PWL2p:sfGFP:NLS reporter strain (CKF3276) strongly accumulated in the appressorial nucleus upon penetration. We also observed that fluorescence intensity decreased in multi-branched invasive hyphae in first invaded cells but then re-increased when the hyphae moved into adjacent cells (Fig. 3.3d, S3.5). This pattern of increase-decrease-re-increase of *PWL2* promoter activity is consistent with the data generated by qRT-PCR and the other promoter reporter construct (PWL2p:EGFP) (Fig. 3.1c, 3.1d). Given that *PWL2* promoter activity changes during the course of infection, we compared fluorescence intensities of sfGFP driven by PWL2p or PWL2p*Δ*repeats at comparable infection stages, specifically focusing on the appressorium that produced young IH (less than two hyphal cells) and invasive hyphae that spread into adjacent cells. Our confocal imaging clearly showed that there was no detectable sfGFP fluorescence in the PWL2p*Δ*repeats:sfGFP:NLS strain (CKF3700) at both infection stages while tdTomato fluorescence driven by RP27p in this strain was equally strong as that in the PWL2p:sfGFP:NLS strain (CKF3276) (Fig. 3.3d, 3.3e, S3.6). These results suggest that the tandem repeats contain a positive regulatory element required for activation of *PWL2* expression during penetration into living rice cells.

The tandem repeats in the *PWL2* promoter contains *cis*-regulatory sequences

To determine if the *PWL2* promoter activity is affected by a change of location or orientation of the tandem repeats in relation to the translation start site, we made a series of promoter constructs by inserting the repeat sequences back into the repeat-deleted promoter (Fig. 3.4). These constructs were individually linked to the sfGFP:NLS reporter, and the promoter activity was measured by quantifying sfGFP fluorescence in transgenic *M. oryzae* strains during appressorium-mediated penetration as described above for Fig. 3.3c-3.3e. We first confirmed that when the three copies of repeats were inserted back into the original location, the promoter activity was fully restored (Original in Fig. 3.4a). Next, we found that insertion of the repeats at the 500-bp upstream from the original location (Non-original in Fig. 3.4a) or in the reversed orientation at the original location (Reverse in Fig. 3.4a) resulted in restoration of the promoter activity, although reduced when compared to the wild-type *PWL2* promoter (reduction of ~50% or ~25%, respectively; Fig. 3.4a). We further showed that the restoration of the promoter activity was specific to the repeats because when a random DNA of the same length as the repeats was inserted into the repeat-deleted promoter, there was no sfGFP fluorescence (Non-specific in Fig. 3.4b). These results suggest that the repeats contain a *cis*-regulatory element controlling inducibility of the *PWL2* promoter, and also that the regulatory activity is not strictly dependent on the location or orientation of the repeats relative to the translation start site. Furthermore, we found that constructs with three repeats had the higher inducibility of the promoter compared to one or two repeats, suggesting that increasing the number of the repeats increases promoter strength (Fig. 3.4b). It is important to note that one repeat, designated R, was generated by taking advantage of *Hind*III sites (AAGCTT), present in all three repeats at conserved locations, which were digested and subsequently ligated to join the 5'-end region of the R1 (14-bp) and the 3'-end

of the R3 (34-bp) (Fig. 3.5a). This single-copy repeat was sufficient for transcription, indicating the presence of a *cis*-regulatory element in each repeat.

Identification of *cis*-regulatory sequences in the tandem repeat of the *PWL2* promoter

Our initial BLAST search revealed that the repeat sequences in the *PWL2* promoter shared some similarity with those in the upstream regions of *M. oryzae* effector and candidate effector genes (Table S3.1). These shared sequences were short, ranging from 10 to 25-bp long, which we mapped on the single copy of the repeat and defined as Region I through IV (Fig. 3.5a**,** S3.8a). Regions I, II, and III are located within the first 24-bp (5'-end, Fig. 3.5a), and Region IV is located in the 3'-end of the repeat (3'-end, Fig. 3.5a). We used a sfGFP:NLS reporter to quantify promoter activity for a series of deletion or substitution mutations in the repeat. We first determined that deletion of the 5'-end (positions 1 – 24), but not the 3'-end (positions 25 – 48), completely abolished promoter activity (Fig. 3.5a,b), suggesting the presence of a *cis*-regulatory element in the 5'-end. To further define the *cis*-regulatory element, we focused our fine-scale deletion and mutation analyses on Regions I, II, and III located at the 5'-end. We found that transversion substitution mutations in each of Regions I (11-bp), II (12-bp), and III (11-bp) reduced promoter activity, and particularly mutations in Region II abolished most of the promoter activity (Fig. 3.5b, S3.8a). These results suggest that the 12-bp motif of the Region II (5'-TTATGCAAGCTT-3') is cis-regulatory sequence. This was further supported by restoration of promoter activity when the 12-bp motif was inserted back into the *PWL2* promoter with deletion of all three tandem repeats (PWL2p*Δ*repeats) (Fig. 3.5c,d).

The 12-bp-like motif is present in the upstream region of *M. oryzae* effector genes

To determine the occurrences of the 12-bp motif (5'-TTATGCAAGCTT-3') in the upstream regions of *M. oryzae* effector genes, we first identified 540 predicted effector genes in the *M. oryzae* genome using EffectorP 1.0 (Sperschneider et al., 2016), and subsequently conducted motif scanning of 1-kb upstream regions of these genes using MEME suite (Grant et al., 2011). We found a total of 126 occurrences of the motif ($p<0.0001$) in the upstream sequences of 106 genes (19.6% of a total of 540 genes), in some of which the motif occurs more than once. The motif-containing genes include some known effector genes, such as *AVR-Pik* (MGG_15972), *BAS4* (MGG_10914), *MAX* (MGG_08414), *MAX* (MGG_09425), *MOCDIP3* (MGG_07986), *MoHEG9* (MGG_00043) and *SPD10* (MGG_11991) (Chen et al., 2013; de Guillen et al., 2015; Mogga et al., 2016; Mosquera et al., 2009; Sharpee et al., 2017; Yoshida et al., 2009) (Table S3.2). A comparison of all 126 motif sequences suggests that the core sequence of the motif is 5'-TGCAAGCTT-3' (Fig. 3.5e).

To determine if the motif-containing effector genes are co-expressed with *PWL2*, we used a time-course qRT-PCR analysis for selected 10 genes that contain the motif in the same orientation and at a similar location (-200 to -350-bp relative to the translation start site) as in the *PWL2* promoter. We found that the five genes showed the similar expression patterns as *PWL2* (Fig. 3.1c and Fig. 3.6). In particular, the expression patterns of *AVR-Pik* and two predicted effector genes (MGG_01953 and MGG_08300) were strikingly similar to that of *PWL2*, exhibiting initial induction at 25 hpi (appressorium-mediated penetration into living cells), repression at 33 hpi (colonization of first-invaded dead cells), and subsequent reinduction at 38 hpi (hyphal cell-to-cell penetration into living cells) (Fig. 3.1c and Fig. 3.6). These results

suggest that the 12-bp motif plays a role in regulating the biotrophy-specific expression of *M. oryzae* effector genes.

Discussion

PWL2 expression is coupled with sequential biotrophic invasion

In this study, we provide evidence that transcriptional regulation of *PWL2* is coupled to the biotrophic phase of *M. oryzae* during colonization of the first two rice cells. In *M. oryzae*, biotrophy is characterized as sequential invasion into living rice cells, starting with the appressorium initially penetrating a living rice cell (~25 hpi), and then highly branched IH penetrating adjacent living cells after colonizing the first invaded cell until cell death (~38 hpi) (Fig. 3**.1a**) (Jones et al., 2017; Kankanala et al., 2007). Our time-course qRT-PCR at the tissue level and GFP reporter-based live cell imaging at single cell resolution consistently showed that *PWL2* expression is induced immediately upon penetrating living rice cells from the appressorium or from IH (Fig. 3.1c,d). This strong expression was in stark contrast to barely detectable expression in the appressorium on the rice cell surface (prior to penetration into the first cell) and highly branched IH in the first-invaded dead rice cell (prior to penetration into the second cell). This two-peaked expression pattern of *PWL2* coincides with localization of the PWL2 protein in BICs, which form when the fungus penetrates new living rice cells (Khang et al., 2010b; Shipman et al., 2017). These suggest that *PWL2* transcription is tightly regulated in coordination with BIC development during biotrophic invasion. Shipman *et al* (2017) made an intriguing observation that cytoplasmic effector proteins, including PWL2, are secreted into the tip BIC and the early side BIC, which can be located more than 32 μm away from the nearest nucleus in the appressorium where this study shows *PWL2* promoter is activated. It remains to be determined how effector trafficking is regulated from the appressorium through the primary

hypha to the distantly located BIC.

PWL2 expression is activated by an unknown signal in living plant cells

Fungal genes that are induced during infection are transcriptionally regulated presumably in response to either or a combination of nutrition conditions, plant-derived inducing compounds, or infection-related fungal development (Basse et al., 2000a; Meyer et al., 2017; Van den Ackerveken et al., 1994; van der Does et al., 2008). Earlier studies by Sweigard et al (1995) showed that *PWL2* transcripts were not detectable when *M. oryzae* was grown in complete, minimal, or nitrogen-depleted medium, thus excluding these nutrition conditions as cues to induce *PWL2* expression. Our finding that *PWL2* expression is induced when the fungus penetrates living cells, but not dead cells, of both rice (host) and onion (nonhost) suggests that the presumed inducer is commonly present in living plant cells (Fig. 3.2). Similar observations have been reported for biotrophy-specific effector genes in other fungi. For instance, expression of the effector gene *Six1* of *Fusasirum oxysporum* is induced upon penetration of the root cortex of living tomato (host) and also in response to cell cultures of tomato and tobacco (non-host) (van der Does et al., 2008). The plant signals that induce *Six1* expression remains unknown. The effector gene *MiSSP7* of *Laccaria bicolor* is expressed during interactions with poplar (host) and *Arabidopsis thaliana* (non-host) roots, and the inducer has been identified as rutin and quercitin, commonly found flavonoids in the exudates of plant roots (Plett et al., 2011). Future studies will be needed to identify inducers and regulatory components for *PWL2*, which can be facilitated by using strategies such as mutagenesis and screening plant compounds using GFP-based reporters (Basse et al., 2002a; Basse et al., 2000a).

Tandem DNA repeats within the *PWL2* promoter contain *cis*-regulatory sequences

Tandem DNA repeat sequences are often associated with gene promoters and function as *cis*-regulatory sequences. For example, tandem repeats are found in 25% of all promoters in the *Saccharomyces cerevisiae* genome (Vinces et al., 2009). Some tandem repeats are shown to directly regulate expression of genes such as the maltose permease gene in *S. cerevisiae* (Bell et al., 1997) and the anthocyanin-regulating transcription factor *MYB10* in apple (Espley et al., 2009). Approximately 52% of the *M. oryzae* genome consists of various repetitive sequences, and a genome-wide analysis is needed to determine how many *M. oryzae* gene promoters, particularly effector gene promoters, are associated with tandem repeats (Raffaele and Kamoun, 2012). The *PWL2* promoter contains three 48-bp imperfect tandem repeats (Fig. 3.3a) (Sweigard et al., 1995b). Using dot plot analyses, we found that promoters of eight additional effector genes beside *PWL2* contain tandem repeats in various number and length in their promoters (Fig. S3.9). There is growing evidence that tandem repeats-containing promoters show higher transcriptional divergence (Vinces et al., 2009). In agreement with this, we found that the inducibility of the *PWL2* promoter varies depending on the copy number of the repeats within the promoter (Fig. 3.4b), and intriguingly, this appears to be further implicated with the role *PWL2* plays during plant infection. *PWL2* confers avirulence against weeping lovegrass, containing a yet-to-be discovered resistance gene, and also presumes to have a virulence role in plants, lacking the resistance gene, based on prevalent presence of *PWL2* in diverse *M. oryzae* populations (Kang et al., 1995; Sweigard et al., 1995b). While characterizing DNA sequences required for *PWL2* avirulence activity, Sweigard *et al* (1995) showed that avirulence was partially lost when the promoter was deleted to contain one and half copies of the repeat or completely lost when deleted further to contain the half copy, whereas avirulence was fully retained with more than

two and half copies of the repeat. This impaired avirulence is likely due to the reduced transcription of *PWL2* that we observed with the reduced copy number of the repeats (Fig. 3.4b). It is possible that a certain level of *PWL2* transcription, correlated with protein production, is required for the PWL2 protein being recognized as an avirulence factor. We suggest that fine-tuned expression of *PWL2* through variations in the repeat copies could be a potential mechanism by which *PWL2* avoids host recognition (losing avirulence activity), while retaining a presumed virulence function, thereby facilitating *M. oryzae*'s host adaptation. Consistent with this, we found that different host-adapted *M. oryzae* strains carry a varying copy number of the repeat in the *PWL2* promoter (Fig. 3.3b). It will be exciting to investigate how repeat copy number variations correlate with *PWL2* expression in these strains and contribute to *M. oryzae*'s adaptibility on different plant species.

We provide evidence that the tandem DNA repeats contain *cis*-regulatory sequences required for biotrophy-specific expression of *PWL2*. Deletion of these repeats resulted in a complete loss of *PWL2* expression, which could be complemented when the repeats were inserted at the original location (Fig. 3.4a). The complementation was specific to the sequences of the repeats because an unrelated DNA sequence in the same length as the repeats failed to complement (Fig. 3.4a). We also determined that the single copy of the repeat contained all sequences sufficient for *PWL2* expression (Fig. 3.4b). These data suggest that each repeat contains *cis*-regulatory sequences, directly regulating gene expression presumed as a transcription factor (TF) binding site rather than a structural component of the promoter. The location and orientation of TF binding sites can have effect on promoter activity (Sharon *et al.*, 2012; Lis & Walther, 2016). Consistent with this, we observed some level of promoter activity even when these repeats were inserted at a distal location or in reverse orientation (Fig. 3.4a).

Further deletion and mutagenesis studies identified a 12-bp motif that is present within each repeat and is sufficient for *PWL2* expression (Fig. 3.5). Addition of the 12-bp motif to PWL2p*Δ*repeats restored the GFP reporter expression upon appressorium-mediated penetration into living rice cells (Fig. 3.5c,d). This motif appears to be involved in regulating expression of other effectors in *M. oryzae*. We found that at least 106 effector or effector candidate genes contain the motif in their promoter regions, and seven of these genes indeed showed the similar expression patterns as *PWL2* (Fig. 3.6), suggesting that they are transcriptionally co-regulated by common transcription factors (Lanver et al., 2018). Whether the motif directly regulates expression of these and other genes containing the 12-bp motif remains to be determined.

Evidence is accumulating that distinct sets of effector genes are coordinately expressed in successive waves during the course of plant infection, reflecting the complexity of effector gene regulation and the diversity of TFs and *cis*-regulatory sequences(Dong et al., 2015; Farfsing et al., 2005; Gervais et al., 2017; Hacquard et al., 2013; Kleemann et al., 2012; Lanver et al., 2018; O'Connell et al., 2012b; Soyer et al., 2014a; Wang et al., 2011). Fungal genomes collectively contain at least 36 different families of TFs, and 13 TFs from 4 families are known for their roles in effector regulation (Lin et al., 2018; Tan and Oliver, 2017a). *M. oryzae* is predicted to contain a total of 495 TFs (4.5% of the 11,054 proteins in *M. oryzae*) (Park et al., 2013), and thus far, MoGti1 is the only TF known to regulate the expression of *M. oryzae* effector genes, including *PWL2 (Li et al., 2016a)*. The precise mechanism of how MoGti1 controls transcription of these effector genes is not known. Our hypothesis is that MoGti1 has an indirect role in activating *PWL2* transcription based on the fact that the 12-bp motif or the rest of the *PWL2* promoter lacks the core binding motif (5’-TTAAAGTTT-3’), recognized by the MoGti1 ortholog, Wor1, in *Candida albicans* (Lohse et al., 2010). Our discovery of the 12-bp motif provides exciting

opportunities for testing this hypothesis, and also predicting new effector candidates based on the presence of the motif in their promoters.

References

Basse, C.W., Kolb, S., and Kahmann, R. (2002). A maize-specifically expressed gene cluster in *Ustilago maydis*. Molecular Microbiology *43*, 75-93.

Basse, C.W., Stumpferl, S., and Kahmann, R. (2000). Characterization of a *Ustilago maydis* gene specifically induced during the biotrophic phase: evidence for negative as well as positive regulation. Molecular and Cellular Biology *20*, 329-339.

Bell, P.J., Higgins, V.J., Dawes, I.W., and Bissinger, P.H. (1997). Tandemly repeated 147 bp elements cause structural and functional variation in divergent *MAL* promoters of *Saccharomyces cerevisiae*. Yeast *13*, 1135-1144.

Che Omar, S., Bentley, M.A., Morieri, G., Preston, G.M., and Gurr, S.J. (2016). Validation of reference genes for robust qRT-PCR gene expression analysis in the rice blast fungus *Magnaporthe oryzae*. PLoS One *11*, e0160637.

Chen, S., Songkumarn, P., Venu, R., Gowda, M., Bellizzi, M., Hu, J., Liu, W., Ebbole, D., Meyers, B., and Mitchell, T. (2013). Identification and characterization of in planta–expressed secreted effector proteins from *Magnaporthe oryzae* that induce cell death in rice. Molecular plant-microbe interactions *26*, 191-202.

Chen, X., and Zhang, J. (2016). The genomic landscape of position effects on protein expression level and noise in yeast. Cell Systems *2*, 347-354.

Crooks, G.E., Hon, G., Chandonia, J.-M., and Brenner, S.E. (2004). WebLogo: a sequence logo generator. Genome Research *14*, 1188-1190.

de Guillen, K., Ortiz-Vallejo, D., Gracy, J., Fournier, E., Kroj, T., and Padilla, A. (2015). Structure analysis uncovers a highly diverse but structurally conserved effector family in phytopathogenic fungi. PLoS Pathogen *11*, e1005228.

Dong, Y., Li, Y., Zhao, M., Jing, M., Liu, X., Liu, M., Guo, X., Zhang, X., Chen, Y., Liu, Y., *et al.* (2015). Global genome and transcriptome analyses of *Magnaporthe oryzae* epidemic isolate 98-06 uncover novel effectors and pathogenicity-related genes, revealing gene gain and lose dynamics in genome evolution. PLoS Pathogen *11*, e1004801.

Espley, R.V., Brendolise, C., Chagne, D., Kutty-Amma, S., Green, S., Volz, R., Putterill, J., Schouten, H.J., Gardiner, S.E., Hellens, R.P., *et al.* (2009). Multiple repeats of a promoter segment causes transcription factor autoregulation in red apples. Plant Cell *21*, 168-183.

Farfsing, J.W., Auffarth, K., and Basse, C.W. (2005). Identification of cis-active elements in *Ustilago maydis mig2* promoters conferring high-level activity during pathogenic growth in maize. Molecular Plant-Microbe Interactions *18*, 75-87.

Gervais, J., Plissonneau, C., Linglin, J., Meyer, M., Labadie, K., Cruaud, C., Fudal, I., Rouxel, T., and Balesdent, M.H. (2017). Different waves of effector genes with contrasted genomic location are expressed by *Leptosphaeria maculans* during cotyledon and stem colonization of oilseed rape. Molecular Plant Pathology *18*, 1113-1126.

Giraldo, M.C., and Valent, B. (2013). Filamentous plant pathogen effectors in action. Nature Reviews Microbiology *11*, 800-814.

Grant, C.E., Bailey, T.L., and Noble, W.S. (2011). FIMO: scanning for occurrences of a given motif. Bioinformatics *27*, 1017-1018.

Hacquard, S., Kracher, B., Maekawa, T., Vernaldi, S., Schulze-Lefert, P., and Ver Loren van Themaat, E. (2013). Mosaic genome structure of the barley powdery mildew pathogen

and conservation of transcriptional programs in divergent hosts. Proceedings of the National Academy of Sciences *110*, E2219-2228.

Hartig, S.M. (2013). Basic image analysis and manipulation in ImageJ. Current Protocols in Molecular Biology *102*, 14.15. 11-14.15. 12.

Jensen, E.C. (2013). Quantitative analysis of histological staining and fluorescence using ImageJ. The Anatomical Record *296*, 378-381.

Jones, K., and Khang, C.H. (2018). Visualizing the movement of *Magnaporthe oryzae* effector proteins in rice cells during infection. In Plant Pathogenic Fungi and Oomycetes (Springer), pp. 103-117.

Jones, K., Kim, D.W., Park, J.S., and Khang, C.H. (2016). Live-cell fluorescence imaging to investigate the dynamics of plant cell death during infection by the rice blast fungus *Magnaporthe oryzae*. BMC Plant Biol *16*, 69.

Jones, K., Zhu, J., Jenkinson, C.B., Kim, D.W., and Khang, C.H. (2017). Disruption of the interfacial membrane leads to *Magnaporthe oryzae* effector re-location and lifestyle switch during rice blast disease. bioRxiv, 177147.

Kang, S., Sweigard, J.A., and Valent, B. (1995). The PWL host specificity gene family in the blast fungus *Magnaporthe grisea*. MPMI-Molecular Plant Microbe Interactions *8*, 939-948.

Kankanala, P., Czymmek, K., and Valent, B. (2007). Roles for rice membrane dynamics and plasmodesmata during biotrophic invasion by the blast fungus. Plant Cell *19*, 706-724.

Khang, C.H., Berruyer, R., Giraldo, M.C., Kankanala, P., Park, S.Y., Czymmek, K., Kang, S., and Valent, B. (2010). Translocation of *Magnaporthe oryzae* effectors into rice cells and their subsequent cell-to-cell movement. Plant Cell *22*, 1388-1403.

Khang, C.H., Park, S.Y., Lee, Y.H., and Kang, S. (2005). A dual selection based, targeted gene replacement tool for *Magnaporthe grisea* and *Fusarium oxysporum*. Fungal Genetics and Biology *42*, 483-492.

Kim, H.-S., Park, S.-Y., Lee, S., Adams, E.L., Czymmek, K., and Kang, S. (2011). Loss of cAMP-dependent protein kinase A affects multiple traits important for root pathogenesis by *Fusarium oxysporum*. Molecular Plant-Microbe Interactions *24*, 719-732.

Kleemann, J., Rincon-Rivera, L.J., Takahara, H., Neumann, U., Ver Loren van Themaat, E., van der Does, H.C., Hacquard, S., Stuber, K., Will, I., Schmalenbach, W., *et al.* (2012). Sequential delivery of host-induced virulence effectors by appressoria and intracellular hyphae of the phytopathogen *Colletotrichum higginsianum*. PLoS Pathogen *8*, e1002643.

Lanver, D., Muller, A.N., Happel, P., Schweizer, G., Haas, F.B., Franitza, M., Pellegrin, C., Reissmann, S., Altmuller, J., Rensing, S.A., *et al.* (2018). The biotrophic development of *Ustilago maydis* studied by RNA-Seq analysis. Plant Cell *30*, 300-323.

Li, X., Zhao, X., Fang, Y., Jiang, X., Duong, T., Fan, C., Huang, C.-C., and Kain, S.R. (1998). Generation of destabilized green fluorescent protein as a transcription reporter. Journal of Biological Chemistry *273*, 34970-34975.

Li, Y., Wang, G., Xu, J.R., and Jiang, C. (2016). Penetration peg formation and invasive hyphae development require stage-specific activation of *MoGTI1* in *Magnaporthe oryzae*. Molecular Plant-Microbe Interactions *29*, 36-45.

Lin, S.Y., Chooi, Y.H., and Solomon, P.S. (2018). The global regulator of pathogenesis PnCon7 positively regulates *Tox3* effector gene expression through direct interaction in the wheat pathogen *Parastagonospora nodorum*. Molecular Microbiology *109*, 78-90.

Livak, K.J., and Schmittgen, T.D. (2001). Analysis of relative gene expression data using real-time quantitative PCR and the 2−ΔΔCT method. Methods *25*, 402-408.

Lohse, M.B., Zordan, R.E., Cain, C.W., and Johnson, A.D. (2010). Distinct class of DNA-binding domains is exemplified by a master regulator of phenotypic switching in *Candida albicans*. Proceedings of the National Academy of Sciences *107*, 14105-14110.

Meyer, M., Bourras, S., Gervais, J., Labadie, K., Cruaud, C., Balesdent, M.H., and Rouxel, T. (2017). Impact of biotic and abiotic factors on the expression of fungal effector-encoding genes in axenic growth conditions. Fungal Genet Biol *99*, 1-12.

Mogga, V., Delventhal, R., Weidenbach, D., Langer, S., Bertram, P.M., Andresen, K., Thines, E., Kroj, T., and Schaffrath, U. (2016). *Magnaporthe oryzae* effectors MoHEG13 and MoHEG16 interfere with host infection and MoHEG13 counteracts cell death caused by *Magnaporthe*-NLPs in tobacco. Plant Cell Reports *35*, 1169-1185.

Mosquera, G., Giraldo, M.C., Khang, C.H., Coughlan, S., and Valent, B. (2009). Interaction transcriptome analysis identifies *Magnaporthe oryzae* BAS1-4 as Biotrophy-associated secreted proteins in rice blast disease. Plant Cell *21*, 1273-1290.

Mullins, E.D., Chen, X., Romaine, P., Raina, R., Geiser, D.M., and Kang, S. (2001). *Agrobacterium*-mediated transformation of *Fusarium oxysporum*: an efficient tool for insertional mutagenesis and gene transfer. Phytopathology *91*, 173-180.

Nelson, B.K., Cai, X., and Nebenführ, A. (2007). A multicolored set of *in vivo* organelle markers for co-localization studies in *Arabidopsis* and other plants. The Plant Journal *51*, 1126-1136.

Nishimura, T., Mochizuki, S., Ishii-Minami, N., Fujisawa, Y., Kawahara, Y., Yoshida, Y., Okada, K., Ando, S., Matsumura, H., Terauchi, R., *et al.* (2016). *Magnaporthe oryzae*

glycine-rich secretion protein, Rbf1 critically participates in pathogenicity through the focal formation of the biotrophic Interfacial complex. PLoS Pathogen *12*, e1005921.

O'Connell, R.J., Thon, M.R., Hacquard, S., Amyotte, S.G., Kleemann, J., Torres, M.F., Damm, U., Buiate, E.A., Epstein, L., Alkan, N., *et al.* (2012). Lifestyle transitions in plant pathogenic *Colletotrichum* fungi deciphered by genome and transcriptome analyses. Nature Genetics *44*, 1060-1065.

Park, S.-Y., Choi, J., Lim, S.-E., Lee, G.-W., Park, J., Kim, Y., Kong, S., Kim, S.R., Rho, H.-S., and Jeon, J. (2013). Global expression profiling of transcription factor genes provides new insights into pathogenicity and stress responses in the rice blast fungus. PLoS pathogens *9*.

Pfeifer, M.A., and Khang, C.H. (2018). A nuclear contortionist: the mitotic migration of *Magnaporthe oryzae* nuclei during plant infection. Mycology *9*, 202-210.

Plett, J.M., Kemppainen, M., Kale, S.D., Kohler, A., Legué, V., Brun, A., Tyler, B.M., Pardo, A.G., and Martin, F. (2011). A secreted effector protein of *Laccaria bicolor* is required for symbiosis development. Current Biology *21*, 1197-1203.

Raffaele, S., and Kamoun, S. (2012). Genome evolution in filamentous plant pathogens: why bigger can be better. Nat Rev Microbiol *10*, 417-430.

Sakulkoo, W., Osés-Ruiz, M., Garcia, E.O., Soanes, D.M., Littlejohn, G.R., Hacker, C., Correia, A., Valent, B., and Talbot, N.J. (2018). A single fungal MAP kinase controls plant cell-to-cell invasion by the rice blast fungus. Science *359*, 1399-1403.

Sanchez-Vallet, A., Fouche, S., Fudal, I., Hartmann, F.E., Soyer, J.L., Tellier, A., and Croll, D. (2018). The genome biology of effector gene evolution in filamentous plant pathogens. Annual Review of Phytopathology.

Sharpee, W., Oh, Y., Yi, M., Franck, W., Eyre, A., Okagaki, L.H., Valent, B., and Dean, R.A. (2017). Identification and characterization of suppressors of plant cell death (SPD) effectors from *Magnaporthe oryzae*. Molecular Plant Pathology *18*, 850-863.

Shipman, E.N., Jones, K., Jenkinson, C.B., Kim, D.W., Zhu, J., and Khang, C.H. (2017). Nuclear and structural dynamics during the establishment of a specialized effector-secreting cell by *Magnaporthe oryzae* in living rice cells. BMC cell biology *18*, 11.

Soanes, D.M., Kershaw, M.J., Cooley, R.N., and Talbot, N.J. (2002). Regulation of the *MPG1* hydrophobin gene in the rice blast fungus *Magnaporthe grisea*. Molecular Plant-Microbe Interactions *15*, 1253-1267.

Soyer, J.L., El Ghalid, M., Glaser, N., Ollivier, B., Linglin, J., Grandaubert, J., Balesdent, M.H., Connolly, L.R., Freitag, M., Rouxel, T., *et al.* (2014). Epigenetic control of effector gene expression in the plant pathogenic fungus *Leptosphaeria maculans*. PLoS Genetics *10*, e1004227.

Sperschneider, J., Gardiner, D.M., Dodds, P.N., Tini, F., Covarelli, L., Singh, K.B., Manners, J.M., and Taylor, J.M. (2016). EffectorP: predicting fungal effector proteins from secretomes using machine learning. New Phytologist *210*, 743-761.

Sweigard, J.A., Carroll, A.M., Kang, S., Farrall, L., Chumley, F.G., and Valent, B. (1995). Identification, cloning, and characterization of *PWL2*, a gene for host species specificity in the rice blast fungus. Plant Cell *7*, 1221-1233.

Tan, K.C., and Oliver, R.P. (2017). Regulation of proteinaceous effector expression in phytopathogenic fungi. PLoS Pathogen *13*, e1006241.

Thompson, J.D., Gibson, T.J., and Higgins, D.G. (2003). Multiple sequence alignment using ClustalW and ClustalX. Current protocols in bioinformatics, 2.3. 1-2.3. 22.

Valent, B., Farrall, L., and Chumley, F.G. (1991). *Magnaporthe grisea* genes for pathogenicity and virulence identified through a series of backcrosses. Genetics *127*, 87-101.

Van den Ackerveken, G., Dunn, R., Cozijnsen, A., Vossen, J., Van den Broek, H., and De Wit, P. (1994). Nitrogen limitation induces expression of the avirulence gene *avr9* in the tomato pathogen *Cladosporium fulvum*. Molecular and General Genetics MGG *243*, 277-285.

van der Does, H.C., Duyvesteijn, R.G., Goltstein, P.M., van Schie, C.C., Manders, E.M., Cornelissen, B.J., and Rep, M. (2008). Expression of effector gene *SIX1* of *Fusarium oxysporum* requires living plant cells. Fungal Genetics and Biology *45*, 1257-1264.

Vinces, M.D., Legendre, M., Caldara, M., Hagihara, M., and Verstrepen, K.J. (2009). Unstable tandem repeats in promoters confer transcriptional evolvability. Science *324*, 1213-1216.

Wang, Q., Han, C., Ferreira, A.O., Yu, X., Ye, W., Tripathy, S., Kale, S.D., Gu, B., Sheng, Y., Sui, Y., *et al.* (2011). Transcriptional programming and functional interactions within the *Phytophthora sojae* RXLR effector repertoire. Plant Cell *23*, 2064-2086.

Xu, J.-R., Urban, M., Sweigard, J.A., and Hamer, J.E. (1997). The *CPKA* gene of *Magnaporthe grisea* is essential for appressorial penetration. Molecular Plant-Microbe Interactions *10*, 187-194.

Yoshida, K., Saitoh, H., Fujisawa, S., Kanzaki, H., Matsumura, H., Yoshida, K., Tosa, Y., Chuma, I., Takano, Y., Win, J., *et al.* (2009). Association genetics reveals three novel avirulence genes from the rice blast fungal pathogen *Magnaporthe oryzae*. Plant Cell *21*, 1573-1591.

Zhang, N., Cai, G., Price, D.C., Crouch, J.A., Gladieux, P., Hillman, B., Khang, C.H., LeBrun, M.-H., Lee, Y.-H., and Luo, J. (2018). Genome wide analysis of the transition to pathogenic lifestyles in *Magnaporthales* fungi. Scientific reports *8*, 5862.

Table

Table S3.1 Effector and effector candidate genes identified by BLAST search of the tandem repeat R1 in promoters of *M. oryzae* genes.

Gene	MGG_#	Length(aa)	SP*	Chromosome	Reference
BAS1	MGG_04795	115	Y	IV (I from NCBI)	Mosquera *et al.*, 2009
BAS2	MGG_09693	102	Y	V(4 from NCBI)	Mosquera *et al.*, 2009
MAX	MGG_08482	142	Y	4	Guillen *et al.*, 2015
AVR-Pita family, metalloproteinase	MGG_14981	226	Y	UK	Khang *et al.*, 2008
Candidate effector	MGG_14156	156	Y	6	Dong *et al.*, 2015
Candidate effector	MGG_18108	174	Y	UK	Dong *et al.*, 2015
Candidate effector	MGG_18105	123	Y	UK	Dong *et al.*, 2015
Candidate effector	MGG_17244	74	Y	4	Dong *et al.*, 2015
Candidate effector	MGG_01953	115	Y	6	Dong *et al.*, 2015
Candidate effector	MGG_09019	193	Y	7	Dong *et al.*, 2015
Candidate effector	MGG_08715	137	Y	6	Dong *et al.*, 2015
Candidate effector	MGG_08799	116	Y	6	Dong *et al.*, 2015
Candidate effector	MGG_09605	182	Y	7	Dong *et al.*, 2015
Candidate effector	MGG_17239	70	Y	4	Dong *et al.*, 2015
Candidate effector	MGG_17425	86	Y	5	Dong *et al.*, 2015

*SP indicates signal peptide that is predicted by SignalP 4.0 Server.

Table S3.2 Predicted effector genes with 12-bp like motif in promoters.

#	MGG_#	Description	Strand	Start	End	p-value	q-value	Matched Sequence
1	MGG_00043	MoHEG9	-	439	450	8.27E-05	0.785	GTATGCAAGCCG
2	MGG_00043	hypothetical protein	+	223	234	2.84E-05	0.652	TAATGCAACCTT
3	MGG_00052	hypothetical protein	+	427	438	9.30E-05	0.818	TTGTGCCAGCGT
4	MGG_00225	hypothetical protein	-	68	79	5.20E-06	0.368	AGATGCAAGCTT
5	MGG_00230	hypothetical protein	+	209	220	9.69E-05	0.818	GGATGCATGCTT
6	MGG_00269	hypothetical protein	-	77	88	9.69E-05	0.818	TGTGGCAAGCTT
7	MGG_00269	hypothetical protein	+	275	286	3.87E-05	0.654	TTACCCAAGCTT
8	MGG_01145	hypothetical protein	+	790	801	5.23E-05	0.773	GTAAGCAAGCTA
9	MGG_01173	hydrophobin	+	905	916	1.46E-05	0.652	TTTTGCAAGCAT
10	MGG_01366	hypothetical protein	-	569	580	3.49E-05	0.654	TTTTGCAAACTT
11	MGG_01530	hypothetical protein	-	688	699	6.21E-05	0.785	GTAGGCGAGCTT
12	MGG_01900	hypothetical protein	-	79	90	4.35E-05	0.701	TTTTGCAATCTT
13	MGG_01953	hypothetical protein	+	692	703	8.43E-07	0.0897	TTATGCAAGCTG
14	MGG_01964	hypothetical protein	+	561	572	2.84E-05	0.652	TAATGCAACCTT
15	MGG_02212	hypothetical protein	-	861	872	4.08E-05	0.668	TTATGCAATCCT
16	MGG_02220	hypothetical protein	-	164	175	4.74E-05	0.741	TTATTCAAGATT
17	MGG_02220	hypothetical protein	+	968	979	4.87E-05	0.751	TTATCCAATCTT
18	MGG_02273	hypothetical protein	+	561	572	7.71E-05	0.785	GTCTGCAAGCTA
19	MGG_02338	hypothetical protein	-	733	744	2.38E-05	0.652	TTAGACAAGCTT
20	MGG_02590	hypothetical protein	+	80	91	8.43E-07	0.0897	GTATGCAAGCTT
21	MGG_02645	hypothetical protein	-	325	336	6.70E-05	0.785	TACTGCAAGCTA
22	MGG_03308	hypothetical protein	+	223	234	6.22E-06	0.389	ATGTGCAAGCTT
23	MGG_03308	hypothetical protein	+	554	565	8.68E-05	0.81	TTCTGCAAGCGG
24	MGG_03308	hypothetical protein	+	578	589	6.21E-05	0.785	GTATGCGAGCTG
25	MGG_03338	cellulose-binding protein	+	598	609	3.37E-05	0.654	TTATGGCAGCTT
26	MGG_03495	hypothetical protein	-	687	698	7.03E-05	0.785	TGAAGCAAGCCT
27	MGG_03495	hypothetical protein	+	297	308	1.60E-05	0.652	TTTTGCGAGCTT
28	MGG_03507	hypothetical protein	+	351	362	9.52E-05	0.818	TTTTGCAGGCTA
29	MGG_03639	hypothetical protein	-	716	727	3.65E-05	0.654	GTATGCAAGTTT
30	MGG_04301	PWL2	+	677	688	8.34E-08	0.0222	TTATGCAAGCTT
31	MGG_04301	PWL2	+	727	738	8.34E-08	0.0222	TTATGCAAGCTT
32	MGG_04301	PWL2	+	779	790	5.00E-07	0.0665	ATATGCAAGCTT
33	MGG_04451	hypothetical protein	-	396	407	9.30E-05	0.818	TGTAGCAAGCTT
34	MGG_04451	hypothetical protein	-	759	770	5.20E-06	0.368	TGATGCAAGCTA
35	MGG_04507	synbindin	+	918	929	9.69E-05	0.818	GGTTGCAAGCTT
36	MGG_04859	hypothetical protein	-	27	38	5.03E-05	0.753	AAAAGCAAGCTT
37	MGG_05091	hypothetical protein	-	154	165	8.27E-05	0.785	GCATGCAAGCGT
38	MGG_05608	hypothetical protein	-	915	926	8.27E-05	0.785	AAATGCATGCTT
39	MGG_05818	hypothetical protein	-	680	691	1.56E-05	0.652	TTATGCATGCGT
40	MGG_05831	hypothetical protein	-	232	243	1.86E-05	0.652	TCTTGCAAGCTT
41	MGG_05896	hypothetical protein	+	272	283	7.71E-05	0.785	TAAGGCACGCTT
42	MGG_06008	hypothetical protein	-	861	872	6.07E-05	0.785	TAGTGCAGGCTT

43	MGG_06359	hypothetical protein	+	331	342	9.52E-05	0.818	TAGTGCTAGCTT
44	MGG_07234	FK506-binding protein 2	+	973	984	5.00E-07	0.0665	TAATGCAAGCTT
45	MGG_07538	hypothetical protein	-	40	51	8.27E-05	0.785	TTCAGCAGGCTT
46	MGG_07538	hypothetical protein	+	863	874	3.80E-05	0.654	TTATGGTAGCTT
47	MGG_07607	hypothetical protein	-	843	854	6.28E-05	0.785	TTAGGCGGGCTT
48	MGG_07810	hypothetical protein	+	486	497	7.71E-05	0.785	TAAGGCACGCTT
49	MGG_07919	hypothetical protein	-	20	31	8.27E-05	0.785	TTTTGCAAGCAA
50	MGG_07952	hypothetical protein	-	638	649	3.49E-05	0.654	TTATGCTAACTT
51	MGG_07986	MoCDIP3	-	929	940	7.71E-05	0.785	TTCTGCAAGCGA
52	MGG_08027	hypothetical protein	-	222	233	7.71E-05	0.785	TACGGCAAGCTT
53	MGG_08300	hypothetical protein	+	789	800	8.27E-05	0.785	GCATGCAAGCTG
54	MGG_08407	hypothetical protein	-	964	975	9.30E-05	0.818	TGCTGCAGGCTT
55	MGG_08407	hypothetical protein	+	430	441	6.49E-05	0.785	AAATGCAAGCCT
56	MGG_08414	Max	-	453	464	3.87E-05	0.654	TTACGCAACCTT
57	MGG_08451	hypothetical protein	-	5	16	4.74E-05	0.741	TTATTCAAGATT
58	MGG_08451	hypothetical protein	-	92	103	6.49E-05	0.785	CAAAGCAAGCTT
59	MGG_08451	hypothetical protein	-	957	968	5.94E-05	0.785	TTGAGCAAGCTG
60	MGG_08451	hypothetical protein	+	86	97	9.30E-05	0.818	AGTTGCAAGCTT
61	MGG_08609	hypothetical protein	+	770	781	7.71E-05	0.785	TCATGCGAGCTA
62	MGG_08799	hypothetical protein	-	599	610	7.03E-05	0.785	CAATGCAAGCTG
63	MGG_08817	hypothetical protein	-	658	669	7.03E-05	0.785	CTATGCAAGCGA
64	MGG_08941	hypothetical protein	+	365	376	9.30E-05	0.818	TGTTGCAAGCAT
65	MGG_09425	Max	-	567	578	9.52E-05	0.818	TTGTGCATGCAT
66	MGG_09724	hypothetical protein	-	770	781	4.08E-05	0.668	TCATTCAAGCTT
67	MGG_09842	hypothetical protein	-	925	936	2.59E-05	0.652	TTGTGCAAGGTT
68	MGG_09844	hypothetical protein	+	559	570	7.63E-06	0.451	TTGTGCAAGCGT
69	MGG_09998	hypothetical protein	-	359	370	8.27E-05	0.785	TAATGCATGCTA
70	MGG_10026	cysteine rich protein	+	791	802	2.94E-05	0.652	TTATGACAGCTT
71	MGG_10217	hypothetical protein	+	60	71	3.65E-05	0.654	TGATTCAAGCTT
72	MGG_10259	hypothetical protein	-	488	499	7.03E-05	0.785	GTATGCAAGCCA
73	MGG_10276	hypothetical protein	-	515	526	8.27E-05	0.785	ATATGCTAGCAT
74	MGG_10276	hypothetical protein	+	513	524	8.27E-05	0.785	TAATGCTAGCAT
75	MGG_10456	hypothetical protein	+	672	683	2.94E-05	0.652	TTATGCCAGATT
76	MGG_10914	BAS4	-	941	952	2.84E-05	0.652	ATATCCAAGCTT
77	MGG_11650	hypothetical protein	+	735	746	8.68E-05	0.81	TGGTGCAAGCTC
78	MGG_11967	hypothetical protein	-	305	316	3.49E-05	0.654	TTTTACAAGCTT
79	MGG_11991	SPD10	+	105	116	1.56E-05	0.652	TGATGCATGCTT
80	MGG_12415	hypothetical protein	+	685	696	1.39E-06	0.134	TTACGCAAGCTT
81	MGG_12445	hypothetical protein	+	908	919	1.60E-05	0.652	TTTTGCAGGCTT
82	MGG_12466	hypothetical protein	+	983	994	7.71E-05	0.785	TGAAGCCAGCTT
83	MGG_12552	hypothetical protein	+	829	840	2.84E-05	0.652	TCATACAAGCTT
84	MGG_12654	hypothetical protein	+	802	813	7.71E-05	0.785	TTCTGCAAGCAG
85	MGG_13019	hypothetical protein	+	40	51	3.37E-05	0.654	TTATTCAAGCAT
86	MGG_13863	PWL2	+	677	688	8.34E-08	0.0222	TTATGCAAGCTT

87	MGG_13863	PWL2	+	727	738	8.34E-08	0.0222	TTATGCAAGCTT
88	MGG_13863	PWL2	+	779	790	5.00E-07	0.0665	ATATGCAAGCTT
89	MGG_13868	hypothetical protein	+	486	497	7.71E-05	0.785	TAAGGCACGCTT
90	MGG_14006	hypothetical protein	-	580	591	1.13E-05	0.634	TGATGCAAGCTC
91	MGG_14374	hypothetical protein	-	596	607	1.76E-05	0.652	TTATGCCCGCTT
92	MGG_14652	hypothetical protein	+	97	108	1.30E-05	0.652	TTGTGCAAGCTC
93	MGG_14836	hypothetical protein	-	232	243	5.00E-07	0.0665	ATATGCAAGCTT
94	MGG_15106	hypothetical protein	+	885	896	7.71E-05	0.785	TAAGGCCAGCTT
95	MGG_15374	hypothetical protein	+	332	343	8.27E-05	0.785	ATAAGCATGCTT
96	MGG_15410	hypothetical protein	-	121	132	7.71E-05	0.785	GTAAGCACGCTT
97	MGG_15539	hypothetical protein	-	738	749	3.49E-05	0.654	TTTTGCAAGATT
98	MGG_15703	hypothetical protein	+	69	80	6.21E-05	0.785	GGATGCGAGCTT
99	MGG_15793	hypothetical protein	-	489	500	3.37E-05	0.654	ATATGCAAGTTT
100	MGG_15972	Avr-Pik	+	468	479	3.83E-06	0.313	TAATGCAAGCAT
101	MGG_15972	Avr-Pik	+	665	676	3.83E-06	0.313	TAATGCAAGCAT
102	MGG_15973	hypothetical protein	-	561	572	3.80E-05	0.654	TTTTGGAAGCTT
103	MGG_16041	hypothetical protein	-	856	867	7.71E-05	0.785	TTCTGCAAGCGA
104	MGG_16058	hypothetical protein	+	765	776	2.59E-05	0.652	TTGTGCAAGGTT
105	MGG_16059	hypothetical protein	-	814	825	1.74E-05	0.652	CTATGCCAGCTT
106	MGG_16175	hypothetical protein	-	490	501	2.84E-05	0.652	TTATGCAAACTC
107	MGG_16188	hypothetical protein	-	650	661	7.71E-05	0.785	TTATGCAGGCAC
108	MGG_16345	hypothetical protein	+	674	685	2.38E-05	0.652	TGATGAAAGCTT
109	MGG_16357	hypothetical protein	+	917	928	9.30E-05	0.818	TTTTGCAAGCAG
110	MGG_16553	hypothetical protein	-	494	505	3.37E-05	0.654	ATATGCAAGTTT
111	MGG_16698	hypothetical protein	+	614	625	2.84E-05	0.652	TAATGCAACCTT
112	MGG_16737	hypothetical protein	+	318	329	5.61E-05	0.785	GTATGCAAGCAG
113	MGG_16939	hypothetical protein	-	364	375	2.13E-05	0.652	TAATGCAAACTT
114	MGG_17022	hypothetical protein	-	73	84	1.93E-05	0.652	TTTTGCTAGCTT
115	MGG_17425	hypothetical protein	-	241	252	3.87E-05	0.654	TTATCCAAGCTC
116	MGG_17463	hypothetical protein	-	766	777	8.27E-05	0.785	TCATGCAAGCGG
117	MGG_17567	hypothetical protein	-	293	304	2.84E-05	0.652	TTACACAAGCTT
118	MGG_17567	hypothetical protein	+	53	64	5.03E-05	0.753	AAAAGCAAGCTT
119	MGG_17579	hypothetical protein	+	465	476	2.59E-05	0.652	TTGTGCAAGGTT
120	MGG_17614	hypothetical protein	+	481	492	2.84E-05	0.652	TAATGCAACCTT
121	MGG_17635	hypothetical protein	+	850	861	2.13E-05	0.652	TAATGCAAACTT
122	MGG_17711	hypothetical protein	+	377	388	6.22E-06	0.389	ATATGCAGGCTT
123	MGG_18013	hypothetical protein	-	985	996	6.28E-05	0.785	TTGGGCGAGCTT
124	MGG_18013	hypothetical protein	+	348	359	2.13E-05	0.652	ATATGAAAGCTT
125	MGG_18062	hypothetical protein	-	365	376	2.13E-05	0.652	TAATGCAAACTT
126	MGG_18122	hypothetical protein	-	493	504	7.03E-05	0.785	GTACGCAAGCAT

Table S3.3 *Magnaporthe oryzae* strains used in this study.

Strain	CKF#	Genotype	Reference
O-137	CKF558	Wild-type, a field isolate from rice in China.	Sweigard *et al.*, 1995
Recipient strain	CKF3209	Transformant of CKF558, expressing a nuclear tdTomato reporter gene under control of a constitutive promoter *M. oryzae RP27*; $G418^R$	This study
PWL2 reporter strain(nuclear)	CKF3276	Transformant of CKF3209, expressing both a constitutive, nuclear tdTomato reporter gene, and a fusion of the *PWL2* promoter with sfGFP:NLS reporter gene; Hyg^R $G418^R$	This study
PWL2 reporter strain(nuclear)	CKF3278	Transformant of CKF3209, expressing both a constitutive, nuclear tdTomato reporter gene, and a fusion of the *PWL2* promoter with sfGFP:NLS reporter gene; Hyg^R $G418^R$	This study
PWL2 reporter strain (cytoplasmic)	CKF3538	Transformant of CKF558, expressing both a constitutive, cytoplasmic tdTomato reporter gene, and a fusion of the *PWL2* promoter with EGFP:PEST reporter gene; Hyg^R $G418^R$	This study
*Δ*repeats	CKF3692	Transformant of CKF3209, expressing both a constitutive, nuclear tdTomato reporter gene, and a fusion of the *PWL2* promoter (without 3-repeats) with sfGFP:NLS reporter gene; Hyg^R $G418^R$	This study
*Δ*repeats	CKF3700	Transformant of CKF3209, expressing both a constitutive, nuclear tdTomato reporter gene, and a fusion of the *PWL2* promoter (without 3-repeats) with sfGFP:NLS reporter gene; Hyg^R $G418^R$	This study
1-repeat	CKF3736	Transformant of CKF3209, expressing both a constitutive, nuclear tdTomato reporter gene, and a fusion of the *PWL2* promoter (1-repeat) with sfGFP:NLS reporter gene; Hyg^R $G418^R$	This study

1-repeat	CKF3737	Transformant of CKF3209, expressing both a constitutive, nuclear tdTomato reporter gene, and a fusion of the *PWL2* promoter (1-repeat) with sfGFP:NLS reporter gene; Hyg^R $G418^R$	This study
Reversed orientation of 3-repeats	CKF3745	Transformant of CKF3209, expressing both a constitutive, nuclear tdTomato reporter gene, and a fusion of the *PWL2* promoter (reversed repeats) with sfGFP:NLS reporter gene; HygR $G418^R$	This study
Reversed orientation of 3-repeats	CKF3748	Transformant of CKF3209, expressing both a constitutive, nuclear tdTomato reporter gene, and a fusion of the *PWL2* promoter (reversed repeats) with sfGFP:NLS reporter gene; Hyg^R $G418^R$	This study
Reversed orientation of 3-repeats	CKF3751	Transformant of CKF3209, expressing both a constitutive, nuclear tdTomato reporter gene, and a fusion of the *PWL2* promoter (reversed repeats) with sfGFP:NLS reporter gene; Hyg^R $G418^R$	This study
Original position of 3-repeats	CKF3757	Transformant of CKF3209, expressing both a constitutive, nuclear tdTomato reporter gene, and a fusion of the *PWL2* promoter (forward repeats) with sfGFP:NLS reporter gene; Hyg^R $G418^R$	This study
Original position of 3-repeats	CKF3758	Transformant of CKF3209, expressing both a constitutive, nuclear tdTomato reporter gene, and a fusion of the *PWL2* promoter (forward repeats) with sfGFP:NLS reporter gene; Hyg^R $G418^R$	This study
Original position of 3-repeats	CKF3760	Transformant of CKF3209, expressing both a constitutive, nuclear tdTomato reporter gene, and a fusion of the *PWL2* promoter (forward repeats) with sfGFP:NLS reporter gene; Hyg^R $G418^R$	This study

Repeats at non-original position	CKF3778	Transformant of CKF3209, expressing both a constitutive, nuclear tdTomato reporter gene, and a fusion of the *PWL2* promoter (repeats at non-original position) with sfGFP:NLS reporter gene; Hyg^R $G418^R$	This study
Repeats at non-original position	CKF3780	Transformant of CKF3209, expressing both a constitutive, nuclear tdTomato reporter gene, and a fusion of the *PWL2* promoter (repeats at non-original position) with sfGFP:NLS reporter gene; Hyg^R $G418^R$	This study
2-repeats	CKF3782	Transformant of CKF3209, expressing both a constitutive, nuclear tdTomato reporter gene, and a fusion of the *PWL2* promoter (2-repeats) with sfGFP:NLS reporter gene; Hyg^R $G418^R$	This study
2-repeats	CKF3784	Transformant of CKF3209, expressing both a constitutive, nuclear tdTomato reporter gene, and a fusion of the *PWL2* promoter (2-repeats) with sfGFP:NLS reporter gene; HygR $G418^R$	This study
2-repeats	CKF3785	Transformant of CKF3209, expressing both a constitutive, nuclear tdTomato reporter gene, and a fusion of the *PWL2* promoter (2-repeats) with sfGFP:NLS reporter gene; Hyg^R $G418^R$	This study
Non-specific DNA replacement	CKF3802	Transformant of CKF3209, expressing both a constitutive, nuclear tdTomato reporter gene, and a fusion of the *PWL2* promoter (non-specific DNA replacement) with sfGFP:NLS reporter gene; Hyg^R $G418^R$	This study
Non-specific DNA replacement	CKF3803	Transformant of CKF3209, expressing both a constitutive, nuclear tdTomato reporter gene, and a fusion of the *PWL2* promoter (non-specific DNA replacement) with sfGFP:NLS reporter gene; Hyg^R $G418^R$	This study

5’-end of one repeat	CKF3820	Transformant of CKF3209, expressing both a constitutive, nuclear tdTomato reporter gene, and a fusion of the *PWL2* promoter (5’-end of one repeat) with sfGFP:NLS reporter gene; Hyg^R $G418^R$	This study
5’-end of one repeat	CKF3821	Transformant of CKF3209, expressing both a constitutive, nuclear tdTomato reporter gene, and a fusion of the *PWL2* promoter (5’-end of one repeat) with sfGFP:NLS reporter gene; HygR $G418^R$	This study
3’-end of one repeat	CKF3852	Transformant of CKF3209, expressing both a constitutive, nuclear tdTomato reporter gene, and a fusion of the *PWL2* promoter (3’-end of one repeat) with sfGFP:NLS reporter gene; Hyg^R $G418^R$	This study
3’-end of one repeat	CKF3853	Transformant of CKF3209, expressing both a constitutive, nuclear tdTomato reporter gene, and a fusion of the *PWL2* promoter (3’-end of one repeat) with sfGFP:NLS reporter gene; Hyg^R $G418^R$	This study
Region II mutation	CKF3885	Transformant of CKF3209, expressing both a constitutive, nuclear tdTomato reporter gene, and a fusion of the *PWL2* promoter (cluster II mutation) with sfGFP:NLS reporter gene; Hyg^R $G418^R$	This study
Region II mutation	CKF3888	Transformant of CKF3209, expressing both a constitutive, nuclear tdTomato reporter gene, and a fusion of the *PWL2* promoter (cluster II mutation) with sfGFP:NLS reporter gene; Hyg^R $G418^R$	This study
Region I mutation	CKF3902	Transformant of CKF3209, expressing both a constitutive, nuclear tdTomato reporter gene, and a fusion of the *PWL2* promoter (cluster I mutation) with sfGFP:NLS reporter gene; Hyg^R $G418^R$	This study

Region I mutation	CKF3906	Transformant of CKF3209, expressing both a constitutive, nuclear tdTomato reporter gene, and a fusion of the *PWL2* promoter (cluster I mutation) with sfGFP:NLS reporter gene; Hyg^R $G418^R$	This study
Region III mutation	CKF3915	Transformant of CKF3209, expressing both a constitutive, nuclear tdTomato reporter gene, and a fusion of the *PWL2* promoter (cluster III mutation) with sfGFP:NLS reporter gene; Hyg^R $G418^R$	This study
Region III mutation	CKF3916	Transformant of CKF3209, expressing both a constitutive, nuclear tdTomato reporter gene, and a fusion of the *PWL2* promoter (cluster III mutation) with sfGFP:NLS reporter gene; Hyg^R $G418^R$	This study
12-bp recovery	CKF3988	Transformant of CKF3209, expressing both a constitutive, nuclear tdTomato reporter gene, and a fusion of the *PWL2* promoter (12-bp recovery) with sfGFP:NLS reporter gene; Hyg^R $G418^R$	This study
12-bp recovery	CKF3989	Transformant of CKF3209, expressing both a constitutive, nuclear tdTomato reporter gene, and a fusion of the *PWL2* promoter (12-bp recovery) with sfGFP:NLS reporter gene; Hyg^R $G418^R$	This study
12-bp recovery	CKF3991	Transformant of CKF3209, expressing both a constitutive, nuclear tdTomato reporter gene, and a fusion of the *PWL2* promoter (12-bp recovery) with sfGFP:NLS reporter gene; Hyg^R $G418^R$	This study

Table S3.4 Key plasmids used in this study.

Clone	Description
pBV578	0.1-kb nuclear localization signal sequence (NLS, *BsrG*I-*BamH*I fragment) and 0.3-kb Nos terminator (*Bgl*II-*EcoR*I fragment) cloned in *BsrG*I-*EcoR*I sites of pAN583 (pBV360, Nelson et al., 2007).
pBV1102	0.5-kb *PWL2* 3'-UTR (PCR product of pCB775 (Sweigard et al., 1995) with primers CKP267 and CKP268) into pGEM-T (Promega).
pCK1292	Cytoplasmic tdTomato expression binary vector derived from pBV141(pBGt, Kim *et al.*, 2011), consisting of 0.5-kb *RP27* promoter (*EcoR*I-*BamH*I fragment), and 1.7-kb tdTomato: *N.crassa* β-tubulin terminator (*BamH*I-*Hind*III fragment) cloned in *EcoR*I-*Hind*III sites of pBV141(pBGt).
pCK1298	*PWL2* nuclear reporter vector, consisting of 872-bp *PWL2* promoter (*EcoR*I-*BamH*I fragment), 0.8-kb EGFP plus NLS (*BamH*I-*Sal*I fragment) and 0.5-kb *PWL2* 3'-UTR (*Not*I-*Xho*I fragment), cloned in *EcoR*I-*Sal*I sites of pBV1 (pBHt2, Mullins *et al.*, 2001).
pCK1528	Nuclear tdTomato expression binary vector derived from pBV141(pBGt, Kim *et al.*, 2011), consisting of 1.0-kb *RP27* promoter (*EcoR*I-*BamH*I fragment), and 1.8-kb tdTomato:NLS: *N.crassa* β-tubulin terminator (*BamH*I-*Hind*III fragment) cloned in *EcoR*I-*Hind*III sites of pBV141(pBGt).
pCK1574	872-bp *PWL2* promoter (from pSK1885 (Khang et al., 2010)) into pJET1.2 (Thermo Fisher Scientific).
pCK1576	1.3-kb sfGFP plus NLS and *PWL2* 3'-UTR into pJET1.2 (Thermo Fisher Scientific).
pCK1586	*PWL2* nuclear reporter vector, consisting of 872-bp *PWL2* promoter (*EcoR*I-*BamH*I fragment), 1.3-kb sfGFP plus NLS and *PWL2* 3'-UTR (*BamH*I-*Xba*I fragment), cloned in *EcoR*I-*Xba*I sites of pBV1.
pCK1714	*PWL2* cytoplasmic reporter vector, consisting of 1.7-kb *PWL2* promoter:EGFP (*EcoR*I-*BsrG*I fragment), 0.12-kb protein degradation signal peptide PEST (*BsrG*I-*Not*I fragment) from pBV118(pd2EGFP-1), and 0.5-kb *PWL2* 3'-UTR (*Not*I-*Xho*I fragment), cloned in *EcoR*I-*Sal*I sites of pBV1(pBHt2).

pCK1790	*PWL2 Δ* repeats reporter vector, consisting of *PWL2* promoter without 3-repeats (*Eco*RI-*BamH*I fragment), 1.3-kb sfGFP plus nuclear localization signal and *PWL2* 3'-UTR (*BamH*I-*Sac*I fragment), cloned in *Eco*RI-*Hind*III sites of pBV1.
pCK1813	*PWL2* 1-repeat reporter vector, consisting of *PWL2* promoter with 1-repeat (*Eco*RI-*BamH*I fragment), 1.3-kb sfGFP plus nuclear localization signal and *PWL2* 3'-UTR (*BamH*I-*Sac*I fragment), cloned in *Eco*RI-*Hind*III sites of pBV1.
pCK1822	*PWL2* reversed repeats reporter vector, consisting of *PWL2* promoter with reversed repeats (*Eco*RI-*BamH*I fragment), 1.3-kb sfGFP plus nuclear localization signal and *PWL2* 3'-UTR (*BamH*I-*Sac*I fragment), cloned in *Eco*RI-*Hind*III sites of pBV1.
pCK1823	*PWL2* forward repeats reporter vector, consisting of *PWL2* promoter with forward repeats (*Eco*RI-*BamH*I fragment), 1.3-kb sfGFP plus nuclear localization signal and *PWL2* 3'-UTR (*BamH*I-*Sac*I fragment), cloned in *Eco*RI-*Hind*III sites of pBV1.
pCK1883	*PWL2* reporter vector with repeats at non-original position, consisting of *PWL2* promoter with repeats at non-original position (*Eco*RI-*BamH*I fragment), 1.3-kb sfGFP plus nuclear localization signal and *PWL2* 3'-UTR (*BamH*I-*Sac*I fragment), cloned in *Eco*RI-*Hind*III sites of pBV1.
pCK1887	*PWL2* 2-repeats reporter vector, consisting of *PWL2* promoter with 2-repeats (*Eco*RI-*BamH*I fragment), 1.3-kb sfGFP plus nuclear localization signal and *PWL2* 3'-UTR (*BamH*I-*Sac*I fragment), cloned in *Eco*RI-*Hind*III sites of pBV1.
pCK1894	*PWL2* reporter vector with non-specific DNA replacement at repeat position, consisting of *PWL2* promoter with non-specific DNA replacement at repeat position (*Eco*RI-*BamH*I fragment), 1.3-kb sfGFP plus nuclear localization signal and *PWL2* 3'-UTR (*BamH*I-*Sac*I fragment), cloned in *Eco*RI-*Hind*III sites of pBV1.
pCK1905	*PWL2* 5'-end of one repeat reporter vector, consisting of *PWL2* promoter with 5'-end of one repeat (*Eco*RI-*BamH*I fragment), 1.3-kb sfGFP plus nuclear localization signal and *PWL2* 3'-UTR (*BamH*I-*Sac*I fragment), cloned in *Eco*RI-*Hind*III sites of pBV1.
pCK1922	*PWL2* 3'-end of one repeat reporter vector, consisting of *PWL2* promoter with 3'-end of one repeat (*Eco*RI-*BamH*I fragment), 1.3-kb sfGFP plus nuclear localization signal and *PWL2* 3'-UTR (*BamH*I-*Sac*I fragment), cloned in *Eco*RI-*Hind*III sites of pBV1.

pCK1969	*PWL2* cluster II mutation reporter vector, consisting of *PWL2* promoter with cluster II mutation (*Eco*RI-*BamH*I fragment), 1.3-kb sfGFP plus nuclear localization signal and *PWL2* 3'-UTR (*BamH*I-*Sac*I fragment), cloned in *Eco*RI-*Hind*III sites of pBV1.
pCK1975	*PWL2* cluster I mutation reporter vector, consisting of *PWL2* promoter with cluster I mutation (*Eco*RI-*BamH*I fragment), 1.3-kb sfGFP plus nuclear localization signal and *PWL2* 3'-UTR (*BamH*I-*Sac*I fragment), cloned in *Eco*RI-*Hind*III sites of pBV1.
pCK1988	*PWL2* cluster III mutation reporter vector, consisting of *PWL2* promoter with cluster III mutation (*Eco*RI-*BamH*I fragment), 1.3-kb sfGFP plus nuclear localization signal and *PWL2* 3'-UTR (*BamH*I-*Sac*I fragment), cloned in *Eco*RI-*Hind*III sites of pBV1.
pCK2004	*PWL2* 12-bp motif recovery reporter vector, consisting of *PWL2* promoter with a 12-bp motif recovery (*Eco*RI-*BamH*I fragment), 1.3-kb sfGFP plus nuclear localization signal and *PWL2* 3'-UTR (*BamH*I-*Sac*I fragment), cloned in *Eco*RI-*Hind*III sites of pBV1.

Table S3.5 PCR primers used in this study.

Name	Sequence [a] (5'-3')	Applications
CKP60	GAATTCGCGTCAGTGAACAAACC	*PWL2* promoter
CKP233	GGATCCCATTTTGAAAGTTTTTAATTTTAAAAAG	*PWL2* promoter
CKP267	GAATCTTTTCACAATGCAGATCAAGGCCCTC	*PWL2* 3'-UTR
CKP268	GAATCTTTTCACAATGGTGAGCAAGGGCGAG	*PWL2* 3'-UTR
CKP402	*CG*GGATCCGTGAGCAAGGGCGAGG	*sfGFP* sequence w/o ATG
CKP403	*GC*TCTAGACTCGAGAAATAGCTTAAAGTAAG	*PWL2* 3'UTR
CKP542	GGTACCAATATATAATTATATATATTAGTACG	*Δ* repeats
CKP543	GGTACCATACAATAAGGGGTTGGCTAATTTATAAG	*Δ* repeats
CKP570	GGTACCTTTTTATTTATGCAAGCTTAC	2-repeats, 3-repeats
CKP571	GGTACCATGTTTTTTATTCGTCCC	2-repeats, 3-repeats
CKP585	GAGCTCTTTTTATTTATGCAAGCTTAC	Repeats at non-original position
CKP586	GAATTCATGTTTTTTATTCGTCCC	Repeats at non-original position
CKP587	GGTACCAGGTCGTTCGCTCCAAGC	Non-specific DNA sequence
CKP588	GGTACCCTGTTACCAGTGGCTGCTGC	Non-specific DNA sequence
CKP619	CGAGTAAGCTTGCATAAAT	5'-end of one repeat
CKP620	ATGCAAGCTTACTCGATACAATAAGGG	5'-end of one repeat
CKP400	AATATATAATTATATATATTAGTACG	3'-end of one repeat
CKP621	TAATATATATAATTATATATTCGGATGGGACGAA	3'-end of one repeat
CKP639	CGCCCGCCCCCAATATATAATTA	Cluster I mutation
CKP640	GGGGGCGGGCGGCAAGCTTACTC	Cluster I mutation
CKP641	CCTAGGTACGCCATAAAAAAATATAT	Cluster II mutation
CKP642	GGCGTACCTAGGACTCGCGGATG	Cluster II mutation
CKP643	ATCTGCCTAGGGCATAAATAAAAA	Cluster III mutation
CKP644	CCTAGGCAGATCGGATGGGACG	Cluster III mutation
CKP665J	AAGCTTGCATAAAATATATAATTATATATATTAG	12-bp motif recovery
CKP666J	TTATGCAAGCTTATACAATAAGGGGTTG	12-bp motif recovery
CKP323	CACTACCTGAGCACCCAGTC	*EGFP* qRT-PCR
CKP324	GAACTCCAGCAGGACCATGT	*EGFP* qRT-PCR
CKP327	GGCGGGTGGACTAACAAACA	*PWL2* qRT-PCR
CKP328	TACCATCCTATCGGGCCCTC	*PWL2* qRT-PCR
CKP333	CGACGTCCGAAAGGATCTGT	*Moactin* qRT-PCR
CKP334	TGCATACGGTCCGAAAGACC	*Moactin* qRT-PCR
CKP667J	GGACCTGACGTTCCTGGAC	*MGG_08300* qRT-PCR
CKP668J	GGTCAGCTTGAGGACCTTGT	*MGG_08300* qRT-PCR
CKP683J	CCGACCGTTATAGCCACTCC	*MGG_01953* qRT-PCR
CKP684J	AACCGGGGATTCTGGCATTC	*MGG_01953* qRT-PCR
CKP679J	CACTTTGGGAACTGTCGCTG	*Avr-Pik* qRT-PCR
CKP680J	TCGGGTACAGGAATACCAGGG	*Avr-Pik* qRT-PCR
T7 promoter	TAATACGACTCACTATAGGG	Sequencing confirmation of clones

[a]Underlined sequences correspond to restriction enzyme sites used for cloning:

*BamH*I (GGATCC), *EcoR*I (GAATTC), *Hind*III (AAGCTT) and *Xba*I (TCTAGA).

Figure

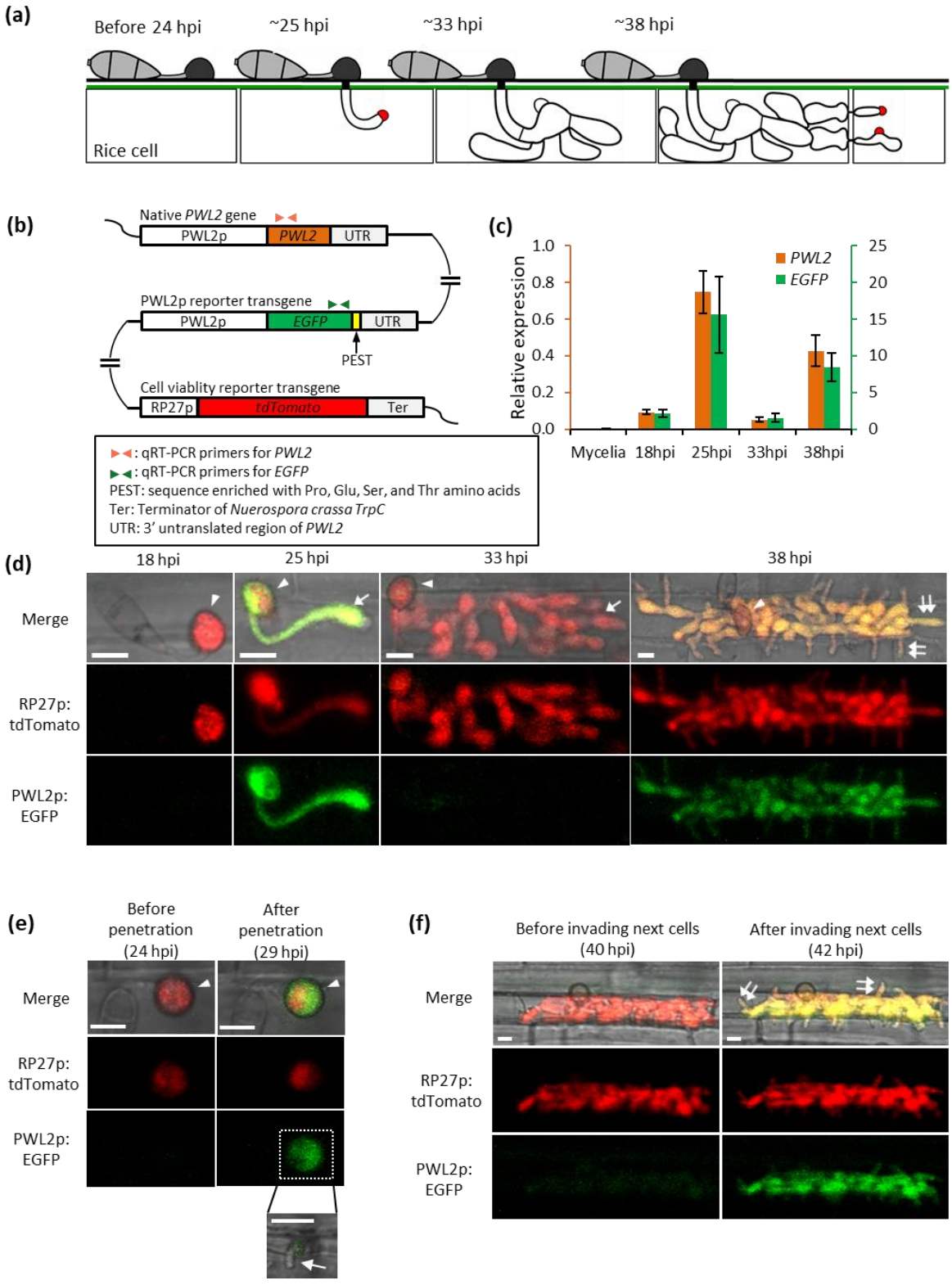
(a)
Before 24 hpi
~25 hpi
~33 hpi
~38 hpi
Rice cell
(b)
Native PWL2 gene
PWL2p
PWL2
UTR
PWL2p reporter transgene
PWL2p
EGFP
UTR
PEST
Cell viablity reporter transgene
RP27p
tdTomato
Ter
►◄: qRT-PCR primers for PWL2
►◄: qRT-PCR primers for EGFP
PEST: sequence enriched with Pro, Glu, Ser, and Thr amino acids
Ter: Terminator of Nuerospora crassa TrpC
UTR: 3' untranslated region of PWL2
(c)
Relative expression
PWL2
EGFP
Mycelia
18hpi
25hpi
33hpi
38hpi
(d)
18 hpi
25 hpi
33 hpi
38 hpi
Merge
RP27p: tdTomato
PWL2p: EGFP
(e)
Before penetration (24 hpi)
After penetration (29 hpi)
Merge
RP27p: tdTomato
PWL2p: EGFP
(f)
Before invading next cells (40 hpi)
After invading next cells (42 hpi)
Merge
RP27p: tdTomato
PWL2p: EGFP

Figure 3.1. Induced *PWL2* expression occurs during appressorium-mediated penetration and cell-to-cell movement of invasive hyphae (IH). (a) Schematic diagram of *M. oryzae* invasion in rice cells. An appressorium on the rice cell surface produces a filamentous hypha that grows inside the living rice cell (~25 hpi). The hyphal tip is associated with a biotrophic interfacial complex (BIC or tip BIC; indicated in red). The hypha subsequently differentiates into branched bulbous IH, and the tip BIC becomes a side BIC positioned on the side of the first bulbous cell (~33 hpi). After filling the first-invaded dead rice cell, IH, associated with BICs, invade adjacent living cells (~38 hpi). (b) Schematic diagram of the native *PWL2* gene and two reporter transgenes, EGFP under control of the *PWL2* promoter (PWL2p:EGFP) and tdTomato under control of the constitutively active *RP27* promoter (P27p:tdTomato), inserted ectopically in *M. oryzae* transformant CKF3538. (c) qRT-PCR expression patterns of native *PWL2* and transgene *EGFP* in CKF3538 with three biological replications. (d) Confocal images of CKF3538 invading rice cells at different stages of infection. (e-f) Time-lapse confocal images showing the activation of the *PWL2* promoter immediately after appressorium-mediated penetration (e) and IH cell-to-cell movement (f). The inset in (e) shows a short filamentous hypha that grew inside the rice cell. Arrows indicate appressoria. Arrowheads indicate some IH in the first invaded cells, and double arrows indicate some IH that have moved to adjacent cells. Bars, 10 μm.

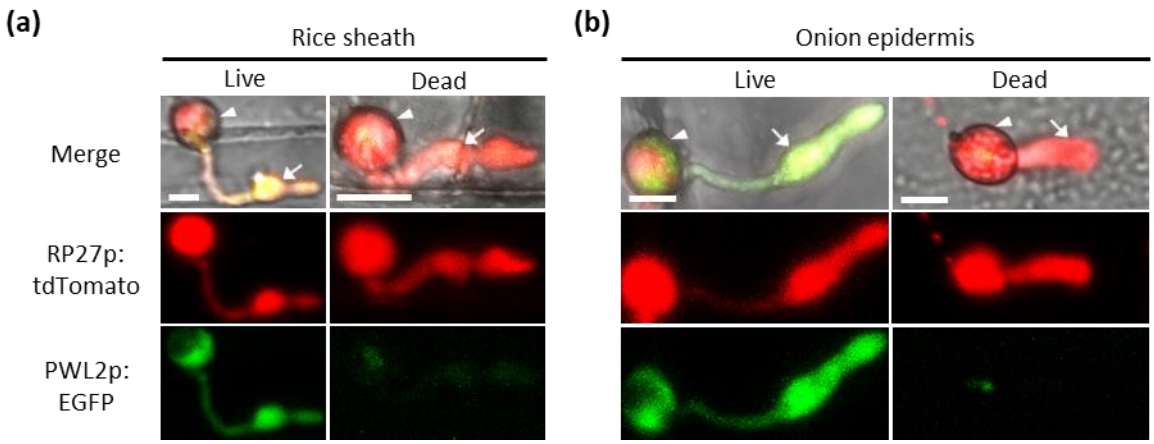

Figure 3.2. Confocal images of *M. oryzae* transformant CKF3538 invading rice cells (a) and nonhost onion cells (b). Note the strong expression of *PWL2* promoter-driven EGFP in living cells but not in dead cells of both rice and onion. The EGFP expression in dead cells was barely detectable even with highly sensitive confocal imaging settings as shown in Fig. S3.3. Bars, 10 μm.

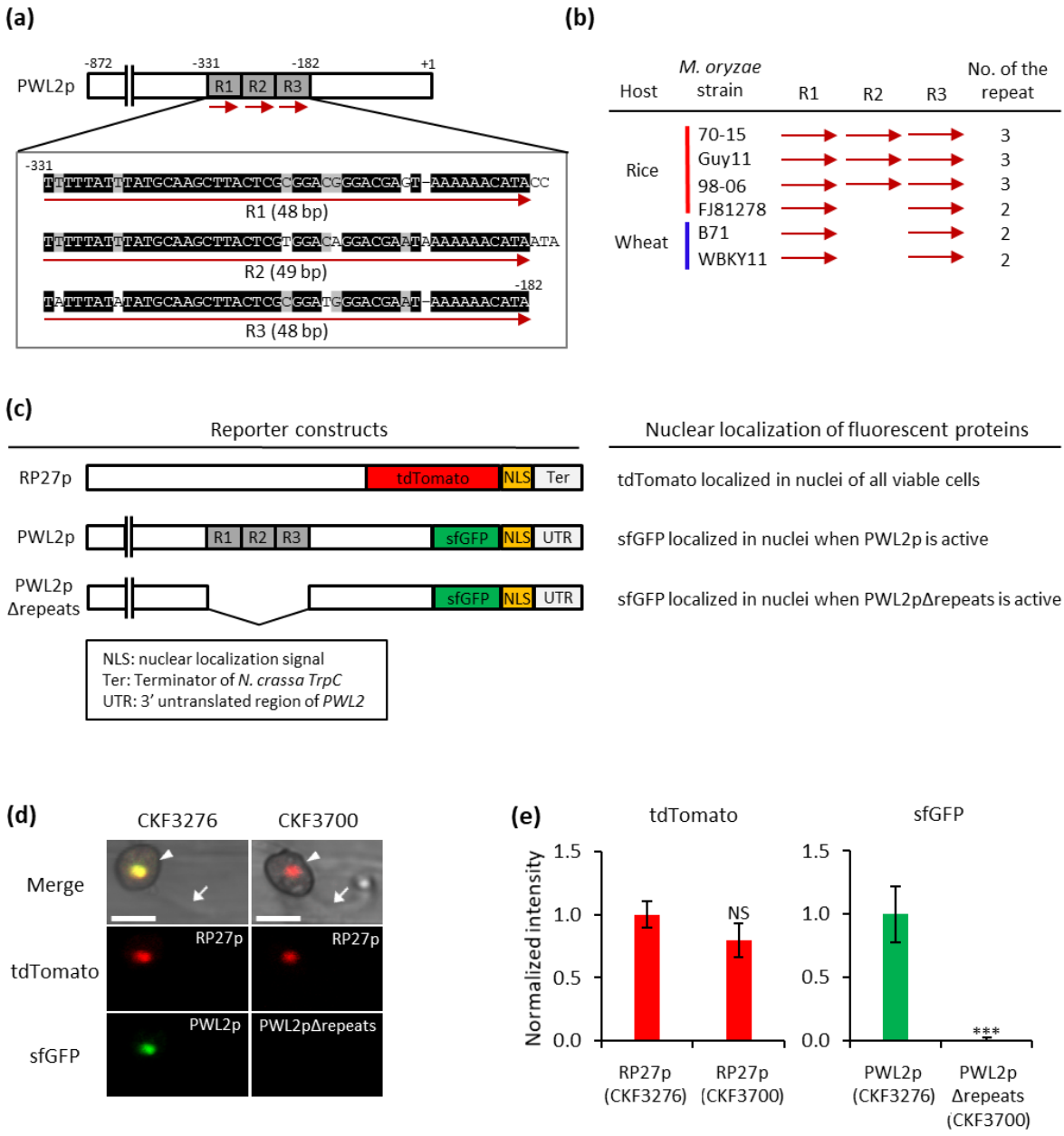

Figure 3.3. The tandem repeat sequences are required for *PWL2* induction during plant infection. (a) The organization and DNA sequences of the three tandem repeats in the *PWL2* promoter (PWL2p). The repeats are denoted as R1, R2, and R3 with red arrows. The numbers indicate the nucleotide positions relative to the translation start site. Black shade indicates sequences conserved in all three repeats, and grey shade indicates sequences conserved in two repeats. (b) Comparison of the repeat copy number in the *PWL2* promoters of six different *M. oryzae* strains, including four

rice-pathogenic (red line) strains, and two wheat pathogenic (blue line) strains. Red arrows indicate the repeats. DNA sequence alignment of the repeats are shown in Fig. S3.4. (c) A schematic representation of the reporter constructs and expected localization of the florescent proteins (red tdTomato and green sfGFP). RP27p is a constitutive promoter. PWL2p is the *PWL2* promoter, and PWL2p*Δ*repeats is the *PWL2* promoter with deletion of all three tandem repeats. (d) Confocal images of *M. oryzae* transformants expressing sfGFP:NLS (green) under control of PWL2p (*M. oryzae* CKF3276) or PWL2p*Δ*repeats (*M. oryzae* CKF3700) at 25hpi. Both transformants constitutively express tdTomato:NLS (red) as a control of visualizing nuclei of viable fungal cells. Arrowheads and arrows indicate, respectively, appressoria and filamentous IH that just penetrated rice cells. Bars, 10 μm. (e) Comparison of normalized fluorescence intensities of tdTomato or sfGFP quantified from nuclei of CKF3276 and CKF3700 at 25 hpi. Data are presented as mean ± SD of more than 10 infection sites for each strain. Two-tailed student t-test was performed to determine statistical difference. *** indicates $p<0.001$, and NS means no significant difference.

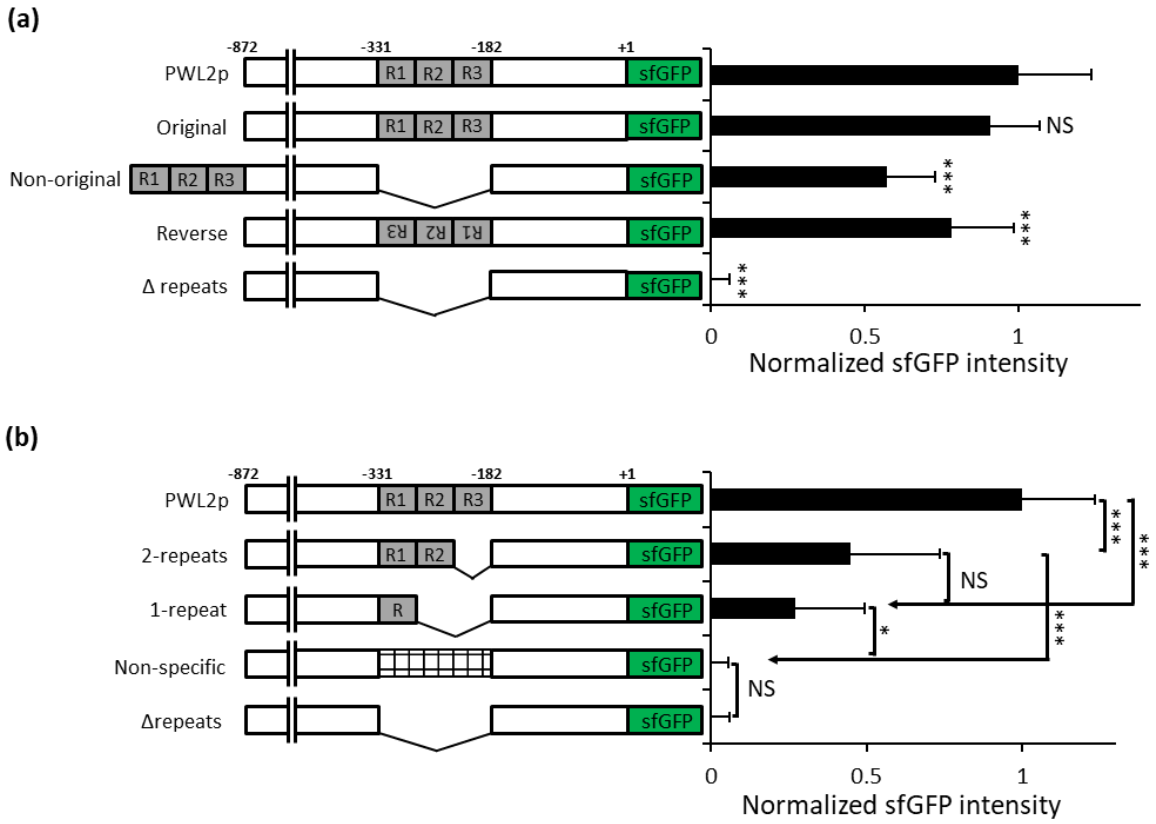

Figure 3.4. Comparison of promoter activity of a series of *PWL2* promoter constructs fused to the sfGFP:NLS reporter. The three tandem repeats in the *PWL2* promoter are denoted as R1, R2, and R3. The numbers indicate the nucleotide positions relative to the translation start site. The promoter activity was measured by quantifying sfGFP fluorescence in nuclei of *M. oryzae* transformants expressing each construct as described for Fig. 3.3c-3.3e. More than two fungal transformants were randomly chosen for each construct, and at least 10 independent infection sites of each transformant were analyzed. The native *PWL2* promoter is indicated as PWL2p, and the promoter with all three repeats being deleted as *Δ*repeats. (a) The repeats were inserted back into the original location (Original) or at the 500-bp upstream from the original location (Non-original) or in the reversed orientation at the original location (Reverse) in the repeat-deleted promoter. Data are presented as mean ± SD. Statistically significant differences were determined using Dunnett's test with PWL2p as the control. *** indicates $p<0.001$, and NS means no

significant difference. (b) Two copies of the repeats were inserted at the original location (2-repeats) in the repeat-deleted promoter. One copy of the repeat (1-repeat), of which DNA sequence is shown in Fig. 3.5a, or a random DNA sequence (Non-specific) was inserted at the original location in the repeat-deleted promoter. Data are presented as mean ± SD. Statistically significant differences were determined using Tukey-Kramer HSD test: *** indicates $p<0.001$, and NS means no significant difference.

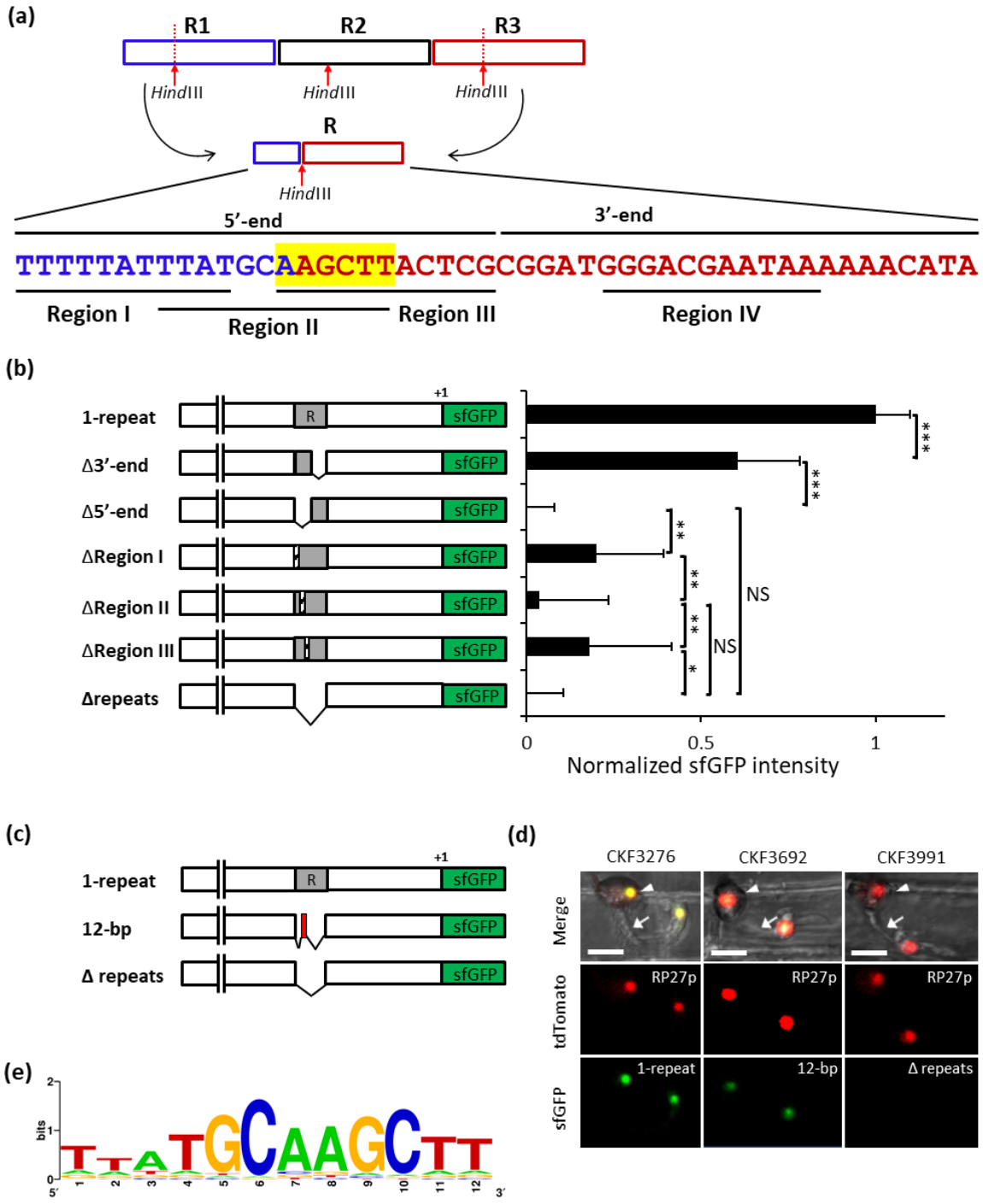

Figure 3.5. The 12-bp motif in the tandem repeat sequence is essential for *PWL2* promoter activity. (a) Schematic diagram of generating the *PWL2* promoter with one repeat (R) by *Hind*III (*AAGCCT*) digestion of the three repeats-containing *PWL2* promoter and ligation to join the 5'-

end region of the R1 (14-bp) and the 3'-end of the R3 (34-bp). The first 24-bp of the R is defined as 5'-end, and the rest 24-bp as 3'-end. The 5'-end was further defined as Region I (11-bp), Region II (12-bp), and Region III (11-bp). (b) The *PWL2* promoter activity with each of the regions defined in (a) being deleted was determined, along with the promoter with one repeat (1-repeat R generated from Fig. 3.5a and the promoter with no repeat (*Δ*repeats), as described for Fig. 3.3c -3.3e. More than two fungal transformants were randomly chosen for each construct, and at least 10 independent infection sites of each transformant were analyzed. Data are presented as mean ± SD. Statistically significant differences were determined by the Tukey-Kramer HSD test. * indicates $p<0.05$, ** indicates $p<0.01$, *** indicates $p<0.001$ and NS means no significant difference was detected at $p<0.05$. (c) Schematic diagram of the *PWL2* promoter with one repeat (1-repeat) or the 12-bp motif in place of the repeat (12-bp; red box corresponding to Region II in Fig. 3.5a) or no repeat (*Δ*repeats) fused to the sfGFP:NLS reporter. (d) Confocal images of *M. oryzae* transformants expressing sfGFP:NLS (green) under control of 1-repeat (*M. oryzae* CKF3736) or 12-bp (*M. oryzae* CKF3991) or *Δ*repeats (*M. oryzae* CKF3692) at 25 hpi. All transformants constitutively express tdTomato:NLS (red) as a control of visualizing nuclei of viable fungal cells. Arrowheads and arrows indicate, respectively, appressoria and filamentous IH that just penetrated rice cells. Note that there are two nuclei (one in the appressorium and another one in the IH cell). More than five independent infection sites were observed for each of 11 random transformants for the 12-bp construct, and all showed the consistent result. Bars, 10 μm. (e) Consensus 12-bp motif sequence generated from 126 sequences similar to the 12-bp motif shown in Fig. 3.5a using WebLogo (Crooks et al., 2004).

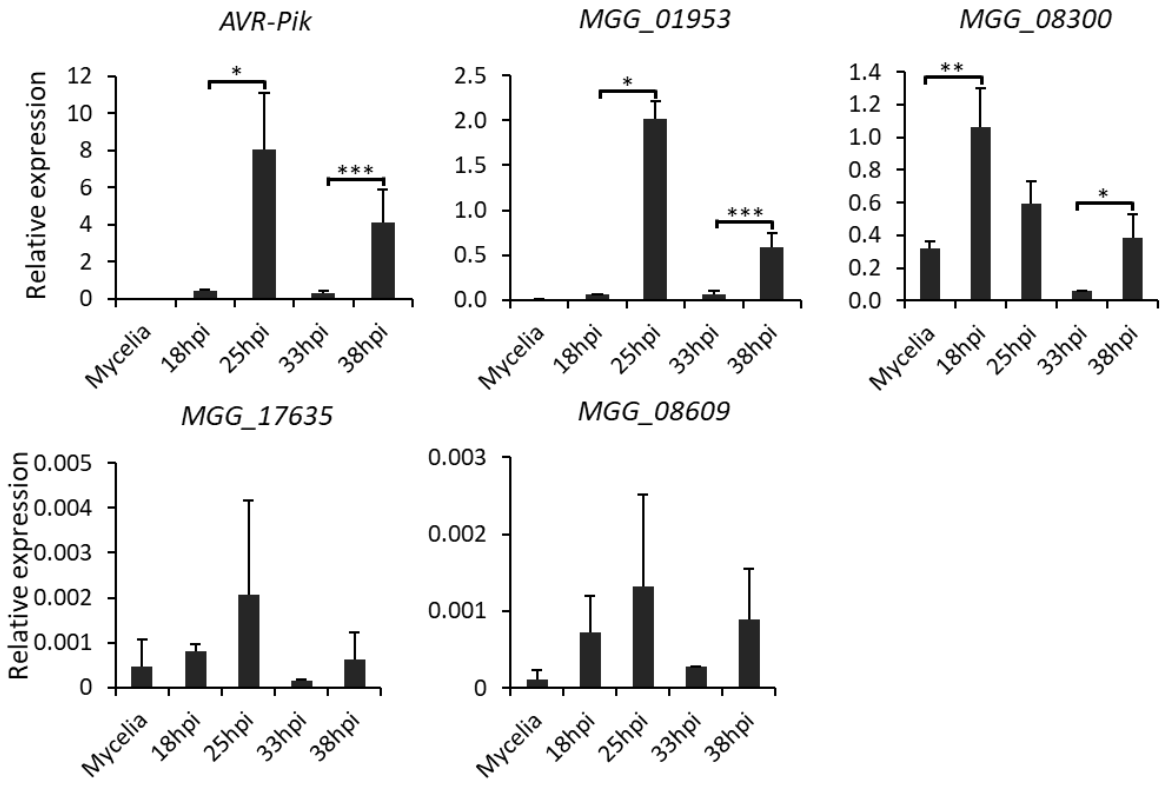

Figure 3.6. qRT-PCR analyses of one known effector gene (*AVR-Pik*) and four candidate effector genes, which all contain the 12-bp like motif in their promoters, show that the expression patterns of these genes are similar to that of *PWL2* (Fig. 3.1c**)** during axenic culture (mycelia) and infection. Data are presented as mean ± SD. Two-tailed student t-test was performed to determine statistical difference. * indicates $p<0.05$, ** indicates $p<0.01$ and *** indicates $p<0.001$.

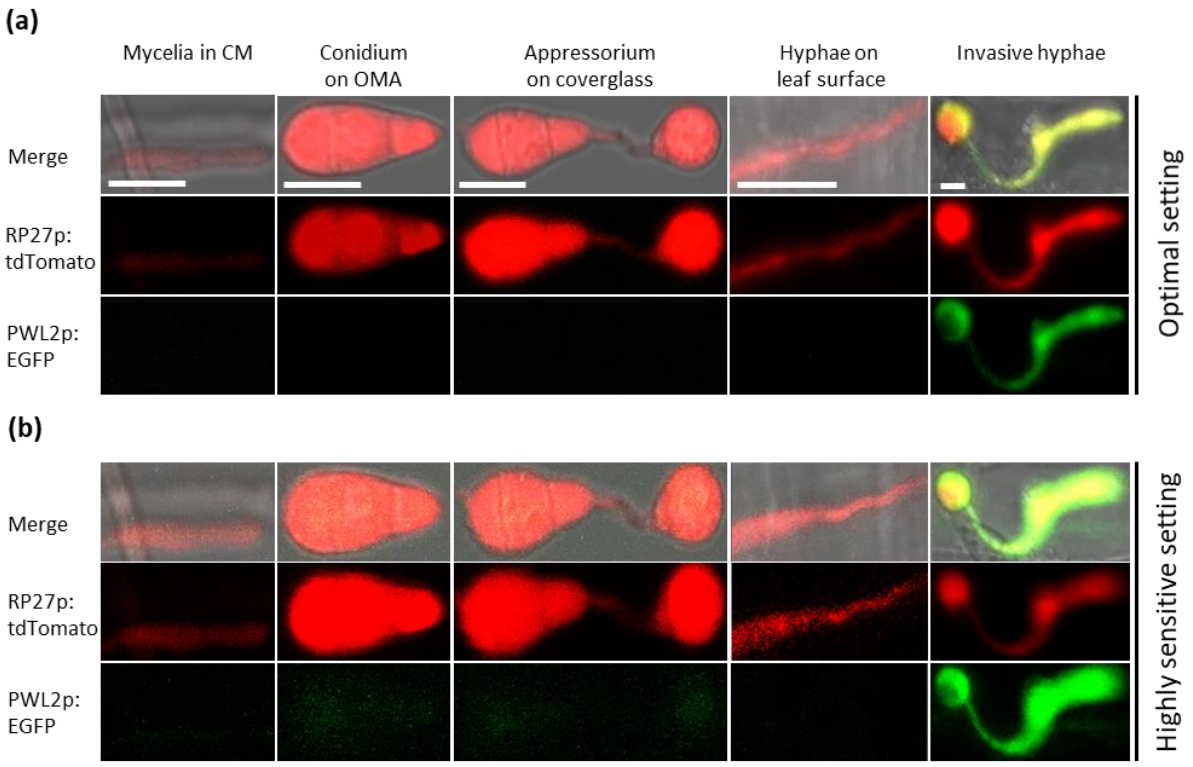

Fig. S3.1 *PWL2* expression is induced during fungal invasion inside of rice cells but not in axenically grown cultures. The *PWL2* expression pattern was monitored at single-cell resolution with CKF3538 at different infection-related development stages. (a) Confocal images with an optimal setting (pinhole: one Airy unit; detect gain: 630) (b) Confocal images with a highly sensitive setting (open pinhole: 10.07 Airy units, almost a nonconfocal image; detector gain: 700). Bars, 10 μm.

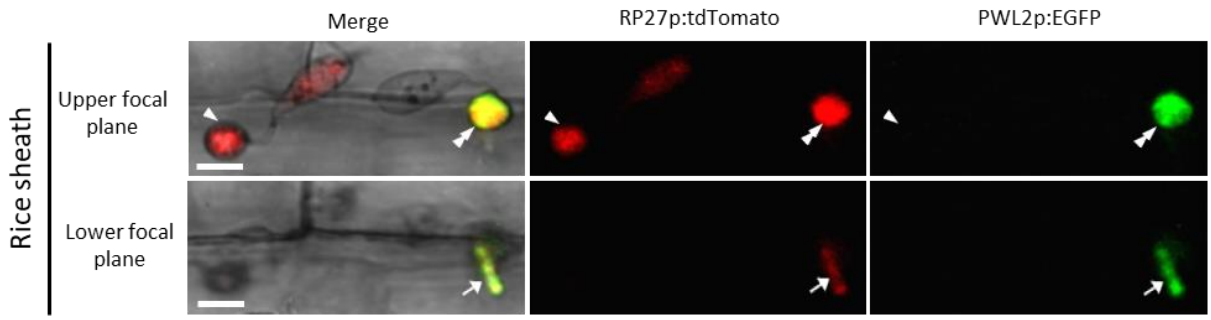

Fig. S3.2 *PWL2* expression is only observed in the appressorium of penetrating epidermal cells of the rice sheath at 25 hpi. Shown are confocal images (CKF3538) of two adjacent infection sites at different Z stack positions: the upper panel was focused on the appressorium z-position, and the lower panel was focused on underneath the appressorium (primary hypha). The left infection site only showed tdTomato fluorescence in appressorium (single arrowhead) but the right infection site showed both tdTomato and EGFP fluorescence in both the penetrating appressorium (double arrowheads) and primary hypha (arrow). Bars, 10 μm.

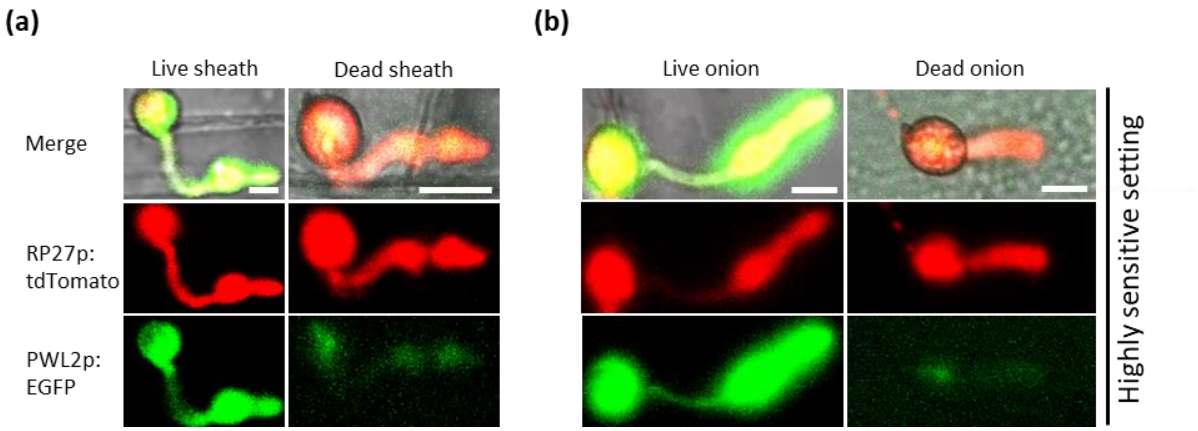

Fig. S3.3 Confocal images of *M. oryzae* transformant CKF3538 invading rice cells and nonhost onion cells with a highly sensitive setting (open pinhole: 10.07 Airy units; detector gain: 700). Bars, 10 μm.

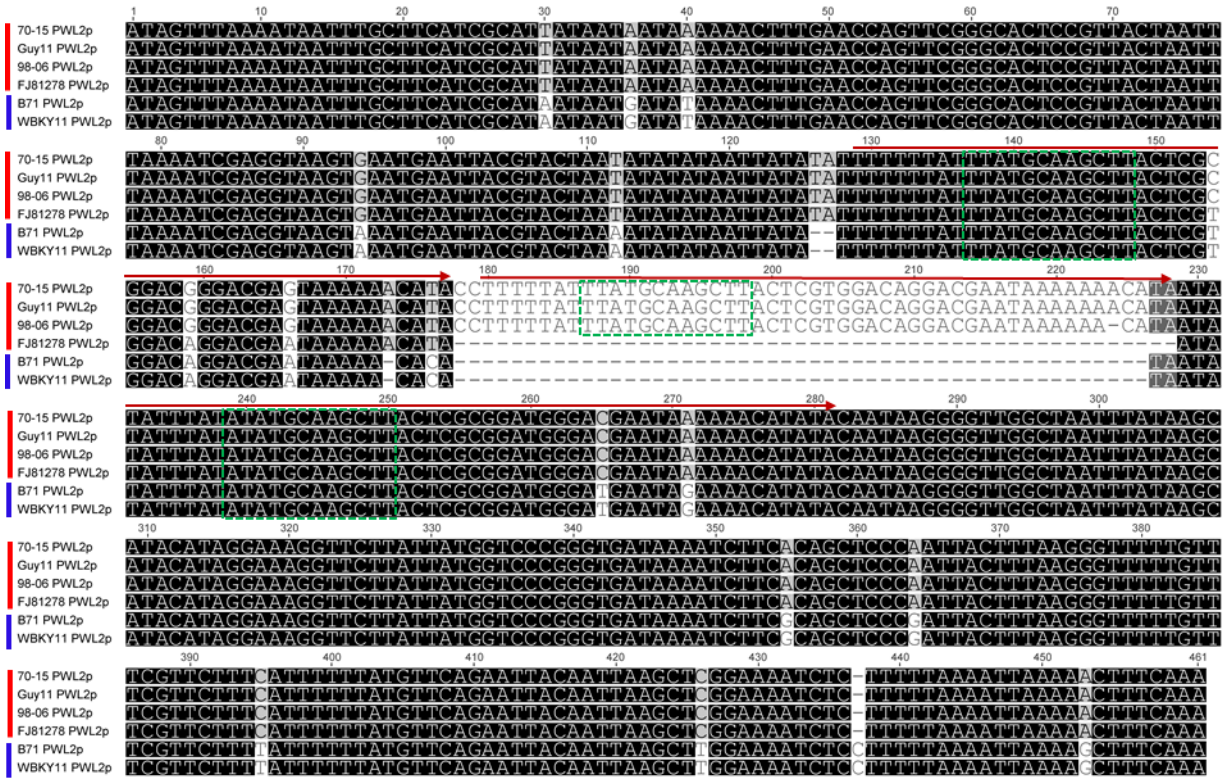

Fig. S3.4 Sequence alignment of the promoter regions of *PWL2* genes from various *M. oryzae* isolates. Identical nucleotides are highlighted on a black background and similar amino acids on a light grey background. Red arrows represent repeats. Green boxes indicate the 12-bp motif identified to be essential for *PWL2* promoter activity (Fig. 3.5).

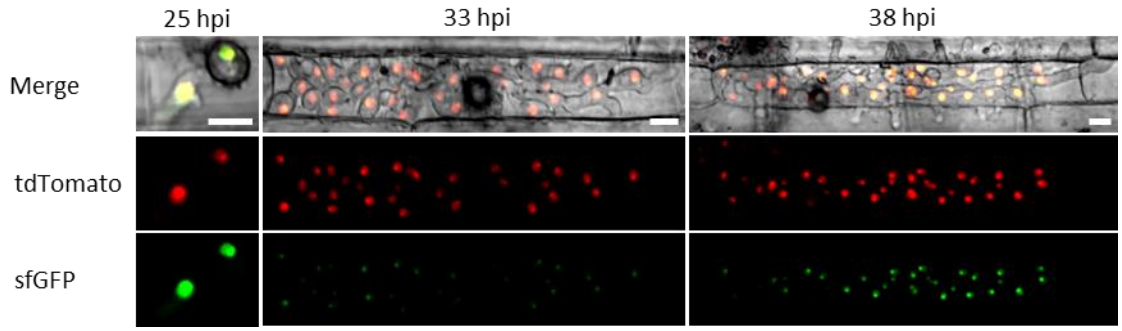

Fig. S3.5 Nucleus-localized fluorescent reporter with the *PWL2* promoter shows a consistent *PWL2* expression pattern. *PWL2* expression pattern was monitored at single-cell resolution with CKF3276 at different stages illustrated in Fig. 3.1a. More than 30 infection sites were observed for each time point. Bars, 10 μm.

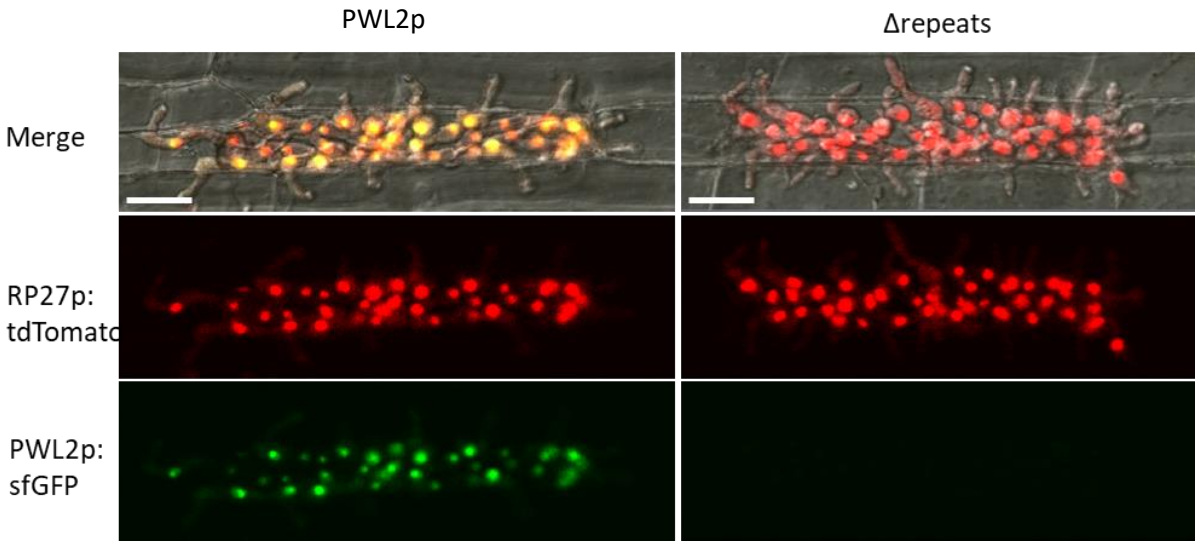

Fig. S3.6 The tandem repeats are required for *PWL2* induction during cell-to-cell movement of invasive hyphae. Confocal images of *M. oryzae* transformants expressing sfGFP:NLS (green) under the control of PWL2p (*M. oryzae* CKF3276) or PWL2p*Δ*repeats (*M. oryzae* CKF3700) at 40 hpi. 10 infection sites were observed for each strain. Bars, 20 μm.

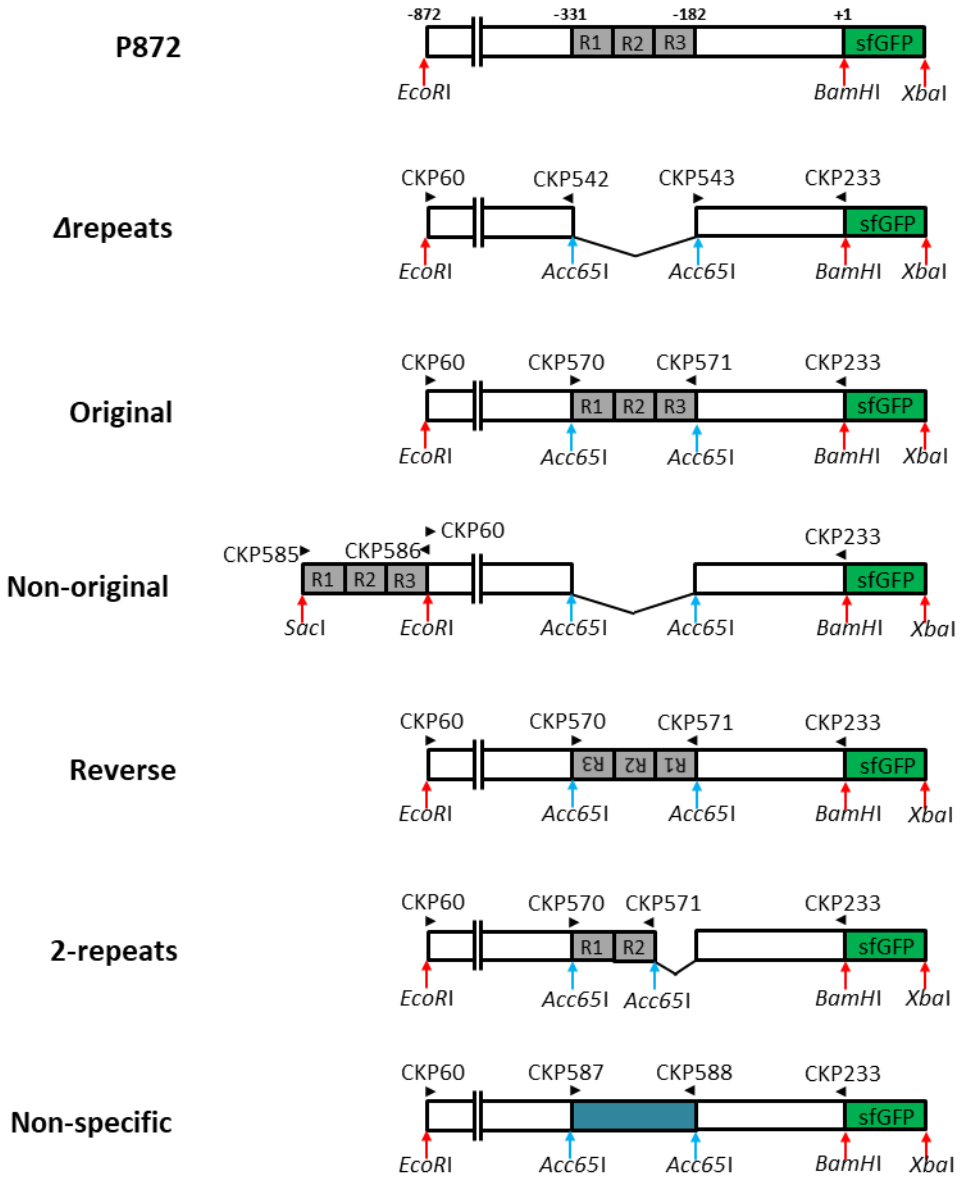

Fig. S3.7 Graphic representation of the *PWL2* promoter region, modified tandem repeats, and the sfGFP fusion constructs used in this study. The construct names are shown on the left and schematic structures on the right. White boxes indicate promoter sequences, gray boxes indicate tandem repeats, tan box indicates non-specific DNA sequence, and green boxes denote sfGFP. Enzyme sites used to make constructs and to modify tandem repeats are indicated by arrows. Primers are indicated with arrowheads and corresponding primer names. Numbers above the boxes indicate nucleotide positions defined relative to the translation start site (A of ATG as +1).

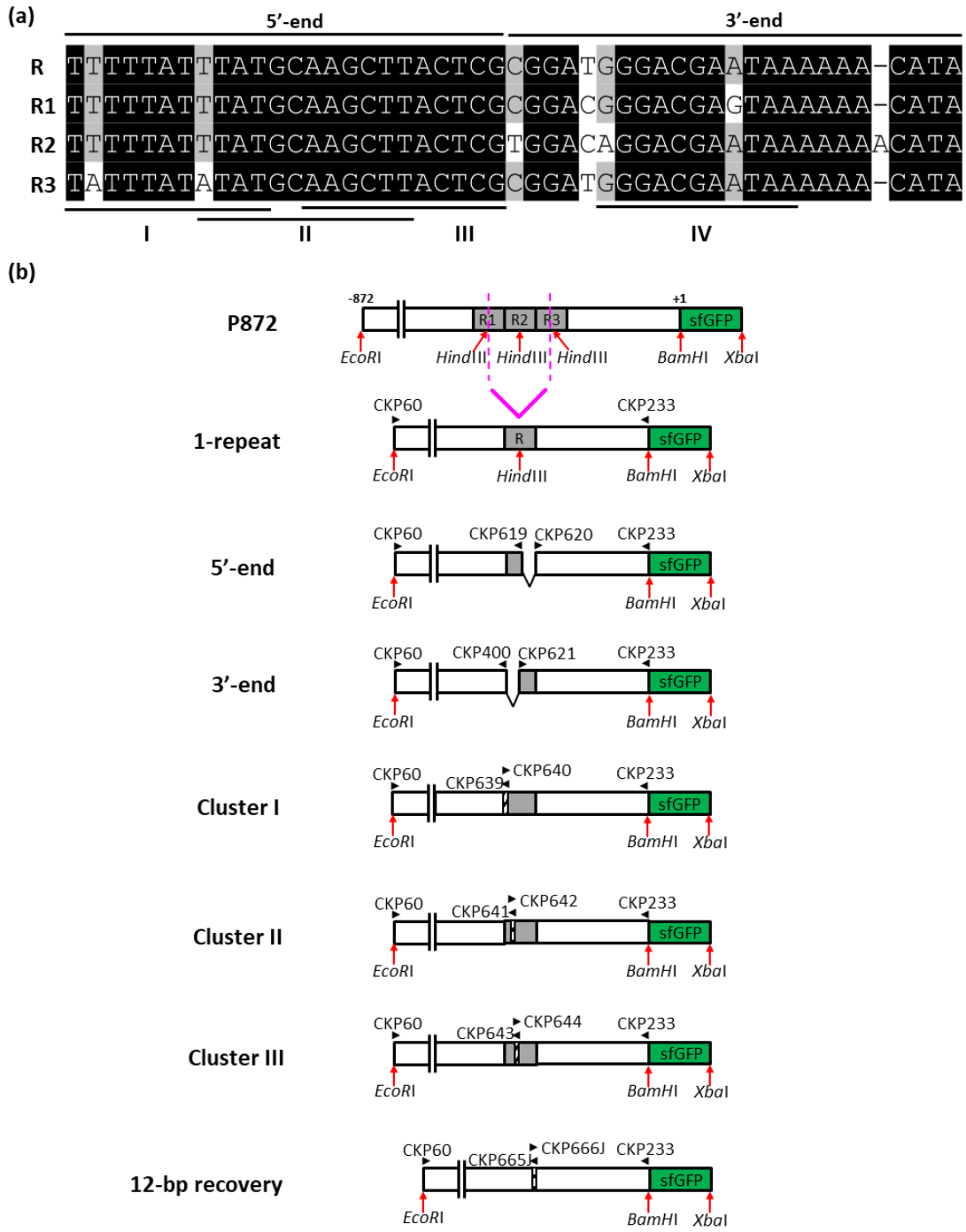

Fig. S3.8 Graphic representation of the deletions and substitutions of one repeat, and the sfGFP fusion constructs used in this study. (a) 5'-end, 3'-end and motifs in different regions (I, II, III) of three repeats (R1, R2, R3) and hybrid repeat (R) are indicated by black lines. (b) The construct names are shown on the left and schematic structures on the right. White boxes indicate promoter

sequences, gray boxes indicate the repeat, and green boxes denote sfGFP. Diagonal stripes indicate substitution sites of clusters. Enzyme sites used to make constructs and to modify tandem repeats are indicated by arrows. A *Hind*III enzyme site is present in each of three repeats, which is used to generate one-repeat construct by *Hind*III digestion and ligation. Deletions of 5'/3'-end, substitutions of clusters, and 12-bp recovery are obtained by fusion PCR with primers indicated with arrowheads and corresponding primer names. Numbers above the boxes indicate nucleotide positions defined relative to the translation start site (A of ATG as +1).

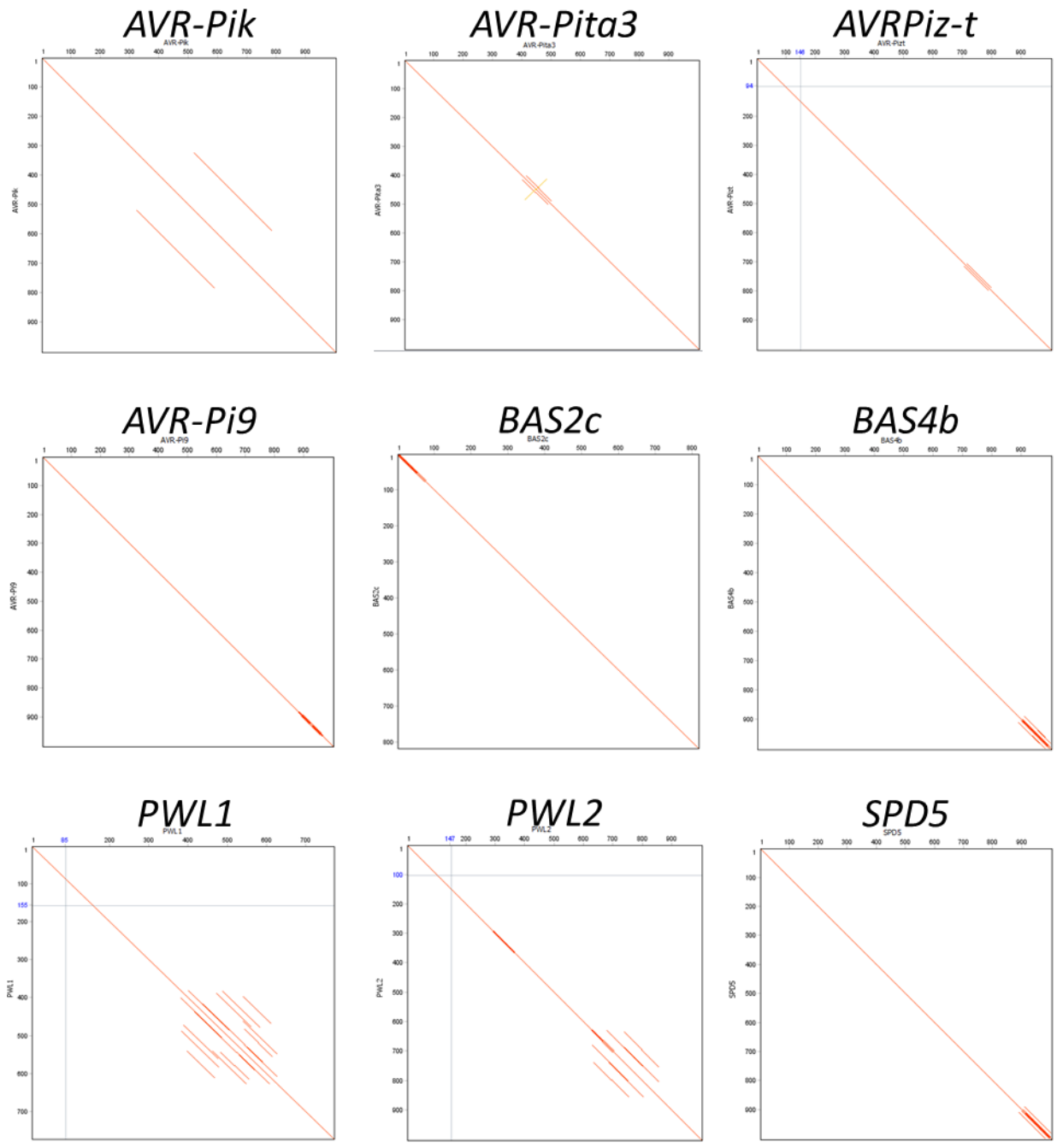

Fig. S3.9 The promoters of multiple effector genes in *M. oryzae* have repeat sequences. The self-dot plots of promoter regions (~1-kb) of different effector genes in *M. oryzae* were generated by Geneious with the following parameters: window size 70 and threshold 85.

CHAPTER 4

LIVE-CELL IMAGING TO INVESTIGATE CELLULAR DYNAMICS OF FINGER MILLET-*MAGNAPORTHE ORYZAE* INTERACTIONS[3]

[3]Jie Zhu, Kathryn Yeary, Margaret Henderson and Chang Hyun Khang. To be submitted to Molecular Plant Pathology.

Abstract

Magnaporthe oryzae is the causal agent of devasting blast disease on many important crop plants, including rice and finger millet (*Eleusine coracana*). *M. oryzae* shows host species specificity, in which individual isolates have a narrow host range. The interaction between blast fungus and rice has been well studied, but host-specific interactions with other plants remain poorly understood. In this present study, we develop a live-cell imaging method based on the optically transparent finger millet leaf sheath tissue to investigate cytological dynamics of the finger millet-*M. oryzae* interaction. Using this method, we found that the finger millet-adapted *M. oryzae* strain (MoE) showed a novel biotrophic interfacial complex (BIC) pattern, multisite BICs, when infecting susceptible finger millet plants. During incompatible interaction between MoE and a susceptible rice cultivar, however, we barely observe rice infection by MoE at both microscopic and macroscopic levels, demonstrating the host species specificity of MoE toward rice. This established finger millet leaf sheath inoculation assay will be a robust tool for further cytological investigations of fungal development and plant responses in finger millet-pathogen interactions.

Introduction

Magnaporthe oryzae is a filamentous fungal pathogen that causes blast disease on more than 50 different grass species, including economically important crops such as rice, wheat, and finger millet. (Dean et al., 2005; Gladieux et al., 2018; Kamoun et al., 2019; Takan et al., 2012). Individual *M. oryzae* isolates typically have a narrow host range (Choi et al., 2013; Kang et al., 1995), and they can be categorized into several pathotypes, according to their adapted host species. Oryzae pathotype strains (MoO) infect rice (*Oryzae sativa*), while Eleusine pathotype strains (MoE) infect finger millet (*Eleusine coracana*) (Couch et al., 2005; Murakami et al., 2000; Yoshida et al., 2016). Host species specificity during plant-microbe interactions is often determined by interactions between resistant (*R*) genes in plants and their cognate avirulence (*AVR*) genes in microbes (Kirzinger and Stavrinides, 2012), in which their interactions result in preventing the microbes from infecting the plants. In *M. oryzae*, *PWL2* and *PWT3* are *AVR* genes that determine host species specificity toward weeping lovegrass and wheat, respectively (Inoue et al., 2017; Kang et al., 1995; Sweigard et al., 1995b). Cellular and molecular mechanisms underlying host specificity remain largely unknown.

Finger millet is widely grown as an important staple crop in sub Saharan Africa, but blast disease causes significant yield losses in this area (Takan, 2004; Takan et al., 2012). Lack of knowledge of *M. oryzae* infection on finger millet has hindered efforts to develop strategies to manage blast disease. Therefore, information about *M. oryzae* infection and host species specificity on finger millet will provide us new perspective to control blast disease on finger millet and other host plants.

Use of the rice sheath infection assay has greatly facilitated cytological understandings of both fungal development and plant responses during *M. oryzae* infection on rice (Koga et al.,

2004; Sakamoto, 1949). *M. oryzae* develops a specialized cell, called an appressorium, to directly penetrate a rice epidermal cell (de Jong et al., 1997). Then the fungus produces invasive hyphae (IH) to proliferate in the first-invaded rice cell and moves into adjacent cells (Kankanala et al., 2007). Cytological studies have revealed that *M. oryzae* is a hemibiotrophic pathogen (Kankanala et al., 2007). The initially-invaded rice cell during infection remains alive but loses viability when IH spread into neighboring cells (Jones et al., 2017; Kankanala et al., 2007). During initial biotrophic invasion, fungal IH are sealed in the extra-invasive hyphal membrane (EIHM) (Kankanala et al., 2007). To suppress plant immune response and manipulate plant cell structure and function, *M. oryzae* secretes and delivers effector proteins into the rice cytoplasm using a specialized structure, called biotrophic interfacial complex (BIC) (Khang et al., 2010a). The tip BIC is formed at the tip of the filamentous primary hypha and then becomes the side BIC, positioned on the side of the first bulbous IH cell, as the fungal hyphae continue to grow (Khang et al., 2010a). Live-cell confocal imaging with fluorescently labelled effector proteins shows that BICs are highly localized structure, showing a single focal fluorescent spot during biotrophic invasion (Giraldo et al., 2013; Khang et al., 2010a; Mosquera et al., 2009).

Magnaporthe oryzae development has been extensively characterized for rice-adapted MoO strains by using various fluorescent reporters coupled with the rice leaf sheath assay. However, little is known about how other pathotypes of *M. oryzae* strains infect their respective host plants and how *M. oryzae* strains fails to infect their non-adapted plants. Here, we developed a finger millet leaf sheath assay and investigated how the finger millet-adapted *M. oryzae* infects finger millet in comparison with the rice-adapted *M. oryzae*.

Materials and Methods

Magnaporthe oryzae isolates, fungal transformation and growth conditions

M. oryzae field isolates O-137 (Sweigard et al., 1995b) and E2 were originally isolated from rice (*Oryzae sativa*) in China and from finger millet (*Eleusine coracana*) in Ethiopia, respectively. Fungal strains were maintained in -20°C freezer as described previously (Valent et al., 1991). Before inoculation, these strains were cultured on oatmeal agar (OMA) plates in a growth chamber with constant light and temperature of 25°C for about 10 days. Fungal mycelia were grown in liquid complete medium for 5 days at 25°C before harvesting for RNA extraction.

To visualize fungal infection at cellular level, we generated transgenic *M. oryzae* strains (Table S4.3). Specifically, MoE (CKF4046) was obtained by transforming finger millet *M. oryzae* wild-type strain E2 with pBV126 (Khang et al., 2010a) using *Agrobacterium*-mediated transformation (Khang et al., 2005). MoO (CKF193) was generated by transforming rice *M. oryzae* wild-type strain O-137 with pBV229. pBV229 was produced by cloning of the hH1 fragment from pBV202 in the XhoI and BamHI sites of pBV126. To visualize effector translocation during finger millet infection by *M. oryzae*, CKF4198 was generated by transforming E2 with pBV591 (Khang et al., 2010a).

Plant materials

Susceptible rice cultivar YT16 and 16 finger millet cultivars including AAUFM-44, IE7, KNE796, and TZA1637, were used in this study. Plants were grown as described previously (Jones et al., 2016). Briefly, all plants were grown from seeds in a growth chamber with long day settings (14/10 h, day/night) under a day-time temperature of 28°C, a night-time temperature of 24°C and 80% humidity. Rice and finger millet plants were grown for 18-20 days and 11-13 days before used for inoculation, respectively.

Whole plant spray inoculation assay

The whole-plant infections were performed with 1×10^5 spores/ml in distilled gelatin solution (0.25%) to assess pathogenicity. Symptoms on the sprayed plants after seven days inoculation were recorded (Valent et al., 1991) and evaluated (Matsunaga et al., 2017) as previously described. Briefly, the marked youngest and/or second youngest leaf that was expanded when being inoculated was examined and documented using EPSON perfection 4870 Photo with 24-bit color, 600 dpi resolutions and same document size (8.5 inch of width and 11.7 inch of height). The diseased leaf area was then measured by ImageJ (Schneider et al., 2012). A single leaf was analyzed each time. Pixels were converted to centimeters using the Set Scale command. Color Threshold with HSB color space was then used to select and measure appropriate thresholds to whole leaf area and specifically diseased leaf area, respectively. Statistical significance was analyzed using One-way ANOVA and Tukey-Kramer HSD.

Plant sheath inoculation assay

Fungal spores were harvested from ~10-day-old cultures in 1 ml distilled water for inoculation. Rice sheath inoculation assay was performed as described (Jones et al., 2016a; Kankanala et al., 2007). For finger millet sheath inoculation assay, leaf sheath of the third leave of the 12-day-old finger millet plant was peeled off and excised. The leaf sheath (~2 cm) was then laid horizontally on a support. 1×10^5 spores/ml in distilled water was injected into the curved cavity and incubated at 25°C until observation. The inoculated sheath was immediately used for staining or confocal microscopy after being hand-trimmed at 30 or 48 hours post inoculation (hpi).

Confocal microscopic analyses of pathogen infection

Fluorescein diacetate (FDA) and propidium iodide (PI) staining were performed as described (Jones et al., 2016). Confocal microscopy was performed on a Zeiss LSM 880 Confocal Microscope with an upright microscope stand. Excitation/emission wavelengths were 488 nm/496 to 544 nm for EGFP/FDA and 543 nm/565 to 617 nm for mCherry/PI. Images were processed using Zen Black software (version 10.0, Zeiss). For PI/FDA staining and effector translocation, all images were recorded at 30 hpi. For quantification of infection stageszfcbgd nnbgbgAZX, the number of infection stages, including appressoria, infecting one plant cell, infecting two or more plant cells, and dead plant cells, were counted at 48 hpi. Each number was then converted into percentage of total infected sites.

RNA isolation and quantitative RT-PCR

Total RNAs from mycelia and sprayed plant leaves by fungal spores (*Magnaporthe*-inoculated) or gelatin (mock-treated) were purified using RNA Clean & Concentrator-5 kit (Zymo research, Cat# R1015) following the manufacturer's instructions. Genomic DNA was digested and removed by Turbo™ DNase (Ambion, Cat# AM1907). 1 µg of total RNA was used to synthesize cDNA with ImProm II Reverse Transcriptase system (Promega). qRT-PCR was performed with CFX96™ (Bio-Rad) systems using the PowerUp™ SYBR™ Green Master Mix (Thermo Fisher/applied biosystem). Thermocycler conditions were as follows: 2 min at 50°C, 10 min at 95°C, followed by 40 cycles of 95°C for 30 sec, 60°C for 60 sec. Each qRT-PCR mixture (final volume 14 µl) contained 7 µl of PowerUp™ SYBR™ Green Master Mix, 1.5 µl of each the forward and reverse primer (3.3 nM concentrations for each), 2 µl of cDNA template and 2 µl of distilled water. Primers used for qRT-PCR assays are listed in Table S4.5. The relative expression level of each gene was calculated by the $2^{-\Delta CT}$ method (Livak and Schmittgen, 2001),

with *O. sativa* actin and *E. coracana* β-tubulin (Reddy et al., 2018) as control housekeeping genes. Briefly, the average threshold cycle (Ct) was normalized to that of the reference gene for each of the treated samples as $2^{-\Delta Ct}$, where ΔCt = (Ct, target gene - Ct, reference gene). Two technical replications for each of three biological replications were performed. Mean and standard deviation were calculated from qRT-PCR results of three biological replicates.

Results and Discussions

Phenotypic analysis of finger millet-*M. oryzae* compatible interactions.

To characterize interaction between finger millet and *M. oryzae*, we exmained >200 *M. oryzae* strains from diseased finger millet plants grown in Eastern Africa (Kenya, Tanzania, Uganda and Ethiopia) and identified a field isolate E2 from Ethiopia as a reference strain. To monitor and compare blast disease, we first developed a whole plant spray inoculation assay and standard lesion types to score degrees of disease symptoms (Fig. S4.1A). Specifically, only youngest and second youngest leaves of ~12-day old finger millet seedings were examined and compared for disease development (Fig. 4.1A). Overall, E2 showed serious symptoms on diverse finger millet cultivars (Table S4.1). We generated transformants of E2, constitutively expressing cytoplasmic green fluorescent protein, and subsequently identify one strain, called MoE (CKF4046, Table S4.3; representing pathotype *Eleusine*), which showed similar growth on oatmeal agar plate and on pathogenicity as E2 strain (Fig. S4.1B). Then, we characterized disease development of MoE on a susceptible finger millet cultivar using the whole plant spray inoculation assay. The timing of symptom development of MoE on *E. coracana* leaves was similar to a rice pathogen on rice leaves (Fig. S4.2). MoE had a visually asymptomatic phase until after ~3 days post inoculation (dpi), when lesions became visible. Then lesions continued to develop and were surrounded by a dark brown margin by ~ 4 dpi. Around same time, leaves

became yellowish and began to shrivel around lesions, which was different from rice pathogen infection on rice. Necrosis was apparent by 5 dpi and lesions increased in size until 6 dpi.

Identification of susceptible and resistant finger millet cultivars by *M. oryzae* infection

To explore cultivar specificity of the finger millet strain, four *E. coracana* cultivars AAUFM-44, IE7, KNE796, and TZA1637, representing various degrees of susceptibility and resistance, were inoculated with MoE spores by spray inoculation. Macroscopic inspection at 7 dpi revealed clear differences of plant responses triggered by the same strain. AAUFM-44, IE7 and KNE796 were highly susceptible to MoE infection, but TZA1637 was resistant (Fig. 4.1B). Moreover, the pathogenicity assays of MoE on 11 finger millet cultivars including AAUFM-44, IE7, and TZA1637 had a similar result. AAUFM-44 and IE7 showed the most severe infection but TZA1637 showed the least (Table S4.2). Hereafter, AAUFM-44 was selected as the susceptible *E. coracana* cultivar to MoE infection for the following investigations.

Development of the finger millet leaf sheath inoculation assay for live-cell imaging.

To investigate fungal infection and plant responses at cellular level during finger millet infection by MoE strain, we developed a finger millet leaf sheath inoculation assay. Briefly, the second or third youngest leaf of the ~12-day-old finger millet seedling was peeled off and excised, then laid horizontally on a support that was placed in a humid petri dish (Fig. 4.2A). Fungal spore suspensions ($1x10^5$/ml) were injected inside of the sheath cavity from one end until suspensions reached the other end. The inoculated leaf sheath was then incubated at 25°C until observation.

Viability of epidermal cells from the inoculated finger millet sheath was determined using two strategies. First, we utilized dual staining of finger miller cells with fluorescein

diacetate (FDA) and propidium iodide (PI) that have been applied to investigate cellular dynamics of plant cell death in rice-*M. oryzae* interaction (Jones et al., 2016a). FDA exclusively stains the cytoplasm of live cells with green fluorescence (Green et al., 2006; Jones et al., 2016a; Saruyama et al., 2013), whereas PI stains nuclei of dead cells and plant cell walls regardless of cell viability with red fluorescence (Chen et al., 2006; Jones et al., 2016a). Confocal microscopy of FDA/PI-stained finger millet sheaths showed bright green fluorescence inside plant cells, but only red fluorescence in plant cell walls (Fig. 4.2B). The presence of FDA staining in the invaded cells and the absence of PI staining in the nucleus indicate that the infected epidermal cells were viable in our excised sheaths. This dual FDA/PI staining pattern in finger millet-*M. oryzae* interaction was similar to the report in rice-*M. oryzae* pathosystem (Jones et al., 2016a).

Next, we inoculated excised finger millet sheath with an E2 transformant expressing fluorescently-labelled PWL2 (PWL2:mCherry:NLS) and BAS4 (BAS4:GFP) effector proteins. PWL2 is a cytoplasmic effector that is preferentially accumulated in BICs before translocating into the plant cytoplasm (Khang et al., 2010a). BAS4 is an apoplastic effector that is secreted and retained within the EIHM compartment (Khang et al., 2010a; Mosquera et al., 2009). Confocal imaging showed that PWL2:mCherry:NLS proteins were predominately accumulated in BICs and BAS4:GFP proteins were uniformly outlined the IH within the EIHM compartment (Fig. 4.2C), which was similar to the patterns previously observed in rice-*M. oryzae* interactions (Khang et al., 2010a; Mosquera et al., 2009). In addition, the accumulation of PWL2:mCherry:NLS in the plant nucleus was also observed (Fig. 4.2C), indicating that the infected plant cells were able to recognize the nuclear localization signal (NLS) attached to PWL2:mCherry and transport the protein into the plant nucleus. Both BICs and EIHM are plant-derived structures and are associated with biotrophic invasion (Giraldo et al., 2013; Kankanala et

al., 2007). Thus, the successful formation of BICs and EIHM in a viable invaded plant cell during fungal infection suggests the establishment of biotrophic invasion of *M. oryzae* on finger millet at the early infection stage.

Novel pattern of the biotrophic interfacial complexes (BICs) during finger millet infection by *M. oryzae*.

By using the finger millet leaf sheath inoculation assay, we demonstrated that the early stage of *M. oryzae* infection on finger millet was a biotrophic invasion. Additionally, we found that BIC and EIHM were formed during the biotrophic invasion on the finger millet plant, indicating conserved features of *M. oryzae* infection on different host plants. However, intriguingly, our live-cell imaging of finger millet-*M. oryzae* interactions revealed that multiple BICs were formed in a clustered or scattered manner (named multisite BICs in this study; 31 out of a total of 37 infection sites; 84%), in addition to a single focal BIC (6 out of 37 infection sites; 16%) at 30 hpi (Fig. 4.2D & E). This is in stark contrast to BICs formed during the rice-*M. oryzae* interaction, in which only a single BIC has been observed (over 1,000 infection sites; Giraldo et al., 2013; Khang et al., 2010; Mosquera et al., 2009). Multisite BICs persistently remained on the first differentiated IH cell, and these BICs were often associated with an uncharacterized small dark body near each fluorescent focus (Fig. 4.2E). This pattern of multisite BICs was consistently observed with a total of seven different fungal transformants in five independent infection assays.

Four *M. oryzae* genes have been known to be implicated with formation or maintenance of the focal BICs during infecting rice cells. The mutation of the t-SNARE protein Sso1 results in a double-BIC phenotype and reduced pathogenicity (Giraldo et al., 2013). Individual deletions of *Rbf1* (required for focal BIC formation 1), *MoSec4* (small GTPase playing roles in membrane

trafficking, protein secretion and fungal development), and *Imp1* (integral membrane protein 1) lead to dispersed puncta or multiple foci of BICs at the early stage of infection (~30 hpi) (Nishimura et al., 2016; Sun et al., 2018; Zheng et al., 2016). It will be interesting to investigate if any of these genes are implicated in multisite BIC formation that we observed with MoE during finger millet infection and what roles multisite BICs play in invasion of finger millet.

Host species specificity of *M. oryzae* isolates on rice and finger millet.

Host species specificity of *M. oryzae* isolated from various plants has been reported (Inoue et al., 2017; Kang et al., 1995; Murakami et al., 2003; Murakami et al., 2000; Sweigard et al., 1995b). Currently, host species specificity is mainly studied at tissue level by pathogenicity assay on different plants, but little information is known at cellular level. Thus, we used the finger millet leaf sheath assay to investigate cellular dynamics of *M. oryzae* interactions with rice (*O. sativa*) and finger millet (*E. coracana*). We inoculated the susceptible *E. coracana* cultivar AAUFM-44 and *O. sativa* cultivar YT16 with spores of the finger millet strain MoE. We found that MoE successfully invaded finger millet cells with colonizing the first invaded cells (276 out of a total of 832 infection sites; 33.2%) and spreading into two to three cells away from the initially invaded finger millet cells (205/832; 24.6%), whereas the same strain failed to penetrate rice cells (Fig. 4.3). Then we used the rice strain MoO (representing pathotype *Oryza*) to inoculate the same susceptible *E. coracana* and *O. sativa* cultivars that we used with MoE. We observed that the most of MoO infections have invaded one to three rice cells but not finger millet cells (63.3% vs. 3.1%, Fig. 4.3). Taken together, we found the similar penetration rates of MoE on susceptible finger millet and MoO on susceptible rice (58.3% vs. 63.3%) but the obvious decrease in penetration and invasion of MoE on rice and MoO on finger millet at 48 hpi

(Fig. 4.3). This demonstrated that both *M. oryzae* strains MoE and MoO show host species specificity toward finger millet and rice plants, respectively.

To further confirm host species specificity of MoE and MoO that was determined by the leaf sheath inoculation assay, we performed a whole plant spray inoculation assay and examined disease development after 7 days inoculation. Consistently, we found severe infection on susceptible finger millet leaves by challenge of the finger millet strain MoE but no obvious symptom by the rice strain MoO (Fig. 4.4A). And vice versa, susceptible rice leaves were heavily infected by MoO but not by MoE (Fig. 4.4B). These results suggested that the host species specificity determined at cellular level by leaf sheath inoculation assay accurately reflected the plant response at tissue level by whole plant spray inoculation assay.

Notably, we observed high percentage of unpenetrated appressoria of MoE on rice and MoO on finger millet (Fig. 4.3). Such phenomenon has also been observed for the infection of a wheat isolate of *M. oryzae* on rice, which showed abundant appressoria without formation of invasive hyphae in epidermal cells (Faivre-Rampant et al., 2008). However, the cytological study of host species specificity may show different responses depending on plant species and host-specific pathotypes of *M. oryzae*. For example, cytological responses of host species specificity of a *M. oryzae* isolate from foxtail millet toward wheat mainly showed hypersensitive reaction (HR) and the formation of a fluorescent papilla in infected epidermal cells (Murakami et al., 2000). Additionally, our result plus previous studies show that all these cytological responses (unpenetrated appressoria, HR and papilla formation) lead to no or slight symptom on plant leaves (Fig. 4.4) (Faivre-Rampant et al., 2008; Murakami et al., 2000). This indicates that the presence of fungal pathogens on plant surface is recognized by plant immune system to prevent fungal infection. Indeed, we found that expression of plant defense related genes (*PR1b*, *PR2*,

PR8) was highly induced during incompatible interactions of *M. oryzae* on nonhost plants (Fig. S4.3), which was similar to that in rice infection by the wheat isolate (Faivre-Rampant et al., 2008). Therefore, the plant responses at the microscopic level are correlated with those at the macroscopic level in *M. oryzae* isolates showing host species specificity. Moreover, cytological responses determining host-species specificity using leaf sheath inoculation assay provide better understandings of host-pathogen interaction within a short time period. First, the fluorescently labelled fungal pathogen coupled with various staining strategies (e.g. FDA/PI and 3′-Diaminobenzidine (DAB)) allows us to comparatively and simultaneously study fungal infection and host responses. Second, the cytological study takes only ~2 days to examine plant responses compared to ~7 days with a spray inoculation assay.

In summary, we developed a live-cell imaging method to visualize cytological dynamics of finger millet-*M. oryzae* interactions. By using this method, we have revealed a novel multisite BICs pattern that seems to be a functionally normal phenotype for *M. oryzae* infection on finger millet. In addition, we demonstrated the utility of the live-cell imaging method for investigating host species specificity of *M. oryzae* on finger millet and rice.

References

Chen, J., Hall, D.E., Murata, J., and De Luca, V. (2006). L-Alanine induces programmed cell death in *V. labrusca* cell suspension cultures. Plant science *171*, 734-744.

Choi, J., Park, S.-Y., Kim, B.-R., Roh, J.-H., Oh, I.-S., Han, S.-S., and Lee, Y.-H. (2013). Comparative analysis of pathogenicity and phylogenetic relationship in *Magnaporthe grisea* species complex. PloS one *8*.

Couch, B.C., Fudal, I., Lebrun, M.-H., Tharreau, D., Valent, B., Van Kim, P., Nottéghem, J.-L., and Kohn, L.M. (2005). Origins of host-specific populations of the blast pathogen *Magnaporthe oryzae* in crop domestication with subsequent expansion of pandemic clones on rice and weeds of rice. Genetics *170*, 613-630.

de Jong, J.C., McCormack, B.J., Smirnoff, N., and Talbot, N.J. (1997). Glycerol generates turgor in rice blast. Nature *389*, 244.

Dean, R.A., Talbot, N.J., Ebbole, D.J., Farman, M.L., Mitchell, T.K., Orbach, M.J., Thon, M., Kulkarni, R., Xu, J.-R., and Pan, H. (2005). The genome sequence of the rice blast fungus Magnaporthe grisea. Nature *434*, 980.

Faivre-Rampant, O., Thomas, J., Allègre, M., Morel, J.B., Tharreau, D., Nottéghem, J.L., Lebrun, M.H., Schaffrath, U., and Piffanelli, P. (2008). Characterization of the model system rice–*Magnaporthe* for the study of nonhost resistance in cereals. New Phytologist *180*, 899-910.

Giraldo, M.C., Dagdas, Y.F., Gupta, Y.K., Mentlak, T.A., Yi, M., Martinez-Rocha, A.L., Saitoh, H., Terauchi, R., Talbot, N.J., and Valent, B. (2013). Two distinct secretion systems

facilitate tissue invasion by the rice blast fungus *Magnaporthe oryzae*. Nat Commun *4*, 1996.

Gladieux, P., Condon, B., Ravel, S., Soanes, D., Maciel, J.L.N., Nhani, A., Chen, L., Terauchi, R., Lebrun, M.-H., and Tharreau, D. (2018). Gene flow between divergent cereal-and grass-specific lineages of the rice blast fungus *Magnaporthe oryzae*. MBio *9*, e01219-01217.

Green, V.S., Stott, D.E., and Diack, M. (2006). Assay for fluorescein diacetate hydrolytic activity: optimization for soil samples. Soil Biology and Biochemistry *38*, 693-701.

Inoue, Y., Vy, T.T., Yoshida, K., Asano, H., Mitsuoka, C., Asuke, S., Anh, V.L., Cumagun, C.J., Chuma, I., and Terauchi, R. (2017). Evolution of the wheat blast fungus through functional losses in a host specificity determinant. Science *357*, 80-83.

Jones, K., Kim, D.W., Park, J.S., and Khang, C.H. (2016). Live-cell fluorescence imaging to investigate the dynamics of plant cell death during infection by the rice blast fungus *Magnaporthe oryzae*. BMC Plant Biol *16*, 69.

Jones, K., Zhu, J., Jenkinson, C.B., Kim, D.W., and Khang, C.H. (2017). Disruption of the interfacial membrane leads to *Magnaporthe oryzae* effector re-location and lifestyle switch during rice blast disease. bioRxiv, 177147.

Kamoun, S., Talbot, N.J., and Islam, M.T. (2019). Plant health emergencies demand open science: Tackling a cereal killer on the run. PLoS Biology *17*, e3000302.

Kang, S., Sweigard, J.A., and Valent, B. (1995). The PWL host specificity gene family in the blast fungus *Magnaporthe grisea*. MPMI-Molecular Plant Microbe Interactions *8*, 939-948.

Kankanala, P., Czymmek, K., and Valent, B. (2007). Roles for rice membrane dynamics and plasmodesmata during biotrophic invasion by the blast fungus. Plant Cell *19*, 706-724.

Khang, C.H., Berruyer, R., Giraldo, M.C., Kankanala, P., Park, S.-Y., Czymmek, K., Kang, S., and Valent, B. (2010). Translocation of *Magnaporthe oryzae* effectors into rice cells and their subsequent cell-to-cell movement. The Plant Cell *22*, 1388-1403.

Khang, C.H., Park, S.Y., Lee, Y.H., and Kang, S. (2005). A dual selection based, targeted gene replacement tool for *Magnaporthe grisea* and *Fusarium oxysporum*. Fungal Genetics and Biology *42*, 483-492.

Kirzinger, M.W., and Stavrinides, J. (2012). Host specificity determinants as a genetic continuum. Trends in microbiology *20*, 88-93.

Koga, H., Dohi, K., Nakayachi, O., and Mori, M. (2004). A novel inoculation method of *Magnaporthe grisea* for cytological observation of the infection process using intact leaf sheaths of rice plants. Physiological and Molecular Plant Pathology *64*, 67-72.

Livak, K.J., and Schmittgen, T.D. (2001). Analysis of relative gene expression data using real-time quantitative PCR and the $2^{-\Delta\Delta CT}$ method. Methods *25*, 402-408.

Matsunaga, T.M., Ogawa, D., Taguchi-Shiobara, F., Ishimoto, M., Matsunaga, S., and Habu, Y. (2017). Direct quantitative evaluation of disease symptoms on living plant leaves growing under natural light. Breed Science *67*, 316-319.

Mosquera, G., Giraldo, M.C., Khang, C.H., Coughlan, S., and Valent, B. (2009). Interaction transcriptome analysis identifies *Magnaporthe oryzae* BAS1-4 as Biotrophy-associated secreted proteins in rice blast disease. Plant Cell *21*, 1273-1290.

Murakami, J., Tomita, R., Kataoka, T., Nakayashiki, H., Tosa, Y., and Mayama, S. (2003). Analysis of host species specificity of *Magnaporthe grisea* toward foxtail millet using a genetic cross between isolates from wheat and foxtail millet. Phytopathology *93*, 42-45.

Murakami, J., Tosa, Y., Kataoka, T., Tomita, R., Kawasaki, J., Chuma, I., Sesumi, Y., Kusaba, M., Nakayashiki, H., and Mayama, S. (2000). Analysis of host species specificity of *Magnaporthe grisea* toward wheat using a genetic cross between isolates from wheat and foxtail millet. Phytopathology *90*, 1060-1067.

Nishimura, T., Mochizuki, S., Ishii-Minami, N., Fujisawa, Y., Kawahara, Y., Yoshida, Y., Okada, K., Ando, S., Matsumura, H., Terauchi, R., *et al.* (2016). *Magnaporthe oryzae* glycine-rich secretion protein, Rbf1 critically participates in pathogenicity through the focal formation of the biotrophic Interfacial complex. PLoS Pathogen *12*, e1005921.

Reddy, P.S., Dhaware, M.G., Reddy, D.S., Reddy, B.P., Divya, K., Sharma, K.K., and Bhatnagar-Mathur, P. (2018). Comprehensive evaluation of candidate reference genes for real-time quantitative PCR (RT-qPCR) data normalization in nutri-cereal finger millet [*Eleusine Coracana* (L.)]. PloS one *13*.

Sakamoto, M. (1949). On the new method of sheath-inoculation of rice plants with blast fungus, *Pyricularia oryzae* Cav. for the study of the disease-resistant nature of the plant. Bull Inst Agr Res Tohoku Univ Jpn *1*, 120-129.

Saruyama, N., Sakakura, Y., Asano, T., Nishiuchi, T., Sasamoto, H., and Kodama, H. (2013). Quantification of metabolic activity of cultured plant cells by vital staining with fluorescein diacetate. Analytical biochemistry *441*, 58-62.

Schneider, C.A., Rasband, W.S., and Eliceiri, K.W. (2012). NIH Image to ImageJ: 25 years of image analysis. Nature Methods *9*, 671.

Sun, G., Elowsky, C., Li, G., and Wilson, R.A. (2018). TOR-autophagy branch signaling via Imp1 dictates plant-microbe biotrophic interface longevity. PLoS genetics *14*, e1007814.

Sweigard, J.A., Carroll, A.M., Kang, S., Farrall, L., Chumley, F.G., and Valent, B. (1995). Identification, cloning, and characterization of *PWL2*, a gene for host species specificity in the rice blast fungus. Plant Cell *7*, 1221-1233.

Takan, J. (2004). Finger millet blast pathogen diversity and management in East Africa: A summary of project activities and outputs. International sorghum and millets newsletter *45*, 66-69.

Takan, J., Chipili, J., Muthumeenakshi, S., Talbot, N., Manyasa, E., Bandyopadhyay, R., Sere, Y., Nutsugah, S., Talhinhas, P., and Hossain, M. (2012). *Magnaporthe oryzae* populations adapted to finger millet and rice exhibit distinctive patterns of genetic diversity, sexuality and host interaction. Molecular biotechnology *50*, 145-158.

Valent, B., Farrall, L., and Chumley, F.G. (1991). *Magnaporthe grisea* genes for pathogenicity and virulence identified through a series of backcrosses. Genetics *127*, 87-101.

Yoshida, K., Saunders, D.G., Mitsuoka, C., Natsume, S., Kosugi, S., Saitoh, H., Inoue, Y., Chuma, I., Tosa, Y., and Cano, L.M. (2016). Host specialization of the blast fungus *Magnaporthe oryzae* is associated with dynamic gain and loss of genes linked to transposable elements. BMC genomics *17*, 370.

Zheng, H., Chen, S., Chen, X., Liu, S., Dang, X., Yang, C., Giraldo, M.C., Oliveira-Garcia, E., Zhou, J., and Wang, Z. (2016). The small GTPase MoSec4 is involved in vegetative development and pathogenicity by regulating the extracellular protein secretion in *Magnaporthe oryzae*. Frontiers in plant science *7*, 1458.

Table

Table S4.1. Virulence of *M. oryzae* E2 strain on different finger millet cultivars

FM#	Original name	Disease scoring*	Mean score
1	GuluE	3,3,3,5	3.5
2	IE1012	3,3,3,4	3.3
3	Okhale-1	1,1,1,1	1.0
4	BKFM0031	1,1,1,1	1.0
5	IE2335	3,3,3,3	3.0
6	AAUFM-44	3,3,4,5,5	4.0
7	IE766	1,1,1,2	1.3
8	KAT/FM	2,3,3,3,4	3.0
9	KNE479	5,5,5	5.0
10	IE7	5,5,5	5.0

*Each score was measured from one leaf of one plant. 3-5 plants per cultivar were tested. Disease scores are the average of scores of each individual leaf harvested per cultivar. Scale is from 0-5 (Fig. S4.1A): 0= no disease, 1= minimal small lesions, 2= many small lesions, 3= many small and a few medium sized lesions, 4= many medium sized lesions, 5= many large lesions or lesions that are dense or merging.

Table S4.2. Virulence of MoE strain on different finger millet cultivars

FM#	Original name	Mean score*
1	GuluE	4.7
3	Okhale-1	4.1
4	BKFM0031	4.0
6	AAUFM-44	5.0
10	IE7	5.0
12	E11	3.0
13	IE255	3.9
14	MD-48	4.4
15	214988	2.9
16	TZA4295	3.8
17	TZA1637	2.1

*Score scale is the same as in the Table S4.1.

Table S4.3. *Magnaporthe oryzae* strains used in this study

Strain	CKF#	Genotype	Reference
O-137	CKF558	Wild-type, a field isolate from rice in China.	Sweigard *et al.*, 1995
E2	CKF4042	Wild-type, a field isolate from finger millet in Ethiopia.	This study
MoO	CKF193	Transformant of the rice isolate O-137, expressing the EGFP fused histone H1 protein under control of a constitutive promoter *M. oryzae P27*; Hyg^R	This study
MoE	CKF4046	Transformant of the finger millet isolate E2, expressing cytoplasmic EGFP reporter gene under control of a constitutive promoter *M. oryzae P27*; Hyg^R	This study
PWL2/BAS4 localization strain	CKF4198	Transformant of the finger millet isolate E2, expressing both a fusion of the *PWL2* promoter and entire coding sequence with the mCherry:NLS reporter gene, and a fusion of the *BAS4* promoter and entire coding sequence with the EGFP reporter gene; Hyg^R	This study

Table S4.4. Key plasmids used in this study

Clone	Description
pBV126	Described in Khang et al., 2010.
pBV229	1.2-kb of hH1:EGFP fragment cloned into XhoI and BamHI sites of pBV126.
pBV591	Described in Khang et al., 2010.

Table S4.5. List of primers used in this study

Gene name	CKP#	Sequence (5'-3')	Size (bp)	Accession No.	Reference
Osactin	CKP331	CGTCTGCGATAATGGAACTG	120	LOC_Os03g50885.1	This study
	CKP332	CCCATTCCGACCATGACACC			
Ecβ-tub	CKP783J	CACCTCCATCCAGGAGATGT	167	Pg/KM105955	Reddy et al., 2018
	CKP784J	GGTGAACTCCATCTCGTCCA			
OsPR1b	CKP816J	CAGGACTACGTGAGGCTCCA	110	LOC_Os01g28450.1	This study
	CKP817J	CTTCTCTGGCTGGCGTAGTT			
OsPR2	CKP818J	CCGGTATGCCTGATGTCTCC	116	LOC_Os07g35560.3	This study
	CKP819J	GTAAACCTCCGTCCCGTCTG			
OsPR8	CKP820J	CCTGCAACTCCGGCCTATAC	108	LOC_Os01g47070.1	This study
	CKP821J	CGGAGCTTGGTTCGCAGT			
EcPR1b	CKP822J	GGGTGGACGAGAAGCAG	84	ELECO.r07.7BG0585710.1	This study
	CKP823J	ACACCACCTGTGTGTAGTG			
EcPR2	CKP824J	GGCCTACGTCAACAACGTGA	103	ELECO.r07.7AG0570850.1	This study
	[illegible]	[illegible]			
EcPR8	CKP826J	CAGTGCCCTTACCCGGACG	93	ELECO.r07.1AG0027350.1	This study
	CKP827J	GCACGGCGGGTTATTGTAGA			

Figure

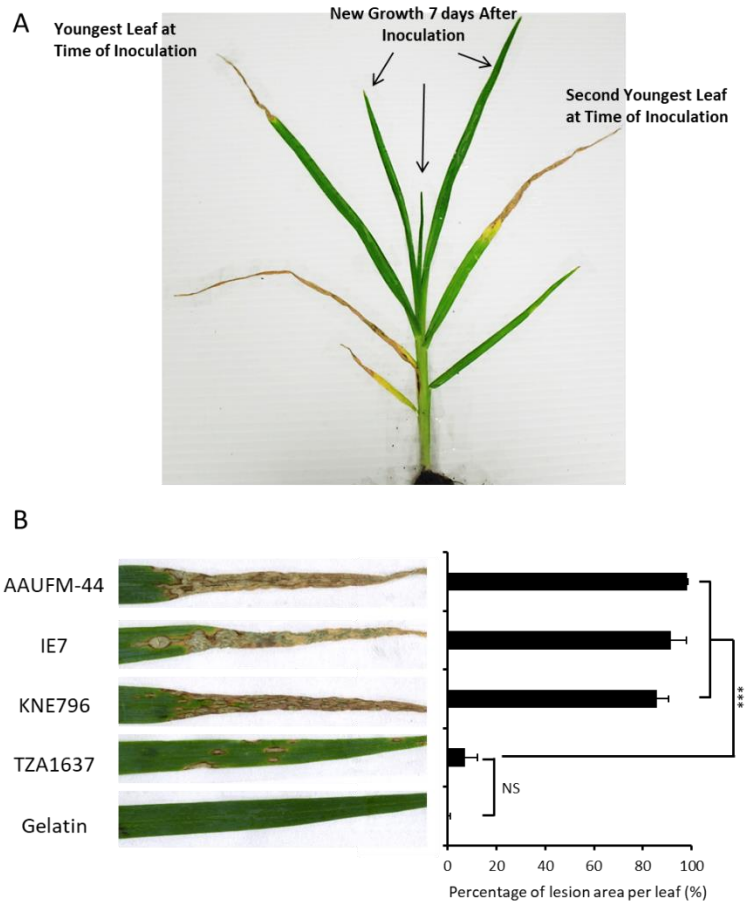

Figure 4.1. Pathogenicity assay of *M. oryzae* pathotype MoE on finger millet using whole plant spray inoculation method. (A) A typical phenotype of the susceptible finger millet cultivar AAUFM-44 after 7 days inoculation under conditions described in Materials and Methods. ~12-day-old finger millet seedlings were incubated with 1x10^5/ml of fungal spores. (B) Comparison of pathogenicity on susceptible and resistant finger millet cultivars. Inoculation with 0.25% gelatin was used as the negative control. Bar chart showed the percentage of lesion area per marked leaf after infection with fungal spores. Error bar equals standard deviation of the mean. *** $p<0.0001$ (Oneway ANOVA and Tukey-Kramer HSD). NS means no significant difference. Two experiments were performed with similar results.

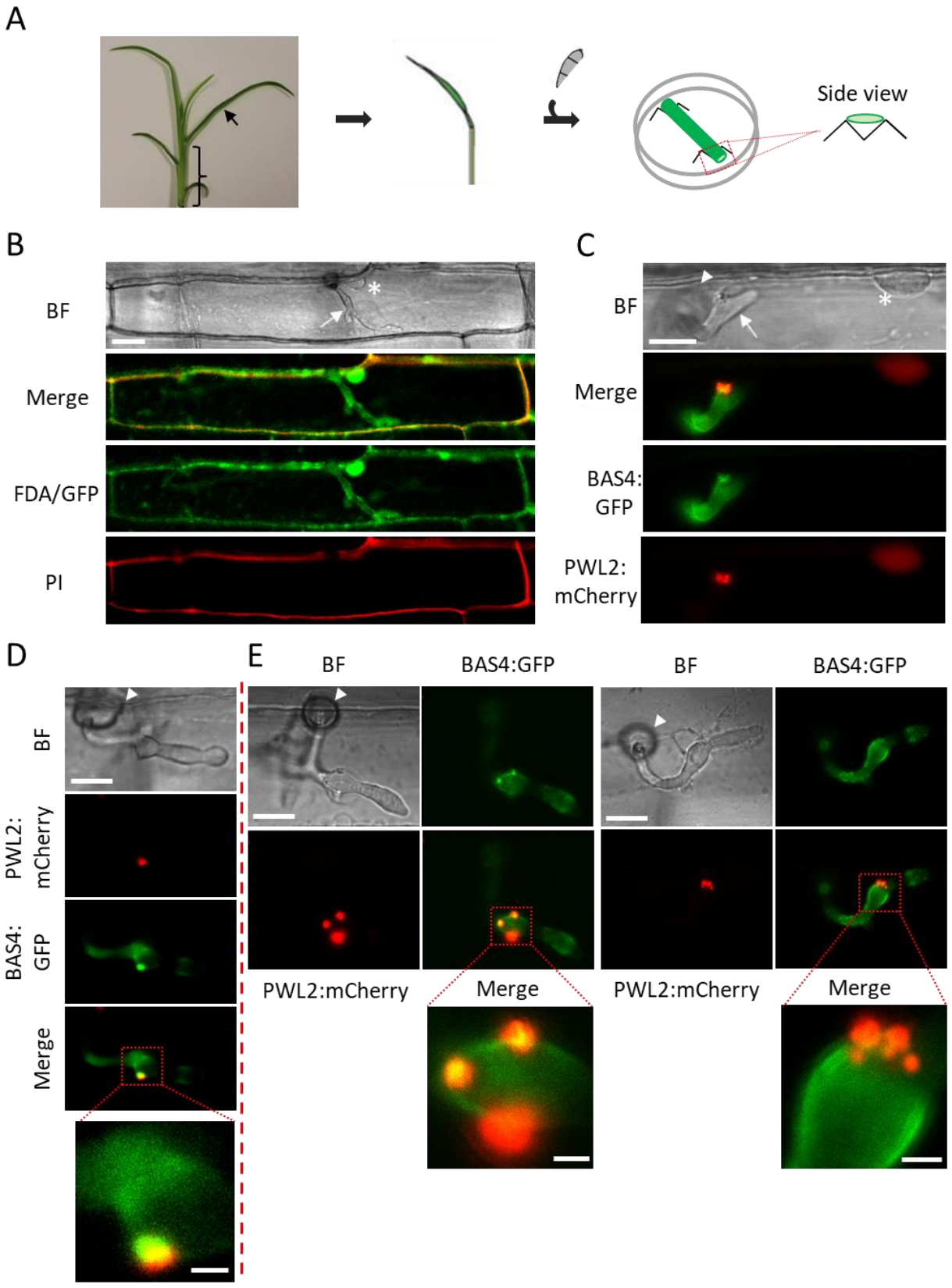
A
Side view
B
BF
Merge
FDA/GFP
PI
C
BF
Merge
BAS4:
GFP
PWL2:
mCherry
D
BF
PWL2:
mCherry
BAS4:
GFP
Merge
E
BF
BAS4:GFP
BF
BAS4:GFP
PWL2:mCherry
Merge
PWL2:mCherry
Merge

Figure 4.2. Development of finger millet leaf sheath inoculation method for live-cell imaging. (A) Schematic diagram of the finger millet leaf sheath inoculation. (B) Confocal image of the susceptible finger millet sheath (AAUFM-44) epidermal cell infected with *M. oryzae* transformant MoE (CKF4046) expressing cytoplasmic EGFP (shown in green inside of plant cell) at 30 hpi and stained with FDA (green around the plant cell and in nucleus) and PI (red around the plant cell). The appressorium (arrowhead) mediated penetration of the plant cell and produced IH (arrow). Asterisk indicates plant nucleus stained with fluorescein. Bar = 20 μm. (C) Cellular localization of PWL2:mCherry:NLS and BAS4:GFP during MoE infection on finger millet epidermal cells at 30 hpi. PWL2:mCherry:NLS was observed to translocate into plant nucleus as indicated by asterisk. Arrowhead indicates appressorium. Bar = 10 μm. The localization of PWL2:mCherry:NLS at BICs was observed two patterns: a single primary BIC (D) and multisite BICs (E). Bars =10 μm. Insets show magnified images of BICs. Inset bars = 2 μm.

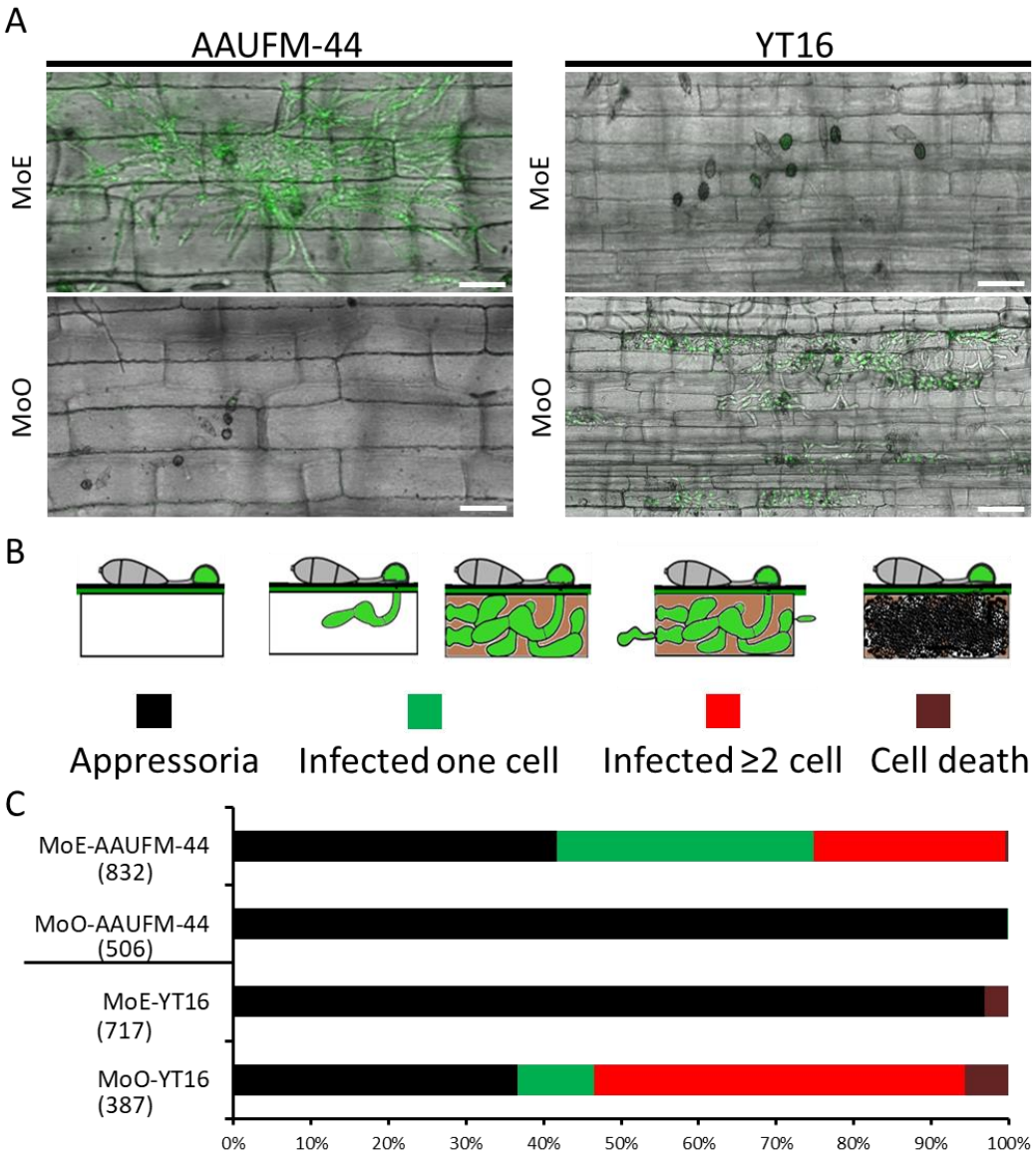

Figure 4.3. Cellular responses of susceptible finger millet and rice to infection of different *M. oryzae* strains. (A) Representative confocal microscopy images of finger millet (AAUFM-44) and rice (YT16) sheath cells infected by GFP-tagged *M. oryzae* isolates MoE and MoO at 48 hpi. Bars = 50 μm. (B) Schematic of various plant infection stages by *M. oryzae*. (C) Distribution of fungal infection progressing at 48 hpi. The number in parentheses indicates the number of infection sites were examined for each interaction. Each bar represents the percentage of the infection stage in all observed infection sites of each interaction.

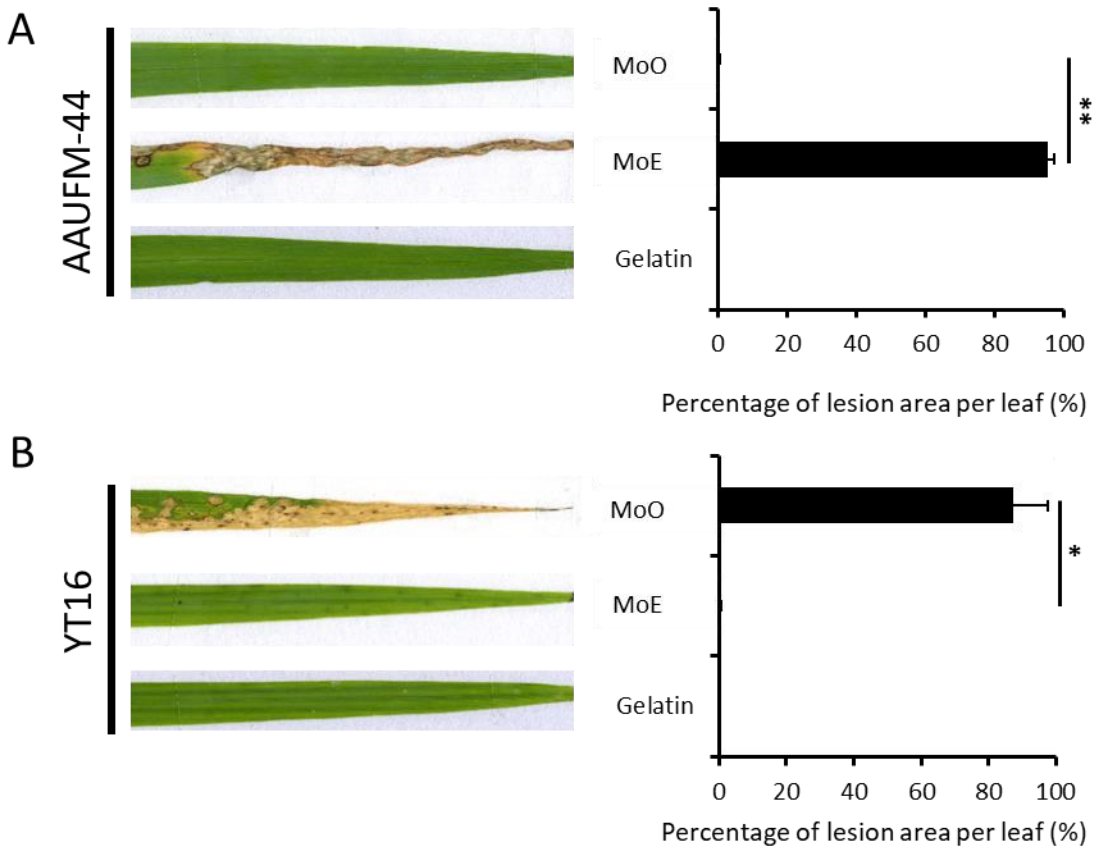

Figure 4.4. *Magnaporthe oryzae* strains isolated from finger millet and rice show host species specificity. Phenotypes of plant-pathogen interactions between *M. oryzae* isolates and finger millet or rice were examined by whole plant spray inoculation assay. 0.25% gelatin was used as the mock control. Disease symptoms were observed after 7 days inoculation. Bar chart showed the percentage of lesion area per marked leaf after infection with fungal spores. Error bar equals standard deviation of the mean. ** $p<0.01$, * $p<0.05$ (student t-test). Two experiments were performed with similar results.

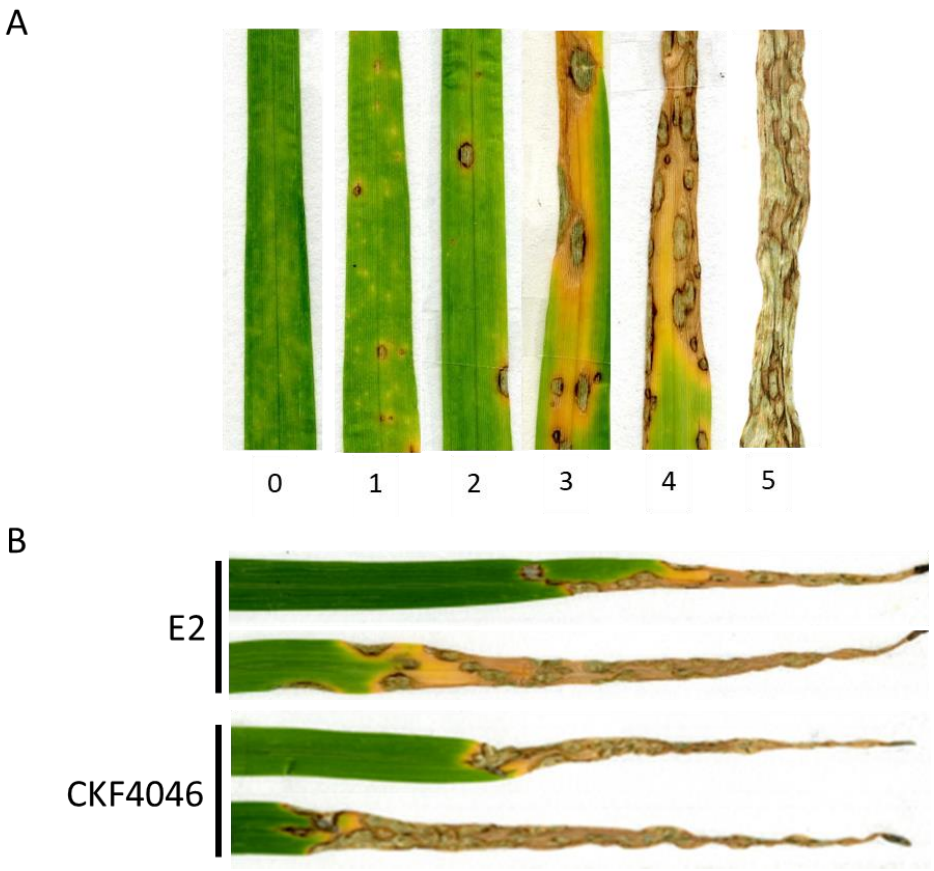

Fig. S4.1. Whole plant spray inoculation assay on finger millet cultivars by *M. oryzae* strain from finger millet. (A) Leaf segments of multiple cultivars (TZA1637, Gulu E, Okhale-1, 214988, and AAUFM-44) showing standard lesion types. Six lesion types have been defined as follows for finger millet seedlings inoculated under conditions described in Materials and Methods. Type 0, no infection; Type 1, very few small lesions with minimal chlorosis; type 2, small to medium lesions with few having visibly grey centers, minimal chlorosis; type 3 several medium to large lesions with some merging, large areas of chlorosis; type 4 many lesions with several merged lesions large areas of chlorosis and some collapsing of the leaf; type 5 complete infection of exposed leaf, large merged lesions collapse of leaf and often complete chlorosis of leaf. (B) The wild-type E2 strain and its transformant (CKF4046) show comparable pathogenicity on finger millet cultivar IE7.

Fig. S4.2. Time-lapse images showing disease progression of *M. oryzae* infection on finger millet. The finger millet cultivar AAUFM-44 was inoculated with MoE spores ($1x10^5$ spores/ml) and the second youngest leaf at inoculation was selected for the time-lapse imaging. Lesions were not observed until about 75hpi when lesions started to appear as discolored spots, indicated by the black circle. As time progressed the lesions expanded and many merged together, while the leaf tissue outside of the lesion margins discolors and eventually shriveled.

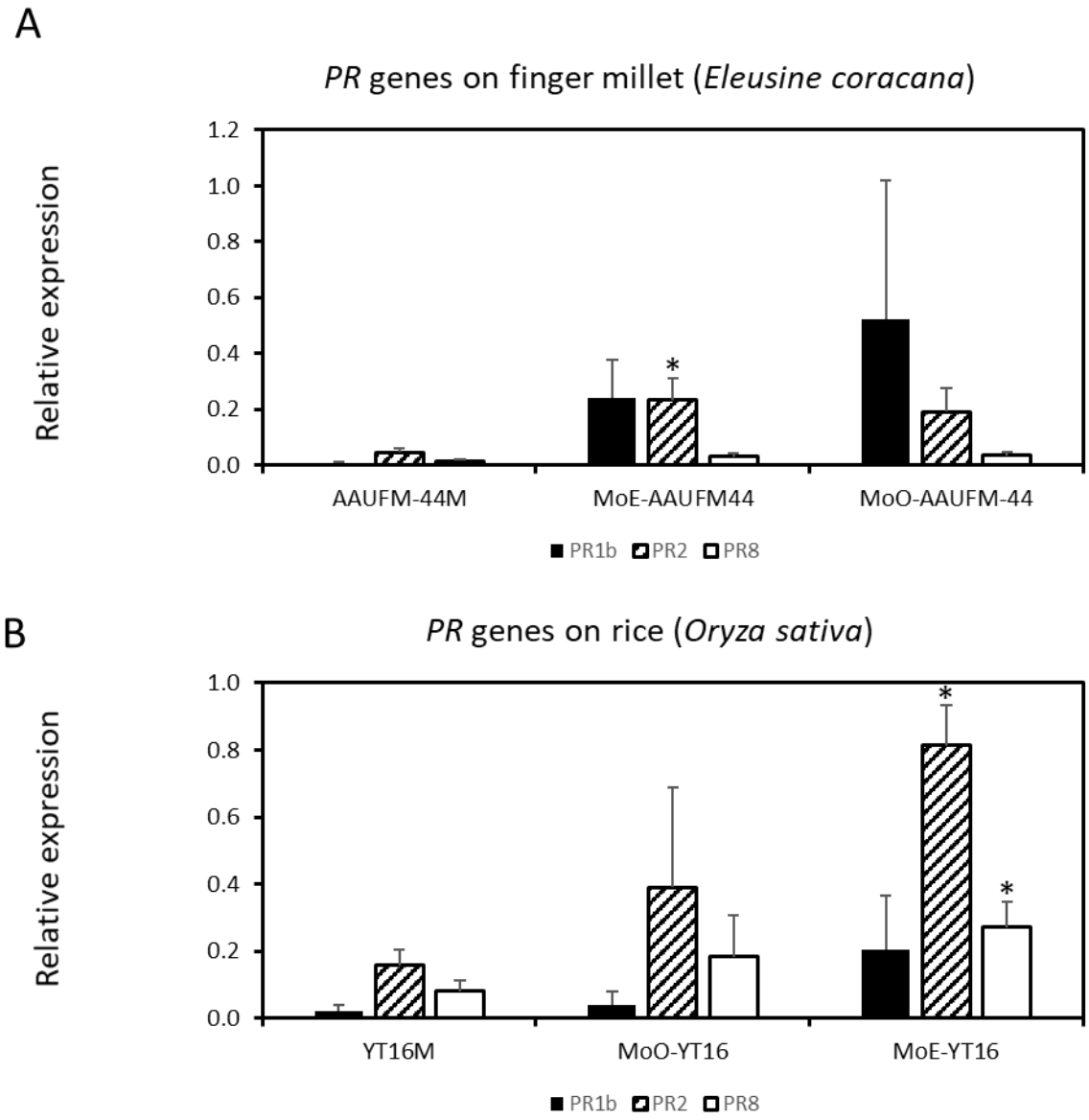

Fig. S4.3. Expression of pathogenesis-related (*PR*) genes in susceptible rice and finger millet plant. Quantitative RT-PCR analysis of expression was used to measure relative transcripts of *PR* genes to rice *actin* gene and finger millet *β-tubulin* gene. Mean values and standard deviation were calculated from three biological replicates. Student t-test was performed to determine statistical difference. * indicates $p<0.05$.

CHAPTER 5

CONCLUSION

Understanding the mechanisms by which plant pathogenic fungi adapt to manipulate plant cell structure, function and immune responses, will provide new insights into pathogen pathogenesis, thus identifying potential plant targets to breed and for engineering durable resistant plant cultivars. *Magnaporthe oryzae*, as a causal agent of the blast disease, affects important crops including rice, wheat and finger millet etc. This research aimed to investigate strategies that the phytopathogenic fungus *M. oryzae* utilizes to infect its host plants on rice and finger millet. In particular, 1) how does *M. oryzae* regulate expression of effector genes to facilitate fungal invasion and to modulate plant immunity? 2) does the infection of *M. oryzae* on finger millet resemble that on rice?

Expression of effector genes is often repressed during mycelial growth in axenic culture and strongly induced during plant infection, yet the mechanism of concerted expression remains largely unknown. By chromatin immunoprecipitation followed by high throughput sequencing (ChIP-seq), in Chapter 2, 40% of known and predicted effector genes were enriched by silencing histone modification trimethylated histone H3 lysine 27 (H3K27me3) during mycelial growth. H3K27me3 loss by the deletion of a histone methyltransferase gene *MoKMT6* responsible for catalyzing H3K27 significantly derepressed overall expression of H3K27me3-enriched effector genes but did not affect non H3K27me3-enriched effector genes through qRT-PCR and transcriptome analyses. Interestingly, expression levels of many H3K27me3-enriched effector genes were also significantly induced by ectopic overexpression of the transcription factor

MoGti1 during mycelial growth, although reprogrammed H3K27me3 pattern at both individual effector gene loci and genome wide was not observed. The MoGti1 overexpression in the absence of H3K27me3 synergistically upregulated expression of 21 effector genes during mycelial growth. Of particularly, 81% (17/21) of these synergistically upregulated effector genes were also highly induced during plant infection at 36 hpi by a wild-type *M. oryae* strain. Taken together, these results suggest that epigenetic control, mediated by H3K27me3, represses expression of H3K27me3-enriched effector genes during mycelial growth, but the transcriptional control, mediated by MoGti1, activates expression of a subset of effector genes during plant infection.

To better understand how expression of an effector gene is transcriptionally regulated, the expression and regulation of the effector gene *PWL2* was characterized at single cell level (Chapter 3). Expression of *PWL2* was successively upregulated at two critical infection stages: appressorium-mediated penetration and invasive hyphae cell-to-cell movement. This induced *PWL2* expression was not host specific but required fungal penetration into living plant cells. *PWL2* promoters in *M. oryzae* isolates from different hosts contained the tandem repeats and showed divergent numbers. Partial or complete deletion of tandem repeats caused a significant decrease or complete loss, respectively, of the promoter activity. Mutation analyses identified the 12-bp *cis*-regulatory sequence in tandem repeats that was required for *PWL2* promoter activation during plant infection. Furthermore, expression of known and predicted effector genes containing the 12-bp motif in their promoters showed consistent pattern to *PWL2* expression during infection. These results suggest that the tandem repeats in the *PWL2* promoter play important roles in transcriptional activity and contain the *cis*-regulatory element that is critical for promoter activity during biotrophic invasion.

M. oryzae is becoming a global threat to production of wheat and finger millet in addition to rice. However, we barely know the infection process of *M. oryzae* on these plants. By developing a finger millet leaf sheath inoculation assay, in Chapter 4, the fungal development during infection of the finger millet (*Eleusine coracana*)-adapted *M. oryzae* (MoE) on finger millet was investigated. I found the formation of both BIC and EIHM as well as the translocation of fluorescently labelled PWL2 effector proteins into plant cytoplasm during early infection, suggesting a biotrophic invasion of *M. oryzae* on finger millet at this stage. Interestingly, a novel BIC pattern, multisite BICs, was uncovered during compatible interaction between MoE and susceptible finger millet, which differed from rice. During incompatible interaction between MoE and a susceptible rice cultivar, however, MoE infection on rice was barely observed microscopically and macroscopically, demonstrating the host species specificity of MoE toward rice. This established finger millet leaf sheath inoculation assay has been shown to be a successful and useful technique for cytological investigations of finger millet-pathogen interactions.

Taken together, this research reveals that the epigenetic control, mediated by H3K27me3, represses expression of H3K27me3-enriched effector genes during mycelial growth, but the transcriptional control, mediated by interaction between transcription factor and *cis*-regulatory element, activates expression of effector genes during plant infection. These indicate a coordinate control of effector gene expression by epigenetic and transcriptional mechanisms in a temporal manner. Besides, the infection of *M. oryzae* on finger millet mostly resembles on rice, showing the formation of EIHM and BIC to establish a biotrophic invasion at the early infection stage, but also displays a different pattern, multisite BICs. This dissertation thus sheds light on pathogenesis of *M. oryzae* on important staple crops rice and finger millet, particularly,

mechanisms controlling expression of effector genes in filamentous fungus and cytological understanding of fungal infection on finger millet.

In this study, I profiled the genomic landscape of histone modifications H3K4me2, H3K9me3, H3K27me3 and H3K36me3 during mycelial growth of *M. oryzae* and demonstrated that H3K27me3 was involved in the repression of effector gene expression at non-inducible condition. However, it remains unknown whether other histone modifications also play roles in effector gene expression in *M. oryzae*. For example, the alteration of H3K9me3 in *Leptosphaeria maculans* results in induced expression of small secreted protein (SSP)-encoding genes during growth in axenic culture (Soyer et al., 2014a). Additionally, both H3K9me3 and H3K27me3 have been indicated to control expression of pathogenicity-related genes, including some putative effector genes, in *Zymoseptoria tritici* (Soyer et al., 2019). In addition to the contribution of other epigenetic marks on effector gene regulation, it is not clear yet if highly and widely upregulated effector gene expression during plant infection is due to altered histone modifications. Previously, the induced expression of putative effector genes and *in planta* exclusively expressed secondary metabolites genes have been reported to be correlated with H3K27me3 reduction at corresponding gene loci (Chujo and Scott, 2014a; Soyer et al., 2019). It thus will be interesting to investigate whether and how the genome-wide redistribution of H3K27me3 and other histone modifications occur to play roles in expression of *M. oryzae* effector genes during plant infection in future experiment.

The identification of the 12-bp motif in *PWL2* promoter represents an important step toward the identification of a novel transcription factor that binds to the motif and therefore to advance our understanding of effector gene regulation in *M. oryzae.* The transcription factor MoGti1 in *M. oryzae* was shown to regulate expression of certain effector genes, including *PWL2*

and *BAS4* (Li et al., 2016a). Interestingly, in contrast to *PWL2* promoter, *BAS4* promoter contained a core binding motif of the Wor1, MoGti1 ortholog in *candida albicans,* and the 12-bp motif in *PWL2* promoter differed from the core binding motif of the Wor1. Therefore, it remains to be determined whether MoGti1 directly or indirectly regulates expression of both *PWL2* and *BAS4*.

Finally, further research remains to elucidate mechanisms underlying multisite BICs and host species specificity observed from finger millet adapted *M. oryzae* isolate. A few genes have been reported to be involved in BIC development during *M. oryzae* infection in rice cells and deletion mutants of these genes showed double-BIC or multiple foci of BICs (Giraldo et al., 2013; Nishimura et al., 2016; Sun et al., 2018; Zheng et al., 2016). Nevertheless, all these mutants showed reduced virulence on rice plants, which was different from my observation showing the completely infected finger millet leaves. Thus, it will be interesting to investigate in future study if the multisite BICs are a host specific pattern to finger millet and if these genes are involved in the formation of multisite BICs during finger millet-*M. oryzae* interaction. In addition, the host species specificity during plant-microbe interaction is often determined by interaction between resistant (R) genes in plant and their cognate avirulence (AVR) genes in microbes (Kirzinger and Stavrinides, 2012). For example, AVR genes *PWL2* and *PWT3* in *M. oryzae* have been revealed to be determinants of host species specificity toward weeping lovegrass and wheat, respectively (Inoue et al., 2017; Kang et al., 1995; Sweigard et al., 1995b). It still remains whether the host species specificity in MoE is also determined by gene-for-gene interaction and what genes are involved.

References

Chujo, T., and Scott, B. (2014). Histone H3K9 and H3K27 methylation regulates fungal alkaloid biosynthesis in a fungal endophyte-plant symbiosis. Molecular Microbiology *92*, 413-434.

Giraldo, M.C., Dagdas, Y.F., Gupta, Y.K., Mentlak, T.A., Yi, M., Martinez-Rocha, A.L., Saitoh, H., Terauchi, R., Talbot, N.J., and Valent, B. (2013). Two distinct secretion systems facilitate tissue invasion by the rice blast fungus *Magnaporthe oryzae*. Nat Commun *4*, 1996.

Inoue, Y., Vy, T.T., Yoshida, K., Asano, H., Mitsuoka, C., Asuke, S., Anh, V.L., Cumagun, C.J., Chuma, I., and Terauchi, R. (2017). Evolution of the wheat blast fungus through functional losses in a host specificity determinant. Science *357*, 80-83.

Kang, S., Sweigard, J.A., and Valent, B. (1995). The PWL host specificity gene family in the blast fungus *Magnaporthe grisea*. MPMI-Molecular Plant Microbe Interactions *8*, 939-948.

Kirzinger, M.W., and Stavrinides, J. (2012). Host specificity determinants as a genetic continuum. Trends in microbiology *20*, 88-93.

Li, Y., Wang, G., Xu, J.R., and Jiang, C. (2016). Penetration peg formation and invasive hyphae development require stage-specific activation of *MoGTI1* in *Magnaporthe oryzae*. Molecular Plant-Microbe Interactions *29*, 36-45.

Nishimura, T., Mochizuki, S., Ishii-Minami, N., Fujisawa, Y., Kawahara, Y., Yoshida, Y., Okada, K., Ando, S., Matsumura, H., Terauchi, R., *et al.* (2016). *Magnaporthe oryzae*

glycine-rich secretion protein, Rbf1 critically participates in pathogenicity through the focal formation of the biotrophic Interfacial complex. PLoS Pathogen *12*, e1005921.

Soyer, J.L., El Ghalid, M., Glaser, N., Ollivier, B., Linglin, J., Grandaubert, J., Balesdent, M.H., Connolly, L.R., Freitag, M., Rouxel, T., *et al.* (2014). Epigenetic control of effector gene expression in the plant pathogenic fungus *Leptosphaeria maculans*. PLoS Genetics *10*, e1004227.

Soyer, J.L., Grandaubert, J., Haueisen, J., Schotanus, K., and Holtgrewe Stukenbrock, E. (2019). In planta chromatin immunoprecipitation in Zymoseptoria tritici reveals chromatin-based regulation of putative effector gene expression. bioRxiv.

Sun, G., Elowsky, C., Li, G., and Wilson, R.A. (2018). TOR-autophagy branch signaling via Imp1 dictates plant-microbe biotrophic interface longevity. PLoS genetics *14*, e1007814.

Sweigard, J.A., Carroll, A.M., Kang, S., Farrall, L., Chumley, F.G., and Valent, B. (1995). Identification, cloning, and characterization of *PWL2*, a gene for host species specificity in the rice blast fungus. Plant Cell *7*, 1221-1233.

Zheng, H., Chen, S., Chen, X., Liu, S., Dang, X., Yang, C., Giraldo, M.C., Oliveira-Garcia, E., Zhou, J., and Wang, Z. (2016). The small GTPase MoSec4 is involved in vegetative development and pathogenicity by regulating the extracellular protein secretion in *Magnaporthe oryzae*. Frontiers in plant science *7*, 1458.